REDUCTIVE COUPLING

AND

TRANSITION METAL CALIXARENE COMPLEXES: METAL-METAL QUADRUPLE BONDS AND POCKETS

By Jacqueline A. Acho

B.S., University of Michigan, Ann Arbor (1989)

SUBMITTED IN PARTIAL FULFILLMENT

OF THE REQUIREMENTS FOR THE

DEGREE OF

DOCTOR OF PHILOSOPHY

at the

MASSACHUSETTS INSTITUTE OF TECHNOLOGY

February, 1995

Signature of Author _____
Department of Chemistry
October 17, 1994

Certified by _____
Stephen J. Lippard
Thesis Supervisor

Accepted by _____
Dietmar Seyferth
Chairman, Departmental Committee on Graduate Students

This doctoral thesis has been examined by a Committee of the Department of Chemistry as follows:

Professor Hans-Conrad zur Loye, Committee Chairman

Professor Stephen J. Lippard
Arthur Amos Noyes Professor of Chemistry

Professor Dietmar Seyferth

To my parents

REDUCTIVE COUPLING

AND

TRANSITION METAL CALIXARENE COMPLEXES: METAL-METAL QUADRUPLE BONDS AND POCKETS

By Jacqueline A. Acho

Submitted to the Department of Chemistry on October XX, 1994 in partial fulfillment of the requirements for the Degree of Doctor of Philosophy

ABSTRACT

Chapter I.

The reductive coupling of two isocyanide ligands to form a coordinated bis(alkylamino)acetylene molecule, previously known for $[M(CNR)_6]$ complexes, M = Mo, W and R = alkyl, has been extended to include the first row transition metal chromium. An improved synthesis and X-ray structure determination of the known precursor molecule, $[Cr(CN\text{-}t\text{-}C_4H_9)_6]$ (**1**), are reported. The coordination geometry is approximately octahedral. A noteworthy feature of the structure is the variability of isocyanide C-N-C bend angles [136.1(9)° to 175(1)°], which correlate linearly with the M-C bond lengths for M = Cr and Mo. Addition of 2 equivalents of HI(aq) to $[Cr(CN\text{-}t\text{-}C_4H_9)_6]$ in THF resulted in carbon-carbon bond formation between two isocyanide ligands to afford $[Cr(t\text{-}C_4H_9HNC{\equiv}CNH\text{-}t\text{-}C_4H_9)(CN\text{-}t\text{-}C_4H_9)_4I]I$ (**2**), which has been characterized by ^1H and $^{13}C\{^1H\}$ NMR, IR spectroscopic, as well as elemental, analyses. The solid-

state structure of **2** was determined in a single crystal X-ray diffraction study. The idealized geometry about the chromium center in **2** is C_{2v} capped trigonal prismatic. Reaction of **2** with excess H_2O_2 resulted in the oxidative removal of the coupled acetylene as (*N,N'*-di-*tert*-butyl)oxamide.

Chapter II.

A brief account of the historical development of calixarene chemistry through the introduction of transition metals to the field in 1986 is presented. Motivation and background for the research presented in Chapters III and IV are provided.

Chapter III.

The preparation of complexes containing metal-metal quadruple bonds supported by calixarene ligands is described. The labile starting materials $[Mo_2(OCCH_3)_2(NCCH_3)_6][BF_4]_2$, a known compound, and $[Mo_2(OCCF_3)_2(NCCH_3)_6][BF_4]_2$ (**1**) were added to solutions of *p-tert*-butyl-calix[4]arene and calix[4]arene that were deprotonated with two equivalents of KH to give, respectively, $[Mo_2(O_2CR)_2(H_2$-*p-tert*-butylcalix[4]arene)] (**2,3**: R = CH_3, CF_3) and $[Mo_2(O_2CR)_2(H_2$-calix[4]arene)] (**4,5**: R = CH_3, CF_3). The dimolybdenum calixarene products **2-5** were studied by ^1H NMR, IR, UV-visible, and Raman spectroscopy. X-ray crystallographic analysis revealed the solid state structure of **2**(THF)·C_6H_6. In **2**(THF)·C_6H_6 a molybdenum-molybdenum quadruple bond (2.1263 (6) Å) is spanned by two bridging acetate ligands and a tetradentate, doubly-deprotonated calixarene macrocycle. Each Mo-Mo unit is weakly

coordinated by an axial THF solvent molecule which is included in the calixarene basket of the neighboring complex.

Chapter IV.

Several transition metal calixarene complexes that are specifically suited to bind guests within the macrocyclic pocket were prepared. The complexes, [Cp*Ta(calix[4]arene)], [Cp*Ta(*p-tert*-butylcalix[4]arene)], and [CpNb(*p-tert*-butylcalix[4]arene)], are all monomeric with electron deficient metal centers protected in the *exo*-calix position by sterically bulky ligands. The spectroscopic and structural characterization of these transition metal calixarene complexes is described. Evidence of small molecule binding at the transition metal center *endo*-calix is provided in the solid state and in solution with the complexes [Cp*Ta(OH_2)(*p-tert*-butylcalix[4]arene)] and [Cp*Ta($NCCH_3$)(*p-tert*-butylcalix-[4]arene)]. By combining the attractive forces of the calixarene pocket and an electron deficient metal center, unusual binding and inclusion within a calixarene macrocycle were observed. This strategy represents a novel contribution to the field of transition metal calixarene chemistry.

Thesis Supervisor: Professor Stephen J. Lippard

Title: Arthur Amos Noyes Professor of Chemistry

Table of Contents

List of Figures

List of Tables

Acknowledgments

This is a wonderful tradition that allows me to put into writing my gratitude to people who have helped me to develop as a chemist and a person during my time here at MIT and before. I hope I can get through this without becoming too sentimental.

About Professor Stephen J. Lippard, the most telling thing that I can say now is that I would do it all over again. Choosing Steve as a research advisor was a more insightful decision than I possibly could have realized four years ago. Steve has a talent for bringing the personal best out of his students, allowing us freedom yet providing guidance. His standards of perfection are not easy to achieve, but they ultimately give us pride in ourselves. Few people put as much heart into their jobs; for this reason I will remember Steve as a professional model, even though my decisions lead me away from scientific research.

Another mentor deserves credit for inspiring me, among many of her students, to pursue graduate studies in chemistry. Professor Seyhan Ege of the University of Michigan introduced me to scientific research and inspired me in one of my greatest loves, teaching. It is also appropriate here that I mention my very fond memories of working with the MIT chemistry undergraduate office as a teaching assistant. Melinda Glidden Cerny organized a program that was beyond even my enthusiastic expectations, and Launa Calendar made the office a home.

From the Lippard laboratories, I have many colleagues to thank. Dr.'s John (flask-switcher) Protasiewicz and Ted (crystallography guru) Carnahan were wonderful chemical "big brothers". From them I learned so so much. What I thank them for most of all is their continued (even after they left) interest in my chemistry and their encouragement, tempered with realism. John, I admire your strength, and I look forward to your wonderful chemistry. Keep the X-rays going so I can pop in for my crystallography fix! Ted, it is fun to watch your career blossom for the many reasons that made you successful here.

I thank Dr. Tong Ren for molecular orbital calculations and many, many helpful discussions that contributed to Chapter III. His crystallographic stamp on our laboratory cannot be discounted either. Speaking of crystallography, I thank Dr.'s Laura Pence and Shibao Yu for taking care of the X-ray facility during my tenure here. I have also benefited from discussions with a visiting scientist, Dr. Tomoaki Tanase, who's quiet positive influence on our lab has been undeniable.

I enjoyed overlapping in the Lippard labs with the inspirational Dr. Kingsley Taft. Dr.'s Steve Bellon and Mike Keck are also quite special in very individual ways, and I enjoyed being in lab with them for too short a while. Thank you to my good friend and fellow classmate Andrew Feig. Your spirit is unstoppable and your unceasing enthusiasm for science buoyed me in dry times. I'll stake out the restaurants in Chicago for your visits (to size up the competition!). May your science always be as golden as your heart. Now for the "sub-subgroup": Linda Doerrer. First, I thank her for the Fenske-Hall calculations she did with great speed and competence for Chapter IV. I am also

deeply grateful for her editorial comments on this thesis. More importantly, I thank her for being an incredibly dependable colleague and great friend. I will miss seeing you and talking to you everyday. I am looking forward to hearing about your progress here and beyond. I admire your determination and I have great faith in you. Joanne Yun. Formally, I thank her for helping me to obtain the Raman spectroscopic data that contributed to Chapter III. I also thank her for the good times we've shared and her remarkable shopping prowess. Dan Lecloux. A personal and professional inspiration as well as a voice of reason. I could say that it's too bad we only overlapped for a year in Boston, but I'm so very grateful for this time that I won't. Light the scientific world on fire.

Outside of the Lippard labs I have some very special friends. Andé Prawoto is a life-long friend I will always cherish, and I deeply appreciate his help and support. Dave Bem (of the Zur Loye lab) has been a great friend and a tremendous support. It sure was fun studying, teaching, discussing research, cooking, gaming.....with this jolly muppet of a guy. Tao (of the Seyferth group) and Shihong Wang and family have given me so many treasured memories. From across the continent, I have been blessed by the steady support of my long-time friend and kindred spirit David Schwartz (at Berkeley). You are very special to me. See you in the windy city!

This brings me to the people who matter most to me in the whole world. It is true that you can't choose your family, so this makes me one of the luckiest people alive. I thank my loving and supportive extended family including cousins, uncles, and aunts. Of these, some people have been especially close and influential. I thank my uncle Jack not only for my name but for years of support and unswerving faith. My grandmother, Edith Kittinger (Minna), loves her family with a strength that could move mountains. I have felt this love and her great friendship all of my life. I know that I will always be able to count on my big brother Mike, and I am so grateful for his deep-down love and support. This brings me to my parents, Barb and Pete Acho. How did I get this lucky? There is just no way to thank them. I have never felt far from their constant support and tremendous love. My father is so sweet. His faith in me and love fill my heart and give me confidence. His calming influence, good advice, and positive spirit have supported and inspired me all of my life. Now you can sit back for a while, dad, and let me bring home the breeeeead! My mother is my ultimate mentor. I am very clearly a product of her patient teaching, as an advisor and role-model. In my adult years I have come to be even more grateful for her friendship. I am never far from you, mom.....and Chicago really is even closer!

Those of you who know me well enough realize that I AM more than a little misty now... So it is best that I end here before I get too carried away. Finally, I do want to thank the Lippard lab members past and present who could not all be mentioned here but certainly contributed to making Steve's group a good place to work, personally and scientifically.

CHAPTER I

The Reductive Coupling of Isocyanide Ligands on a Chromium Metal Center[1,2]

Introduction

Following the discovery of the reductive coupling of two isocyanide ligands in $[Mo(CN\text{-}t\text{-}C_4H_9)_6I]I$,[3] much work has been carried out to extend the generality of the reaction and to elucidate the mechanism of carbon-carbon bond formation.[4,5] Work from our laboratory extended the reductive coupling chemistry both to CO complexes and to group V transition metals. Reductive coupling of CO ligands, originally studied with niobium and tantalum, was recently achieved with vanadium with two unexpected results.[6] Not only was the coupled acetylene ligand more readily removed from the metal than for the Nb and Ta analogs, but the smaller vanadium center afforded an unprecedented 6-coordinate cation, $[V(Me_3SiOC{\equiv}COSiMe_3)(dmpe)_2]^+$ (eq. 1).

$$Na[V(CO)_2(dmpe)_2] \xrightarrow{2\ Me_3SiOTf} [V(Me_3SiOC{\equiv}COSiMe_3)(dmpe)_2]OTf \quad (1)$$

Given these differences between the chemistry of a first row compared to second and third row group V transition metal complexes, we were interested to extend the reductive coupling of group VI Mo and W isocyanide complexes to the first row congener Cr. Reductive coupling of isocyanides on Group VI metal centers is well precedented for the second and third row metals.[3,5,7-12] Reductive coupling was first discovered during a study of seven-coordinate molybdenum isocyanide complexes. Refluxing a solution of $[Mo(CN\text{-}t\text{-}C_4H_9)_6I]I$ in slightly wet THF overnight in the presence of zinc dust produced the coupled product $[Mo(t\text{-}C_4H_9HNC{\equiv}CNH\text{-}t\text{-}C_4H_9)(CN\text{-}t\text{-}C_4H_9)_4I]I$.[3] Subsequent mechanistic studies revealed that the reaction pathway, shown in eq. 2,[8] involves reduction of the $[Mo(CNR)_6I]^+$ cation first to afford the homoleptic Mo^0 isocyanide complex,

$$[Mo(CNR)_6I]^+ \xrightarrow[THF]{Zn} [Mo(CNR)_6] \xrightarrow{HX}$$

$$\{[Mo(\equiv CNHR)(CNR)_5]X\} \xrightarrow{HX} [Mo(RHNC\equiv CNHR)(CNR)_4X]X \qquad (2)$$

R = alkyl; X = halide, triflate

$[Mo(CNR)_6]$, which was isolated as a discrete intermediate. Subsequent addition of one equivalent of acid transformed this compound to a metal alkylaminocarbyne complex which, although not isolated, was postulated to exist by analogy to reactions carried out with silylating agents instead of HX. Addition of a second equivalent of HX triggered C-C bond formation, yielding the metal-bound acetylene complex, $[Mo(RHNC\equiv CNHR)(CNR)_4X]X$. Since the chromium analog of $[Mo(CNR)_6]$ for R = t-C_4H_9, $[Cr(CN\text{-}t\text{-}C_4H_9)_6]$, is a known compound, [13,14] we wondered whether it might be possible to couple the isocyanide ligands in this molecule by similar chemistry. To do so would not only extend the reaction to a new metal center but would provide a powerful test of the generality of the reaction mechanism. Moreover, since among the few homoleptic isocyanide complexes of Cr(0), X-ray crystal structures are available only for two aryl isocyanide complexes, $[Cr(CNPh)_6]$[15] and $[Cr\{CN(i\text{-}Pr)_2Ph\}_6]$[16], and just one alkyl isocyanide, $[Cr(CNCF_3)_6]$,[17] we also carried out an X-ray diffraction study of **1**. This information allows an examination of geometric factors that might relate to its propensity to undergo reductive coupling. Information of this kind was valuable in understanding the reactivity of $[Mo(CN\text{-}t\text{-}C_4H_9)_6]$.[8] Knowledge of the structure also helps to assess the changes that take place upon reductive coupling of two adjacent ligands in **1**.

Experimental Section

General Procedures. All manipulations were carried out in a Vacuum Atmospheres nitrogen-filled dry box or by using standard Schlenk line techniques. Solvents were distilled under nitrogen. Tetrahydrofuran (THF), toluene, and pentane were distilled from sodium benzophenone ketyl. NMR spectra were obtained on a Varian XL-300 spectrometer at room temperature. IR spectra were recorded on a Bio-Rad FTS7 Fourier Transform instrument. GC/MS studies were performed on a 12 m Hewlett-Packard Model 5971 A system with a fluid phase methylsilicone column. The yield was determined by comparison to an internal standard (naphthalene).

Materials. *tert*-Butyl isocyanide, $CrCl_2$, and H_2O_2 (30%) were purchased from commercial vendors and used without further purification. Hydriodic acid (HI, 57%) was deoxygenated prior to use by purging the solution with argon for 10 minutes.

Synthesis. [Cr(CN-t-C_4H_9)$_6$] (1). The preparation of [Cr(CN-*t*-C_4H_9)$_6$], a known compound,[13,14] was carried out as previously reported for [Mo(CN-*t*-C_4H_9)$_6$][8] with minor changes. To a suspension of $CrCl_2$ (139 mg, 1.13 mmol) in 20 mL of THF was added excess 1% Na/Hg amalgam (29.8 g Hg, 0.302 g Na, 13.1 mmol Na) and CN-*t*-C_4H_9 (566 mg, 6.81 mmol). The reaction mixture was stirred vigorously for 3 h in the absence of light. The green-yellow solution was decanted from the amalgam and filtered through silica gel. The solvent was removed from the orange-brown filtrate in vacuo, and the resulting solid was extracted into 50 mL of pentane. Evaporation of the pentane left 430 mg (69%) of bright orange air- and light-sensitive product which could be recrystallized from pentane to give an orange crystalline product. IR (pentane): 2955 (w), 2088 (sh), 1953 (sh), 1919 (sh), 1883 (vs, br), 1842 (sh), 1390 (w), 1361 (m), 1211 (m) cm^{-1}. ^1H

NMR (C_6D_6): 1.35 ppm (s). Anal. Calcd. for $C_{30}H_{54}N_6Cr$: C, 65.42; H, 9.88; N, 15.26. Found: C, 65.50; H, 10.01; N, 15.28.

[Cr(t-C_4H_9HNC≡CNH-t-C_4H_9)(CN-t-C_4H_9)$_4$I]I (2). To a bright orange solution of [Cr(CN-*t*-C_4H_9)$_6$] (**1**) (200 mg, 0.363 mmol) in 15 mL of THF was added 2 equiv of aqueous HI (57%, 109 μL, 0.729 mmol). The solution immediately turned brown. After stirring for 1 h, the solution was passed through a one inch pad of silica. The solvent was evaporated and the red-brown product was washed with several portions of pentane, and 252 mg (0.312 mmol, 86%) of **2** were collected on a fritted funnel. The product was judged to be >95% pure by ^{1}H NMR spectroscopy and could be further purified by recrystallization from THF at -30 °C. IR (KBr): 3151 (m), 3106 (m), 2978 (s), 2121 (br, vs), 1608 (vs), 1520 (m), 1464 (s), 1369 (s), 1203 (vs), 1034 (w), 728 (w), 584 (m), 554 (m) cm^{-1}. ^{1}H NMR ($CDCl_3$): δ 10.51 (br, N*H*), 1.74 (s, *t*-C_4H_9NHCCNH-*t*-C_4H_9), 1.44 (s, CN-t-C_4H_9) ppm. $^{13}C\{^1H\}$ NMR ($CDCl_3$): δ 30.1 ($C(CH_3)_3$), 31.1 ($C(CH_3)_3$), 56.2 ($C(CH_3)_3$), 56.8 ($C(CH_3)_3$), 168.1 (M-C), 208.9 (C≡C) ppm. Anal. Calcd. for $C_{30}H_{56}N_6I_2Cr$: C, 44.67; H, 7.00; N, 10.42. Found: C, 44.63; H, 6.92; N, 10.24.

Reaction of [Cr(t-C_4H_9HNC≡CNH-t-C_4H_9)(CN-t-C_4H_9)$_4$I]I (2) with H_2O_2; Removal of the Coupled Ligand as N,N'-Di-tert-butyl Oxamide. A solution of 0.074 g (0.091 mmol) of [Cr(*t*-C_4H_9HNC≡CNH-*t*-C_4H_9)(CN-*t*-C_4H_9)$_4$I]I (**2**) in 10 mL THF was prepared. To the stirred brown solution were added 10 equiv of H_2O_2 (30 μL, 0.98 mmol). The reaction was allowed to stir for 14 h and then filtered to remove a thin layer of fine brown precipitate. The orange filtrate was analyzed by GC/MS and found to contain N, N'-di-*tert*-butyl oxamide (M^+ = 200) in 28% yield.

X-ray Structure Determinations of [Cr(CN-t-C_4H_9)$_6$] (1) and [Cr(t-C_4H_9HNC≡CNH-t-C_4H_9)(CN-t-C_4H_9)$_4$I]I (2). Bright orange crystals of **1** were grown by cooling to -30 °C a concentrated solution in pentane in the dark. The

crystals were transferred to a cold stage and a block-shaped specimen of dimensions 0.2 x 0.3 x 0.4 mm was mounted on the tip of a quartz fiber with silicone grease. Study on the diffractometer at -72 °C indicated a primitive monoclinic cell. The crystal quality was judged to be acceptable based on open counter ω-scans of several low angle reflections ($\Delta\bar{\omega}_{1/2}$ = 0.23°, no fine structure) and on axial photographs. A shroud was draped over the diffractometer to exclude room light. The unit cell parameters and intensity data were obtained by methods common in our laboratory,[18] details of which are provided in Table 1.1. Systematic absences and intensity statistics indicated the acentric space group $P2_1$, a choice later confirmed by the structure solution. The chromium atoms of the two molecules in the asymmetric unit were located by direct methods. The remaining non-hydrogen positions were determined by subsequent iterative least square refinements and difference Fourier maps. Most non-hydrogen atoms were refined anisotropically. Rotational disorder of methyl carbons on four of the *tert*-butyl groups resulted in high B_{eq} values. A two-site model for the methyl carbon atoms on these *tert*-butyl groups was introduced with 50% occupancy and isotropic temperature factors. All hydrogen atoms were placed in calculated positions and fixed to the attached carbon atoms (d_{C-H} = 0.95 Å, B_H = 1.2 B_C). The enantiomorph reported is that which refined to the lower R_w value. The largest residual peak in the final difference Fourier map was 0.39 $e^-/Å^3$, located at a distance of 0.82 Å from C223.

Deep red-brown crystals of **2** were grown by slowly cooling a warm saturated solution in toluene to -30 °C. The crystals were coated in Exxon Paratone-N, and an irregularly shaped specimen of dimensions 0.2 x 0.3 x 0.4 mm was frozen on the tip of a quartz fiber in a cold stream of N_2 at -72 °C. Preliminary studies indicated a primitive monoclinic cell. The crystal quality was judged to be acceptable based on open counter ω-scans of several low angle

reflections ($\Delta\bar{\omega}_{1/2}$ = 0.23°, no fine structure) and on axial photographs. The unit cell parameters and intensity data were obtained by methods standard in our laboratory,[18] details of which are provided in Table 1.1. An empirical psi-scan absorption correction was applied to the data. Systematic absences and intensity statistics were consistent with the centrosymmetric space group $P2_1/n$. The two iodine atoms and the chromium atom were located by direct methods. The remaining non-hydrogen atoms were located by subsequent iterative least square refinements and difference Fourier maps. All non-hydrogen atoms were refined anisotropically. Hydrogen atoms H1 and H2 of the protonated bis(alkylamino)acetylene ligand were located on a difference Fourier map. Other hydrogen atoms were calculated and fixed on the attached carbon atoms (d_{C-H} = 0.95 Å, $B_H = 1.2\ B_C$). The largest residual peak in the final difference Fourier map was 1.18 $e^-/Å^3$, at a distance of 0.96 Å from the I2 anion.

Results and Discussion

The preparation of $[Cr(CN\text{-}t\text{-}C_4H_9)_6]$ (**1**) reported here is more convenient and less expensive than earlier syntheses. The compound was first made from $[Cr(C_8H_8)_3]$,[13] which is obtained by metal atom vapor techniques. It was later reported that red-brown crystals of **1** could be obtained in 24 hours by reducing $[Cr_2(CO_2CH_3)_4]$ with sodium amalgam in the presence of excess *tert*-butyl isocyanide.[14] We found that the homoleptic compound **1** could be readily synthesized by the procedure reported previously for $[Mo(CN\text{-}t\text{-}C_4H_9)_6]$.[8] The reduction of $CrCl_2$ by 1% sodium amalgam in THF in the presence of approximately 6 equivalents of *tert*-butyl isocyanide afforded good yields of the bright orange product **1** (eq. 3). The photosensitivity of **1** was noticed both in solution and in the crystalline state, for the bright orange color darkens to red-

brown over several hours when the compound is exposed to light. The low C≡NR stretching frequency (1883 cm^{-1}) in the solution IR spectrum of **1** suggested a highly electron-dense metal center and considerable π-back donation, indicating the compound to be a good candidate for the reductive coupling reaction.[5] The presumed π-backbonding was corroborated by the X-ray structure determination.

$$CrCl_2 \xrightarrow[\text{THF, RT, 3 h}\\ \text{in the dark}]{\text{1\% Na/Hg, 6 CN-}t\text{-}C_4H_9} [Cr(CN\text{-}t\text{-}C_4H_9)_6] \quad \mathbf{1}, 69\% \qquad (3)$$

An ORTEP diagram of one of the molecules in the asymmetric unit of **1** is shown in Figure 1.1. Final positional and thermal parameters, anisotropic thermal parameters, and selected bond distances and angles are summarized in Tables 1.2, 1.3 and 1.4, respectively. Compound **1** is isomorphous and isostructural with $[Mo(CN\text{-}t\text{-}C_4H_9)_6]$,[8] differing only in the nature of the *tert*-butyl group disorder. The geometry at the Cr center is approximately octahedral. As in the case of $[Mo(CN\text{-}t\text{-}C_4H_9)_6]$, the most notable feature of the structure is the variety of isocyanide ligand bend angles, ranging from severely bent, 136.1(9)° for C13-N13-C131, to nearly linear, 175(1)° for C23-N23-C231. The average bending angle for the twelve crystallographically independent isocyanide ligands is 153°, a value indicative of a highly electron rich Cr center donating π electrons to the ligands. This phenomenon is well-known for low valent metal isocyanide complexes and is also postulated to promote the reductive coupling reaction by increasing the electrophilicity of the isocyanide ligands, as discussed previously.[8] As illustrated in Figure 1.2, there is an approximately linear relationship between the isocyanide ligand C-N-C angles and the corresponding metal-carbon bond lengths for $[Mo(CN\text{-}t\text{-}C_4H_9)_6]$ and **1**.

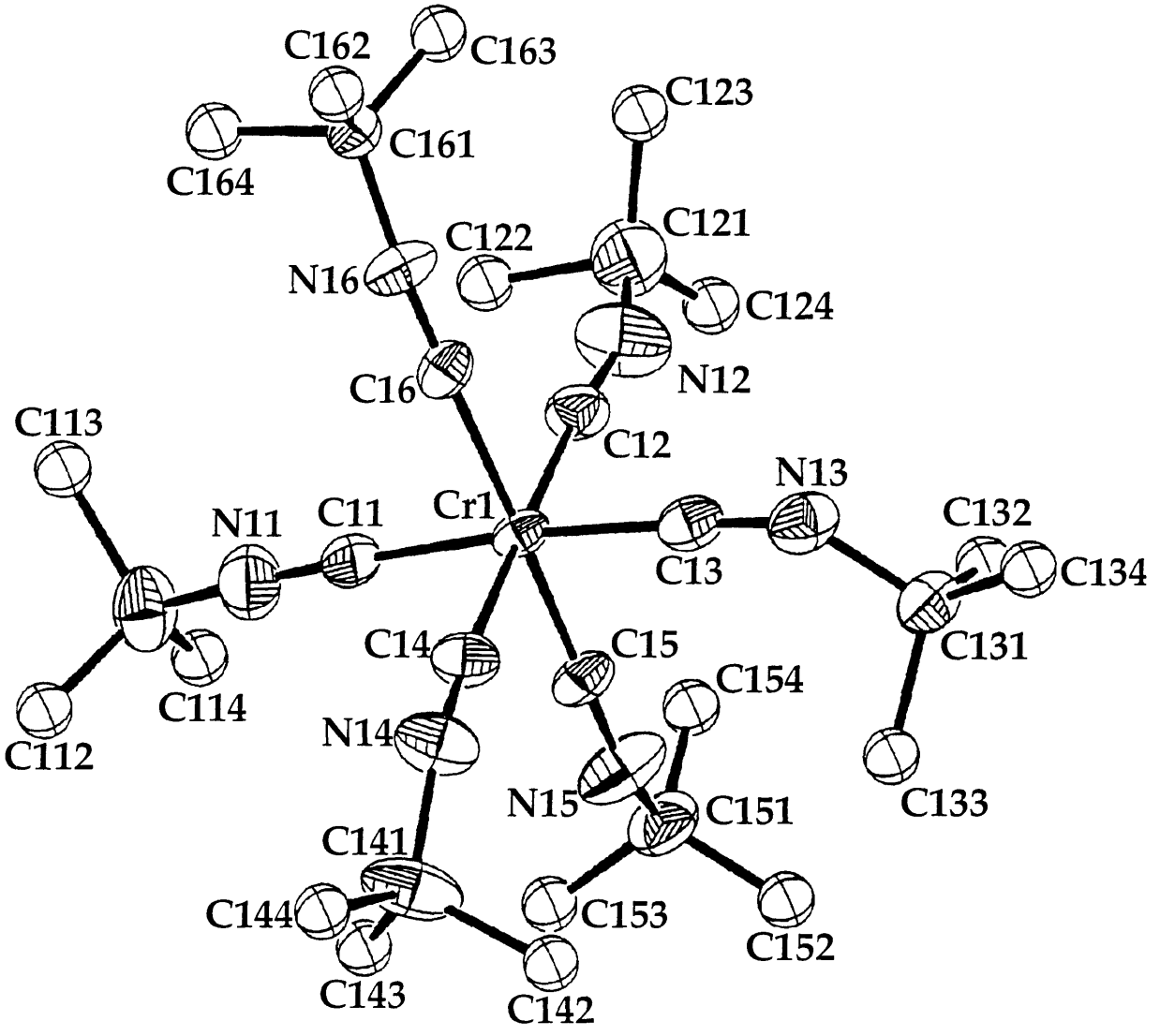

Figure 1.1. An ORTEP diagram of one of the two molecules of $[Cr(CN\text{-}t\text{-}C_4H_9)_6]$ (**1**) in the crystallographic asymmetric unit, showing the atom labeling scheme and the 40% probability thermal ellipsoids. The second molecule contains the atoms Cr2, C21, N21, C211, etc. The methyl carbons of the *tert*-butyl groups are displayed as 3 Å isotropic spheres for clarity.

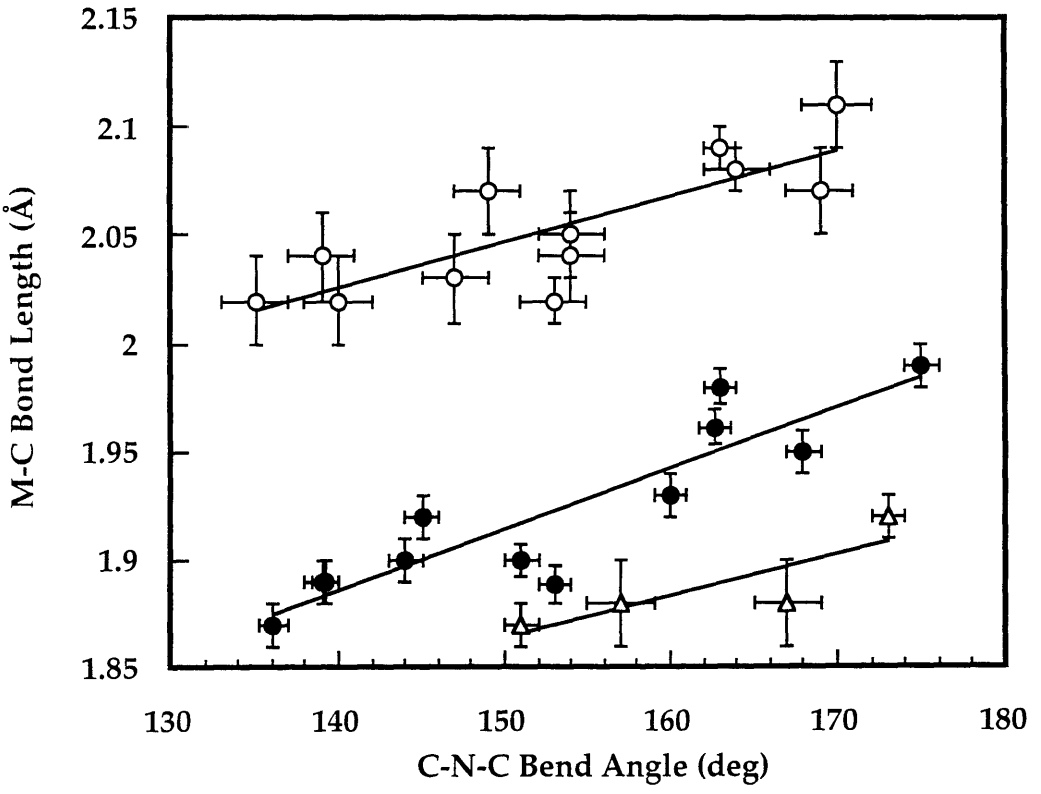

Figure 1.2. Plot of the isocyanide ligand C-N-C bend angle versus M-C bond length for $[Mo(CN\text{-}t\text{-}C_4H_9)_6]$ (open circles), $[Cr(CN\text{-}t\text{-}C_4H_9)_6]$ (**1**) (filled circles), and $[Cr(CNCF_3)_6]$ (triangles). Solid lines represent the best least squares fit to a linear relationship. Error bars denote ± 1 esd.

This relationship reflects the resonance structures **I** and **II** shown below. Figure 1.2 further reveals that $[Cr(CNCF_3)_6]$ behaves similarly,[17] but the aromatic homoleptic analogues exhibit little bending of the C-N-C angles because of resonance structures **III**.

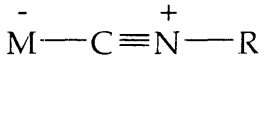

I

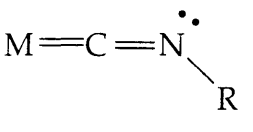

II

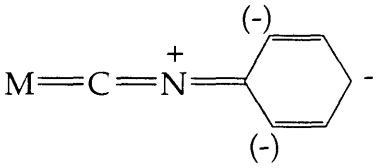

III

Addition of 2 equivalents of HI to a THF solution of **1** resulted in the reductive coupling of two adjacent isocyanide ligands to produce $[Cr(t\text{-}C_4H_9HNC{\equiv}CNH\text{-}t\text{-}C_4H_9)(CN\text{-}t\text{-}C_4H_9)_4I]I$ (**2**), as indicated in eq. 4. The best results were obtained when the reaction solution was purified by passage

$$\underset{\mathbf{1}}{[Cr(CN\text{-}t\text{-}C_4H_9)_6]} \xrightarrow[\text{THF, RT, 1 hr}]{\text{2 HI (aq, 57\%)}} \underset{\mathbf{2}\text{ , 86\%}}{[Cr(t\text{-}C_4H_9NHC{\equiv}CNH\text{-}t\text{-}C_4H_9)(CN\text{-}t\text{-}C_4H_9)_4I]I} \qquad (4)$$

through silica gel before evaporating the solvent, presumably to remove water remaining from the aqueous acid. The relatively air-stable product decomposes over time in the presence of water. The coupled product **2** was identified by its IR, ^1H NMR, and $^{13}C\{^1H\}$ NMR spectra. A strong peak at 1604 cm^{-1} in the infrared spectrum is indicative of a metal-coordinated acetylene ligand of the form (RHNC≡CNHR). Bands at 3151 and 3106 cm^{-1}, arising from N-H stretching modes, further indicated coupled product formation. The ^1H NMR spectrum supports these assignments. Peaks at 1.43, 1.74, and 10.51 ppm in a ratio of 18:9:2 can be assigned, respectively, to *tert*-butyl protons on linear ($CN\text{-}t\text{-}C_4H_9$) ligands,

tert-butyl protons on the bound acetylene, and N-H protons. Further support for a bound acetylene is provided by a resonance in the ^{13}C NMR spectrum at 209 ppm. Definitive structural proof in the solid state was provided by the X-ray diffraction study.

An ORTEP diagram of the cation of **2** is shown in Figure 1.3. Final positional and thermal parameters, anisotropic temperature facors, selected bond distances, and bond angles for **2** are summarized in Tables 1.5, 1.6, and 1.7, and 1.8, respectively. The Cr center has C_{2v} capped trigonal prismatic geometry, taking the bound acetylene to occupy two coordination sites. The core structure of **2** is very similar to that of the molybdenum analog, [Mo(*t*-C_4H_9HNC≡CNH-*t*-C_4H_9)(CN-*t*-C_4H_9)$_4$I]I.[19] Table 1.9 compares the interbond angles about the metal centers of [Cr(*t*-C_4H_9HNC≡CNH-*t*-C_4H_9)(CN-*t*-C_4H_9)$_4$I]I (**2**) and [Mo(*t*-C_4H_9HNC≡CNH-*t*-C_4H_9)(CN-*t*-C_4H_9)$_4$I]I to angles expected for the possible geometries expected of seven-coordinate complexes. This "twenty-one angle test"[20] shows that the metal centers of both complexes have approximate C_{2v} capped trigonal prismatic geometry, taking the bound acetylene to occupy two coordination sites. The metrical parameters of the coupled ligands in the two are compared in Figure 1.4, which reveals some noteworthy differences. The metal-carbon distance is 0.11 Å shorter in **2** than for the molybdenum analog, corresponding to the differences in their atomic radii [Cr(0) = 1.29 Å; Mo(0) = 1.40 Å].[21] This difference in turn produces a slightly larger C1-Cr-C2 angle (approximately 3°) in **2**. Figure 1.5 shows a packing diagram of **2**·toluene, salient features of which are the close contacts between the ionic iodide I2, and the N-H protons on the coordinated aminoacetylene ligand, I2···N1 = 3.613(4) Å (I2···H1 = 2.560 Å) and I2···N2 = 3.646(4) Å (I2···H2 = 2.721 Å). This interaction was also observed in the lattice structure of [Mo(*t*-C_4H_9HNC≡CNH-*t*-C_4H_9)(CN-*t*-C_4H_9)$_4$I]I, I2···N2 = 3.72 Å (I2···H1 = 3.05Å) and I2···N2 = 3.68 Å (I2···H2 = 2.81 Å).

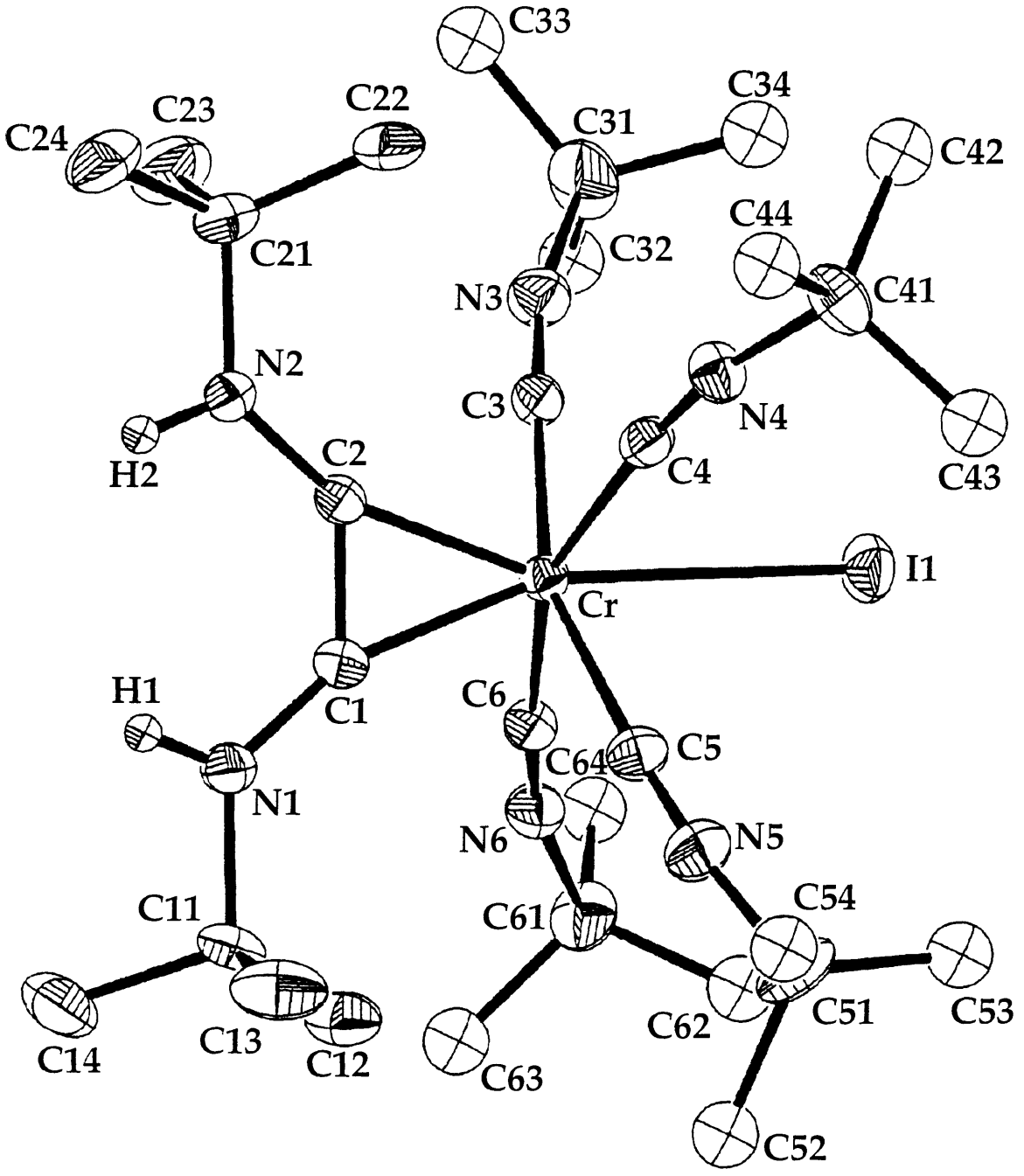

Figure 1.3. An ORTEP diagram of [Cr(*t*-$C_4H_9HNC{\equiv}CNH$-*t*-C_4H_9)(CN-*t*-$C_4H_9)_4I$]I (**2**), showing the atom labeling scheme and the 40% probability ellipsoids. The methyl carbons on C3-C6 are represented as 3 Å isotropic spheres for clarity.

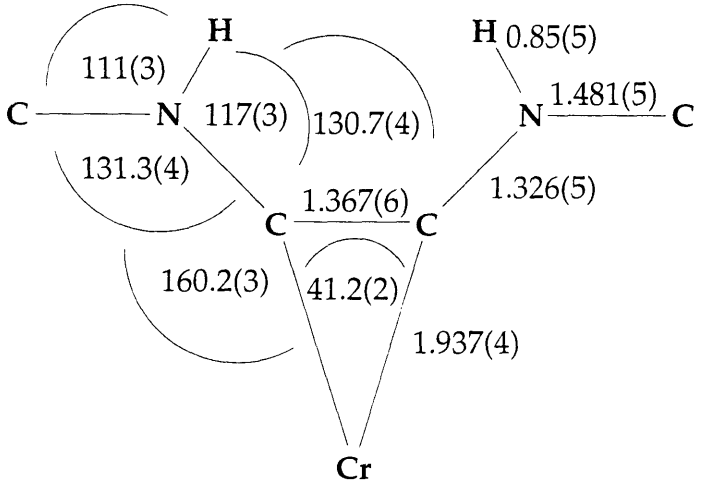

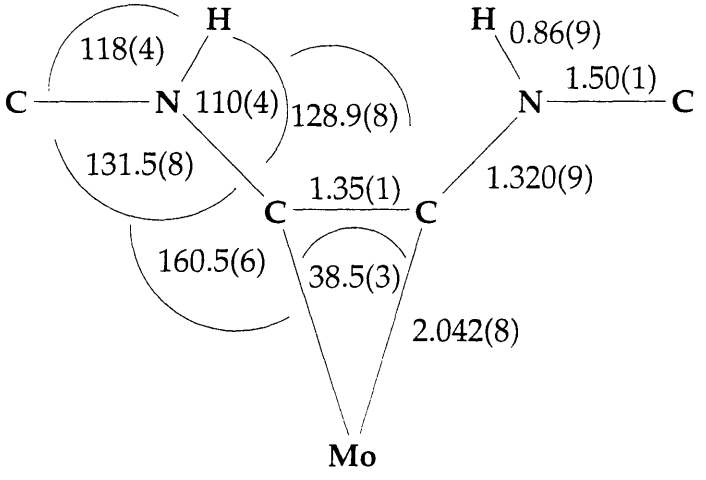

Figure 1.4. A comparison of the bond distances (Å) and angles (deg) about the cores of [Cr(*t*-$C_4H_9HNC{\equiv}CNH$-*t*-C_4H_9)(CN-*t*-C_4H_9)$_4$ I]I (**2**) and the corresponding molybdenum coupled product, [Mo(*t*-$C_4H_9HNC{\equiv}CNH$-*t*-C_4H_9)(CN-*t*-C_4H_9)$_4$I]I. Numbers in parentheses are estimated standard deviations in the last significant figure.

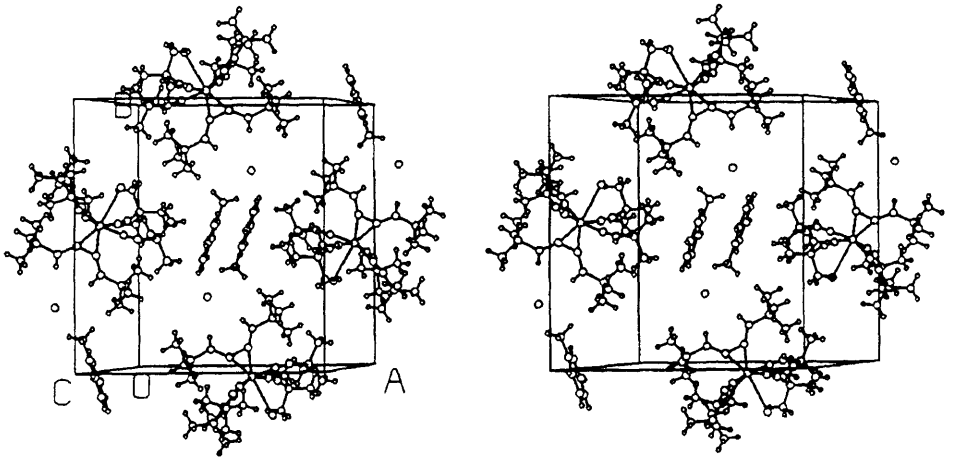

Figure 1.5. A packing diagram in stereo view of [Cr(*t*-$C_4H_9HNC{\equiv}CNH$-*t*-C_4H_9)(CN-*t*-C_4H_9)$_4$I]I (**2**). Hydrogen atoms and solvent molecules (toluene) are included.

As reported for [Mo(*t*-$C_4H_9HNC{\equiv}CNH$-*t*-C_4H_9)(CN-*t*-C_4H_9)$_4$I]I,[7] removal of the coupled ligand from **2** with the C-C bond intact could be accomplished oxidatively (eq. 5). Addition of excess H_2O_2 to [Cr(*t*-$C_4H_9HNC{\equiv}CNH$-*t*-C_4H_9)(CN-*t*-C_4H_9)$_4$I]I (**2**) in THF resulted in the formation of a product with a retention time and mass spectrum by GC-MS analysis identical to those of a genuine sample of (*N,N'*-di-*tert*-butyl)oxamide.[7] The 28% yield of oxamide achieved from this oxidation was comparable to those reported previously from oxidations of [Mo(*t*-$C_4H_9HNC{\equiv}CNH$-*t*-C_4H_9)(CN-*t*-C_4H_9)$_4$I]I.

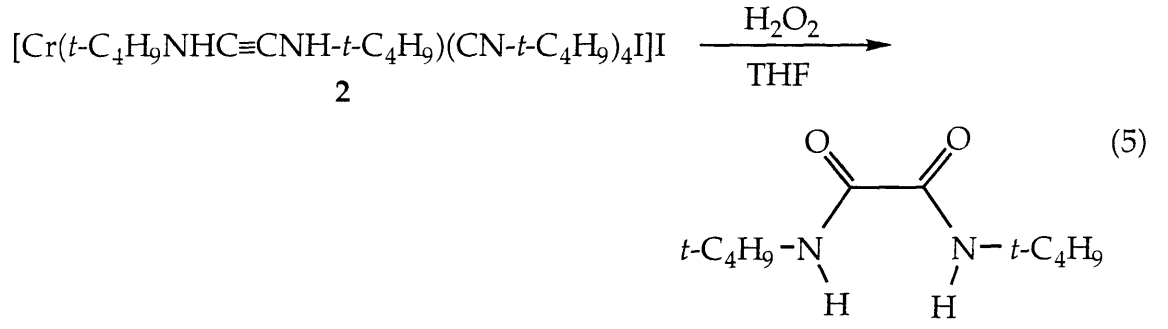

(5)

It is interesting to note that the complex [*cis*-$Cr(CO)_2(dmpe)_2$][22] did not undergo the reductive coupling reaction when exposed to electrophiles such as Me_3SiBr, Me_3SiOTf, and Et_3OBF_4, despite the reductive coupling of isoelectronic species such as Na[*cis*-$M(CO)_2(dmpe)_2$]$^-$ (M = V, Ta, Nb).[6,23-27] The relative resistance of [*cis*-$Cr(CO)_2(dmpe)_2$][22] to electrophiles was not surprising, however. A correlation between high electron density at the metal center and ease of reductive coupling has been established.[9] The electron density at the chromium center in [*cis*-$Cr(CO)_2(dmpe)_2$][22] is relatively low as evidenced by the carbonyl stretching frequencies in the IR spectrum (1824 and 1759 cm^{-1}). Moreover, the seemingly simple chemistry of the closely related complex [*cis*-$Cr(CO)_2(dpe)_2$] was recently de-convoluted[28] to reveal that solutions of the complex also contain [*trans*-$Cr(CO)_2(dpe)_2$] and [*trans*-$Cr(CO)_2(dpe)_2$]$^+$, both of

which are poor candidates for the reductive coupling reaction for geometrical as well as electronic reasons. The negative results obtained from reductive coupling attempts on [*cis*-$Cr(CO)_2(dpe)_2$] are thus consistent with our present understanding of the reductive coupling reaction.

Conclusions

A convenient synthesis of [$Cr(CN\text{-}t\text{-}C_4H_9)_6$] (**1**) has been reported. The structural characterization of this compound augments the small body of X-ray diffraction studies of homoleptic Cr(0) isocyanide compounds. The large bend angles of the CNR groups in this molecule indicate a highly electron dense metal center, as was seen earlier for [$Mo(CN\text{-}t\text{-}C_4H_9)_6$], and attest to its propensity to undergo reductive coupling. A linear relationship between M-CNR distances and MC-N-R bend angles was found. Reductive coupling of two isocyanide ligands of **1** upon addition of 2 equivalents of HI afforded [$Cr(t\text{-}C_4H_9HNC{\equiv}CNH\text{-}t\text{-}C_4H_9)(CN\text{-}t\text{-}C_4H_9)_4I]I$ (**2**). This reaction extends the reductive coupling reaction of isocyanide ligands to a first row transition metal. A crystal structure of **2** revealed its similarity to the analogous coupled product [$Mo(t\text{-}C_4H_9HNC{\equiv}CNH\text{-}t\text{-}C_4H_9)(CN\text{-}t\text{-}C_4H_9)_4I]I$. Oxidative removal of the coupled ligand from **2** as the corresponding di-*tert*butyl oxamide was also achieved.

References and Notes

(1) Most of this work has appeared previously in a slightly altered form in reference (2), © 1994 American Chemical Society.

(2) Acho, J. A.; Lippard, S. J. *Organometallics* **1994**, *13*, 1294.

(3) Lam, C. T.; Corfield, P. W. R.; Lippard, S. J. *J. Am. Chem. Soc.* **1977**, *99*, 617.

(4) Carnahan, E. M.; Protasiewicz, J. D.; Lippard, S. J. *Acc. Chem. Res.* **1993**, *26*, 90.

(5) Vrtis, R. N.; Lippard, S. J. *Israel J. Chem.* **1990**, *30*, 331.

(6) Protasiewicz, J. D.; Lippard, S. J. *J. Am. Chem. Soc.* **1991**, *113*, 6564.

(7) Giandomenico, C. M.; Lam, C. T.; Lippard, S. J. *J. Am. Chem. Soc.* **1982**, *104*, 1263.

(8) Carnahan, E. M.; Lippard, S. J. *J. Chem. Soc., Dalton Trans.* **1991**, 699.

(9) Caravana, C.; Giandomenico, C. M.; Lippard, S. J. *Inorg. Chem.* **1982**, *21*, 1860.

(10) Filippou, A. C.; Grünleitner, W.; Völkl, C.; Kiprof, P. *Angew. Chem. Int. Ed. Eng.* **1991**, *30*, 1167.

(11) Filippou, A. C.; Völkl, C.; Grünleitner, W.; Kiprof, P. J. *J. Organomet. Chem.* **1992**, *434*, 201.

(12) Fraústo da Silva, J. J. R.; Pellinghelli, M. A.; Pombeiro, A. J. L.; Richards, R. L.; Tiripicchio, A.; Wang, Y. *J. Organomet. Chem.* **1993**, *454*, C8.

(13) Timms, P. L.; Turney, T. W. *J. Chem. Soc., Dalton Trans.* **1976**, 2021.

(14) Chiu, K. W.; Howard, C. G.; Wilkinson, G.; Galas, A. M. R.; Hursthouse, M. B. *Polyhedron* **1982**, *1*, 803.

(15) Ljungström, E. *Acta Chem. Scand., Ser. A* **1978**, *A32(1)*, 47.

(16) Anderson, K. A.; Scott, B.; Wherland, S.; Willett, R. D. *Acta. Crystallogr., Sect. C: Cryst. Struct. Commun.* **1991**, *C47(11)*, 2337.

(17) Lentz, D. *J. Organomet. Chem.* **1990**, *381*, 205.

(18) Carnahan, E. M.; Rardin, R. L.; Bott, S. G.; Lippard, S. J. *Inorg. Chem.* **1992**, *31*, 5193.

(19) Corfield, P. W. R.; Baltusis, L. M.; Lippard, S. J. *Inorg. Chem.* **1981**, *20*, 922.

(20) Giandomenico, C. M.; Dewan, J. C.; Lippard, S. J. *J. Am. Chem. Soc.* **1981**, *103*, 1407.

(21) Wells, A. F. *Structural Inorganic Chemistry*; Oxford University Press: Oxford, 1984.

(22) Salt, J. E.; Girolami, G. S.; Wilkinson, G.; Motevalli, M.; Thornton-Pett, M.; Hursthouse, M. B. *J. Chem. Soc., Dalton Trans.* **1985**, 685.

(23) Bianconi, P. A.; Williams, I. D.; Engeler, M. P.; Lippard, S. J. *J. Am. Chem. Soc.* **1986**, *108*, 311.

(24) Bianconi, P. A.; Vrtis, R. N.; Rao, C. P.; Williams, I. D.; Engler, M. P.; Lippard, S. J. *Organometallics* **1987**, *6*, 1968.

(25) Vrtis, R. N.; Rao, C. P.; Warner, S.; Lippard, S. J. *J. Am. Chem. Soc.* **1988**, *110*, 2669.

(26) Vrtis, R. N.; Liu, S.; Rao, C. P.; Bott, S. G.; Lippard, S. J. *Organometallics* **1991**, *10*, 275.

(27) Protasiewicz, J.; Lippard, S. J. *J. Am. Chem. Soc.* **1991**, *113*, 6564.

(28) Bond, A. M.; Colton, R.; Cooper, J. B.; Traeger, J. C.; Walter, J. N.; Way, D. M. *Organometallics* **1994**, *13*, 3434.

Table 1.1. X-ray Crystallographic Information for [Cr(CN-*t*-C_4H_9)$_6$] (1) and [Cr(*t*-C_4H_9HNC≡CNH-*t*-C_4H_9)(CN-*t*-C_4H_9)$_4$I]I·toluene (2)[a]

	(1)	(2)
formula	$C_{30}H_{54}N_6Cr$	$C_{37}H_{64}N_6I_2Cr$
mol wt (g/mol)	550.8	898.8
a (Å)	17.688 (6)	15.927 (4)
b (Å)	11.912 (1)	17.397 (2)
c (Å)	19.221 (6)	17.351 (4)
β (deg)	116.65 (1)	111.363 (1)
V (Å^3)	3619 (2)	4477 (2)
T (°C)	-71.7	-71.7
Z	4	4
ρ_{calc}	1.011	1.333
space group	$P2_1$	$P2_1/n$
2*θ* limits (deg)	3-54	3-50
data limits	+h+k±l	+h+k±l
μ (cm^{-1})	3.303	16.42
total data	8280	8663
unique data[b]	4851	5523
no. of parameters	657	415
p factor	0.03	0.03
R[c] =	0.060	0.035
R_w =	0.070	0.042

[a] Data were collected on an Enraf Nonius CAD-4F kappa geometry diffractometer using Mo K_α radiation. [b] Observation criterion $I > 3\sigma(I)$. [c] $R = \Sigma||F_o|-|F_c||/\Sigma|F_o|$, $R_w = [\Sigma w(|F_o|-|F_c|)^2/\Sigma w|F_o|^2]^{1/2}$, where $w = 1/\sigma(F)$, as defined in Carnahan, E. M.; Rardin, R. L.; Bott, S. G.; Lippard, S. J. *Inorg. Chem.* **1992**, *31*, 5193.

Table 1.2. Final Positional Parameters for [Cr(CN-*t*-C_4H_9)$_6$] (1)[a]

atom	*x*	*y*	*z*	B_{eq} Å^{2} [b]
Cr(1)	0.78923 (8)	0.1764	0.51317 (8)	2.69 (3)
Cr(2)	0.79466 (8)	0.4081 (1)	0.00710 (7)	2.64 (3)
N(11)	0.8169 (5)	0.3278 (8)	0.6571 (5)	5.2 (2)
N(12)	0.7085 (6)	0.3737 (8)	0.3989 (6)	6.2 (3)
N(13)	0.7360 (5)	0.0208 (7)	0.3711 (5)	4.2 (2)
N(14)	0.8554 (6)	-0.0292 (7)	0.6207 (5)	5.0 (2)
N(15)	0.6137 (5)	0.1354 (8)	0.5041 (6)	6.1 (2)
N(16)	0.9587 (4)	0.2689 (6)	0.5212 (4)	4.3 (2)
N(21)	0.7262 (5)	0.2195 (7)	-0.1143 (5)	3.8 (2)
N(22)	0.7078 (6)	0.5819 (8)	-0.1233 (5)	5.5 (2)
N(23)	0.8550 (6)	0.5916 (8)	0.1392 (5)	4.5 (2)
N(24)	0.8558 (5)	0.2335 (7)	0.1401 (5)	4.9 (2)
N(25)	0.9607 (5)	0.4786 (6)	-0.0024 (4)	4.2 (2)
N(26)	0.6245 (5)	0.3910 (8)	0.0126 (5)	5.8(2)
C(11)	0.8090 (5)	0.2695 (8)	0.6030 (5)	3.6 (2)
C(12)	0.7397 (6)	0.3025 (8)	0.4442 (6)	3.8 (2)
C(13)	0.7595 (6)	0.0831 (8)	0.4266 (6)	3.5 (2)
C(14)	0.8332 (6)	0.0509 (9)	0.5806 (6)	3.7 (2)
C(15)	0.6812 (5)	0.1507 (8)	0.5074 (5)	3.5 (2)
C(16)	0.8961 (5)	0.2321 (7)	0.5188 (5)	3.3 (2)
C(21)	0.7551 (5)	0.2930 (7)	-0.0685 (5)	2.8 (2)
C(22)	0.7428 (6)	0.5172 (8)	-0.0715 (6)	3.4 (2)
C(23)	0.8314 (6)	0.5251 (8)	0.0899 (6)	3.4 (2)
C(24)	0.8366 (5)	0.2983 (8)	0.0891 (6)	3.2 (2)

Table 1.2 (cont). Final Positional Parameters for [Cr(CN-*t*-C_4H_9)$_6$] (1)

atom	*x*	*y*	*z*	B_{eq} Å$^{2\,b}$
C(25)	0.9010 (5)	0.4452 (7)	0.0015 (5)	3.4 (2)
C(26)	0.6891 (5)	0.3998 (8)	0.0105 (5)	3.2 (2)
C(111)	0.8085 (7)	0.404 (1)	0.7109 (6)	5.4 (3)
C(112)	0.8431 (9)	0.352 (1)	0.7900 (7)	8.4 (4)
C(113)	0.871 (1)	0.502 (1)	0.719 (1)	12.6 (6)
C(114)	0.7220 (9)	0.435 (2)	0.688 (1)	16.4 (7)
C(121)	0.6781 (7)	0.480 (1)	0.3689 (7)	5.8 (3)
C(122)	0.698 (2)	0.550 (2)	0.442 (2)	23 (1)
C(123)	0.729 (1)	0.526 (1)	0.332 (1)	13.4 (7)
C(124)	0.593 (1)	0.483 (3)	0.323 (2)	28 (1)
C(131)	0.6598 (6)	-0.0449 (8)	0.3250 (5)	4.1 (2)
C(132)	0.5899 (7)	0.041 (1)	0.2784 (7)	6.8 (3)
C(133)	0.6363 (7)	-0.112 (1)	0.3803 (6)	6.6 (3)
C(134)	0.6768 (7)	-0.121 (1)	0.2717 (6)	5.4 (3)
C(141)	0.8337 (9)	-0.103 (1)	0.6692 (8)	6.7 (4)
C(142)	0.771 (1)	-0.193 (2)	0.617 (1)	14.6 (7)
C(143)	0.781 (2)	-0.037 (1)	0.699 (1)	16.6 (9)
C(144)	0.912 (1)	-0.155 (2)	0.730 (1)	14.5 (7)
C(151)	0.5304 (6)	0.169 (1)	0.4872 (6)	4.9 (3)
C(152)	0.4668 (8)	0.092 (2)	0.443 (1)	12.4 (6)
C(153)	0.528 (1)	0.199 (2)	0.562 (1)	13.7 (7)
C(154)	0.513 (1)	0.272 (2)	0.439 (1)	14.8 (8)
C(161)	1.0193 (5)	0.3428 (9)	0.5145 (5)	3.7 (2)
C(162)	1.0961 (7)	0.282 (1)	0.5246 (8)	8.4 (4)

Table 1.2 (cont). Final Positional Parameters for [Cr(CN-*t*-C_4H_9)$_6$] (1)

atom	*x*	*y*	*z*	B_{eq} Å^2 [b]
C(163)	0.9818 (9)	0.407 (2)	0.442 (1)	11.9 (6)
C(164)	1.047 (1)	0.424 (1)	0.5836 (9)	10.4 (5)
C(211)	0.6443 (5)	0.1660 (8)	-0.1612 (5)	4.0 (2)
C(212)	0.5820 (7)	0.255 (1)	-0.2051 (7)	7.9 (4)
C(213)	0.6205 (9)	0.105 (1)	-0.1065 (8)	8.3 (4)
C(214)	0.6545 (7)	0.086 (1)	-0.2168 (6)	6.2 (3)
C(221)	0.6889 (6)	0.7039 (8)	-0.1351 (6)	4.7 (2)
C(222)	0.728 (1)	0.747 (2)	-0.186 (1)	5.8 (5)
C(223)	0.723 (1)	0.763 (2)	-0.054 (1)	5.2 (4)
C(224)	0.590 (1)	0.721 (2)	-0.183 (1)	5.5 (5)
C(231)	0.8832 (6)	0.666 (1)	0.2038 (6)	4.6 (2)
C(232)	0.954 (1)	0.727 (2)	0.213 (1)	21 (1)
C(233)	0.811 (1)	0.737 (2)	0.195 (1)	17.6 (8)
C(234)	0.907 (1)	0.594 (2)	0.2752 (9)	13.0 (6)
C(241)	0.8276 (7)	0.173 (1)	0.1921 (7)	5.7 (3)
C(242)	0.895 (1)	0.096 (2)	0.242 (1)	12.8 (6)
C(243)	0.747 (1)	0.110 (2)	0.1373 (9)	13.3 (6)
C(244)	0.801 (1)	0.258 (1)	0.234 (1)	10.7 (6)
C(251)	1.0279 (5)	0.5507 (9)	-0.0001 (6)	4.5 (2)
C(252)	0.993 (1)	0.659 (2)	-0.033 (1)	6.1 (5)
C(253)	1.071 (1)	0.489 (2)	-0.044 (1)	3.4 (3)
C(254)	1.095 (1)	0.545 (2)	0.092 (1)	4.8 (4)
C(261)	0.5556 (7)	0.440 (1)	0.0234 (7)	5.5 (3)
C(262)	0.516 (2)	0.361 (2)	0.055 (1)	5.5 (5)

Table 1.2 (cont). Final Positional Parameters for [Cr(CN-*t*-C_4H_9)$_6$] (1)

atom	*x*	*y*	*z*	B_{eq} Å$^{2\,b}$
C(263)	0.598 (1)	0.545 (2)	0.082 (1)	4.4 (4)
C(264)	0.487 (2)	0.498 (3)	-0.060 (2)	7.4 (7)
C(222B)	0.771 (2)	0.760 (3)	-0.126 (2)	9.7 (8)
C(223B)	0.613 (3)	0.725 (4)	-0.126 (2)	12 (1)
C(224B)	0.640 (2)	0.722 (3)	-0.232 (2)	9.5 (8)
C(252B)	0.986 (2)	0.622 (3)	-0.084 (2)	8.4 (7)
C(253B)	1.109 (2)	0.488 (3)	0.008 (2)	9.4 (8)
C(254B)	1.051 (2)	0.638 (2)	0.065 (1)	7.7 (6)
C(262B)	0.559 (2)	0.366 (2)	0.099 (1)	7.1 (6)
C(263B)	0.539 (3)	0.553 (4)	0.016 (3)	15 (1)
C(264B)	0.474 (2)	0.401 (3)	-0.048 (2)	10.4 (8)

[a]Numbers in parentheses are errors in the last significant figure. See Fig. 1.1 for atom labeling scheme. [b]$B_{eq} = 4/3\,[a^2\beta_{11} + b^2\beta_{22} + c^2\beta_{33} + 2ab\cos(\gamma)\beta_{12} + 2ac\cos(\beta)\beta_{13} + 2bc\cos(\alpha)\beta_{23}]$

Table 1.3. Anisotropic Thermal Parameters for [Cr(CN-*t*-C_4H_9)$_6$] (1)[a]

atom	U_{11}	U_{22}	U_{33}	U_{12}	U_{13}	U_{23}
Cr(1)	0.0306 (7)	0.0226 (8)	0.0485 (8)	-0.0000 (7)	0.0172 (7)	0.0042 (7)
Cr(2)	0.0426 (9)	0.0202 (8)	0.0471 (8)	-0.0016 (7)	0.0288 (8)	-0.0014 (7)
N(11)	0.066 (6)	0.074 (7)	0.053 (5)	-0.003 (5)	0.024 (5)	-0.010 (5)
N(12)	0.091 (7)	0.053 (7)	0.087 (7)	0.028 (5)	0.036 (6)	0.042 (6)
N(13)	0.064 (5)	0.039 (5)	0.065 (5)	-0.001 (4)	0.034 (5)	-0.007 (4)
N(14)	0.088 (6)	0.042 (5)	0.081 (6)	0.025 (5)	0.055 (6)	0.027 (5)
N(15)	0.052 (5)	0.058 (6)	0.132 (8)	-0.012 (5)	0.049 (6)	-0.009 (6)
N(16)	0.052 (4)	0.040 (5)	0.081 (6)	-0.014 (4)	0.038 (4)	-0.004 (4)
N(21)	0.056 (5)	0.033 (5)	0.061 (5)	-0.000 (4)	0.031 (4)	-0.008 (4)
N(22)	0.102 (8)	0.035 (5)	0.072 (7)	0.008 (5)	0.038 (6)	0.008 (5)
N(23)	0.068 (6)	0.055 (6)	0.054 (6)	-0.010 (5)	0.032 (5)	-0.021 (5)
N(24)	0.065 (5)	0.050 (6)	0.073 (6)	0.008 (5)	0.031 (5)	0.025 (5)
N(25)	0.050 (5)	0.043 (5)	0.073 (5)	-0.010 (4)	0.034 (4)	-0.011 (4)
N(26)	0.064 (5)	0.064 (7)	0.112 (7)	-0.004 (5)	0.059 (5)	-0.006 (6)
C(11)	0.054 (6)	0.038 (5)	0.045 (5)	-0.007 (5)	0.021 (5)	0.010 (4)
C(12)	0.054 (6)	0.036 (6)	0.048 (6)	-0.000 (5)	0.018 (5)	0.008 (5)
C(13)	0.042 (5)	0.034 (6)	0.056 (6)	0.002 (5)	0.022 (5)	0.006 (5)
C(14)	0.055 (6)	0.039 (6)	0.056 (6)	0.009 (5)	0.033 (5)	0.011 (5)
C(15)	0.044 (5)	0.024 (5)	0.059 (6)	-0.005 (4)	0.018 (5)	0.005 (4)
C(16)	0.042 (5)	0.028 (5)	0.050 (5)	-0.001 (4)	0.017 (4)	-0.006 (4)
C(21)	0.041 (5)	0.029 (5)	0.044 (5)	0.003 (4)	0.028 (4)	0.005 (4)
C(22)	0.055 (6)	0.032 (6)	0.038 (5)	-0.002 (5)	0.016 (5)	-0.002 (5)
C(23)	0.054 (6)	0.034 (6)	0.054 (6)	0.000 (5)	0.035 (5)	0.004 (5)
C(24)	0.038 (5)	0.029 (5)	0.052 (6)	0.002 (4)	0.017 (5)	-0.001 (4)
C(25)	0.050 (5)	0.029 (5)	0.055 (6)	-0.003 (4)	0.030 (5)	-0.010 (4)

Table 1.3 (cont). Anisotropic Thermal Parameters for [Cr(CN-*t*-C_4H_9)$_6$] (1)

atom	U_{11}	U_{22}	U_{33}	U_{12}	U_{13}	U_{23}
C(26)	0.049 (5)	0.024 (5)	0.059 (5)	0.003 (4)	0.034 (4)	0.001 (4)
C(111)	0.081 (7)	0.051 (7)	0.061 (6)	0.010 (7)	0.021 (6)	-0.012 (6)
C(112)	0.15 (1)	0.10 (1)	0.074 (8)	0.01 (1)	0.053 (9)	-0.006 (8)
C(113)	0.27 (2)	0.06 (1)	0.13 (1)	-0.08 (1)	0.08 (2)	-0.01 (1)
C(114)	0.09 (1)	0.28 (3)	0.17 (2)	0.10 (1)	-0.01 (1)	-0.13 (2)
C(121)	0.075 (8)	0.063 (8)	0.094 (9)	0.027 (6)	0.048 (7)	0.041 (7)
C(122)	0.62 (5)	0.07 (1)	0.26 (3)	0.00 (2)	0.27 (3)	-0.05 (2)
C(123)	0.23 (2)	0.12 (1)	0.26 (2)	0.05 (1)	0.20 (2)	0.10 (2)
C(124)	0.05 (1)	0.52 (5)	0.39 (3)	0.02 (2)	0.00 (1)	0.37 (4)
C(131)	0.047 (5)	0.047 (6)	0.061 (6)	-0.012 (5)	0.024 (5)	-0.010 (5)
C(132)	0.063 (7)	0.074 (9)	0.092 (9)	0.012 (6)	0.010 (6)	-0.000 (7)
C(133)	0.089 (8)	0.09 (1)	0.085 (8)	-0.048 (8)	0.047 (7)	-0.030 (7)
C(134)	0.089 (8)	0.056 (7)	0.065 (6)	-0.019 (6)	0.037 (6)	-0.025 (5)
C(141)	0.13 (1)	0.053 (8)	0.11 (1)	0.028 (8)	0.09 (1)	0.041 (8)
C(142)	0.25 (2)	0.12 (2)	0.17 (2)	-0.08 (2)	0.07 (2)	0.05 (1)
C(143)	0.42 (3)	0.10 (1)	0.28 (2)	0.04 (2)	0.32 (3)	0.05 (2)
C(144)	0.16 (2)	0.16 (2)	0.24 (2)	0.06 (1)	0.10 (2)	0.16 (2)
C(151)	0.044 (5)	0.067 (8)	0.078 (7)	-0.011 (6)	0.031 (5)	-0.004 (7)
C(152)	0.057 (8)	0.18 (2)	0.23 (2)	-0.04 (1)	0.06 (1)	-0.11 (2)
C(153)	0.13 (1)	0.29 (3)	0.13 (1)	-0.03 (2)	0.08 (1)	-0.07 (2)
C(154)	0.12 (1)	0.20 (2)	0.24 (2)	0.06 (2)	0.08 (1)	0.10 (2)
C(161)	0.034 (4)	0.067 (6)	0.036 (5)	-0.014 (4)	0.012 (4)	0.001 (5)
C(162)	0.084 (8)	0.08 (1)	0.17 (1)	-0.008 (8)	0.08 (1)	0.01 (1)
C(163)	0.10 (1)	0.20 (2)	0.16 (1)	-0.00 (1)	0.06 (1)	0.09 (2)
C(164)	0.16 (1)	0.12 (1)	0.15 (1)	-0.10 (1)	0.09 (1)	-0.06 (1)

Table 1.3 (cont). Anisotropic Thermal Parameters for [Cr(CN-*t*-C_4H_9)$_6$] (1)

atom	U_{11}	U_{22}	U_{33}	U_{12}	U_{13}	U_{23}
C(211)	0.040 (4)	0.044 (6)	0.067 (6)	-0.001 (5)	0.023 (4)	-0.014 (5)
C(212)	0.064 (7)	0.10 (1)	0.10 (1)	0.027 (7)	-0.001 (7)	-0.013 (8)
C(213)	0.13 (1)	0.08 (1)	0.15 (1)	-0.053 (9)	0.10 (1)	-0.024 (9)
C(214)	0.082 (8)	0.066 (8)	0.067 (7)	0.001 (7)	0.017 (6)	-0.031 (6)
C(221)	0.061 (6)	0.026 (5)	0.095 (8)	0.001 (4)	0.037 (6)	0.023 (5)
C(231)	0.077 (7)	0.048 (6)	0.068 (6)	-0.016 (6)	0.046 (6)	-0.031 (6)
C(232)	0.26 (2)	0.34 (3)	0.30 (2)	-0.25 (2)	0.24 (2)	-0.27 (2)
C(233)	0.13 (1)	0.24 (2)	0.20 (2)	0.06 (2)	-0.01 (1)	-0.16 (2)
C(234)	0.26 (2)	0.14 (2)	0.09 (1)	-0.03 (2)	0.07 (1)	0.00 (1)
C(241)	0.065 (6)	0.061 (8)	0.084 (8)	-0.014 (7)	0.028 (6)	0.025 (7)
C(242)	0.13 (1)	0.19 (2)	0.17 (2)	0.05 (1)	0.07 (1)	0.14 (1)
C(243)	0.18 (2)	0.18 (2)	0.12 (1)	-0.13 (1)	0.05 (1)	0.02 (1)
C(244)	0.21 (2)	0.11 (1)	0.13 (1)	0.00 (1)	0.12 (1)	-0.00 (1)
C(251)	0.045 (5)	0.059 (6)	0.081 (7)	-0.023 (5)	0.041 (5)	-0.029 (6)
C(261)	0.060 (6)	0.075 (9)	0.101 (8)	0.004 (6)	0.061 (7)	0.001 (7)

[a] Numbers in parentheses are estimated standard deviations in the last significant digit. The anisotropic temperature factors are of the form $\exp[-2\pi^2(U_{11}h^2a^{*2} \ldots +2U_{12}hka^*b^* = \ldots)]$.

Table 1.4. Selected Interatomic Bond Distances (Å) and Angles (deg) for [Cr(CN-*t*-C_4H_9)$_6$] (1)[a]

		Bond Distances	
Cr1-C11	1.95 (1)	Cr2-C21	1.89 (1)
Cr1-C12	1.93 (1)	Cr2-C22	1.89 (1)
Cr1-C13	1.87 (1)	Cr2-C23	1.99 (1)
Cr1-C14	1.90 (1)	Cr2-C24	1.92 (1)
Cr1-C15	1.889 (9)	Cr2-C25	1.980 (8)
Cr1-C16	1.961 (8)	Cr2-C26	1.900 (7)
mean C-N	1.18 (2)[b]	range C-N	1.16 (1)-1.21 (1)
mean N-C(Bu^t)	1.45 (3)[b]	range N-C(Bu^t)	1.40 (1)-1.49 (1)
mean C-C(Me)	1.52 (7)[b]	range C-C(Me)	1.36 (2)-1.67 (3)
		Bond Angles	
mean *cis* C-Cr-C	90 (4)[b]	range *cis* C-Cr-C	84.5 (4)-99.8 (4)
mean *trans* C-Cr-C	173 (3)[b]	range *trans* C-Cr-C	169.5 (4)-177.5 (4)
mean Cr-C-N	176 (2)[b]	range Cr-C-N	172.9 (8)-179.6 (8)
C11-N11-C111	168 (1)	C21-N21-C211	139.2 (8)
C12-N12-C121	160 (1)	C22-N22-C221	139 (1)
C13-N13-C131	136.1 (9)	C23-N23-C231	175 (1)
C14-N14-C141	144 (1)	C24-N24-C241	145 (1)
C15-N15-C151	153 (1)	C25-N25-C251	163.0 (9)
C16-N16-C161	162.7 (9)	C26-N26-C261	151 (1)

[a]See footnote a, Table 1.2. [b]Numbers in parentheses are the standard deviations of the mean.

Table 1.5. Final Positional Parameters and B(eq) for [Cr(*t*-$C_4H_9HNC{\equiv}CNH$-*t*-C_4H_9)(CN-*t*-C_4H_9)$_4$I]I (2)[a]

atom	*x*	*y*	*z*	B_{eq} Å^{2} [b]
I(1)	0.13384 (2)	0.67698 (2)	0.80548 (2)	2.92 (1)
I(2)	0.17263 (3)	0.76435 (2)	0.34591 (3)	5.09 (2)
Cr(1)	0.03686 (4)	0.53465 (4)	0.76495 (4)	1.73 (2)
N(1)	-0.1436 (2)	0.4336 (2)	0.7231 (2)	2.3 (2)
N(2)	0.0294 (3)	0.3553 (2)	0.7193 (2)	2.3 (1)
N(3)	0.2243 (2)	0.4845 (2)	0.8939 (2)	2.8 (2)
N(4)	0.1108 (2)	0.5537 (2)	0.6220 (2)	2.4 (1)
N(5)	-0.1062 (3)	0.6486 (2)	0.6498 (2)	3.0 (2)
N(6)	-0.0074 (2)	0.5930 (2)	0.9169 (2)	2.5 (1)
C(1)	-0.0621 (3)	0.4616 (2)	0.7380 (2)	1.9 (2)
C(2)	0.0147 (3)	0.4267 (2)	0.7380 (2)	1.8 (2)
C(3)	0.1547 (3)	0.5009 (2)	0.8453 (3)	2.0 (2)
C(4)	0.0854 (3)	0.5425 (2)	0.6751 (3)	2.1 (2)
C(5)	-0.0553 (3)	0.6059 (2)	0.6937 (3)	2.3 (2)
C(6)	0.0072 (3)	0.5681 (2)	0.8617 (3)	2.2 (2)
C(11)	-0.2294 (3)	0.4718 (3)	0.7172 (3)	2.7 (2)
C(12)	-0.2130 (3)	0.5406 (3)	0.7730 (3)	3.3 (2)
C(13)	-0.2784 (3)	0.4936 (4)	0.6271 (3)	4.3 (2)
C(14)	-0.2846 (3)	0.4119 (3)	0.7425 (4)	4.2 (2)
C(21)	0.1145 (3)	0.3169 (3)	0.7253 (3)	2.8 (2)
C(22)	0.1737 (3)	0.3698 (3)	0.6981 (3)	3.5 (2)
C(23)	0.1633 (4)	0.2906 (3)	0.8141 (4)	4.4 (2)
C(24)	0.0878 (4)	0.2469 (3)	0.6683 (4)	4.2 (2)

Table 1.5 (cont). Final Positional Parameters and B(eq) for [Cr(*t*-$C_4H_9HNC{\equiv}CNH$-*t*-C_4H_9)(CN-*t*-C_4H_9)$_4$I]I (2)

atom	*x*	*y*	*z*	B_{eq} Å$^{2\,b}$
C(31)	0.3163 (3)	0.4844 (3)	0.9541 (4)	4.5 (2)
C(32)	0.3122 (5)	0.5033 (6)	1.0372 (5)	9.0 (4)
C(33)	0.3561 (4)	0.4056 (4)	0.9562 (6)	8.8 (4)
C(34)	0.3664 (4)	0.5470 (4)	0.9292 (5)	7.8 (4)
C(41)	0.1469 (3)	0.5861 (3)	0.5623 (3)	3.2 (2)
C(42)	0.2474 (4)	0.5847 (4)	0.6021 (4)	5.8 (3)
C(43)	0.1138 (5)	0.6693 (4)	0.5482 (4)	6.0 (3)
C(44)	0.1116 (5)	0.5406 (5)	0.4842 (4)	6.8 (4)
C(51)	-0.1600 (4)	0.7125 (3)	0.6041 (4)	4.1 (2)
C(52)	-0.2421 (7)	0.7189 (5)	0.6298 (7)	11.6 (6)
C(53)	-0.1045 (7)	0.7822 (4)	0.6282 (7)	13.2 (6)
C(54)	-0.1912 (7)	0.6948 (5)	0.5165 (5)	10.1 (5)
C(61)	-0.0172 (4)	0.6420 (3)	0.9811 (3)	3.2 (2)
C(62)	-0.0295 (6)	0.7228 (3)	0.9488 (5)	6.8 (4)
C(63)	-0.0973 (4)	0.6146 (4)	1.0004 (4)	4.8 (3)
C(64)	0.0680 (4)	0.6307 (4)	1.0571 (4)	5.9 (3)
C(100)	-0.0037 (6)	0.1208 (5)	0.8787 (6)	10.0 (5)
C(101)	0.0177 (4)	0.0462 (4)	0.8504 (4)	5.1 (3)
C(102)	0.0058 (4)	0.0356 (4)	0.7686 (4)	4.9 (3)
C(103)	0.0278 (5)	-0.0336 (6)	0.7426 (5)	7.2 (4)
C(104)	0.0591 (6)	-0.0916 (5)	0.7969 (9)	9.5 (5)
C(105)	0.0709 (6)	-0.0847 (7)	0.8762 (8)	10.4 (6)
C(106)	0.0501 (5)	-0.0140 (6)	0.9039 (5)	7.0 (4)

Table 1.5 (cont). Final Positional Parameters and B(eq) for [Cr(*t*-$C_4H_9HNC{\equiv}CNH$-*t*-C_4H_9)(CN-*t*-$C_4H_9)_4I$]I (2)

atom	*x*	*y*	*z*	B_{eq} Å$^{2\,b}$
H(1)	-0.152 (3)	0.388 (2)	0.710 (2)	1.2 (9)
H(2)	-0.014 (3)	0.324 (3)	0.707 (3)	3 (1)

[a]Numbers in parentheses are estimated standard deviations of the last significant figure. See Fig. 1.3 for atom labeling scheme. [b]$B_{eq} = 4/3\ [a^2\beta_{11} + b^2\beta_{22} + c^2\beta_{33} + 2ab\cos(\gamma)\beta_{12} + 2ac\cos(\beta)\beta_{13} + 2bc\cos(\alpha)\beta_{23}]$

Table 1.6. Anisotropic Thermal Parameters for [Cr(*t*-$C_4H_9HNC{\equiv}CNH$-*t*-C_4H_9)(CN-*t*-C_4H_9)$_4$I]I (2)[a]

atom	U_{11}	U_{22}	U_{33}	U_{12}	U_{13}	U_{23}
I(1)	0.0412 (2)	0.0283 (2)	0.0417 (2)	-0.0090 (1)	0.0153 (1)	-0.0058 (1)
I(2)	0.0586 (3)	0.0414 (2)	0.1019 (4)	-0.0201 (2)	0.0395 (2)	-0.0191 (2)
Cr(1)	0.0213 (4)	0.0220 (3)	0.0219 (4)	0.0006 (3)	0.0075 (3)	-0.0011 (3)
N(1)	0.025 (2)	0.027 (2)	0.037 (2)	0.000 (2)	0.012 (2)	-0.005 (2)
N(2)	0.025 (2)	0.023 (2)	0.040 (2)	0.001 (2)	0.013 (2)	-0.003 (2)
N(3)	0.028 (2)	0.037 (2)	0.036 (2)	0.001 (2)	0.007 (2)	-0.000 (2)
N(4)	0.035 (2)	0.034 (2)	0.027 (2)	-0.005 (2)	0.016 (2)	-0.004 (2)
N(5)	0.038 (2)	0.035 (2)	0.037 (2)	0.008 (2)	0.011 (2)	0.005 (2)
N(6)	0.032 (2)	0.032 (2)	0.035 (2)	0.000 (2)	0.016 (2)	-0.002 (2)
C(1)	0.023 (2)	0.029 (2)	0.020 (2)	0.001 (2)	0.008 (2)	-0.002 (2)
C(2)	0.023 (2)	0.027 (2)	0.020 (2)	-0.001 (2)	0.010 (2)	0.000 (2)
C(3)	0.027 (2)	0.026 (2)	0.027 (2)	-0.000 (2)	0.013 (2)	0.001 (2)
C(4)	0.025 (2)	0.024 (2)	0.030 (3)	0.002 (2)	0.007 (2)	-0.003 (2)
C(5)	0.032 (3)	0.031 (2)	0.026 (2)	0.003 (2)	0.012 (2)	-0.003 (2)
C(6)	0.023 (2)	0.027 (2)	0.030 (3)	-0.000 (2)	0.009 (2)	-0.000 (2)
C(11)	0.019 (2)	0.046 (3)	0.038 (3)	0.004 (2)	0.013 (2)	0.000 (2)
C(12)	0.036 (3)	0.049 (3)	0.046 (3)	0.007 (2)	0.019 (2)	-0.007 (2)
C(13)	0.036 (3)	0.078 (4)	0.043 (3)	0.015 (3)	0.008 (2)	-0.006 (3)
C(14)	0.036 (3)	0.065 (4)	0.066 (4)	-0.007 (3)	0.028 (3)	-0.005 (3)
C(21)	0.031 (3)	0.032 (3)	0.044 (3)	0.010 (2)	0.015 (2)	0.000 (2)
C(22)	0.042 (3)	0.040 (3)	0.063 (4)	0.013 (2)	0.033 (3)	0.001 (3)
C(23)	0.056 (4)	0.052 (3)	0.061 (4)	0.021 (3)	0.024 (3)	0.020 (3)
C(24)	0.053 (3)	0.034 (3)	0.077 (4)	0.009 (3)	0.027 (3)	-0.012 (3)
C(31)	0.027 (3)	0.058 (4)	0.065 (4)	-0.007 (3)	-0.007 (3)	0.013 (3)

Table 1.6 (cont). Anisotropic Thermal Parameters for [Cr(*t*-$C_4H_9HNC{\equiv}CNH$-*t*-C_4H_9)(CN-*t*-C_4H_9)$_4$I]I (2)

atom	U_{11}	U_{22}	U_{33}	U_{12}	U_{13}	U_{23}
C(32)	0.091 (6)	0.159 (8)	0.054 (5)	-0.041 (6)	-0.019 (4)	0.001 (5)
C(33)	0.039 (4)	0.086 (5)	0.168 (9)	0.012 (4)	-0.011 (5)	0.038 (5)
C(34)	0.034 (3)	0.095 (6)	0.142 (7)	-0.015 (4)	0.003 (4)	0.047 (5)
C(41)	0.038 (3)	0.054 (3)	0.034 (3)	-0.010 (2)	0.019 (2)	0.002 (2)
C(42)	0.044 (4)	0.096 (5)	0.089 (5)	-0.009 (4)	0.034 (4)	0.003 (4)
C(43)	0.094 (5)	0.072 (4)	0.069 (4)	0.007 (4)	0.040 (4)	0.037 (4)
C(44)	0.100 (5)	0.134 (6)	0.038 (3)	-0.058 (5)	0.043 (4)	-0.029 (4)
C(51)	0.056 (4)	0.036 (3)	0.055 (4)	0.026 (3)	0.012 (3)	0.014 (3)
C(52)	0.133 (8)	0.119 (7)	0.23 (1)	0.092 (7)	0.112 (9)	0.081 (8)
C(53)	0.146 (9)	0.042 (4)	0.22 (1)	-0.005 (5)	-0.042 (8)	0.047 (6)
C(54)	0.18 (1)	0.109 (7)	0.051 (5)	0.068 (7)	-0.005 (5)	0.034 (5)
C(61)	0.056 (3)	0.036 (3)	0.034 (3)	-0.002 (2)	0.023 (3)	-0.012 (2)
C(62)	0.160 (8)	0.037 (3)	0.098 (6)	0.003 (4)	0.088 (6)	-0.009 (3)
C(63)	0.076 (4)	0.069 (4)	0.053 (4)	0.007 (3)	0.044 (3)	-0.005 (3)
C(64)	0.073 (4)	0.100 (5)	0.044 (4)	-0.017 (4)	0.011 (3)	-0.030 (4)
C(100)	0.099 (6)	0.118 (7)	0.20 (1)	-0.056 (6)	0.100 (7)	-0.092 (7)
C(101)	0.047 (4)	0.068 (4)	0.079 (5)	-0.024 (3)	0.024 (3)	-0.014 (4)
C(102)	0.046 (4)	0.075 (5)	0.058 (4)	-0.007 (3)	0.010 (3)	0.008 (3)
C(103)	0.064 (5)	0.116 (7)	0.088 (6)	-0.011 (5)	0.021 (4)	-0.033 (5)
C(104)	0.050 (5)	0.053 (5)	0.23 (1)	0.008 (4)	0.013 (7)	-0.012 (7)
C(105)	0.065 (6)	0.105 (8)	0.18 (1)	-0.022 (6)	-0.012 (7)	0.077 (9)
C(106)	0.060 (5)	0.127 (7)	0.070 (5)	-0.033 (5)	0.013 (4)	0.026 (5)

Table 1.6 (cont). Anisotropic Thermal Parameters for [Cr(*t*-$C_4H_9HNC{\equiv}CNH$-*t*-C_4H_9)(CN-*t*-C_4H_9)$_4$I]I (2)

---

[a] Numbers in parentheses are estimated standard deviations in the last significant digit. The anisotropic temperature factors are of the form $\exp[-2\pi^2(U_{11}h^2a^{*2} \ldots +2U_{12}hka^*b^* = \ldots)]$.

Table 1.7. Selected Interatomic Distances (Å) for [Cr(*t*-$C_4H_9HNC{\equiv}CNH$-*t*-C_4H_9)(CN-*t*-C_4H_9)$_4$I]I (2)[a]

Cr-I1	2.8670 (8)	N1-C11	1.488 (5)
Cr-C1	1.944 (4)	N2-C21	1.481 (5)
Cr-C2	1.937 (4)	C3-N3	1.159 (5)
Cr-C3	1.976 (4)	C4-N4	1.149 (5)
Cr-C4	1.982 (5)	C5-N5	1.157 (5)
Cr-C5	1.974 (4)	C6-N6	1.149 (5)
Cr-C6	1.989 (5)	N3-C31	1.457 (6)
C1-C2	1.367 (6)	N4-C41	1.468 (6)
C1-N1	1.321 (5)	N5-C51	1.451 (6)
C2-N2	1.326 (5)	N6-C61	1.451 (6)
N1-H1	0.82 (4)	mean C-C(methyl)	1.51 (2)[b]
N2-H2	0.85 (5)	range C-C(methyl)	1.451 (9)-1.53 (1)

[a]See footnote **a**, Table 1.4. [b]Numbers in parentheses are the standard deviations of the mean.

Table 1.8. Selected Bond Angles (deg) for [Cr(*t*-$C_4H_9HNC{\equiv}CNH$-*t*-C_4H_9)(CN-*t*-$C_4H_9)_4$I]I (2)[a]

I1-Cr-C3	78.2 (1)	Cr-C4-N4	173.9 (4)
I1-Cr-C4	78.7 (1)	Cr-C5-N5	176.4 (4)
I1-Cr-C5	79.8 (1)	Cr-C6-N6	174.7 (4)
I1-Cr-C6	79.2 (1)	C1-C2-N2	130.9 (4)
C1-Cr-C2	41.2 (2)	C2-C1-N1	130.7 (4)
C1-Cr-C3	117.0 (2)	C1-N1-C11	131.3 (4)
C1-Cr-C5	84.7 (2)	C2-N2-C21	130.0 (4)
C2-Cr-C4	88.0 (2)	C1-N1-H1	117 (3)
C2-Cr-C6	114.2 (2)	C2-N2-H2	118 (3)
C3-Cr-C4	91.9 (2)	C11-N1-H1	111 (3)
C3-Cr-C5	158.0 (2)	C21-N2-H2	112 (3)
C4-Cr-C6	157.6 (2)	C3-N3-C31	165.5 (5)
C5-Cr-C6	89.7 (2)	C4-N4-C41	166.7 (4)
Cr-C1-N1	160.2 (3)	C5-N5-C51	169.9 (5)
Cr-C2-N2	159.2 (3)	C6-N6-C61	165.7 (4)
Cr-C3-N3	176.8 (4)		

range N-C-C(methyl)		range C(methyl)-C-C(methyl)	
groups 1 and 2	106.3 (4)-111.8 (4)	groups 1 and 2	109.4 (4)-111.6 (4)
groups 3-6	106.0 (4)-108.8 (5)	groups 3-6	108.5 (7)-114.4 (8)
mean N-C-C(methyl)		mean C(methyl)-C-C(methyl)	
groups 1 and 2	109 (2)[b]	groups 1 and 2	110.2 (8)[b]
groups 3-6	108 (1)[b]	groups 3-6	111 (2)[b]

[a]Estimated standard deviations in the least significant figure are given in parentheses. [b]Numbers in parentheses are the standard deviations of the mean.

Table 1.9. Twenty-one Angle Test for [Cr(*t*-$C_4H_9HNC{\equiv}CNH$-*t*-C_4H_9)(CN-*t*-$C_4H_9)_4I$]I and [Mo(*t*-$C_4H_9HNC{\equiv}CNH$-*t*-C_4H_9)(CN-*t*-$C_4H_9)_4I$]I[a]

	Cr	Mo	PB (D_{5h})	CTP(C_{2v})	CO(C_{3v})	4:3 (C_s)
1	160.1	161.7	180.0	164.0	160.0	170.0
2	158.6	160.4	144.0	164.0	160.0	153.6
3	158.0	159.8	144.0	144.2	160.0	153.6
4	157.6	157.8	144.0	144.2	130.0	130.8
5	117.0	114.4	144.0	119.0	130.0	130.8
6	115.4	114.0	144.0	119.0	130.0	120.0
7	114.2	112.6	90.0	118.8	108.9	120.0
8	111.7	112.0	90.0	118.8	108.9	108.8
9	91.9	90.5	90.0	99.0	108.9	108.8
10	89.7	89.5	90.0	99.0	83.1	89.4
11	88.5	89.3	90.0	83.7	83.1	89.4
12	88.0	87.6	90.0	83.7	83.1	83.1
13	87.0	87.0	90.0	80.3	82.0	83.1
14	85.7	86.8	90.0	80.3	82.0	83.1
15	84.7	83.4	90.0	78.8	82.0	75.5
16	83.0	85.8	90.0	78.6	82.0	75.5
17	79.8	81.2	72.0	75.2	82.0	75.5
18	79.2	79.6	72.0	75.2	82.0	75.5
19	78.7	79.5	72.0	75.0	70.0	73.3
20	78.2	78.5	72.0	75.0	70.0	73.3
21	41.2	38.5	72.0	71.5	70.0	70.0

Table 1.9 (cont). Twenty-one Angle Test for [Cr(*t*-$C_4H_9HNC{\equiv}CNH$-*t*-C_4H_9)(CN-*t*-C_4H_9)$_4$I]I and [Mo(*t*-$C_4H_9HNC{\equiv}CNH$-*t*-C_4H_9)(CN-*t*-C_4H_9)$_4$I]I[a]

---

[a]Angles are listed by decreasing size. Abbreviations are : PB, pentagonal bipyramid; CTP, capped trigonal prism; CO, capped octahedron; 4:3, the 4:3 "piano stool" structure.

CHAPTER II
Calixarene Macrocycles and Transition Metals

The macrocyclic compounds shown in Figure 2.1 were first called "calixarenes" by C. David Gutsche in 1978.[1] The name is derived from the Greek *calix*, meaning "vase" or "chalice", and *arene*, describing the repeating aryl residues in the macrocyclic array. Suitably named, the salient features of these compounds are their cone-like shape and hydrophobicity. Despite their long history, calixarene macrocycles have received much attention only in recent years. Over a century ago, Adolf von Bayer reported the reaction of phenols with aldehydes in the presence of acid.[2-4] The products were complex, difficult to characterize, and in some cases, "kettartige" or "cement-like". From these humble beginnings, and through a century of research into the nature of the products and optimal conditions for their preparation,[5] came the inexpensive and convenient one-pot syntheses of the calix[4,6,8]arene macrocycles from the condensation of phenol with formaldehyde as shown in Figure 2.2.[6] Starting with the simple calixarenes, workers in the last half of this century developed methods for contouring their shapes and placing a variety of functional groups on the rim of the cavity. Several accounts of the historical development of this field are available.[7,8]

One especially convenient aspect of working with calixarene macrocycles is their characteristic and simple ^{1}H NMR spectra, which reveal the geometry and symmetry of calixarene products. *p-tert*-Butylcalix[4]arene,[9] for example, has 5 resonances in its ^{1}H NMR spectrum: singlets in the phenol, phenyl, and *tert*-butyl regions, and two broadened doublets corresponding to the diastereotopic methylene protons, as shown in Figure 2.3. The methylene region of the spectrum is the most informative. The chemical shift of the *axial* methylene protons, those closest to the phenolic oxygen atoms, lie downfield of the *equatorial* methylene protons, which

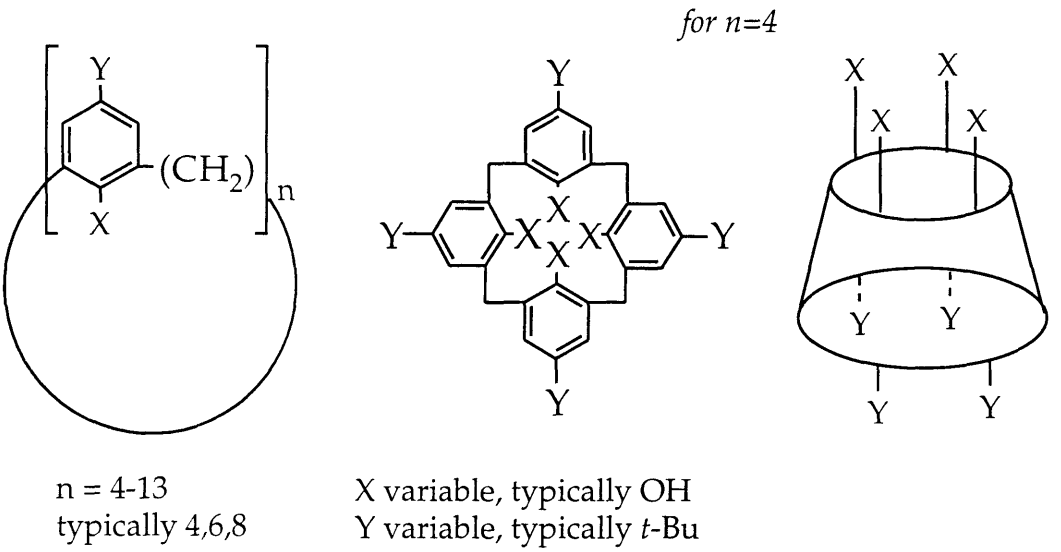

n = 4-13
typically 4,6,8

X variable, typically OH
Y variable, typically *t*-Bu

Figure 2.1. Three standard depictions of calixarenes.

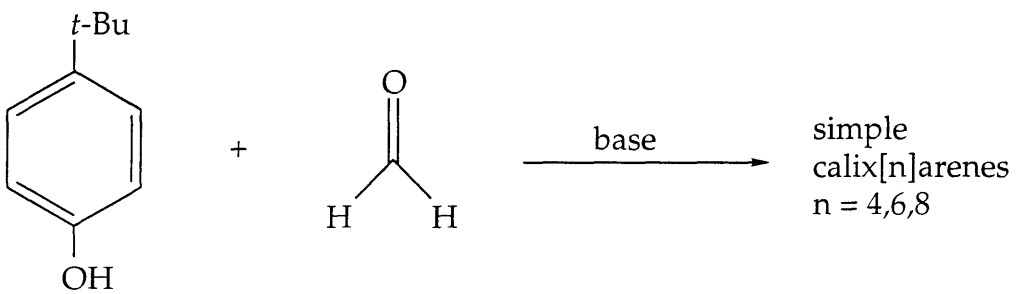

$ 0.03/g

$ 0.01/mL

~30 g
1 day
$ 2.38

Figure 2.2. Synthetic convenience and economic advantage of calix[4,6,8]arenes.[10]

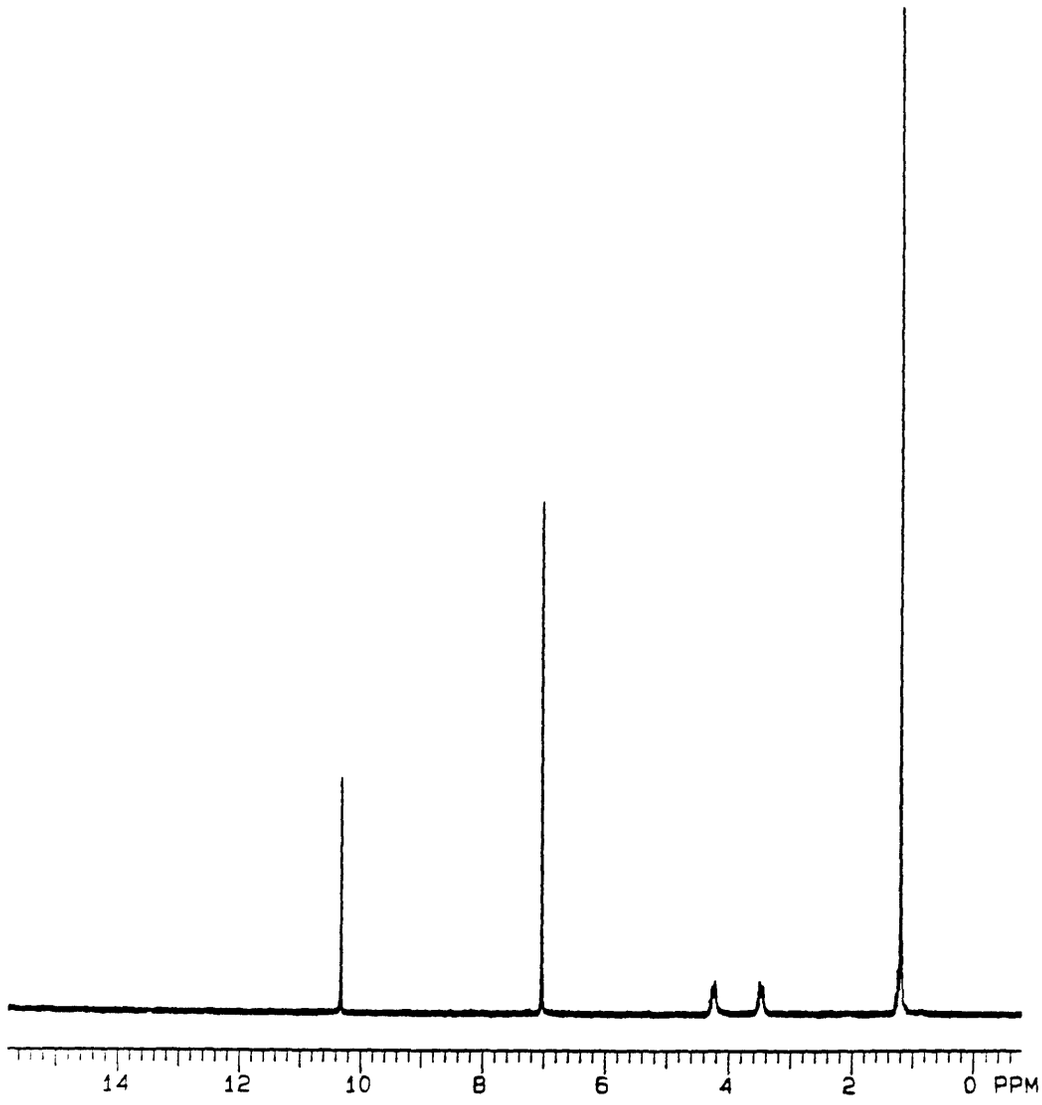

Figure 2.3. ^{1}H NMR spectrum ($CDCl_3$) of *p-tert*-butylcalix[4]arene.

are shielded due to their proximity to the aromatic rings. Although geometrically inequivalent, at room temperature the methylene protons are exchanging rapidly as the *p-tert*-butylcalixarene converts from one cone conformer to the other. The methylene protons of a geometrically-fixed calixarene ligand, however, are inequivalent at room temperature and give rise to sharp doublets in the ^{1}H NMR spectrum. The methylene region also reveals the symmetry of calixarene macrocycles and any products containing them. Calixarenes in which all the methylene protons are symmetry-related have only two doublets in the methylene region. As the methylene positions become inequivalent, *n* pairs of doublets appear in the ^{1}H NMR spectrum, where n is the number of methylene position types.

Calixarenes have become prevalent in recent literature not only for their ease of preparations, but also for their range of reactivity. Calixarene ligands have host-guest capabilities, similar to crown-type compounds,[11] and are potential tetradentate binding ligands for transition metals, like porphyrins.[12] Calixarenes also have sequestration properties due to their three-dimensional structures, comparable to those of cryptands and cyclodextrins.[13-16]

Early interest in calixarenes stemmed from their ability to complex alkali and alkaline earth metal cations,[17,18] neutral molecules,[19-21] organic cations,[22,23] organic anions,[24] lanthanide ions,[25] and UO_2^{2+}.[26] Two examples of inclusion of neutral molecules in the solid state are of toluene by *p-tert*-butylcalix[4]arene (**1**) and of acetonitrile by tetra-ethyl-*p-tert*-butylcalix[4]arene tetracarbonate (**2**), as depicted in Figure 2.4. This ability of calixarenes to include neutral molecules has been ascribed to attractive "alkyl-phenyl" or "CH_3-π" interactions.[27]

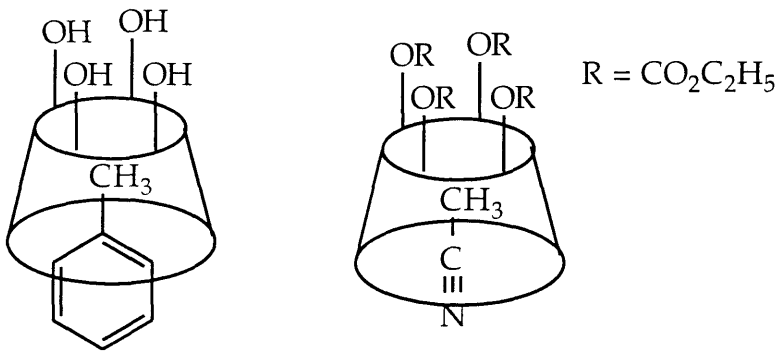

1 2

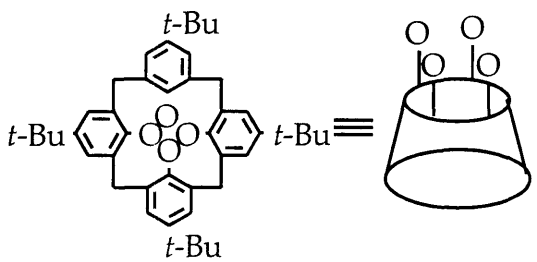

Figure 2.4. Schematic representations of the calixarene inclusion complexes: toluene included by *p-tert*-butylcalix[4]arene (**1**) and acetonitrile included by tetra-ethyl-*p-tert*-butylcalix[4]arene tetracarbonate (**2**).

It was not until 1985 that the first transition metal calixarene complexes were reported.[28] A variety of transition metal amines (M=Ti, Fe, Co) were allowed to react with para-*tert*-butylcalix[4]arene to yield [(Ti{*p*-*tert*-butyl-calix[4]arene})$_2$] (**3**), [(Fe(NH$_3$){*p*-*tert*-butyl-calix[4]areneOSiMe$_3$})$_2$] (**4**), and [(Co$_3${*p*-*tert*-butyl-calix[4]areneOSiMe$_3$}$_2$(THF)] (**5**). The simplest case resulted from the reaction of the calixarene with [Ti(NMe$_2$)$_4$], which afforded the aryloxido compound **3** in good yield. All of the products **3-5** were characterized by X-ray crystallography, and the structures are shown schematically in Figure 2.5. Soon thereafter, transition metal complexes were reported for calix[6]arene[29] and calix[8]arene.[30,31] The products [{H$_2$-calix[6]arene}{TiCl$_2$(μ-O)TiCl$_3$}]$_2$ (**6**) and [calix[8]arene{Ti(O-*i*Pr)}$_2$][RNH$_3$] (**7**) are schematically depicted in Figure 2.6. These and other similar compounds[32-36] opened the field of transition metal calixarene chemistry.

Floriani and coworkers, by considering the calix[4]arene ligand as an oxido-matrix with fourfold symmetry, produced a transition metal calixarene compound with an open coordination site directed into the basket.[37] The reaction of MoOCl$_4$ and *p*-*tert*-butylcalix[4]arene produced the intriguing compound [(*p*-*tert*-butylcalix[4]arene)·(*p*-*tert*-butylcalix[4]arene)(Mo=O)·H$_2$O-·Ph-NO$_2$] (**8**) upon recrystallization from wet nitrobenzene. The structurally characterized product **8** is shown in Figure 2.7. It is interesting to note that water is weakly bound to the transition metal center inside a calixarene pocket in the solid state (Mo-OH$_2$, 2.41 (2) Å). Also shown in Figure 2.7 is a similar tungsten complex [(calix[4]arene)(W=O)·CH$_3$COOH] (**9**) that was synthesized by an analogous procedure.[38] Again, solvent of crystallization (CH$_3$COOH) showed weak *endo*-calix coordination to the metal center (W-OAc, 2.39 (4) Å).

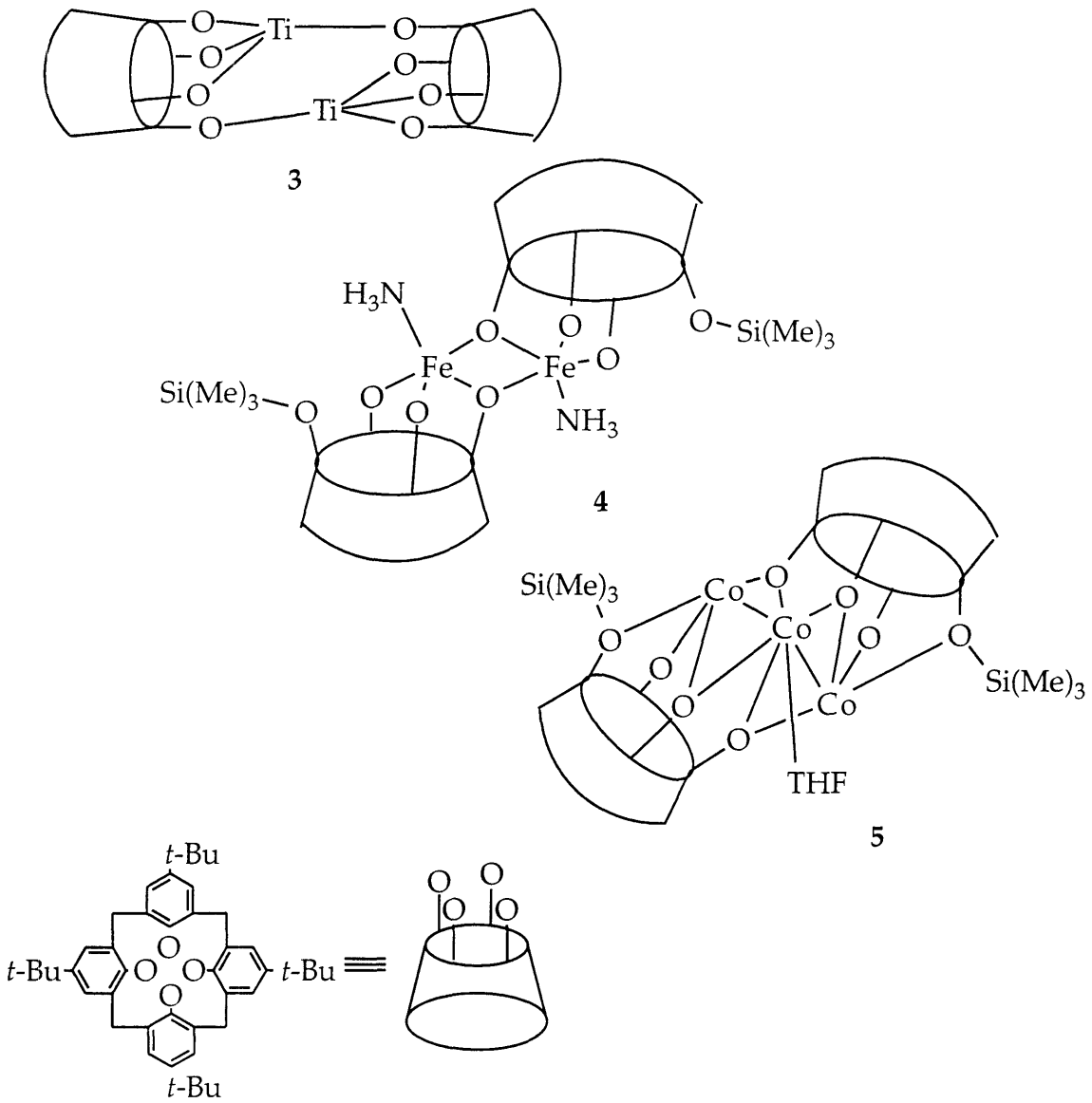

Figure 2.5. Schematic representations of the first transition metal calixarene complexes: [(Ti{*p-tert*-butyl-calix[4]arene})$_2$] (**3**), [(Fe(NH_3){*p-tert*-butyl-calix[4]areneOSiMe$_3$})$_2$] (**4**), and [(Co$_3${*p-tert*-butylcalix[4]areneOSiMe$_3$}$_2$-(THF)] (**5**) prepared by Power and coworkers.[28]

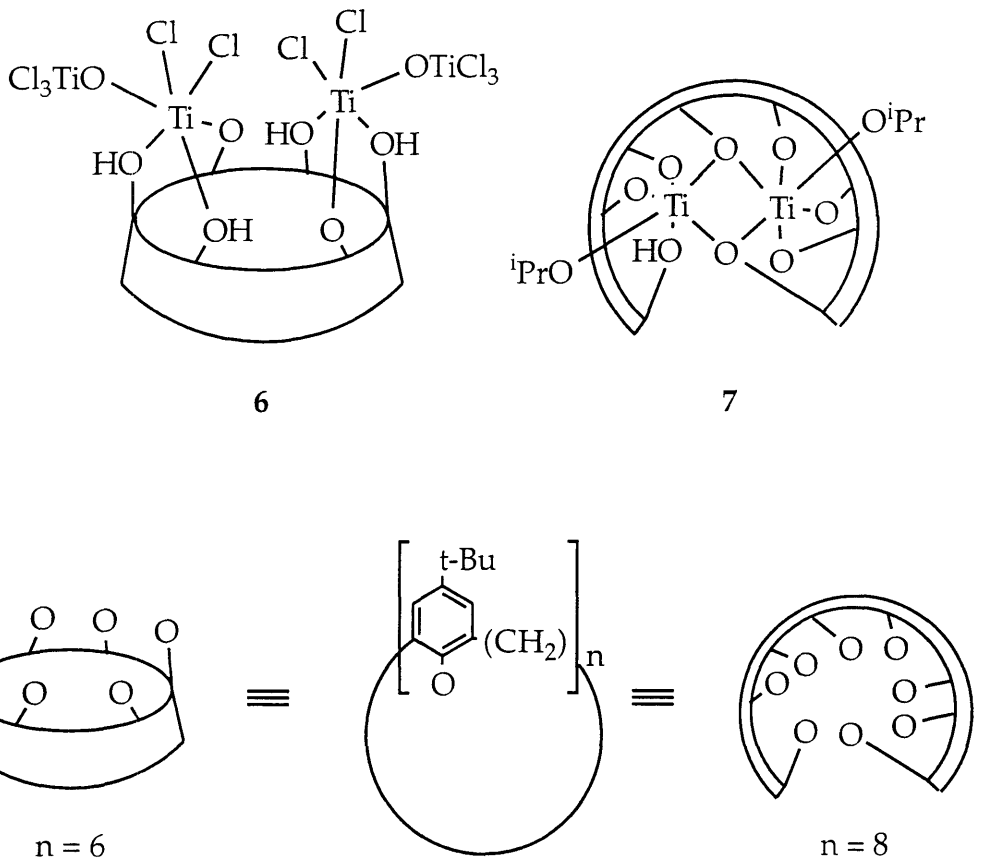

Figure 2.6. Schematic representations of [{H_2-calix[6]arene}{$TiCl_2$(μ-O)$TiCl_3$}]$_2$ (**6**)[29] and [calix[8]arene{Ti(O-*i*Pr)}$_2$][RNH_3] (**7**).[30,31]

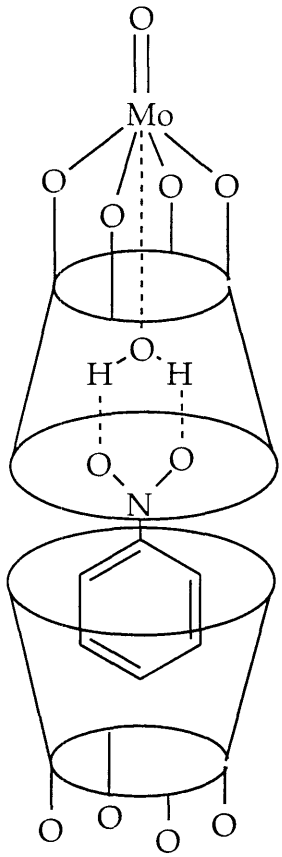

8

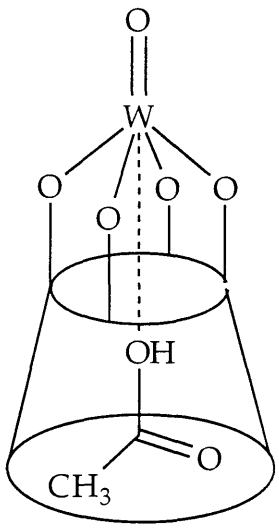

9

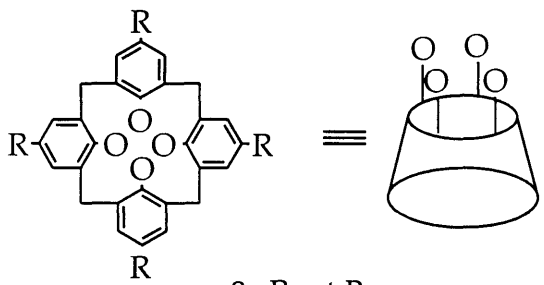

8: R = *t*-Bu
9: R = H

Figure 2.7. Representations of [(*p-tert*-butylcalix[4]arene)·(*p-tert*-butylcalix[4]arene)(Mo=O)·H_2O·Ph-NO_2] (**8**) and [(calix[4]arene)(W=O)·CH_3COOH] (**9**) prepared by Floriani and coworkers.

Enticed by the attractive properties of the calixarene pocket as a host for unusual ligands and the relative rarity of transition metals in this class, we began a program of transition metal calixarene chemistry, the results of which are discussed in the remainder of this thesis. The application of calixarene ligands to the area of metal-metal quadruply bonded complexes is presented in Chapter III. The synthesis and characterization of several dimolbydenum (II) calixarene complexes are described. The effect of binding the methylene-tethered, geometrically-hindered phenol and phenoxide donors of *p-tert*-butylcalix[4]arene and calix[4]arene to the $[Mo\underline{\underline{4}}Mo]^{4+}$ moiety has been explored by spectroscopic and X-ray crystallographic techniques. Chapter IV introduces transition metal calixarene complexes that are specifically suited to bind small molecules in the *endo*-calix position. The preparation of several electron-deficient $Cp^{(*)}$Mcalixarene complexes is described. X-ray crystallography was used to reveal the structural features of these "pocket" compounds and their inclusion complexes. Both chapters represent novel contributions to the field of transition metal calixarene chemistry.

References

(1) Gutsche, C. D.; Muthukrishnan, R. *J. Org. Chem.* **1978**, *43*, 4905.

(2) Baeyer, A. *Chem. Ber.* **1872**, *5*, 25.

(3) Baeyer, A. *Chem. Ber.* **1872**, *5*, 280.

(4) Baeyer, A. *Chem. Ber.* **1872**, *5*, 1094.

(5) Gutsche, C. D. In *Calixarenes: A Versatile Class of Macrocyclic Compounds*; J. Vicens and V. Böhmer, Ed.; Kluwer Academic Publishers: Dordrecht, 1990; Vol. 3; pp 3-61.

(6) Preparations of standard calix[4,6,8]arenes: (a) Gutsche, C. D.; Iqbal, M. *Org. Synth* **1989**, *68*, 234. (b) Gutsche, C. D.; Dhawan, B.; Leonis, M.; Stewart, D. *Org. Synth.* **1989**, *68*, 238. (c) Munch, J. H.; Gutsche, C. D. *Org. Synth.* **1989**, *68*, 243.

(7) Böhmer, V.; Vicens, J. In *Calixarenes: A Versatile Class of Macrocyclic Compounds*; J. Vicens and V. Böhmer, Ed.; Kluwer Academic Publishers: Dordrecht, 1990; Vol. 3; pp 39-61.

(8) Gutsche, C. D. *Calixarenes*; The Royal Society of Chemistry: Cambridge, 1989; Vol. 1.

(9) Gutsche, C. D.; Iqbal, M. *Org. Synth.* **1989**, *68*, 234.

(10) Aldrich Chemical Company Catalog, 1993

(11) *Synthetic Multidentate Macrocyclic Compounds*; Izatt, R. M.; Christensen, J. J., Ed.; Academic Press: New York, 1978.

(12) *Porphyrins*; Gouterman, M.; Rentzepis, P. M.; Straub, K. D., Ed.; American Chemical Society: Washington, DC, 1986.

(13) Cram, D. J.; Cram, J. M. *Science* **1974**, *183*, 803.

(14) Cram, D. J.; Cram, J. M. *Acc. Chem. Res.* **1978**, *11*, 8.

(15) Szejtli, J. *Cyclodextrins and their Inclusion Compounds*; Akademiai Kiado: Budapest, 1982.

(16) Bender, M. L.; Komiyama, M. *Cyclodextrin Chemistry*; Springer-Verlag: Berlin, 1978.

(17) Izatt, R. M.; Lamb, J. D.; Hawkins, R. T.; Brown, P. R.; Izatt, S. R.; Christensen, J. J. *J. Am. Chem. Soc.* **1983**, *105*, 1782.

(18) Izatt, S. R.; Hawkins, R. T.; Christensen, J. J.; Izatt, R. M. *J. Am. Chem. Soc.* **1985**, *107*, 63.

(19) Andreetti, G. D.; Ungaro, R.; Pochini, A. *J. Chem. Soc., Chem. Commun.* **1979**, 1005.

(20) Gutsche, C. D.; Dhawan, B.; No, K. H.; Muthukrishnan, R. *J. Am. Chem. Soc.* **1981**, *103*, 3782.

(21) Coruzzi, M.; Andreetti, G. D.; Bocchi, V.; Pochini, A. *J. Chem. Soc., Perkin II* **1982**, 1133.

(22) Bauer, L. J.; Gutsche, C. D. *J. Am. Chem. Soc.* **1985**, *107*, 6063.

(23) Gutsche, C. D.; Iqbal, M.; Alam, I. *J. Am. Chem. Soc.* **1987**, *109*, 4314.

(24) Arimura, T.; Edamitsu, S.; Shinkai, S.; Manabe, O.; Muramatsu, T.; Tashiro, M. *Chem. Lett.* **1987**, 2269.

(25) Bunzli, J. G.; Harrowfield, J. M. In *Calixarenes: A Versatile Class of Macrocyclic Compounds*; J. Vicens and V. Bohmer, Ed.; Kluwer Academic Publishers: Dordrecht, 1991.

(26) Shinkai, S.; Koreishi, H.; Ueda, K.; Arimura, T.; Manabe, O. *J. Am. Chem. Soc.* **1987**, *109*, 6371.

(27) Andreetti, G. D.; Ori, O.; Ugozzoli, F.; Alfieri, C.; Pochini, A.; Ungaro, R. *J. Incl. Phenom.* **1988**, *6*, 523.

(28) Olmstead, M. M.; Sigel, G.; Hope, H.; Xu, X.; Power, P. P. *J. Am. Chem. Soc.* **1985**, *107*, 8087.

(29) Bott, S. G.; Coleman, A. W.; Atwood, J. L. *J. Chem. Soc., Chem. Commun.* **1986**, 610.

(30) Hofmeister, G. E.; Hahn, F. E.; Pedersen, S. F. *J. Am. Chem. Soc.* **1989**, *111*, 2318.

(31) Hofmeister, G. E.; Alvarado, E.; Leary, J. A.; Yoon, D. J.; Pedersen, S. F. *J. Am. Chem. Soc.* **1990**, *112*, 8843.

(32) Furphy, B. M.; Harrowfield, J. M.; Kepert, D. L.; Skelton, B. W. *Inorg. Chem.* **1987**, *26*, 4231.

(33) Andreetti, G. D.; Calestani, G.; Ugozzoli, F.; Arduini, A. *J. Incl. Phenom.* **1987**, *5*, 123.

(34) Furphy, B. M.; Harrowfield, J. M.; Ogden, M. I. *J. Chem. Soc., Dalton Trans.* **1989**, 2217.

(35) Englehardt, L. M.; Furphy, B. M.; Harrowfield, J. M.; White, A. H. *Aust. J. Chem.* **1988**, *41*, 1465.

(36) Corazza, F.; Floriani, C.; Angiola, C. V.; Guastini, C. *J. Chem. Soc., Chem. Commun.* **1990**, 1083.

(37) Corazza, F.; Floriani, C.; Chiesi-Villa, A.; Guastini, C. *J. Chem. Soc., Chem. Commun.* **1990**, 640.

(38) Corazza, F.; Floriani, C.; Chiesi-Villa, A.; Rizzoli, C. *Inorg. Chem.* **1991**, *30*, 4465.

CHAPTER III

Calixarene Complexes of the Molybdenum-Molybdenum Quadruple Bond

Introduction

Calixarenes[1] have enjoyed substantial attention in the last decade. Named for the chalice-like cone conformation of the tetramer shown in Figure 3.1, these macrocyclic polyphenols are easy to prepare in a variety of sizes.[2] They can encapsulate small molecules and ions[3] and provide multiple binding sites for transition metals.[4] A brief summary of this work is given in Chapter II. Although the field of metal-metal multiple bonding is replete with complexes containing alkoxide and aryloxide ligands,[5] there were no examples of such complexes with the methylene-tethered, geometrically-hindered phenoxides of calixarene macrocycles. In order to study the effect of binding these ligands to the dimolybdenum quadruple bond, we undertook the preparation of such complexes by allowing the conveniently prepared, labile starting material $[Mo_2(O_2CCH_3)_2(NCMe)_6][BF_4]_2$[6,7] to react with the deprotonated calix[4]arene and *p-tert*-butyl-calix[4]arene macrocycles.[8] A related starting material, $[Mo_2(O_2CCF_3)_2(NCMe)_6][BF_4]_2$, was also synthesized and employed. These products represent the first examples of a new class of calixarene complexes of the metal-metal quadruple bond.

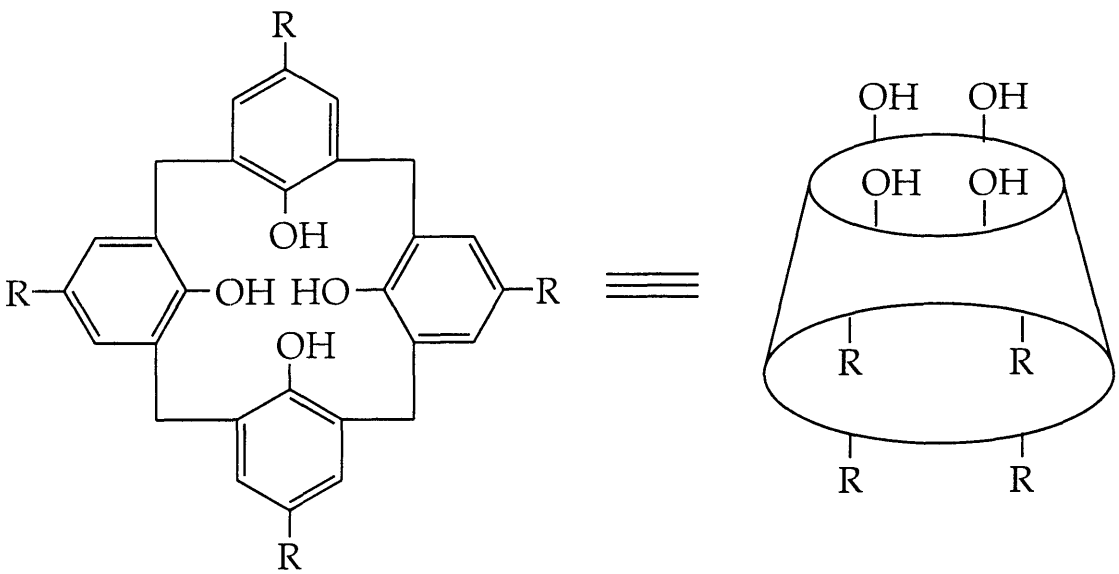

Figure 3.1. Two representations of calix[4]arenes (calix[4]arene for R = H, and *p-tert*-butyl-calix[4]arene for R = *tert*-butyl).

Experimental Section

General Considerations. All procedures were carried out in a nitrogen-filled drybox or by using standard Schlenk line techniques. Acetonitrile was distilled from CaH_2. All other solvents were distilled under nitrogen from purple sodium benzophenone ketyl. Calix[4]arene[9] and *p-tert*-butyl-calix[4]arene[10] were prepared according to the literature procedures and dried at 120 °C under vacuum for 24 hours. $[Mo_2(O_2CCF_3)_4]$[11] and $[Mo_2(O_2CCH_3)_2(NCMe)_6][BF_4]_2$[6,7] were also prepared according to published procedures. Potassium hydride was purchased as a mineral oil suspension from Aldrich Chemical Company and rinsed with pentane prior to use. All other reagents were obtained from commercial sources and used without further purification. NMR spectra were recorded on a Varian XL-300 spectrometer at room temperature. All IR spectra were run on a Bio-Rad FTS7 Fourier Transform instrument. UV-visible spectra were recorded on a Hewlett Packard 8452A diode array spectrophotometer.

Preparation of $[Mo_2(O_2CCF_3)_2(NCCH_3)_6][BF_4]_2$ (1). Yellow crystals of $[Mo_2(O_2CCF_3)_4]$[11] (450 mg, 0.0699 mmol) were added to a solution of Me_3OBF_4 (207 gm, 1.399 mmol) in 15 mL of acetonitrile. As the yellow solids dissolved, the reaction mixture turned orange in color, then red-orange and then pink. The reaction was allowed to stir for 20 h. The solvent was then removed in vacuo and the crude product was washed with 10 mL of DME to remove any residual starting materials. The insoluble pink solids were collected on a fritted funnel, rinsed twice with 10 mL of pentane, and vacuum dried to give 73% (426 mg, 0.508 mmol) of the pink product **1**. The resulting powder was judged to be >95% pure by ^1H NMR spectroscopy and could be further recrystallized from hot acetonitrile. Anal. Calcd for $C_{14}H_{15}N_5O_4B_2F_{14}Mo_2$ (**1**-$NCCH_3$): C, 21.10; H, 1.90;

N, 8.79. Found: C, 20.74; H, 1.92; N, 8.48. IR (CsI, Nujol): 2323 (s), 2294 (s), 1599 (s), 1377 (m), 1241 (s), 1196 (vs), 1077 (vs, υ B-F), 1027 (s), 954 (m), 867 (m), 776 (m), 736 (s), 526 (m), 316 (w) cm^{-1}. ^1H NMR ($NCCD_3$, 300 MHz): δ 1.96 (s, Mo-$NCCH_3$) ppm. UV-vis (THF): λ_{max}, nm (ε/Mo $cm^{-1}M^{-1}$) 382 (440), 528 (857).

Preparation of [$Mo_2(O_2CCH_3)_2$(H$_2$-*p-tert*-butylcalix[4]arene)] (2). To a stirred suspension of *p-tert*-butylcalix[4]arene (114 mg, 0.154 mmol) in 20 mL of THF were added 2 equiv of KH (12 mg, 0.299 mmol). The reaction solution was stirred for at least 2 h, during which time it effervesced and clarified. One equiv of insoluble pink [$Mo_2(O_2CCH_3)_2(NCCH_3)_6](BF_4)_2$] (**1**) (112 mg, 0.153 mmol) was then added. Over the next hour the pink solids disappeared, producing a red-orange solution. The solvent was removed in vacuo and the product was extracted into pentane. Concentration of the pentane solution and cooling to -30 °C overnight resulted in air-sensitive, fluffy orange-pink crystals (107 mg, 0.112 mg) in 73% yield. Anal. Calcd for $C_{48}H_{60}O_8Mo_2$ (**2**): C, 60.25; H, 6.32. Found: C, 59.99; H, 6.15. IR (CsI, Nujol): 1304 (s), 1267 (m), 1205 (s), 1042 (m), 872 (m), 824 (m), 788 (m), 745 (m), 680 (m), 618 (w), 527 (w), 478 (w), 381 (w), 343 (w), 309 (w) cm^{-1}. ^1H NMR (THF-d_8, 300 MHz): δ 1.26 (s, 36H; *t*-Bu), 1.78 (br, 8H; *axial* THF), 2.57 (d, *J* = 12 Hz, 2H; CH_2), 2.92 (s, 6H; O_2CCH_3), 3.07 (d, *J* = 12 Hz, 2H; CH_2), 3.75 (d, *J* = 12 Hz, 2H; CH_2), 3.63 (br, 8H; *axial* THF), 4.57 (d, *J* = 12 Hz, 2H; CH_2), 7.13 (dd, *J* = 12 Hz, 3Hz, 8H; Ph), 16.94 (s, 2H; Mo-OHPh) ppm. UV-vis (THF): λ_{max}, nm (ε/Mo $M^{-1}cm^{-1}$) 379 (1213), 514 (875).

Preparation of [$Mo_2(O_2CCF_3)_2$(H$_2$-*p-tert*-butylcalix[4]arene)] (3). *p-tert*-Butylcalix[4]arene (100 mg, 0.135 mmol) was stirred vigorously with 2 equiv of KH (11mg, 0.274 mmol) in 15 mL of THF for 2 hours. To the resulting clear, colorless solution was added solid pink [$Mo_2(O_2CCF_3)_2(NCCH_3)_6][BF_4]_2$ (**1**) (113 mg, 0.135 mmol). The reaction suspension was stirred overnight, during which time the solids disappeared and a dark red-orange color developed. The solvent

was removed in vacuo and the product was extracted with pentane. The pentane extract was filtered through Celite and concentrated to dryness. Recrystallization from pentane with a few drops of THF afforded orange-pink crystals of **3** in 39% yield (56 mg, 0.052 mmol). Anal. Calcd for $C_{48}H_{54}O_8F_6Mo_2$ (**3**): C, 54.14; H, 5.11. Found: C, 54.02; H, 5.14. IR (CsI, Nujol): 1598 (m), 1305 (m), 1265 (w), 1195 (s), 1161 (m), 1128 (m), 1033 (m), 969 (m), 923 (m), 911 (m), 870 (m), 824 (m), 732 (s), 619 (w), 557 (w), 358 (w) cm^{-1}. ^1H NMR (THF-d_8, 300 MHz): δ 1.22 (s, 36H; *t*-Bu), 1.78 (br, 8H; *axial* THF), 2.54 (d, *J* = 12 Hz, 2H; CH_2), 3.08 (d, *J* = 12 Hz, 2H; CH_2), 3.63 (br, 8H; *axial* THF), 3.81 (d, *J* = 12 Hz, 2H; CH_2), 4.51 (d, *J* = 12 Hz, 2H; CH_2), 7.16 (s, 8H; Ph), 16.96 (s, 2H; Mo-OHPh) ppm. UV-vis (THF): λ_{max}, nm (ε/Mo $M^{-1}cm^{-1}$) 338 (4396), 414 (3049), 530 (1005).

Preparation of $[Mo_2(O_2CCH_3)_2(H_2\text{-calix[4]arene})]$ (4). A 15 mL THF solution of calix[4]arene (100 mg, 0.236 mmol) was stirred with 2 equiv of KH (19 mg, 0.474 mmol) for at least one hour, until gas evolution ceased. To the resulting solution was added 1 equiv of $[Mo_2(O_2CCH_3)_2(NCCH_3)_6](BF_4)_2$ (172 mg, 0.236 mmol). The insoluble pink solids disappeared over 1 h and a wine-red solution developed. The solution was passed through an inch pad of Celite saturated with THF to remove any traces of starting material, and the solvent was evaporated from the filtrate. A red-orange, highly air-sensitive solid remained. The product was soluble in THF, DME, acetonitrile, and toluene, but insoluble in diethyl ether and pentane. Anal. Calcd for $C_{32}H_{28}O_8Mo_2$ (**1**): C, 52.47; H, 3.85. Found: C, 52.47; H, 4.27. IR (CsI, Nujol): 1594 (w), 1298 (m), 1262 (m), 1218 (m), 1100 (sh), 1076 (m), 1029 (m), 968 (m), 891 (m), 856 (m), 824 (m), 745 (m), 727 (m), 676 (m), 613 (w), 580 (w), 472 (w), 464 (w), 376 (w), 340 (w) cm^{-1}. ^1H NMR (THF-d_8, 300 MHz): δ 1.78 (br, 8H; *axial* THF), 2.55 (s, *J* = 12 Hz, 2H; CH_2), 2.89 (s, 6H; O_2CCH_3), 3.04 (d, *J* = 12 Hz, 2H; CH_2), 3.63 (br, 8H; *axial* THF), 3.72 (d, *J* = 12 Hz, 2H; CH_2), 4.54 (d, *J* = 12 Hz, 2H; CH_2), 6.55 (t, *J* = 6 Hz, 4H; Ph),

7.06 (d, J = 6 Hz, 8H Ph), 16.94 (s, 2H; Mo-OHPh) ppm. UV-vis (THF) λ_{max}, nm (ε/Mo $M^{-1}cm^{-1}$) 380 (712), 512 (591).

Preparation of $[Mo_2(O_2CCF_3)_2(H_2\text{-calix[4]arene})]$ (5). To a stirred solution of calix[4]arene (100mg, 0.236 mmol) in 15 mL of THF was added 2 equiv of KH (19 mg, 0.474 mmol). The effervescent solution was allowed to react for at least 2 hours before solid pink $[Mo_2(O_2CCF_3)_2(NCCH_3)_6][BF_4]_2$ (**1**) (198 mg, 0.236 mmol) was added. The pink solid disappeared and a red-orange color developed as the reaction was stirred overnight. The solvent was then removed in vacuo, and the product extracted with pentane. Concentrating the pentane solution to dryness produced bright orange microcrystals in 71% yield (140 mg, 0.166 mmol). Larger crystals could be grown by slow diffusion of pentane into a toluene solution of **5** with a few drops of THF. Anal. Calcd for $C_{39}H_{30}O_8F_6Mo_2$ (**5**·toluene): C, 50.23; H, 3.24. Found: C, 50.59; H, 4.15. IR (CsI, Nujol): 1605 (s), 1377 (m), 1367 (sh), 1296 (w), 1263 (m), 1196 (vs), 1163 (s), 1100 (m), 1034 (m), 968 (m), 858 (m), 825 (w), 752 (s), 732 (vs), 668 (w)613 (w), 581 (w), 547 (w), 499 (w), 472 (w), 358 (w) cm^{-1}. ^1H NMR (THF-d_8, 300 MHz): δ 1.78 (br, 8H; *axial* THF), 2.55 (d, J = 12 Hz, 2H; CH_2), 3.10 (d, J = 12 Hz, 2H; CH_2), 3.63 (br, 8H; *axial* THF), 3.83 (d, J = 12 Hz, 2H; CH_2), 4.53 (d, J = 12 Hz, 2H; CH_2), 6.65 (t, J = 6 Hz, 4H; Ph), 7.13 (d, J = 6 Hz, 8H; Ph), 17.00 (s, 2H; Mo-OHPh) ppm. UV-vis (THF) λ_{max}, nm (ε/Mo $M^{-1}cm^{-1}$) 338 (4056), 412 (2220), 528 (716).

X-ray Crystallography.

$[Mo_2(O_2CCH_3)_2(H_2$-*p*-*tert*-butylcalix[4]arene)(THF)]·C_6H_6 (2(THF)·C_6H_6). Air-sensitive X-ray quality crystals of **2**(THF)·C_6H_6 could be grown by slow evaporation of pentane into a benzene solution of **2** containing a few drops of THF. A bright red-orange block of dimensions 0.5 X 0.4 X 0.15 mm was mounted on a quartz fiber from a liquid nitrogen cold stage and studied on an Enraf-Nonius CAD4 diffractometer at -73.8 °C by methods commonly employed

in our laboratory,[12] details of which are provided in Table 3.1. Unit cell parameters were determined from 25 reflections with $20<2\theta<30$. Crystal quality was judged to be acceptable by open counter ω-scans of several low-angle reflections ($\Delta\bar{\omega}_{1/2} = 0.27^{o}$, no fine structure) and axial photographs. Systematic absences and intensity statistics were consistent with the monoclinic space group $P2_1/c$. The structure was solved by conventional direct methods and refined by full matrix least-squares procedures. All non-hydrogen atoms were refined anisotropically, and the phenol hydrogen atoms, H1 and H2, were located on the difference map and allowed to refine isotropically. Other hydrogen atoms were calculated and fixed on the attached carbon atoms ($d_{C-H} = 0.95$ Å, $B_H = 1.2\ B_C$). Lorentz and polarization corrections were applied, as was an empirical absorption correction based on psi-scans. The largest residual peak in the final difference Fourier map was 0.7 $e^-/Å^3$, at a distance of 1.04 Å from Mo2. Positional and thermal parameters for non-hydrogen atoms, H1, and H2 are given in Table 3.2. Anisotropic thermal parameters for non-hydrogen atoms are given in Table 3.3.

Raman Spectroscopy. $[Mo_2(O_2CCH_3)_2(H_2$-*p*-*tert*-butylcalix[4]arene)] (2), $[Mo_2(O_2CCF_3)_2(H_2$-*p*-*tert*-butylcalix[4]arene)] (3), $[Mo_2(O_2CCH_3)_2(H_2$-calix[4]arene)] (4), and $[Mo_2(O_2CCF_3)_2(H_2$-calix[4]arene)] (5). Raman spectra were recorded by using a Spex spectrometer, with excitation by a Coherent Innova 90 argon ion laser. Peak positions on this model are accurate to within 2 cm^{-1}. The samples were 0.14 M solutions in THF measured at room temperature with excitation at $\lambda_o = 514.5$ cm^{-1} and a spectral slit width of 400 μm. Spectra were recorded with 200-500 milliwatts of power, while spinning the samples. A total of 200-500 scans were taken at a rate of approximately 1 scan per second.

Results and Discussion

$[Mo_2(O_2CCF_3)_2(NCCH_3)_6][BF_4]_2$ (1). The preparation of $[Mo_2(O_2CCF_3)_2(NCCH_3)_6][BF_4]_2$ (**1**) proved to be as facile as the syntheses of the previously reported complexes $[Mo_2(O_2CR_3)_2(NCCR_3)_4L_2][BF4]_2$ (R = H, CH_3; L = $NCCH_3$, O_3SCF_3)[6,7] Unlike the original preparations of this class of compounds in which an excess of Me_3OBF_4 was used, $[Mo_2(O_2CCF_3)_2(NCCH_3)_6][BF_4]_2$ (**1**) was best prepared with stochiometric amounts of $[Mo_2(O_2CCF_3)_4]$ and Me_3OBF_4. The reaction of 2 equivalents of Me_3OBF_4 in acetonitrile with $[Mo_2(O_2CCF_3)_4]$ proceeded through an array of colors to afford the bright pink product **1** in good yield. Complex **1** can be stored indefinitely under aerobic and anhydrous conditions, is very soluble in acetonitrile, and is moderately soluble in other polar solvents such as DME and THF. The spectroscopic properties of **1** are similar to those of its analogs. The ^1H NMR spectrum shows only one resonance for the $NCCH_3$ groups (δ = 1.96 ppm) at nearly the same shift as the solvent, suggesting rapid exchange of the axial and equatorial $NCCH_3$ groups of the product with each other and with the solvent. The IR spectrum of **1** in Nujol shows strong peaks (υ = 2323, 2294 cm^{-1}) corresponding to the C≡N vibrations of the bound acetonitrile ligands. The lowest energy band in the UV-visible absorption spectrum of the product occurs at 528 nm which is comparable to the lowest energy band in the spectrum of $[Mo_2(O_2CCH_3)_2(NCCH_3)_6][BF_4]_2$ at 531 nm[7] attributed to a metal-metal $\delta \rightarrow \delta^*$ transition. Analytical results for **1** are correspond to the loss of one axial ligand, consistent with elemental analyses of analogs of **1**[6,7] and the solvent lability demonstrated by ^1H NMR mentioned above.

Preparation of $[Mo_2(O_2CCH_3)_2(H_2$-*p*-*tert*-butylcalix[4]arene)] (2), $[Mo_2(O_2CCF_3)_2(H_2$-*p*-*tert*-butylcalix[4]arene)] (3), $[Mo_2(O_2CCH_3)_2(H_2$-calix[4]arene)] (4), and $[Mo_2(O_2CCF_3)_2(H_2$-calix[4]arene)] (5). The complexes $[Mo_2(O_2CR_3)_2(NCCH_3)_6][BF_4]_2$ (R = CH_3, CF_3 (**1**)) proved to be useful starting materials for the preparation of calixarene-substituted dimolybdenum quadruply bonded products **2-5**. The labile acetonitrile ligands were readily displaced by doubly-deprotonated calixarene macrocycles. Reaction progress was monitored in THF by the disappearance of the insoluble starting material. The neutral products were purified by extraction into non-polar solvents and filtration to remove salts and residual starting materials. The products are extremely air-sensitive in the solid state as well as in solution.

One advantage in using calix[4]arene ligands in transition metal chemistry is the characteristic ^1H NMR spectra of their diamagnetic complexes.[1,13] Metal incorporation and the overall symmetry of the molecule are immediately apparent from the shape and number of doublets corresponding to the methylene protons of the calix[4]arene ligand. The presence of 4 sets of sharp methylene doublets in the ^1H NMR spectra of **2-5** indicated products with approximately twofold symmetry and geometrically fixed calixarene ligands. In THF-d_8, the NMR spectra of **2-5** contain broad peaks at 1.78 and 3.63 ppm, only slightly downfield of the chemical shift of the solvent, suggesting axial coordination of the complexes by THF in solution. This coordination was confirmed in the solid state, as follows.

Structural Results.

$[Mo_2(O_2CCH_3)_2(H_2$-*p*-*tert*-butylcalix[4]arene)(THF)]·C_6H_6 [(2)(THF)]·C_6H_6. The solid state structure of **2**(THF)·C_6H_6 was revealed in an X-ray diffraction study. An ORTEP diagram of **2**(THF) is shown in Figure 3.2, and selected bond distances and angles are given in Table 3.4. The molecule

crystallizes in the space group $P2_1/c$ and has no crystallographically imposed symmetry elements. No disorder was encountered in the structure refinement. Final positional parameters, and selected bond distances and angles are summarized in Tables 3.2 and 3.3, respectively. The dimolybdenum core of **2**(THF) is bridged by two bidentate acetate ligands and spanned in a tetradentate fashion by the doubly-deprotonated calixarene macrocycle. The bridging tetradentate coordination of **2**(THF) is similar to the bridging bis-bidentate coordination of the tetraazamacrocyclic H_2TMTAA (5,7,12,14-tetramethyldibenzo[*b*,*i*][1,4,8,11]-tetraazacyclotetradecine) ligand in $[Mo_2(O_2CCH_3)_2$-(TMTAA)].[14] In both molecules, the Mo-$\underline{4}$-Mo core is spanned by the macrocyclic ligands as well as two bridging carboxylate ligands. A more common binding motif for tetradentate ligands was seen in the complexes $[\{Mo(TMTAA)\}_2]$,[15,16] $[\{Mo(acacen)\}_2]$,[17] $[\{Mo(TPP)\}_2]$,[18] $[\{Mo(OEP)\}_2]$,[19] and $[\{Mo(TOEP)\}_2]$.[20] In these complexes, each molybdenum atom is individually coordinated by one macrocycle, leaving the Mo-$\underline{4}$-Mo core unbridged.

The Mo-Mo distance of 2.1263 (6) Å and the eclipsed geometry of the Mo_2O_8 core are consistent with the presence of a quadruple bond.[21,22] The Mo-$\underline{4}$-Mo separation as well as the Mo-O_{ligand} distances of **2**(THF) can be compared with the relevant structural features of some other $[Mo_2]^{4+}$ complexes with carboxylate, alkoxide, or phenoxide ligands. As shown in Table 3.5, the metal-metal distance in **2**(THF) is about 0.03 Å longer than the distance of Mo1-Mo2 in the carboxylate complexes $[Mo_2(O_2CCH_3)_4]$ and $[Mo_2(O_2CCF_3)_4]$. The Mo-$\underline{4}$-Mo separation and Mo-O_{ligand} distances of **2**(THF) are more similar to corresponding values in the alkoxide and phenoxide complexes listed in Table 3.5. As was proposed for these latter compounds,[23,24] repulsive interactions of electrons in the filled p_π phenol and phenoxide oxygen atomic orbitals with those in the filled Mo-Mo δ orbital of **2**(THF)·C_6H_6 are likely to occur. This interaction is possible

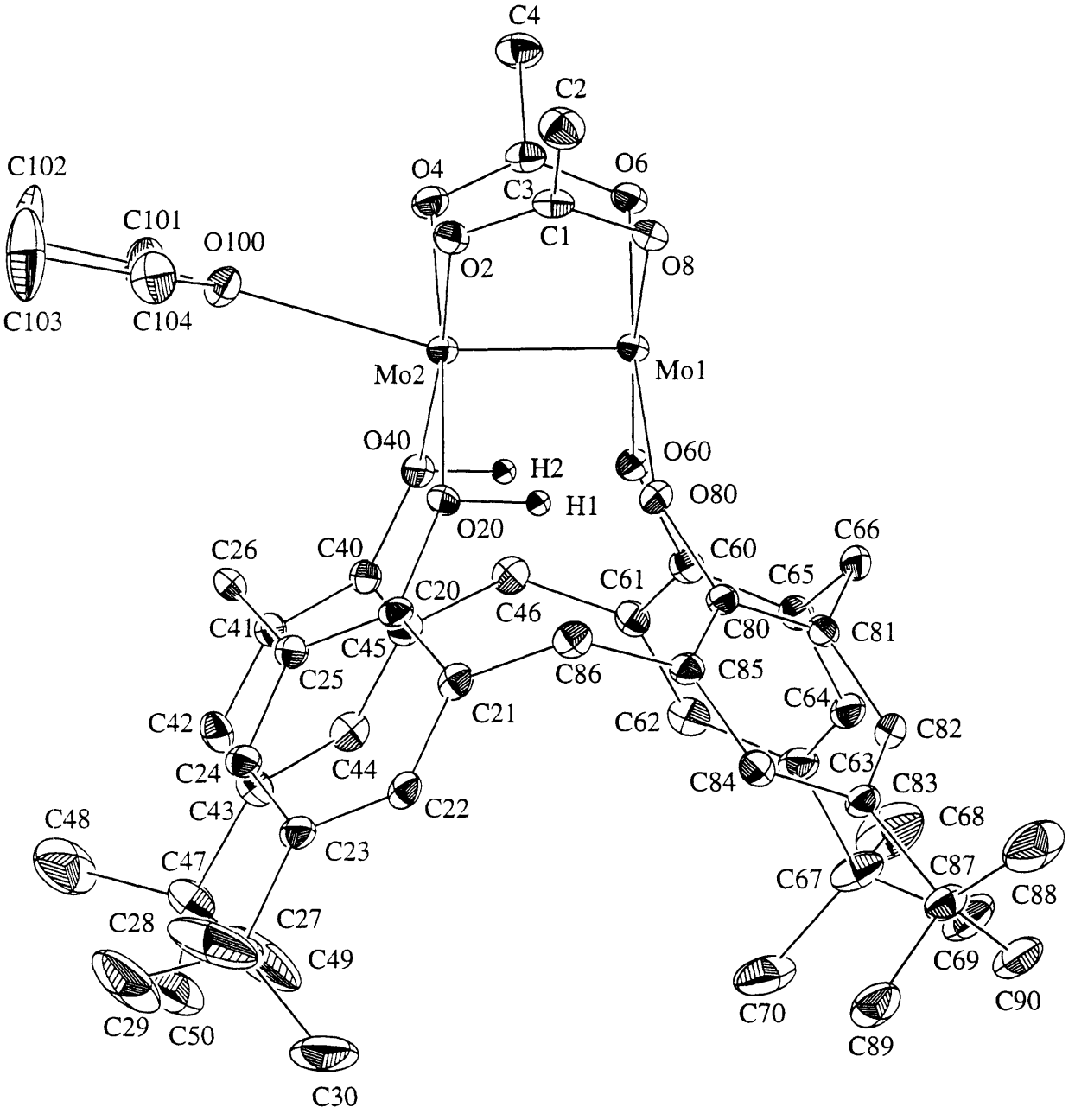

Figure 3.2. An ORTEP drawing of $[Mo_2(O_2CCH_3)_2(H_2$-*p*-*tert*-butylcalix[4]arene)(THF)], **2**(THF), showing the 30% thermal ellipsoids for all non-hydrogen atoms and the atom labeling scheme.

in the bridging mode of calixarene binding found in **2**(THF)·C_6H_6 for which the average Mo-O-C(calix) angle is 145°, consistent with approximate sp^2 hybridization of the oxygen atoms.

The hydrogen atoms H1 and H2 were located and refined without difficulty, revealing asymmetric hydrogen bonding interactions (O20-H1 = 1.06 (5), H1···O80 = 1.32 (6) Å; O40-H2 = 0.99 (5), H2···O60 = 1.43 (5) Å) parallel to the Mo$\equiv$Mo vector in the solid state. These hydrogen bonds are extremely strong (O40···O60 = 2.403 (4) Å, O20···O80 = 2.380 (4) Å) compared to other asymmetric hydrogen bonds, such as those in the complexes $[M_2(O\text{-}i\text{-}Pr)_8(HO\text{-}i\text{-}Pr)_2]$ (M = Zr, Ce) for which the O···O separation was 2.76-2.78 Å.[25,26] The metal-metal distances in these latter complexes (3.50 Å for M = Zr and 3.77 Å for M = Ce) indicate nonbonding interactions. In contrast, in the dimolybdenum quadruply-bonded complexes $[Mo_2(O\text{-}i\text{-}Pr)_4(HO\text{-}i\text{-}Pr)_4]$ and $[Mo_2(O\text{-c-Pen})_4(HO\text{-c-Pen})_4]$ the O···O distances were also quite short, *ca.* 2.40 Å.[24] The hydrogen atoms were not located in these structures. In solution, complexes **2-5** show only one resonance for the hydrogen bonded hydroxyl protons in the ^1H NMR, at *ca.* 16.9 ppm. Similarly, the hydroxyl proton chemical shift of the $[Mo_2(OR)_4(HOR)_4]$ complexes is at ca. 12.5 ppm.[24] These chemical shifts are significantly downfield of the δ = 6.3 ppm shift of the hydroxyl protons of $[Zr_2(O\text{-i-Pr})_8(HO\text{-i-Pr})_2]$,[25,26] in which the metals are not bonded to one another. These differences reflect the large diamagnetic anisotropy of the Mo$\equiv$Mo bond.[27,28]

As shown in Figure 3.2, there is a THF molecule bound axially to molybdenum atom of **2** in the solid state. Although axial ligation of the metal-metal quadruple bond is well-precedented, it is more usual in dichromium compounds, where there are typically two such ligands rather than one.[5] The Mo-O(THF) distance of 2.552 (3) Å is among the shortest reported for the dimolybdenum complexes axially ligated by THF. Examples include

$[Mo_2(S_2COC_2H_5)_4(THF)_2]$ (Mo-O(THF) = 2.795 (1) Å),[29] $[Mo_2\{(2,6\text{-}Me_2C_6H_3)NC(H)O\}_4(THF)_2]$ (Mo-O(THF) = 2.564 (5) Å),[30] $[Mo_2\{(2,6\text{-}Me_2C_6H_3)N)_2CCH_3\}_2(O_2CCH_3)_2(THF)_2]$ (Mo-O(THF) = 2.709 (6) Å),[31] and $[Mo(C_5H_3O_2S)_4(THF)_2]$ (Mo-O(THF) = 2.593 (5) Å).[32] A remarkable feature of the extended lattice of **2**(THF) can be seen in the packing diagrams (Figures 3.3 and 3.4). The axially-coordinated THF molecule of one complex is included in the pocket of the calixarene in the neighboring complex. Inclusion by the *p-tert*-butylcalix[4]arene macrocycle has been seen in the solid state for a variety of neutral molecules, such as toluene,[33] benzene and xylene,[34] and anisole.[34] Such inclusion has been explained in part by invoking alkyl-phenyl interactions.[35] In the case of **2**(THF), the calixarene macrocycle has aided in the organization of an intimately connected extended structure as shown in Figure 3.5. Each complex is weakly coordinated to the neighboring molecules through axial interactions via Mo-O bonds with Mo···O distances of 3.45 Å, and the axial ligation of a THF molecule included in the next calixarene basket. The closest *endo*-calix interaction of 3.50 Å occurs between C102 of the THF molecule and the plane of the phenyl ring C20-C25. This value is similar to that found in other calixarene inclusion complexes.[36,37]

Electronic Spectra of Products 2-5. All of the compounds **2-5** are highly colored in various shades of red and orange and their UV-visible absorption spectra share common features. The UV-visible spectrum of **2** in THF is shown as an example in Figure 3.6. The lowest energy transitions for **2-5** occur at λ_{max}, nm (ε/Mo $cm^{-1}M^{-1}$) 514 (875), 530 (1005), 512 (591), and 528 (719), respectively.

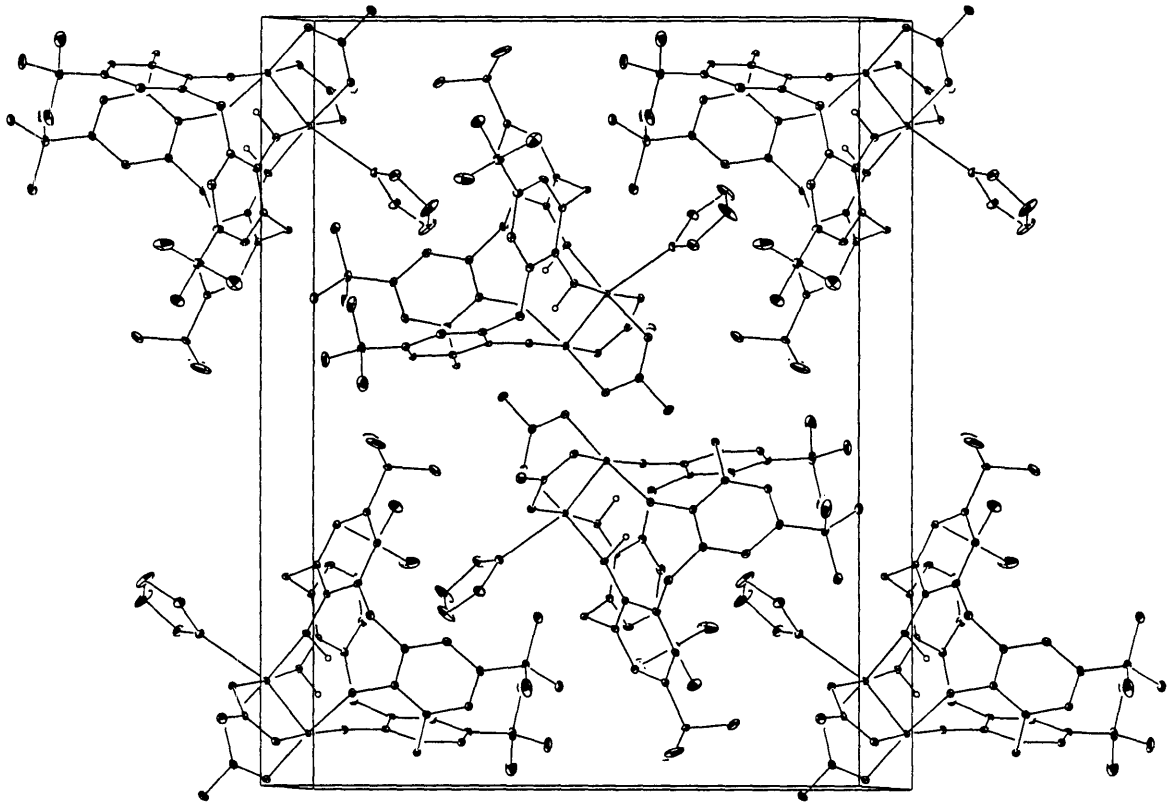

Figure 3.3. An ORTEP packing diagram of $[Mo_2(O_2CCH_3)_2(H_2$-*p*-*tert*-butyl-calix[4]arene)(THF)], (**2**)(THF). Benzene molecules in the lattice were omitted for clarity.

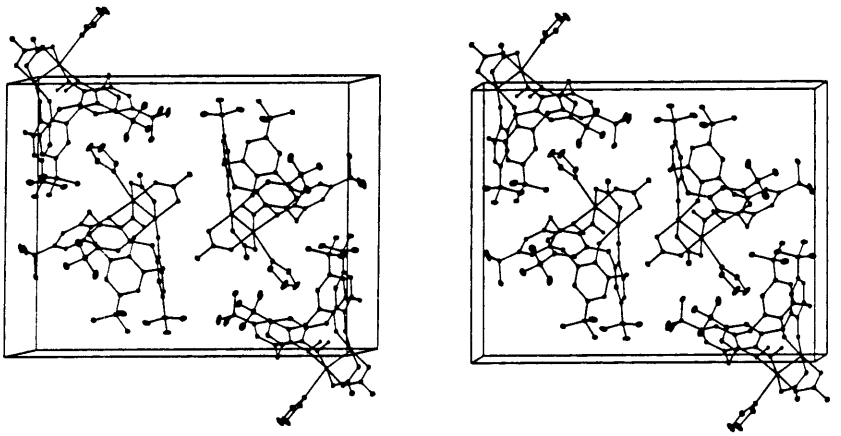

Figure 3.4. A stereo ORTEP drawing of $[Mo_2(O_2CCH_3)_2(H_2$-*p*-*tert*-butylcalix[4]arene)(THF)], (**2**)(THF). Benzene molecules in the lattice were omitted for clarity.

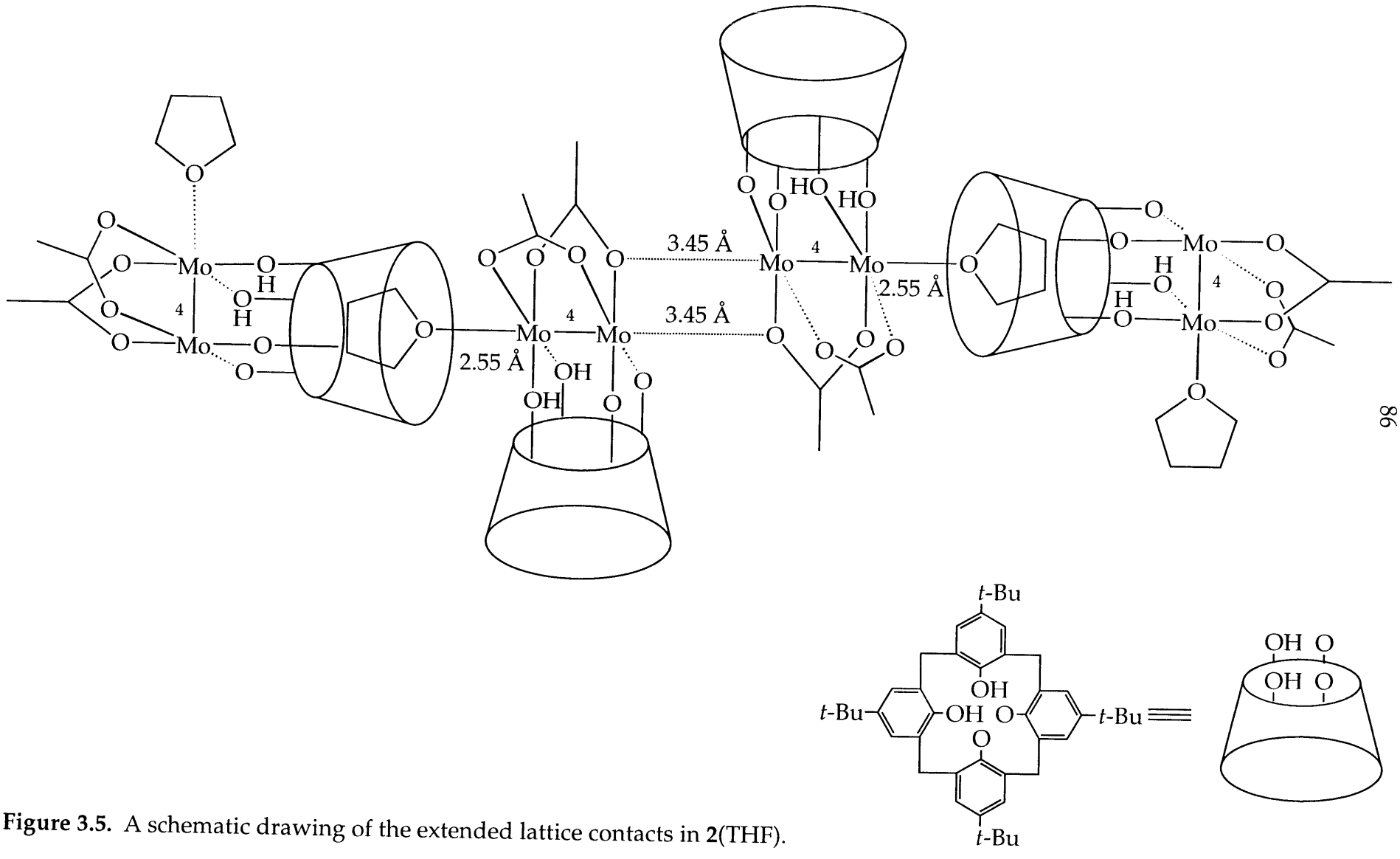

Figure 3.5. A schematic drawing of the extended lattice contacts in **2**(THF).

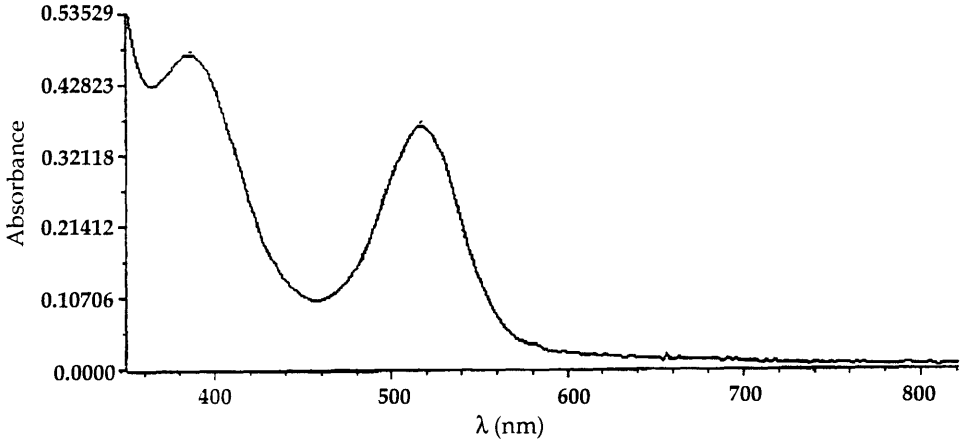

Figure 3.6. UV-visible spectrum of $[Mo_2(O_2CCH_3)_2(H_2$-*p*-*tert*-butylcalix-[4]arene)] (**2**).

These data are similar to the lowest energy transitions seen for other $[Mo_2]^{4+}$ complexes, such as $[Mo_2(O_2CCH_3)_4]$ (λ_{max}, 435 nm; ε, 150 $M^{-1}cm^{-1}$)[38] and $[Mo_2(O_2CCF_3)_4]$ (λ_{max}, 435 nm; ε, 120 $M^{-1}cm^{-1}$),[11] which were assigned as metal-metal $\delta \rightarrow \delta^*$ transitions. The experimentally observed red-shift of this band in the calixarene substituted products **2-5** is consistent with preliminary Fenske-Hall calculations on **2**, revealing significant antibonding contributions from the lone pairs of the phenol and phenoxide moieties of the calixarene macrocycle to the Mo-Mo δ orbital.[39] Moreover, the intensities of the $\delta \rightarrow \delta^*$ transitions of **2-5** are considerably larger than the intensities of the corresponding bands in $[Mo_2(O_2CCH_3)_4]$ and $[Mo_2(O_2CCF_3)_4]$. This result is also consistent with the effects of ligand orbital mixing with δ,δ^* orbitals.[40] Higher energy bands

observed in the electronic spectra of **2-5** are due to ligand to metal charge transfer.

Vibrational Spectroscopy. Resonance Raman Studies of $[Mo_2(O_2CCH_3)_2(H_2$-*p*-*tert*-butylcalix[4]arene)] (2), $[Mo_2(O_2CCF_3)_2(H_2$-*p*-*tert*-butylcalix[4]arene)] (3), $[Mo_2(O_2CCH_3)_2(H_2$-calix[4]arene)] (4), and $[Mo_2(O_2CCF_3)_2(H_2$-calix[4]arene)] (5). The 250-500 cm^{-1} region of the Raman spectra of **2-5** in THF are shown in Figures 3.7-3.10, respectively. The position, intensity, and breadth of the bands at 378, 360, 379, 357 cm^{-1} for **2-5**, respectively, are characteristic of the totally symmetric υ(Mo-Mo) vibration.[41] For complexes **2-5**, which have approximate C_{2v} symmetry, the totally symmetric vibration has A_1 symmetry.

The choice of excitation at 514.5 nm in the Raman studies of **2-5** was made to coincide with their δ-δ^* transitions, providing resonance enhancement of the bands. Resonance enhancement of the Raman spectra for molybdenum-molybdenum quadruply-bonded species was first observed in 1973,[42] and since has been widely utilized then for the study of metal-metal bonded species.[41] In general, the frequency of the Raman vibration increases with the order of the bond being investigated.[43,44] In the case of quadruply-bonded dimolybdenum complexes, the assignment of the A_1 vibration as molybdenum-molybdenum stretching is only a rough approximation, since there is most likely also some ligand character. A comparison of Raman and infrared frequencies for the A_1 vibration and Mo$\underline{4}$Mo bond distances for some dimolybdenum complexes, including **2-5**, is made in Table 3.6. These data suggest that, although there is not a strict correlation between Raman frequencies and Mo$\underline{4}$Mo bond distances, **2** occupies a predictable position in a discernible pattern. In this series, the higher the frequency of the Raman band corresponding to the A_1 vibration, the shorter the Mo$\underline{4}$Mo bond. Axial ligands can also have a substantial effect on the

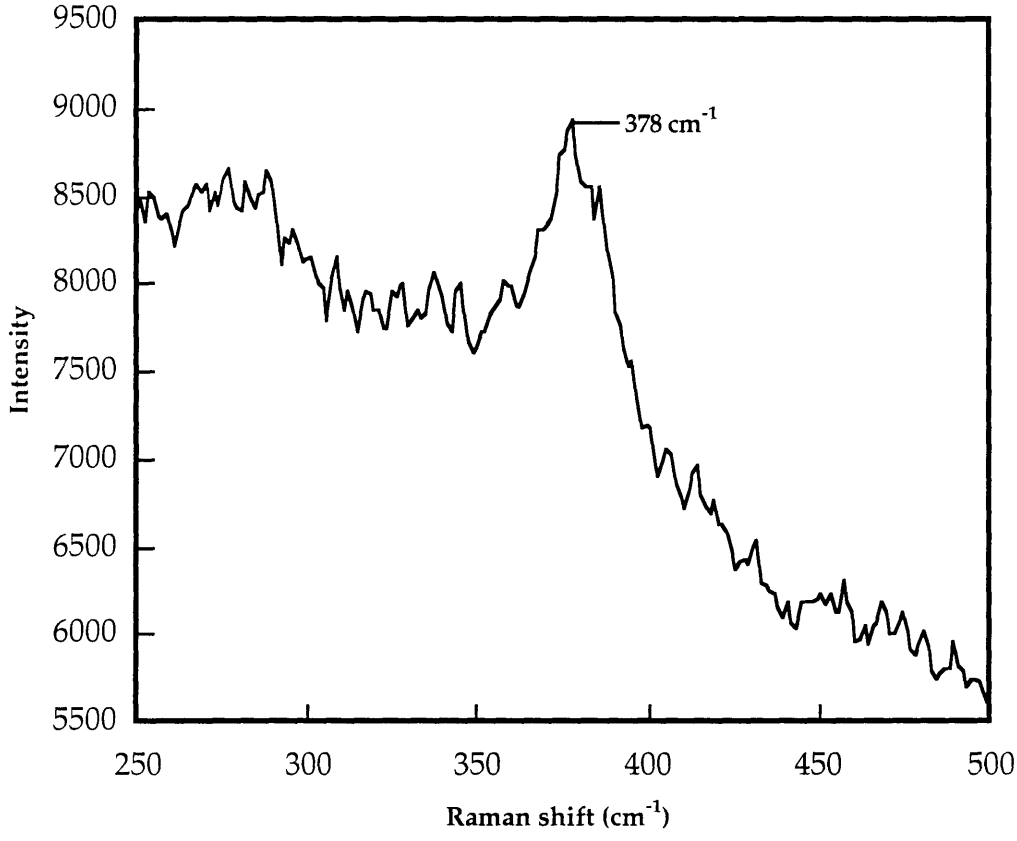

Figure 3.7. Resonance Raman spectrum (250-500 cm^{-1}) of $[Mo_2(O_2CCH_3)_2(H_2$-*p*-*tert*-butylcalix[4]arene)] (**2**) recorded in THF solution with 514.5 nm excitation.

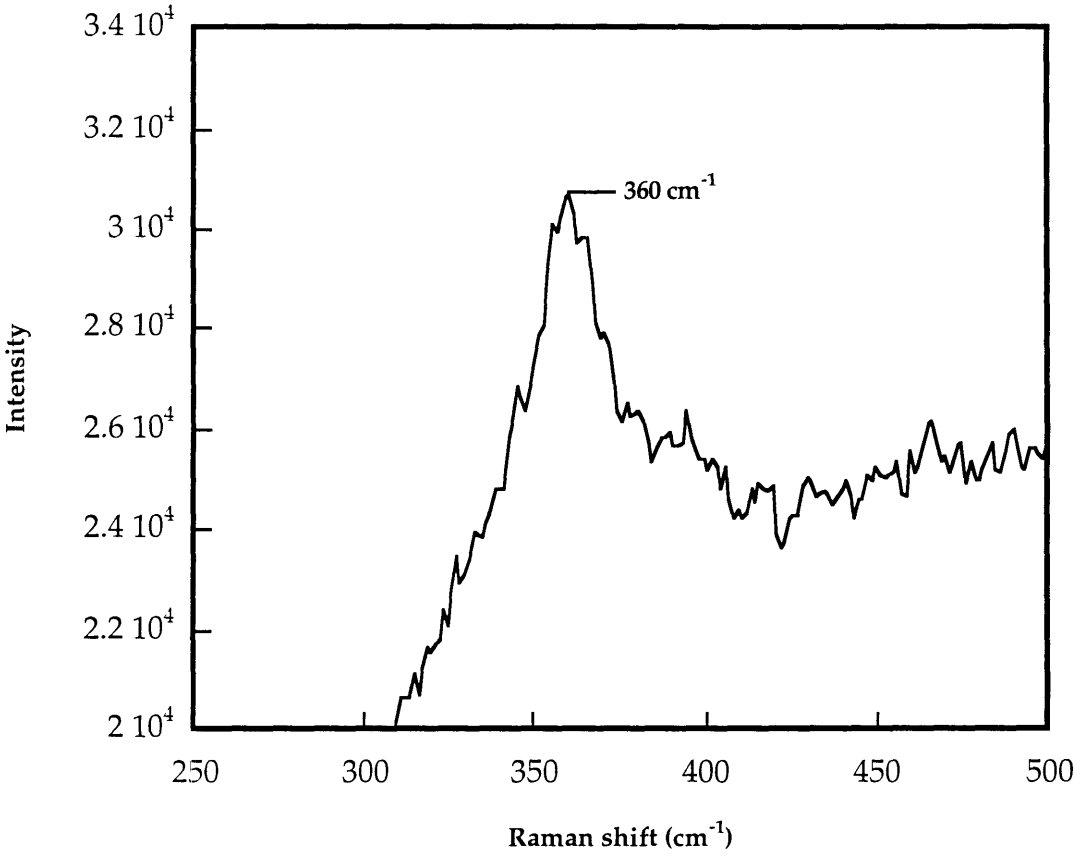

Figure 3.8. Resonance Raman spectrum (250-500 cm^{-1}) of $[Mo_2(O_2CCF_3)_2(H_2$-*p*-*tert*-butylcalix[4]arene)] (**3**) recorded in THF solution with 514.5 nm excitation.

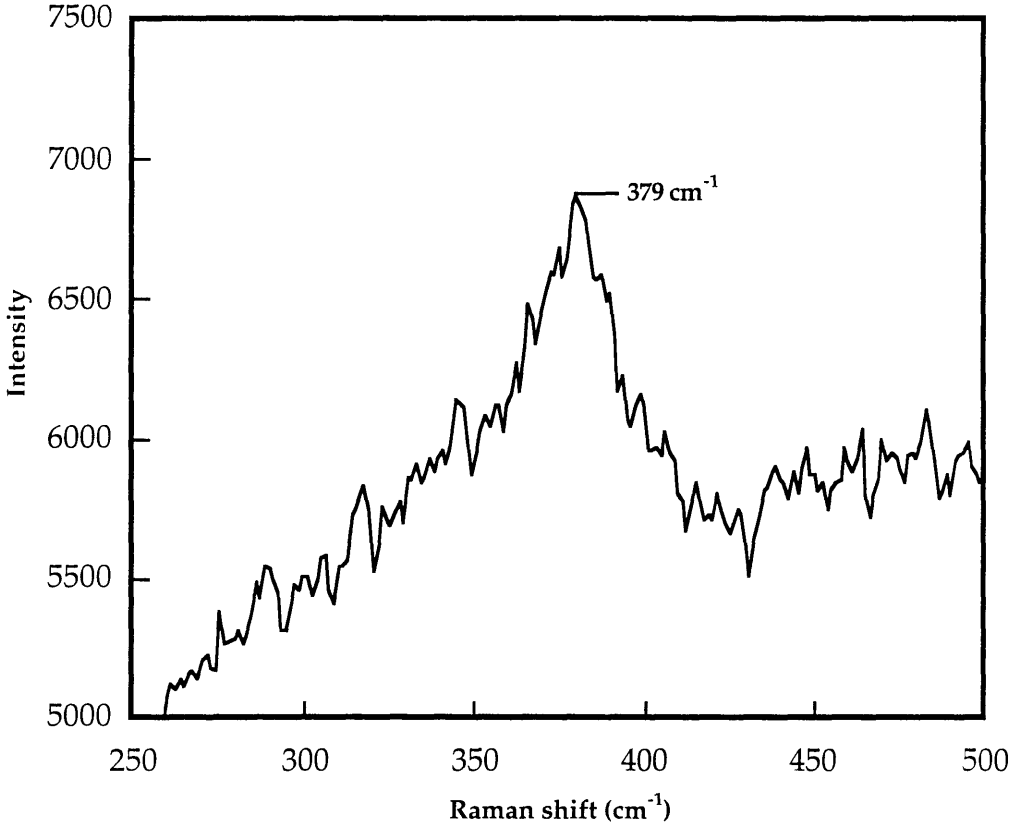

Figure 3.9. Resonance Raman spectrum (250-500 cm^{-1}) of $[Mo_2(O_2CCH_3)_2(H_2$-calix[4]arene)] (**4**) recorded in THF solution with 514.5 nm excitation.

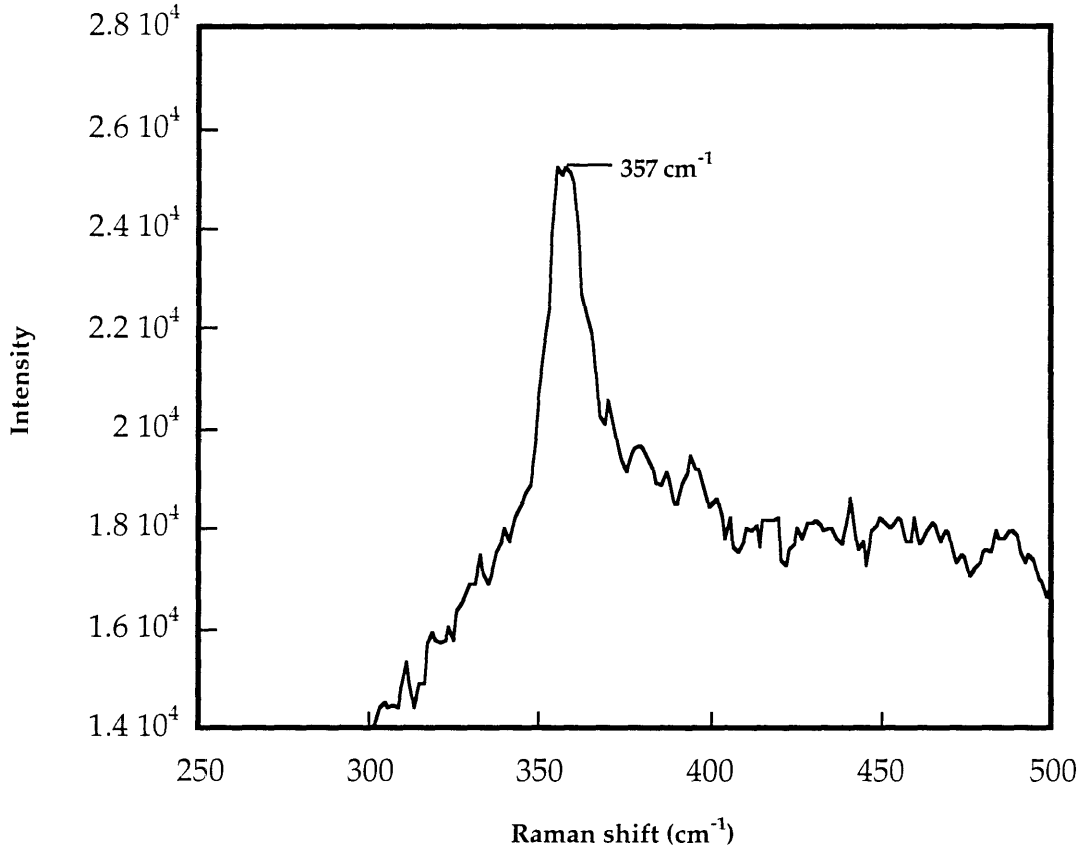

Figure 3.10. Resonance Raman spectrum (250-500 cm^{-1}) of $[Mo_2(O_2CCF_3)_2(H_2$-calix[4]arene)] (**5**) recorded in THF solution with 514.5 nm excitation.

observed frequency of the A_1 vibration, lowering the value by 30-40 cm^{-1}, as seen in comparing ν(Mo-Mo) of 397 cm^{-1} for $[Mo_2(O_2CCF_3)]$ and 367 cm^{-1} for $[Mo_2(O_2CCF_3)(py)_2]$ in Table 3.6. ^1H NMR and structural evidence support axial ligation of **2-5** by THF, and this effect must also be taken into account in the resonance Raman spectra of **2-5** in THF solution. The products **2-5**, unlike many of the published dimolybdenum quadruply-bonded complexes, do not have centers of inversion. The rule of mutual exclusion does not apply,[45] and the A_1 vibration of **2-5** is also IR active, giving rise to stretches at 381, 376, 358, and 358 cm^{-1}, respectively.

Conclusions

Four novel calix[4]arene complexes of the dimolybdenum quadruple bond have been prepared by reacting doubly-deprotonated calix[4]arene and *p-tert*-butylcalix[4]arene with the labile complexes $[Mo_2(O_2CCH_3)_2(NCCH_3)_6]$-$[BF_4]_2$ and $[Mo_2(O_2CCF_3)_2(NCCH_3)_6][BF_4]_2$ (**1**), a new and effective starting material for quadruply-bonded dimolybdenum products. The geometry and electronic structure of the products $[Mo_2(O_2CCH_3)_2(H_2$-*p-tert*-butylcalix[4]arene)] (**2**), $[Mo_2(O_2CCF_3)_2(H_2$-*p-tert*-butylcalix[4]arene)] (**3**), $[Mo_2(O_2CCH_3)_2(H_2$calix[4]-arene)] (**4**), and $[Mo_2(O_2CCF_3)_2(H_2$-calix[4]arene)] (**5**) were probed by ^1H NMR, X-ray crystallography, and electronic and vibrational spectroscopy. These studies indicate that the bridging mode of calixarene binding in this class of complexes allows for interaction of filled ligand orbitals with the Mo-Mo δ bond, a result supported by preliminary Fenske-Hall calculations on **2**(THF). In the solid state, $[Mo_2(O_2CCH_3)_2(H_2$-*p-tert*-butylcalix[4]arene)(THF)]·C_6H_6 (2(THF)-

·C_6H_6) has an intimately connected extended structure organized in part by the inclusion capability of the *p-tert*-butylcalix[4]arene macrocycle.

References

(1) Gutsche, C. D. *Calixarenes*; The Royal Society of Chemistry: Cambridge, 1989; Vol. 1.

(2) Preparations of standard calix[4,6,8]arenes: (a) Gutsche, C. D.; Iqbal, M. *Org. Synth* **1989**, *68*, 234. (b) Gutsche, C. D.; Dhawan, B.; Leonis, M.; Stewart, D. *Org. Synth.* **1989**, *68*, 238. (c) Munch, J. H.; Gutsche, C. D. *Org. Synth.* **1989**, *68*, 243.

(3) For some examples, see: (a) Andreetti, G.D. *J. Chem. Soc., Chem. Commun.* **1979**, 1005. (b) McKervey, M.A.; Seward, E.M. *J. Org. Chem. 51*, **1986**, 3581. (c) Bott, S.G.; Coleman, A.W.; Atwood, J.L. *J. Am. Chem. Soc.* **1986**, *108*, 1709. (d) Andreetti, G.D.; Ugozzoli, F.; Ungaro, R.; Pochini, A. in *Inclusion Compounds*; Atwood, J. L., ed.; Oxford Science: New York, 1984; Vol 4. (e) Atwood, J.L.; Orr, G.W.; Juneja, R.K.; Bott, S.G.; Hamada, F. *Pure & Appl. Chem.* **1993**, *65*, 1471.

(4) Examples include: (a) Olmstead, M.M.; Sigel, G.; Hope, H.; Xu, X.; Power, P.P. *J. Am. Chem. Soc.* **1985**, *107*, 8087. (b) Bott, S.G.; Coleman, A.W.; Atwood, J.L. *J. Chem. Soc., Chem. Commun.* **1986**, 610. (c) Hofmeister, G.E.; Hahn, F.E.; Pedersen, S.F. *J. Am. Chem. Soc.* **1989**, *111*, 2318. (d) Hofmeister, G.E.; Alvarado, E.; Leary, J. A.; Yoon, D. J.; Pedersen, S.F. *J. Am. Chem. Soc.* **1990**, *112*, 8843. (e) Corazza, F.; Floriani, C.; Chiesi-Villa, A.; Guastini, C. *J. Chem. Soc., Chem. Commun.* **1990**, 640. (f) Corazza, F.; Floriani, C.; Chiesi-Villa, A.; Guastini, C. *J. Chem. Soc., Chem. Commun.* **1990**, 1083. (g) Corazza, F.; Floriani, C.; Chiesi-Villa, A.; Rizzoli, C. *Inorg. Chem.* **1991**, *30*, 4465.

(5) Cotton, F. A.; Walton, R. A. *Multiple Bonds Between Metal Atoms;* 2nd ed. ; Oxford University Press: New York, 1993.

(6) Cotton, F. A.; Reid, A. H.; Schwotzer, W. *Inorg. Chem.* **1985**, *24*, 3965.

(7) Pimblett, G.; Garner, C. D.; Clegg, W. *J. Chem. Soc., Dalton Trans.* **1986**, 1257.

(8) A preliminary report of this work has been accepted for publication: Acho, J. A.; Lippard, S. J. *Inorg. Chim. Acta*, **1994**, in press.

(9) Gutsche, C. D.; Levine, J. A.; Sujeeth, P. K. *J. Org. Chem.* **1985**, *50*, 5802.

(10) Gutsche, C. D.; Iqbal, M. *Org. Synth.* **1989**, *68*, 234.

(11) Cotton, F. A.; Norman, J. G. *J. Coord. Chem.* **1971**, *1*, 161.

(12) Carnahan, E. M.; Rardin, R. L.; Bott, S. G.; Lippard, S. J. *Inorg. Chem.* **1992**, *31*, 5193.

(13) Chapter II of this thesis.

(14) Kerbaol, J. M.; Furet, E.; Guerchais, J. E.; Le Mest, Y.; Saillard, J. Y.; Sala-Pala, J.; Toupet, L. *Inorg. Chem.* **1993**, *32*, 713.

(15) Mandon, D.; Giraudon, J.-M.; Toupet, L.; Sala-Pala, J.; Guerchais, J. E. *J. Am. Chem. Soc.* **1987**, *109*, 3490.

(16) Cotton, F. A.; Czuchajowska, J.; Feng, X. *Inorg. Chem.* **1990**, *29*, 4329.

(17) Pennesi, G.; Floriani, C.; Chiesi-Villa, A.; Guastini, C. *J. Chem. Soc., Chem. Commun.* **1988**, 350.

(18) Yang, C.-H.; Dzugan, S. J.; Goedken, V. L. *J. Chem. Soc., Chem. Commun.* **1986**, 1313.

(19) Tait, C. D.; Garner, J. M.; Collman, J. P.; Sattelberger, A. P.; Woodruff, W. H. *J. Am. Chem. Soc.* **1989**, *111*, 9072.

(20) Collman, J. P.; Garner, J. M.; Hembre, R. T.; Ha, Y. *J. Am. Chem. Soc.* **1992**, *114*, 1292.

(21) Cotton, F. A.; Curtis, N. F.; Harris, C. B.; Johnson, B. F. G.; Lippard, S. J.; Mague, J. T.; Robinson, W. R.; Wood, J. S. *Science* **1964**, *145*, 1305.

(22) Cotton, F. A. *Inorg. Chem.* **1965**, *4*, 334.

(23) Chisholm, M. H.; Folting, K.; Huffman, J. C.; Tatz, R. J. *J. Am. Chem. Soc.* **1984**, *106*, 1153.

(24) Chisholm, M. H.; Folting, K.; Huffman, J. C.; Putilina, E. F.; Streib, W. E.; Tatz, R. J. *Inorg. Chem.* **1993**, *32*, 3771.

(25) Vaarstra, B. A.; Huffman, J. C.; Gradeff, P. S.; Hubert-Pfalzgraf, L. G.; Daran, J.-C.; Parraud, S.; Yunlu, K.; Caulton, K. G. *Inorg. Chem.* **1990**, *29*, 3126.

(26) Huggins, B. A.; Ellis, P. D.; Gradeff, P. S.; Vaarstra, B. A.; Yunla, K.; Huffman, J. C.; Caulton, K. G. *Inorg. Chem.* **1991**, *30*, 1720.

(27) San Filippo Jr., J. *Inorg. Chem.* **1972**, *11*, 3140.

(28) Cotton, F. A.; Kitagawa, S. *Polyhedron* **1988**, *7*, 1673.

(29) Ricard, L.; Karagiannidis, P.; Weiss, R. *Inorg. Chem.* **1973**, *12*, 2179.

(30) Cotton, F. A.; Ilsley, W. H. *Inorg. Chem.* **1980**, *19*, 3586.

(31) Cotton, F. A.; Ilsley, W. H.; Kaim, W. *Inorg. Chem.* **1981**, *20*, 930.

(32) Cotton, F. A.; Falvello, L. R.; Reid, A. H.; Roth, W. J. *Acta Cryst.* **1990**, *C46*, 1815.

(33) Andreetti, G. D. *J. Chem. Soc., Chem. Commun.* **1979**, 1005.

(34) Coruzzi, M.; Andreetti, G. D.; Bocchi, V.; Pochini, A.; Ungaro, R. *J. Chem. Soc., Perkin Trans. 2* **1982**, 1133.

(35) Andreetti, G. D.; Ori, O.; Ugozzoli, F.; Alfieri, C.; Pochini, A.; Ungaro, R. *J. Incl. Phenom.* **1988**, *6*, 523.

(36) Gutsche, C. D. *The Calixarenes*; Springer-Verlag: Berlin, 1984.

(37) Vicens, J.; Böhmer, V. *Calixarenes: A Versatile Class of Macrocyclic Compounds*; Kluwer Academic Publishers: Dordrecht, 1991.

(38) Martin, D. S.; Newman, R. A.; Fanwick, P. E. *Inorg. Chem.* **1979**, *18*, 2511.

(39) T. Ren (Florida Inst. of Tech.), personal communication.

(40) Hopkins, M. D.; Gray, H. B.; Miskowski, V. M. *Polyhedron* **1987**, *6*, 705.

(41) Clark, R. J. H.; Dines, T. J. *Angew. Chem., Int. Ed. Engl.* **1986**, *25*, 131.

(42) Angell, C. L.; Cotton, F. A.; Frenz, B. A.; Webb, T. R. *J. Chem. Soc., Chem. Commun.* **1973**, 399.

(43) Long, T. V.; Plane, R. A. *J. Chem. Phys.* **1965**, *43*, 457.

(44) Quicksall, C. O.; Spiro, T. G. *Inorg. Chem.* **1970**, *9*, 1045.

(45) Cotton, F. A. *Chemical Applications of Group Theory;* 3rd Edn. ; John Wiley and Sons: New York, 1993.

(46) Cotton, F. A.; Mester, Z. C.; Webb, T. R. *Acta Crystallogr., Sect. B* **1974**, *B30*, 2768.

(47) Abbott, R. G.; Cotton, F. A.; Falvello, L. R. *Inorg. Chem.* **1990**, *29*, 514.

(48) Cotton, F. A.; Wiesinger, K. J. *Inorg. Chem.* **1991**, *30*, 750.

(49) Bratton, W. K.; Cotton, F. A.; Debeau, M.; Walton, R. A. *J. Coord. Chem.* **1971**, *1971*, 121.

(50) San Filippo Jr., J.; Sniadoch, H. J. *Inorg. Chem.* **1973**, *12*, 2326.

(51) Ketteringham, A. P.; Oldham, C. *J. Chem. Soc., Dalton Trans.* **1973**, 1067.

(52) Clark, R. J. H.; Hempleman, A. J.; Kurmoo, M. *J. Chem. Soc., Dalton Trans.* **1988**, 973.

(53) Cotton, F. A.; Norman, J. G. *J. Am. Chem. Soc.* **1972**, *94*, 5967.

(54) Clark, R. J. H.; Franks, M. L. *J. Am. Chem. Soc.* **1975**, *97*, 2691.

(55) Brencic, J. V.; Cotton, F. A. *Inorg. Chem.* **1969**, *8*, 2698.

(56) Brencic, J. V.; Cotton, F. A. *Inorg. Chem.* **1969**, *8*, 7.

Table 3.1. X-ray Crystallographic Information for $[Mo_2(O_2CCH_3)_2(H_2$-*p*-*tert*-butylcalix[4]arene)(THF)]·C_6H_6 (2(THF)·C_6H_6). [a]

	(2)(THF)·C_6H_6
formula	$C_{58}H_{74}O_9Mo_2$
a (Å)	12.533 (2)
b (Å)	23.515 (3)
c (Å)	18.520 (2)
β (deg)	95.66 (2)
V (Å^3)	5432 (1)
T (°C)	-73.8
fw	1107.10
Z	4
ρ_{calc} (g/cm^3)	1.35
space group	$P2_1/c$
2θ limits (deg)	3-50
data limits	+h+k±l
μ (cm^{-1})	5.14
no. of total data	10775
no. of unique data	9787
R(merge)[b]	3.6
no. of unique observed[c] data	6251
no. of LS parameters	630
p factor	0.03
R[d] =	0.040
R_w =	0.042

[a] Data were collected on an Enraf Nonius CAD-4F kappa geometry diffractometer using Mo K_α radiation. [b] R(merge) = $\Sigma_{i=1}^{n}\Sigma_{j=1}^{m} | \langle F_i^2\rangle - F_{ij}^2 | / \Sigma_{i=1}^{n} m \times \langle F_i^2\rangle$ where n = number of reflections observed more than once, m = number of times a given reflection was observed, and $\langle F_i^2\rangle$ is the average value of F^2 for reflection i. [c] Observation criterion $I > 3\sigma(I)$. [d] $R = \Sigma | |F_o| - |F_c| | / \Sigma |F_o|$, $R_w = [\Sigma w (|F_o| - |F_c|)^2 / \Sigma w |F_o|^2]^{1/2}$, where $w = 1/\sigma(F)$, as defined in Carnahan, E. M.; Rardin, R. L.; Bott, S. G.; Lippard, S. J. *Inorg. Chem.* **1992**, *31*, 5193.

Table 3.2. Final Positional Parameters and B(eq) for $[Mo_2(O_2CCH_3)_2(H_2$-*p*-*tert*-butylcalix[4]arene)(THF)]·C_6H_6 (2)(THF)·C_6H_6 .[a]

atom	x	y	z	B(eq) Å$^{2\,b}$
Mo(1)	0.076149(33)	0.427805(17)	1.496705(21)	1.82(2)
Mo(2)	0.124205(32)	0.359315(17)	1.432370(21)	1.77(2)
O(2)	-0.01714(25)	0.36607(13)	1.36396(16)	2.2(1)
O(4)	0.20471(25)	0.41614(13)	1.36949(16)	2.2(1)
O(6)	0.15026(25)	0.48736(13)	1.43519(16)	2.2(1)
O(8)	-0.06722(25)	0.43743(13)	1.43096(16)	2.2(1)
O(20)	0.04272(24)	0.29712(13)	1.49181(17)	1.9(1)
O(40)	0.27119(25)	0.34497(13)	1.49919(17)	2.1(1)
O(60)	0.21662(24)	0.42337(13)	1.57012(16)	2.0(1)
O(80)	-0.00633(25)	0.37468(13)	1.56407(16)	2.2(1)
O(100)	0.17139(26)	0.29836(14)	1.32604(17)	2.5(1)
C(1)	-0.08515(38)	0.40370(20)	1.37739(25)	2.2(2)
C(2)	-0.18913(42)	0.40692(23)	1.33137(28)	3.2(2)
C(3)	0.20110(38)	0.46844(21)	1.38398(24)	2.2(2)
C(4)	0.25925(41)	0.51004(22)	1.33987(27)	2.9(2)
C(20)	0.05049(38)	0.24551(19)	1.52683(23)	2.0(2)
C(21)	-0.03045(37)	0.23158(19)	1.57143(24)	2.0(2)
C(22)	-0.02710(39)	0.17846(20)	1.60341(24)	2.2(2)
C(23)	0.05232(40)	0.13885(20)	1.59339(24)	2.3(2)
C(24)	0.13156(38)	0.15540(19)	1.55049(24)	2.1(2)
C(25)	0.13302(35)	0.20835(19)	1.51719(23)	1.9(2)
C(26)	0.22593(38)	0.22386(19)	1.47492(25)	2.1(2)
C(27)	0.05094(46)	0.07957(21)	1.62757(27)	2.9(2)
C(28)	-0.04819(71)	0.04885(29)	1.59974(45)	8.5(5)
C(29)	0.14540(75)	0.04407(31)	1.61140(52)	9.1(5)
C(30)	0.05900(78)	0.08445(28)	1.70832(37)	7.4(4)
C(40)	0.33440(36)	0.30525(19)	1.53704(24)	1.9(2)
C(41)	0.31887(36)	0.24678(19)	1.52404(24)	1.8(2)
C(42)	0.38961(39)	0.20955(19)	1.56166(26)	2.4(2)
C(43)	0.47204(38)	0.22637(21)	1.61232(27)	2.5(2)
C(44)	0.48301(36)	0.28431(22)	1.62409(25)	2.4(2)
C(45)	0.41623(37)	0.32394(20)	1.58740(25)	2.1(2)

Table 3.2 (cont). Final Positional Parameters and B(eq) for $[Mo_2(O_2CCH_3)_2(H_2$-*p-tert*-butylcalix[4]arene)(THF)]·C_6H_6 (2)(THF)·C_6H_6

atom	x	y	z	B(eq) Å$^{2\,b}$
C(46)	0.43072(37)	0.38687(20)	1.60467(25)	2.2(2)
C(47)	0.54584(44)	0.18238(24)	1.65164(32)	3.5(3)
C(48)	0.61906(54)	0.15712(32)	1.59850(42)	6.3(4)
C(49)	0.61346(74)	0.20758(31)	1.71437(47)	9.7(5)
C(50)	0.48142(52)	0.13356(28)	1.67993(36)	5.2(3)
C(60)	0.25387(38)	0.42308(19)	1.64271(25)	2.1(2)
C(61)	0.36017(38)	0.40824(19)	1.66116(25)	2.1(2)
C(62)	0.40053(39)	0.41029(21)	1.73376(27)	2.6(2)
C(63)	0.33890(40)	0.42707(20)	1.78854(25)	2.4(2)
C(64)	0.23311(40)	0.43988(19)	1.76775(24)	2.2(2)
C(65)	0.18677(38)	0.43864(19)	1.69609(24)	2.1(2)
C(66)	0.06948(37)	0.45225(19)	1.67936(24)	2.0(2)
C(67)	0.38971(45)	0.42956(26)	1.86736(26)	3.5(3)
C(68)	0.47886(59)	0.47412(33)	1.87306(33)	6.1(4)
C(69)	0.30911(54)	0.44354(30)	1.91998(29)	5.0(3)
C(70)	0.43910(49)	0.37135(31)	1.88829(31)	4.8(3)
C(80)	-0.03380(34)	0.36483(20)	1.63262(23)	1.8(2)
C(81)	-0.00381(35)	0.40253(19)	1.68895(24)	1.8(2)
C(82)	-0.04040(37)	0.39192(20)	1.75631(24)	2.2(2)
C(83)	-0.10424(36)	0.34546(20)	1.76989(24)	2.1(2)
C(84)	-0.12760(36)	0.30758(20)	1.71210(26)	2.1(2)
C(85)	-0.09363(35)	0.31644(20)	1.64387(24)	1.9(2)
C(86)	-0.11956(37)	0.27321(20)	1.58387(25)	2.3(2)
C(87)	-0.15352(40)	0.33822(23)	1.84192(26)	2.7(2)
C(88)	-0.26335(54)	0.36694(36)	1.83397(35)	6.5(4)
C(89)	-0.16732(52)	0.27556(25)	1.86172(29)	4.2(3)
C(90)	-0.08468(53)	0.36593(25)	1.90421(28)	4.1(3)
C(101)	0.10176(44)	0.25751(23)	1.28650(30)	3.5(3)
C(102)	0.17045(57)	0.22752(34)	1.23708(45)	7.1(4)
C(103)	0.26651(73)	0.25265(37)	1.24241(52)	9.5(6)
C(104)	0.27459(43)	0.29527(24)	1.30117(31)	3.7(3)
C(200)	0.64187(51)	0.05447(28)	0.96505(34)	4.5(3)

Table 3.2 (cont). Final Positional Parameters and B(eq) for $[Mo_2(O_2CCH_3)_2(H_2$-*p-tert*-butylcalix[4]arene)(THF)]·C_6H_6 (2)(THF)·C_6H_6 .

atom	x	y	z	B(eq) Å$^{2\,b}$
C(201)	0.68447(47)	0.10393(31)	0.99323(33)	4.5(3)
C(202)	0.63177(53)	0.15466(29)	0.97604(35)	4.6(3)
C(203)	0.53954(53)	0.15455(28)	0.93172(36)	4.7(3)
C(204)	0.49721(50)	0.10439(30)	0.90348(35)	4.9(3)
C(205)	0.54970(53)	0.05424(28)	0.91987(35)	4.8(3)
H(1)	0.0142(42)	0.3294(23)	1.5253(28)	5(1)
H(2)	0.2589(39)	0.3777(21)	1.5307(26)	3(1)

[a]Numbers in parentheses are estimated standard deviations of the last significant figure. See Figure 3.2 for atom labeling scheme. [b]$B_{eq} = 4/3\ [a^2\beta_{11} + b^2\beta_{22} + c^2\beta_{33} + 2ab\cos(\gamma)\beta_{12} + 2ac\cos(\beta)\beta_{13} + 2bc\cos(\alpha)\beta_{23}]$

Table 3.3. Complete Anisotropic Thermal Parameters for $[Mo_2(O_2CCH_3)_2(H_2$-*p-tert*-butylcalix[4]arene)(THF)]·C_6H_6 (2)(THF)·C_6H_6[a]

atom	U11	U22	U33	U12	U13	U23
Mo(1)	0.03088(23)	0.01845(21)	0.02001(21)	0.00106(18)	0.00285(17)	0.00282(17)
Mo(2)	0.02941(22)	0.01933(21)	0.01880(21)	-0.00031(18)	0.00342(16)	0.00207(17)
O(2)	0.0326(18)	0.0249(19)	0.0259(18)	0.0024(16)	-0.0005(15)	0.0020(15)
O(4)	0.0339(19)	0.0279(20)	0.0227(18)	-0.0023(15)	0.0049(15)	0.0033(14)
O(6)	0.0379(20)	0.0203(18)	0.0255(18)	0.0008(15)	0.0011(15)	0.0040(14)
O(8)	0.0318(18)	0.0236(18)	0.0269(18)	0.0040(15)	0.0016(15)	0.0049(15)
O(20)	0.0327(19)	0.0167(17)	0.0255(18)	-0.0003(14)	0.0070(15)	0.0048(14)
O(40)	0.0326(19)	0.0231(18)	0.0230(18)	0.0003(15)	0.0018(14)	-0.0008(14)
O(60)	0.0285(17)	0.0242(17)	0.0214(17)	-0.0002(14)	0.0017(14)	-0.0002(14)
O(80)	0.0367(19)	0.0256(18)	0.0216(17)	0.0023(15)	0.0079(15)	0.0008(14)
O(100)	0.0366(20)	0.0311(20)	0.0267(18)	-0.0079(16)	0.0081(15)	-0.0048(15)
C(1)	0.0297(27)	0.0275(27)	0.0243(26)	-0.0028(22)	-0.0002(21)	0.0087(21)
C(2)	0.0379(31)	0.0424(34)	0.0393(32)	0.0023(26)	-0.0058(26)	0.0021(25)
C(3)	0.0311(27)	0.0294(29)	0.0228(26)	-0.0033(22)	-0.0027(21)	0.0051(22)
C(4)	0.0439(32)	0.0315(30)	0.0369(31)	-0.0078(25)	0.0062(25)	0.0108(24)
C(20)	0.0355(28)	0.0210(25)	0.0170(24)	-0.0060(21)	-0.0009(20)	-0.0000(19)
C(21)	0.0279(26)	0.0260(27)	0.0233(25)	-0.0068(21)	0.0002(21)	-0.0046(20)
C(22)	0.0393(29)	0.0226(26)	0.0220(26)	-0.0109(22)	0.0055(22)	-0.0062(20)
C(23)	0.0452(30)	0.0227(26)	0.0203(25)	-0.0050(23)	0.0004(22)	-0.0015(21)
C(24)	0.0352(27)	0.0224(26)	0.0211(25)	-0.0023(21)	-0.0038(21)	-0.0007(20)
C(25)	0.0277(25)	0.0210(25)	0.0215(24)	-0.0036(20)	-0.0020(20)	-0.0028(20)
C(26)	0.0354(28)	0.0174(25)	0.0288(27)	0.0040(21)	0.0040(22)	0.0022(20)
C(27)	0.0613(37)	0.0209(27)	0.0271(28)	-0.0069(26)	0.0003(25)	0.0076(21)
C(28)	0.1411(79)	0.0362(42)	0.1308(72)	-0.0371(46)	-0.0624(62)	0.0388(44)
C(29)	0.1420(82)	0.0417(46)	0.1750(90)	0.0267(49)	0.0844(72)	0.0545(53)
C(30)	0.1854(90)	0.0438(44)	0.0503(43)	-0.0143(50)	-0.0032(51)	0.0240(34)
C(40)	0.0233(25)	0.0266(27)	0.0244(26)	0.0044(20)	0.0066(20)	0.0016(20)
C(41)	0.0219(24)	0.0233(26)	0.0243(25)	0.0016(20)	0.0029(20)	-0.0004(20)
C(42)	0.0356(28)	0.0174(24)	0.0378(29)	-0.0019(22)	0.0041(23)	-0.0040(22)
C(43)	0.0287(27)	0.0273(29)	0.0398(31)	0.0046(22)	0.0015(23)	0.0014(23)
C(44)	0.0249(26)	0.0369(30)	0.0287(27)	-0.0025(23)	0.0019(21)	-0.0009(23)
C(45)	0.0270(26)	0.0274(28)	0.0272(27)	-0.0025(21)	0.0080(21)	0.0011(21)

Table 3.3 (cont). Complete Anisotropic Thermal Parameters for $[Mo_2(O_2CCH_3)_2(H_2$-*p*-*tert*-butylcalix[4]arene)(THF)]·C_6H_6 (2)(THF)·C_6H_6[a]

atom	U11	U22	U33	U12	U13	U23
C(46)	0.0249(25)	0.0308(28)	0.0267(26)	-0.0033(21)	-0.0019(21)	-0.0026(21)
C(47)	0.0379(32)	0.0383(34)	0.0536(38)	0.0112(26)	-0.0041(28)	0.0089(28)
C(48)	0.0563(44)	0.0834(57)	0.1013(61)	0.0343(41)	0.0147(42)	0.0268(46)
C(49)	0.1576(85)	0.0467(47)	0.1381(76)	0.0234(52)	-0.1133(68)	-0.0026(48)
C(50)	0.0618(43)	0.0556(45)	0.0790(49)	0.0197(36)	0.0047(37)	0.0242(37)
C(60)	0.0368(28)	0.0147(24)	0.0276(26)	-0.0082(21)	0.0028(22)	-0.0011(19)
C(61)	0.0319(27)	0.0176(25)	0.0310(28)	-0.0054(20)	0.0043(22)	-0.0010(20)
C(62)	0.0303(28)	0.0304(29)	0.0361(30)	-0.0021(22)	-0.0006(23)	0.0030(23)
C(63)	0.0440(31)	0.0247(26)	0.0237(26)	-0.0065(24)	0.0003(22)	0.0024(21)
C(64)	0.0406(30)	0.0227(26)	0.0218(25)	-0.0060(22)	0.0022(22)	-0.0030(20)
C(65)	0.0335(27)	0.0189(25)	0.0272(26)	-0.0042(21)	0.0031(21)	-0.0006(20)
C(66)	0.0334(27)	0.0209(25)	0.0237(25)	-0.0008(21)	0.0057(21)	-0.0023(20)
C(67)	0.0492(35)	0.0609(39)	0.0225(28)	-0.0132(31)	-0.0043(25)	0.0027(27)
C(68)	0.0886(55)	0.0937(60)	0.0450(40)	-0.0367(46)	-0.0136(38)	-0.0109(39)
C(69)	0.0770(47)	0.0888(54)	0.0218(30)	0.0127(40)	-0.0004(30)	-0.0038(32)
C(70)	0.0516(38)	0.0964(56)	0.0359(34)	0.0131(38)	0.0024(29)	0.0228(35)
C(80)	0.0226(23)	0.0267(27)	0.0208(24)	0.0070(20)	0.0040(19)	0.0033(20)
C(81)	0.0229(24)	0.0201(24)	0.0256(26)	0.0026(19)	0.0052(20)	0.0028(20)
C(82)	0.0339(27)	0.0276(28)	0.0216(25)	0.0046(22)	0.0044(21)	-0.0021(21)
C(83)	0.0277(26)	0.0327(29)	0.0216(25)	0.0031(22)	0.0074(20)	0.0032(21)
C(84)	0.0239(25)	0.0255(27)	0.0331(28)	0.0011(20)	0.0091(21)	0.0038(21)
C(85)	0.0232(25)	0.0277(27)	0.0222(25)	0.0036(20)	0.0001(20)	0.0022(20)
C(86)	0.0274(26)	0.0305(29)	0.0290(28)	-0.0059(22)	0.0048(22)	0.0009(21)
C(87)	0.0351(30)	0.0446(33)	0.0243(27)	-0.0003(25)	0.0087(23)	0.0050(23)
C(88)	0.0634(46)	0.1341(72)	0.0538(43)	0.0410(48)	0.0318(37)	0.0253(46)
C(89)	0.0800(46)	0.0476(38)	0.0371(34)	-0.0199(33)	0.0237(32)	0.0023(28)
C(90)	0.0869(48)	0.0464(38)	0.0251(30)	-0.0195(34)	0.0119(31)	-0.0011(26)
C(101)	0.0389(32)	0.0412(34)	0.0504(36)	-0.0091(27)	-0.0019(27)	-0.0097(28)
C(102)	0.0562(46)	0.0915(62)	0.1205(68)	-0.0001(42)	0.0017(46)	-0.0791(54)
C(103)	0.1099(72)	0.1125(73)	0.1530(85)	-0.0477(58)	0.0878(66)	-0.1017(66)
C(104)	0.0381(32)	0.0458(36)	0.0582(39)	-0.0082(27)	0.0175(29)	-0.0146(30)
C(200)	0.0546(41)	0.0618(46)	0.0548(40)	0.0126(35)	-0.0022(33)	0.0124(34)

Table 3.3 (cont). Complete Anisotropic Thermal Parameters for $[Mo_2(O_2CCH_3)_2(H_2$-*p*-*tert*-butylcalix[4]arene)(THF)]·C_6H_6 (2)(THF)·C_6H_6[a]

atom	U11	U22	U33	U12	U13	U23
C(201)	0.0394(35)	0.0840(54)	0.0472(39)	-0.0003(36)	-0.0055(29)	0.0050(36)
C(202)	0.0545(41)	0.0662(48)	0.0564(42)	-0.0003(36)	0.0083(34)	-0.0099(35)
C(203)	0.0557(41)	0.0544(43)	0.0682(46)	0.0154(34)	0.0124(35)	0.0056(35)
C(204)	0.0464(39)	0.0729(50)	0.0614(44)	0.0122(37)	-0.0138(33)	0.0038(38)
C(205)	0.0610(44)	0.0563(44)	0.0630(45)	0.0045(35)	-0.0055(36)	-0.0047(34)

[a]See Figure 3.2 for atom labeling scheme. Numbers in parentheses are estimated standard deviations in the last significant digit. The anisotropic temperature factors are of the form $\exp[-2\pi^2(U_{11}h^2a^{*2} \ldots +2U_{12}hka^*b^* = \ldots)]$.

Table 3.4. Selected Interatomic Bond Distances (Å) and Angles (deg) for $[Mo_2(O_2CCH_3)_2(H_2$-*p*-*tert*-butylcalix[4]arene)(THF)]·C_6H_6 (2)(THF)·C_6H_6 [a]

Bond Distances (Å)

Mo(1)-Mo(2)	2.1263(6)	O(2)-C(1)	1.271(5)
Mo(1)-O(6)	2.081(3)	O(4)-C(3)	1.261(5)
Mo(1)-O(8)	2.083(3)	O(6)-C(3)	1.274(5)
Mo(1)-O(60)	2.120(3)	O(8)-C(1)	1.273(5)
Mo(1)-O(80)	2.107(3)	O(20)-C(20)	1.376(5)
Mo(2)-O(2)	2.082(3)	O(20)-H(1)	1.06(5)
Mo(2)-O(4)	2.095(3)	O(40)-C(40)	1.373(5)
Mo(2)-O(20)	2.148(3)	O(40)-H(2)	0.99(5)
Mo(2)-O(40)	2.144(3)	O(60)-C(60)	1.380(5)
O(100)-Mo(2)	2.552(3)	O(80)-C(80)	1.368(5)

Bond Angles (deg)

Mo(2)-Mo(1)-O(6)	92.12(9)	O(2)-Mo(2)-O(4)	92.3(1)
Mo(2)-Mo(1)-O(8)	91.77(9)	O(2)-Mo(2)-O(20)	86.9(1)
Mo(2)-Mo(1)-O(60)	93.35(8)	O(2)-Mo(2)-O(40)	175.0(1)
Mo(2)-Mo(1)-O(80)	93.73(9)	O(4)-Mo(2)-O(20)	176.5(1)
O(6)-Mo(1)-O(8)	90.7(1)	O(4)-Mo(2)-O(40)	89.3(1)
O(6)-Mo(1)-O(60)	89.8(1)	O(20)-Mo(2)-O(40)	91.2(1)
O(6)-Mo(1)-O(80)	174.0(1)	Mo(2)-O(2)-C(1)	118.8(3)
O(8)-Mo(1)-O(60)	174.8(1)	Mo(2)-O(4)-C(3)	118.3(3)
O(8)-Mo(1)-O(80)	88.0(1)	Mo(1)-O(6)-C(3)	117.1(3)
O(60)-Mo(1)-O(80)	90.9(1)	Mo(1)-O(8)-C(1)	117.6(3)
Mo(1)-Mo(2)-O(2)	90.67(9)	Mo(2)-O(20)-C(20)	145.8(3)
Mo(1)-Mo(2)-O(4)	90.38(9)	Mo(2)-O(40)-C(40)	145.4(3)
Mo(1)-Mo(2)-O(20)	93.08(9)	Mo(1)-O(60)-C(60)	143.7(3)
Mo(1)-Mo(2)-O(40)	94.07(9)	Mo(1)-O(80)-C(80)	146.4(3)

[a]See Figure 3.2 for atom labeling scheme. Estimated standard deviations in the least significant figure are given in parentheses.

Table 3.5. Structural Parameters for Some $[Mo_2]^{4+}$ Complexes

	Bond Distances, Å	
Compound	Mo-Mo	average Mo-O
$[Mo_2(O_2CCH_3)_2(H_2$-*p*-*tert*-butylcalix[4]arene)(THF)]		2.11 (O_{calix})
(**2**)(THF)	2.1263 (6)	2.15 (HO_{calix})
		2.08 ($O_{acetate}$)
$[Mo_2(O_2CCH_3)_4]$[46]	2.0934 (8)	2.12
$[Mo_2(O_2CCF_3)_4]$[11]	2.090 (4)	2.06
$[Mo_2(O_2CCH_3)_2(TMTAA)]$*,[14]	2.106 (1)	2.12
$[Mo_2(O$-*i*-$Pr)_4(HO$-*i*-$Pr)_4]$[24]	2.110 (3)	2.09 (OR)
		2.17 (HOR)
$[Mo_2(O$-*i*-$Pr)_4(py)_4]$[24]	2.195 (1)	2.03
$[Mo_2(OC_6F_5)_4(HNMe_2)_4]$[47]	2.140 (2)	2.07
$[Mo_2(OC_6F_5)_4(PMe_3)_4]$[48]	2.146 (2)	2.09

*TMTAA=5,7,12,14-tetramethylldibenzo[*b*,*i*][1,4,8,11]tetraazacyclotetradecine

Table 3.6. Raman and Infrared Frequencies (cm^{-1}) and Bond Distances (Å) for Some $[Mo_2]^{4+}$ Complexes

Compound	Raman Frequency (cm^{-1})	Infrared Frequency (cm^{-1})	Mo-Mo Distance (Å)
$[Mo_2(O_2CCH_3)_4]$	404[49-52]		2.0934 (8)[46]
$[Mo_2(O_2CCF_3)_4]$	397[11,50]		2.090 (4)[11]
$[Mo_2(O_2CCH_3)_2(H_2$-*p*-*tert*-butylcalix[4]-arene)(THF)]	378[a]	381	2.1263 (6)
[(**2**)(THF)]			
$[Mo_2(O_2CCH_3)_2(H_2$-calix[4]arene)]	379[a]	376	
(**4**)			
$[Mo_2(O_2CCF_3)_4(py)_2]$	367[11,50]		2.129 (2)[53]
$[Mo_2(O_2CCF_3)_2(H_2$-*p*-*tert*-butylcalix[4]-arene)]	360[a]	358	
(**3**)			
$[Mo_2(O_2CCF_3)_2(H_2$-calix[4]-arene)]	357[a]	358	
(**5**)			
$[(enH_2)_2(Mo_2Cl_8)]\cdot 2H_2O$	348[42,54]		2.134 (1)[55]
$[K_4Mo_2Cl_8]\cdot 2H_2O$	345[42,54]		2.139 (4)[56]

[a]Spectra recorded as 0.14 M solutions in THF

CHAPTER IV

The Synthesis and Inclusion Behavior of Pentamethylcyclopentadienyl and Cyclopentadienyl Tantalum and Niobium Metal Calixarene Complexes

Introduction

Calixarene[1] macrocycles have long history, but have caught the attention of transition metal chemists only in the last decade. Bayer first reported his investigations into the reactions of phenols with formaldehydes in 1872,[2-4] but more than a century passed before convenient, high-yield syntheses of the standard calix[n]arenes (n = 4, 6, 8) were available.[5] These elegant macrocycles were named "calixarenes" by Gutsche for the shape of their cone conformation, reminiscent of a Grecian *calix*. Two standard depictions of tetrameric calixarenes are shown in Figure 4.1.

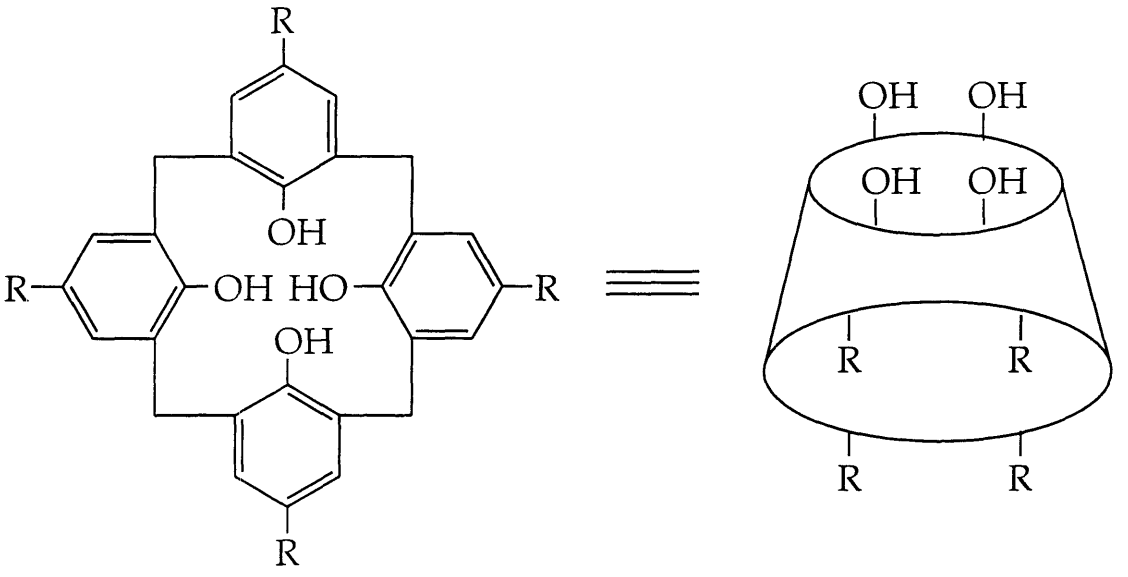

Figure 4.1. Two representations of calix[4]arenes (calix[4]arene for R = H, and *p-tert*-butylcalix[4]arene for R = *tert*-butyl).

The first transition metal calixarene complexes, [(Ti{*p-tert*-butylcalix[4]arene})$_2$], [(Fe(NH_3){*p-tert*-butylcalix[4]areneOSiMe_3})$_2$], and [(Co_3{*p-tert*-butylcalix[4]areneOSiMe_3}$_2$(THF)], were prepared from the reaction of transition

metal amines (M=Ti, Fe, Co) with para-*tert*-butylcalix[4]arene (Figure 2.5).[6] Other early transition metal calixarene complexes include [{H_2-calix[6]arene}{$TiCl_2(\mu$-O)$TiCl_3$}]$_2$[7] and [calix[8]arene{Ti(O-*i*Pr)}$_2$][RNH_3] (Figure 2.6).[8,9] These complexes, among other contributions,[10-14] formed the basis for transition metal calixarene chemistry.

Frequently compared to cyclodextrins and cryptands, calixarenes have attracted attention for their ability to include small molecules in the solid state.[15] The first X-ray structural determination of a calixarene, *p-tert*-butylcalix[4]arene, for example, revealed the *endo*-calix inclusion of a toluene molecule.[16] This inclusion capacity of calixarenes has been attributed in part to attractive host-guest "alkyl-phenyl" or "CH_3-π" interactions.[17] This property extends to transition metal calixarene complexes. Mononuclear products with open coordination sites directed into the calixarene basket,[18,19] [(*p*-*tert*-butylcalix[4]arene)·(*p-tert*-butylcalix[4]arene)(Mo=O)·H_2O·$PhNO_2$] and [(calix[4]-arene)(W=O)·CH_3COOH], coordinate solvent in the solid state, as shown in Figure 2.7.

This interesting property of the calixarene pocket to include guest molecules and the relative paucity of transition metals in this class led us to initiate a program of transition metal calixarene chemistry. In Chapter III of this thesis, we reported the preparation and characterization of novel calix[4]arene and *p-tert*-butyl-calix[4]arene complexes of the dimolybdenum quadruple bond. Inclusion of an axially-ligated THF molecule by the calixarene pocket of a neighboring complex helped to organize an extended lattice structure of [$Mo_2(O_2CCH_3)_2$(H_2-*p-tert*-butylcalix[4]arene)(THF)]·C_6H_6 in the solid state.[20] In the present chapter we examine the inclusion capabilities of discrete transition metal calixarene complexes. Our aim was to produce mononuclear products with electron-deficient metal centers protected from reaction in the *exo*-calixarene

position by sterically-demanding cyclopentadienyl and pentamethylcyclopentadienyl ligands, with available sites for binding nucleophiles at the *endo*-calix site. We describe the synthesis and characterization of [Cp*Ta(calix[4]arene)], [Cp*Ta(*p-tert*-butylcalix[4]arene)], [CpNb(*p-tert*-butylcalix[4]arene)] and the *endo*-calix inclusion complexes, [Cp*Ta(OH_2)(*p-tert*-butylcalix[4]arene)] and [Cp*Ta($NCCH_3$)(*p-tert*-butylcalix[4]arene)].

Experimental Section

General Considerations. All manipulations were carried out in a nitrogen-filled dry box or by using standard Schlenk line techniques. Solvents were distilled under nitrogen. Tetrahydrofuran (THF), dimethoxyethane (DME), pentane, toluene, and diethyl ether were distilled from sodium benzophenone ketyl. Methylene chloride and acetonitrile were distilled from CaH_2. Calix[4]arene[21] and *p-tert*-butylcalix[4]arene[22] were prepared according to published procedures and dried at 130 °C under vacuum for 24 hours. Cp*$TaCl_4$ was purchased from Strem Chemical and purified by washing with benzene and recrystallizing from toluene. $CpNbCl_4$ was purchased from Strem Chemicals and required no further purification. n-Butyllithium was purchased from Aldrich Chemical Company as a 1.6 M solution in hexanes and used as received. NMR spectra were obtained on a Varian XL-300 spectrometer at room temperature unless otherwise indicated. All IR spectra were recorded on a Bio-Rad FTS7 Fourier transform instrument. Mass spectra were obtained on a Finnigan 8200 system mass spectrometer.

Preparation of [Cp*Ta(calix[4]arene)] (1). *Method A:* Calix[4]arene (200 mg, 0.471 mmol) and Cp*$TaCl_4$ (230 mg, 0.502 mmol) were suspended in 50 mL

of toluene in a 100 mL round bottom flask fitted with a sidearm. The reaction mixture clarified as it was brought to reflux under a flow of argon gas. The evolution of HCl gas was followed by holding moist pH paper over the reaction exhaust and continued for 48 hours. The reaction mixture was then allowed to cool to room temperature, and filtered, and the solvent was evaporated. The off-white product **1** (248 mg, 0.337 mmol) was collected in 72% yield.

Method B: Calix[4]arene (100 mg, 0.236 mmol) was deprotonated with 4 equiv of KH (38 mg, 0.947 mmol) in 15 mL of THF. The vigorous effervescence diminished after 1 h, leaving a colorless solution. Cp^*TaCl_4 (108 mg, 0.236 mmol) was added, producing a yellow color upon dissolution. The reaction was stirred for 3 h, passed through a 1 inch pad of alumina, and the solvent was evaporated. Following a pentane wash and drying in vacuo, the off-white product **1** (99 mg, 0.134 mmol) was collected in 57% yield. Recrystallization by layering pentane onto a toluene solution of **1** at -40 °C afforded X-ray quality crystals. IR (KBr): 3001 (w), 2962 (w), 2947 (w), 2919 (m), 1588 (m), 1464 (vs), 1448 (vs), 1426 (s), 1310 (sh), 1293 (s), 1270 (vs), 1256 (s), 1244 (sh), 1221 (s), 1203 (s), 1083 (m), 1070 (m), 935 (m), 921 (s), 882 (m), 860 (m), 847 (m), 835 (m), 751 (vs), 744 (sh), 727 (m), 698 (m), 597 (w), 577 (w), 532 (m), 514 (m) cm^{-1}. ^1H NMR ($CDCl_3$, 300 MHz): δ 2.49 (s, 15H; Cp*(Me)), 3.20 (d, J = 12 Hz, 4H; CH_2), 4.32 (d, J = 12 Hz, 4H; CH_2)), 6.60 (t, J = 6 Hz, 4H; Ph), 6.97 (d, J = 6 Hz, 8H; Ph) ppm. MS(EI): 736 (M^+, 100), 601 ([M-Cp*]$^+$, 58), 368 (28), 351 (8). Anal. Calcd. for $C_{38}H_{35}O_4Ta$ (**1**): C, 61.96; H, 4.79. Found: C 61.55; H, 4.85.

Preparation of [Cp*Ta(*p-tert*-butylcalix[4]arene)] (2a). *Method A:* A vigorously stirred suspension of Cp^*TaCl_4 (318 mg, 0.694 mmol) and *p-tert*-butylcalix[4]arene (550 mg, 0.742 mmol) was brought to reflux in 50 mL of toluene under a purge of argon gas. The resulting solution evolved HCl gas which could be monitored by holding moist pH paper over the exhaust of

reaction; acid production ceased after 48 hours. Evaporation of the solvent left a light yellow powder, **2a** (621 mg, 0.646 mmol) in 93% yield. The crude product was judged to be >95% pure by its ^{1}H NMR spectrum and could be recrystallized by vapor diffusion of pentane into a toluene solution of **2a** to give crystals suitable for X-ray diffraction studies.

Method B: *p-tert*-Butyl-calix[4]arene (250 mg, 0.337 mmol) was deprotonated by an excess of KH (78 mg, 1.94 mmol) in 15 mL of DME. The suspension clarified then developed a fluffy white precipitate. Gas evolution ceased after 1 h of vigorous stirring. To the resulting white suspension was added Cp*$TaCl_4$ (100 mg, 0.437 mmol). The reaction clarified and turned deep orange as it was stirred over 12 h. After concentration of the orange solution to dryness, extraction of the resulting solid with CH_2Cl_2, and evaporation of the solvent from the filtrate, the light yellow product **2a** (244 mg, 0.254 mmol) was obtained in 58% yield. IR (KBr): 3038 (sh), 2952 (vs, br), 1471 (vs), 1365 (m), 1311 (s), 1254 (s), 1204 (vs), 1110 (m), 1027 (w), 924 (m), 873 (m), 834 (m), 794 (m), 763 (w), 736 (w), 543 (m), 429 (sh), 403 (m) cm^{-1}. ^{1}H NMR ($CDCl_3$, 300 MHz): δ 1.19 (s, 36H; *t*-Bu), 2.46 (s, 15H; Cp*(Me)), 3.18 (d, J = 12 Hz, 4H; CH_2), 4.34 (d, J = 12 Hz, 4H; CH_2), 7.01 (s, 8H; Ph) ppm. MS(EI): 961 (M^+, 100), 946 ($[M-CH_3]^+$, 62), 904 ($[M-(t\text{-Bu})]^+$, 2), 465 (40). Anal. Calcd for $C_{54}H_{67}O_4Ta$ (**2a**): C, 67.49; H, 7.03. Found: C, 67.18; H, 7.10.

Preparation of [Cp*Ta(OH_2)(*p-tert*-butylcalix[4]arene)] (2b). Dissolution of complex **2a** in wet acetone followed by slow evaporation of solvent and filtration produced X-ray quality crystals of complex **2b** in essentially quantitative yield. IR (KBr): 3480 (m), 3425 (m), 3036 (m), 2954 (s), 2914 (sh), 1715 (m), 1595 (w), 1459 (vs), 1427 (sh), 1361 (m), 1305 (s), 1255 (sh), 1203 (s), 1116 (m), 1023 (w), 919 (m), 873 (m), 830 (s), 796 (m), 761 (m), 678 (w), 543 (m), 498 (w), 417 (m) cm^{-1}. ^{1}H NMR ($CDCl_3$, 300 MHz): δ 1.19 (s, 36H; *t*-Bu), 2.16 (s, 6H;

$(CH_3)_2CO$), 2.23 (br, 2H; Ta-OH_2), 2.41 (s, 15H; Cp*(Me)), 3.14 (d, J = 12 Hz, 4H; CH_2), 4.25 (d, J = 12 Hz, 4H; CH_2), 7.01 (s, 8H; Ph) ppm. Anal. Calcd for $C_{57}H_{75}O_6Ta$ (**2b**·acetone): C, 66.01; H, 7.29. Found: C, 65.59; H, 7.26.

Preparation of [Cp*Ta(NCCH$_3$)(*p-tert*-butylcalix[4]arene)] (2c). Complex **2a** (200 mg, 0.208 mmol) was dissolved in 10 mL of CH_2Cl_2. When 3 mL of CH_3CN were added dropwise to the light yellow reaction solution, the color bleached and a waxy white precipitate developed. Additional CH_2Cl_2 was added to dissolve the precipitate. Cooling the colorless solution for several hours at -30 °C produced the first crop of large X-ray quality block-shaped crystals which were filtered, crushed, and dried in vacuo. Concentration and cooling of the mother liquor afforded more crystals, resulting in a 94% (196 mg, 0.196 mmol) overall yield. IR (KBr): 2954 (vs, br), 2920 (vs, br), 2864 (vs, br), 2714 (w), 2332 (s), 2302 (m), 1480 (vs), 1392 (s), 1360 (vs), 1307 (vs), 1258 (vs), 1206 (vs), 1162 (sh), 1128 (s), 1107 (s), 1024 (m), 950 (m), 919 (vs), 888 (m), 871 (s), 833 (vs), 800 (vs), 763 (s), 678 (m), 588 (m), 543 (vs), 500 (s) cm^{-1}. ^1H NMR ($CDCl_3$, 300 MHz): δ -0.28 (br, 3H; Ta-$NCCH_3$), 1.19 (s, 36H; *t*-Bu), 2.44 (s, 15H; Cp*(Me)), 3.16 (d, J = 12 Hz, 4H; CH_2), 4.26 (d, J = 12 Hz, 4H; CH_2), 7.09 (s, 8H; Ph) ppm. Anal. Calcd for $C_{56.5}H_{71}O_4NClTa$ (**2c**·0.5 CH_2Cl_2): C, 64.97; H, 6.85; N, 1.34. Found: C, 64.52; H, 6.65; N, 1.64.

Preparation of [CpNb(*p-tert*-butylcalix[4]arene)] (3). *Method A: p-tert*-Butyl-calix[4]arene (500 mg, 0.736 mmol) and $CpNbCl_4$ (221 mg, 0.737 mmol) were loaded into a 200 mL round bottom flask fitted with a side arm and suspended in 100 mL of toluene. The rust-colored reaction solution clarified and evolved HCl as it was brought to reflux under a flow of argon gas. The reaction was refluxed for 2 days, during which time the color faded to yellow. The solvent was removed in vacuo, and the crude product was extracted into diethyl

ether. Filtration, followed by evaporation of the ether, afforded the yellow product **3** (426 mg, 0.530 mmol) in 72% yield.

Method B: *p-tert*-Butyl-calix[4]arene (100 mg, 0.135 mmol) was deprotonated with 4 equiv of KH (22 mg, 0.548 mmol) in THF over one hour. $CpNbCl_4$ (40 mg, 0.133 mmol) was added to the reaction flask and the reaction was stirred for 2 h. The resulting yellow-brown solution was passed through a one inch pad of alumina and the solvent was evaporated. The yellow product **3** (73 mg, 0.091 mmol) was isolated in 68% yield. The product could be recrystallized from pentane at -40 °C. IR (KBr): 3420 (m), 2956 (s), 2913 (sh), 2870 (sh), 1752 (w), 1561 (m), 1463 (vs), 1402 (sh), 1364 (w), 1294 (s), 1255 (sh), 1202 (s), 1114 (m), 1077 (sh), 1026 (w), 920 (m), 876 (m), 821 (vs), 763 (m), 676 (w), 575 (sh), 548 (s), 498 (m), 421 (s) cm^{-1}. ^1H NMR ($CDCl_3$, 300 MHz): δ 1.19 (s, 36H; *t*-Bu), 3.15 (d, J = 12 Hz, 4H; CH_2), 4.37 (d, J = 12 Hz, 4H; CH_2), 7.00 (s, 8H; Ph), 7.06 (s, 5H; Cp) ppm. MS(EI): 802 (M^+, 100), 787 ($[M-CH_3]^+$, 67), 386 (34). Anal. Calcd for $C_{49}H_{57}O_4Nb$ (3): C, 73.30; H, 7.16. Found: C, 73.27; H, 7.14.

X-ray Crystallography.

General procedures. Details of the crystal data and the data collection parameters for **1** and **2a-c** are reported in Table 4.1. Intensity data were obtained on an Enraf-Nonius CAD-4 diffractometer by using graphite monochromated Mo Kα radiation and methods previously described.[23] Unit cell parameters were determined and refined from 25 reflections with $2\theta > 20^o$. All data were corrected for Lorentz and polarization effects. The observed structure factors were averaged for equivalent reflections.

[Cp*Ta(calix[4]arene)] (1). Very pale yellow crystals grew when pentane was allowed to diffuse slowly into a toluene solution of **1**. A rod of dimensions 0.2 X 0.2 X 0.5 was mounted vertically on the end of a quartz fiber with silicone grease. The crystal was transferred to the diffractometer and studied at low

temperature. Crystal quality was determined to be good from axial photographs and open-counter ω-scans of several low-angle reflections ($\Delta\bar{\omega}_{1/2}$ = 0.24°) which showed no fine structure. The crystal had 2/m Laue symmetry and systematic absences consistent with the centrosymmetric space group $P2_1/c$ (No. 14). Each asymmetric unit contains one molecule of **1**. There are no solvent molecules in the lattice. The tantalum and oxygen atoms were located by direct methods. All other non hydrogen atoms were found through least squares refinement and difference Fourier procedures. Hydrogen atoms were generated and fixed to ride on attached carbon atoms (d_{C-H} = 0.95 Å, B_H = 1.2 B_C). The largest residual peak found in the final difference Fourier map was 1.1 $e^-/Å^3$, located at a distance of 1.03 Å from the tantalum atom. Final atomic positional and anisotropic thermal parameters for non-hydrogen atoms are given in Tables 4.2 and 4.3.

[Cp*Ta(*p-tert*-butylcalix[4]arene)] (2a). Very pale yellow crystals were grown from slow diffusion of pentane into a toluene solution of **2a** at -40 °C. A block-shaped specimen of dimensions 0.5 X 0.4 X 0.3 mm was transferred to a liquid nitrogen cold stage and mounted with silicone grease on the tip of a quartz fiber. The crystal was transferred to the diffractometer and studied at low temperature, revealing 2/m Laue symmetry. Crystal quality was judged to be acceptable based on axial photographs and open counter ω-scans of several low angle reflections with $\Delta\bar{\omega}_{1/2}$ = 0.23° and no fine structure. Systematic absences were consistent with the space group $P2_1/c$ (No. 14). An empirical psi-scan absorption correction was applied to the data. The positions of the tantalum and oxygen atoms were determined by direct methods. All other non-hydrogen atom were located by a series of least-squares refinements and difference Fourier techniques. In the asymmetric unit, there are one molecule of **2a**, two molecules of toluene, and one molecule of pentane. All non-hydrogen atoms except for

those of the pentane molecule were allowed to refine anisotropically. The carbon atoms of the lattice pentane molecule were refined isotropically. The central carbon in the pentane is disordered over two positions related by a crystallographic inversion center. A two-site model was introduced for these positions with 50% occupancy each. All hydrogen atoms were placed in calculated positions and fixed to the attached carbon atoms (d_{C-H} = 0.95 Å, B_H = 1.2 B_C). The largest residual peak in the final difference Fourier map was 0.7 $e^-/Å^3$, located at a distance of 0.72 Å from the C208 of the pentane molecule in the lattice. Final atomic positional and anisotropic thermal parameters for non-hydrogen atoms are given in Tables 4.4 and 4.5.

[Cp*Ta(OH$_2$)(*p-tert*-butylcalix[4]arene)] (2b). Colorless crystals of **2b** were grown by slow evaporation of a moist acetone solution of **2a**. A parallelepiped of **2b** (dimensions 0.25 x 0.40 x 0.40 mm) was mounted on the end of a quartz fiber in Paratone N oil from Exxon. The crystal was judged to be acceptable based on open counter ω-scans of several low-angle reflections ($\Delta\bar{\omega}_{1/2}$ = 0.21°, no fine structure) and by axial photographs. Examination on the diffractometer revealed 2/m Laue symmetry and systematic absences consistent with space group $P2_1/n$ (No. 14).[24] A psi-scan absorption correction was applied to the data. The tantalum atom was found by direct methods. All remaining non-hydrogen atoms were located by subsequent least-squares refinements and difference Fourier maps. Hydrogen atoms H1 and H2 were located on the difference map and refined isotropically. The remaining hydrogen atoms were placed in calculated positions and fixed to the attached carbon atoms (d_{C-H} = 0.95 Å, B_H = 1.2 B_C). The largest residual peak in the final difference Fourier map was 1.6 $e^-/Å^3$, located at a distance of 0.97 Å from the tantalum atom. Final atomic positional parameters for all refined atoms are given in Table 4.6. Anisotropic thermal parameters for non-hydrogen atoms are given in Table 4.7.

[Cp*Ta(NCCH$_3$)(*p-tert*-butylcalix[4]arene)] (2c). Large blocks of colorless crystals of **2c** grew overnight at -40°C from a $CH_2Cl_2/NCCH_3$ solution of **2a**. An irregular crystal of dimensions 0.5 X 0.3 X 0.3 mm was covered in Exxon's Paratone N and maneuvered onto the end of a quartz fiber. Study on the diffractometer at low temperature indicated a triclinic crystal system. Quality of the crystal was judged to be good on the basis of axial photographs and open-counter ω-scans of several low-angle reflections ($\Delta\bar{\omega}_{1/2}$ = 0.24°, no fine structure). Intensity statistics indicated the centrosymmetric space group $P\bar{1}$ (No. 2). An empirical psi-scan absorption correction was applied to the data. There are two molecules of **2c** in the crystallographic asymmetric unit. For each molecule of **2c**, there are 2.5 molecules of CH_2Cl_2 in the lattice. Tantalum and oxygen atoms were located by direct methods. All other non-hydrogen atoms were located by iterative least-squares refinements and difference Fourier procedures. Hydrogen atom positions were calculated and fixed to ride on attached carbon atoms (d_{C-H} = 0.95 Å, B_H = 1.2 B_C). Final refinement yielded the residuals given in Table 4.1. The largest residual peak found in the final difference Fourier map was 0.6 $e^-/Å^3$, located at a distance of 1.56 Å from C128 of the disordered pentane molecule in the lattice. Final atomic positional and anisotropic thermal parameters for non-hydrogen atoms are given in Tables 4.8 and 4.9.

Variable Temperature ^{2}H NMR Studies of [Cp*Ta(NCCD$_3$)(p-tert-butyl-calix[4]arene)] (2c-d$_3$). Crystals of **2c-d$_3$**·2.5 CH_2Cl_2 were grown by cooling a solution of **2a** in $CH_2Cl_2/NCCD_3$ to -30 °C. The crystals were crushed and dried in vacuo overnight, removing the solvent of crystallization. To a solution of **2c-d$_3$** (50 mg, 0.050 mmol) in 2 mL CH_2Cl_2 in an NMR tube was added 1-5 equivalents of $NCCD_3$ (2.5-12.5 μL) via microliter syringe. Spectra were collected on a Varian XL300 spectrometer with a multinuclear probe and externally referenced to C_6D_6 in benzene. Temperatures were calibrated according to an

internal calibration method on the machine, using pure methanol. Sweep widths of 6500 Hz were scanned for features before focusing on the observed peaks.

***Endo*-calix Deprotonation of $NCCH_3$: Reaction of [Cp*Ta($NCCH_3$)(*p-tert*-butylcalix[4]arene)] (2c) with Butyllithium.** Microcrystalline **2c** (50 mg, 0.050 mmol) was prepared as above and added to a stirred solution of n-butyllithium (45 μL, 0.074 mmol) in 5 mL of THF. The colorless solution took on a yellow hue and was allowed to stir for one hour. The solvent was then evaporated in vacuo, and the crude product analyzed by IR and ^{1}H NMR spectroscopy. IR (KBr): 2952 (sh), 2921 (vs), 2854 (vs), 1461 (vs), 1374 (m), 1307 (m), 1257 (m), 1204 (m), 1026 (w), 919 (w), 870 (w), 833 (w), 800 (w), 673 (w) cm^{-1}. ^{1}H NMR (C_6D_6, 300 MHz): δ -0.48 (s, 2H; Ta-$NCCH_2$), 1.19 (s, 36 H; *t*-Bu), 2.34 (s, 15H; Cp*(Me)), 3.26 (d, J = 12 Hz, 4H; CH_2), 4.52 (d, J = 12 Hz, 4H; CH_2), 7.11 (s, 8H; Ph) ppm.

Results and Discussion

Syntheses of [Cp*Ta(calix[4]arene)] (1), [Cp*Ta(*p-tert*-butylcalix[4]arene)] (2a), and [CpNb(*p-tert*-butylcalix[4]arene)] (3). Transition metal calixarene complexes **1**, **2a**, and **3** were prepared by two routes, from the protonated or deprotonated ligand. In the former method, the pentamethylcyclopentadienyl or cyclopentadienyl metal tetrachloride was allowed to react over approximately two days with the calixarene macrocycle in refluxing toluene. The reactions were easily monitored by following the evolution of HCl gas and produced very good yields of the desired products. With some loss in yield, preparation from the anionic ligands gave the desired products in less time. In the latter procedure, the calixarene macrocycles were

first deprotonated and then allowed to react in situ with the pentamethylcyclopentadienyl or cyclopentadienyl metal tetrachloride. Residual calixarene or transition metal starting materials were removed when necessary by extracting the products into non-polar solvents or passing a solution of the crude mixture through alumina. All of the products were hygroscopic but otherwise very stable and soluble in a variety of polar and nonpolar solvents.

The nature of products **1**, **2a**, and **3** was readily determined by ^{1}H NMR and IR spectroscopy, mass spectrometry, and elemental analysis. Calix[4]arene and *p-tert*-butyl-calix[4]arene macrocycles give rise to very characteristic and uncomplicated ^{1}H NMR spectra (see Figure 2.3, for example). In the free ligands, the diastereotopic protons on the methylene groups tethering the phenol moieties give rise to a pair of broad doublets, due to interconversion of cone conformers.[21,22] The most obvious sign of calixarene ligand metallation, is the dramatic sharpening of this pair of doublets due to the rigid cone conformation imparted to the ligand, as explained in Chapter II of this thesis. This effect is illustrated in Figure 4.2, which shows the methylene regions in the ^{1}H NMR spectra of the free *p-tert*-butylcalix[4]arene and the geometrically fixed product [Cp*Ta(*p-tert*-butylcalix[4]arene)] (**2a**). As in the free ligands, the presence of only one pair of doublets in the ^{1}H NMR spectra of the products **1**, **2a**, and **3**, suggested approximate fourfold symmetry in solution. Further evidence of metal incorporation onto the calixarene ligands was provided by the disappearance of the phenol resonance at *ca.* 9-10 ppm present in the ^{1}H NMR spectra of the free ligands, and the appearance of a resonances at *ca.* 2.5 ppm or 7.1 ppm assignable, respectively, to pentamethylcyclopentadienyl or cyclopentadienyl ligands on the transition metals. The IR spectra of the products

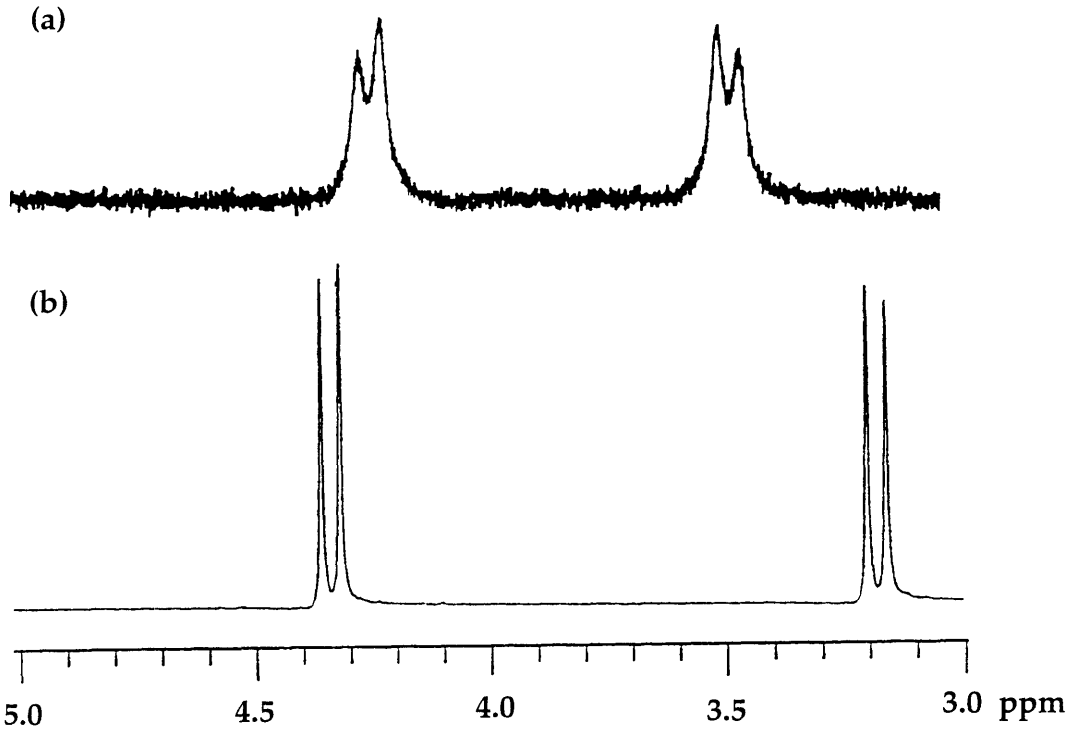

Figure 4.2. The methylene regions of the ^{1}H NMR spectra of free (a) *p-tert*-butylcalix[4]arene and (b) [Cp*Ta(*p-tert*-butylcalix[4]arene)] (**2a**).

1, **2a**, and **3** were also informative when compared with those of the free ligands, revealing the disappearance of the broad band arising from the PhO-H stretch of the free ligand, and a new band in the 750-850 region, assignable to M-O stretch (M = Ta, Nb).[25] Mass spectrometry and elemental analyses further supported the assignments of **1**, **2a**, and **3**.

Structures of [Cp*Ta(calix[4]arene)] (1) and [Cp*Ta(*p-tert*-butyl-calix[4]arene)]·toluene·pentane (2a)·2 toluene·pentane. Single crystal X-ray analyses revealed the nature of products **1** and **2a** in the solid state, and their structures are shown in Figures 4.3 and 4.4, respectively. Selected bond distances and angles for **1** and (**2a**)·2 toluene·pentane are given in Tables 4.10 and 4.11 respectively. Both complexes are comprised of a Cp*Ta moiety mounted onto the tetraphenoxide rim of a calixarene, at the top of the macrocyclic pocket. In the solid state these products are distorted from the fourfold symmetry of the free ligands, producing elliptical rather than circular calixarene cavities. This shape can be seen by looking down the vector containing the centroid of the Cp(*) ring and the Ta atom as shown for both **1** and (**2a**)·2 toluene·pentane in Figure 4.5, and by analysis of metrical parameters. There is approximately a 30° difference in the endo-calix angles O20-Ta-O60 and O40-Ta-O80 for both **1** and (**2a**)·2 toluene·pentane. The Ta-O_{calix} distances for both complexes also vary, with Ta-O20 and Ta-O60 being at least 0.1 Å shorter than Ta-O40 and Ta-O80. The Ta-O-C_{calix} angles range from ca. 124° to almost linear, as well, and the trans angles Ta-O20-O20 and Ta-O60-C6O are 34-55° larger than Ta-O40-O40 and Ta-O80-C8O. The bending of the calixarene macrocycles in **1** and **2a** can be understood in part by considering that both contain Ta(V) d^0 metal centers and are formally 14 e^- complexes. The phenoxide groups of the calixarenes are capable of donating π as well as σ electrons, the relative contributions of which are reflected in the shortening of the Ta-O distances and a related increase in the Ta-O-Ph

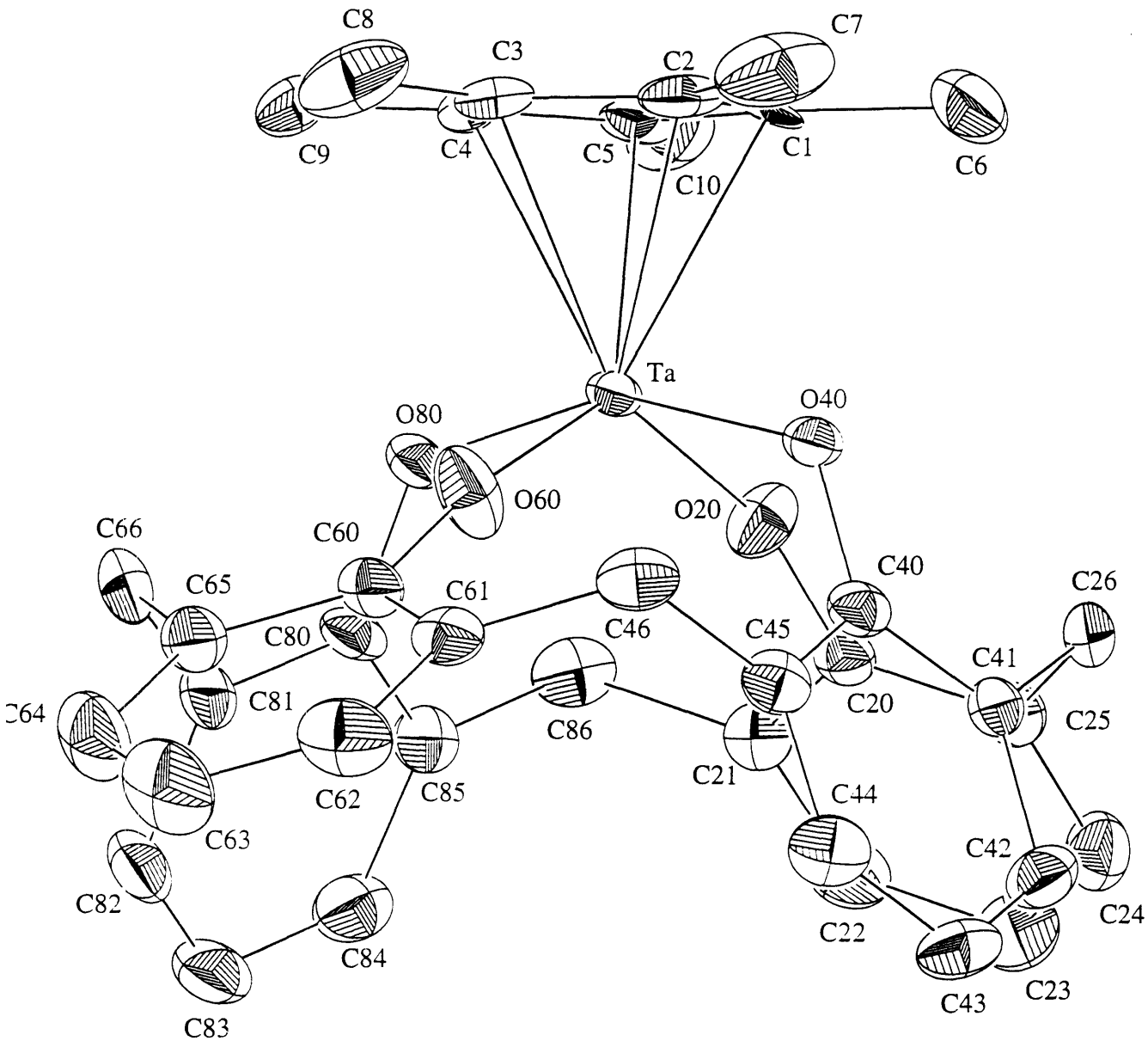

Figure 4.3. An ORTEP diagram of [Cp*Ta(calix[4]arene)] (**1**) showing the atom labeling scheme and the 50% probability ellipsoids.

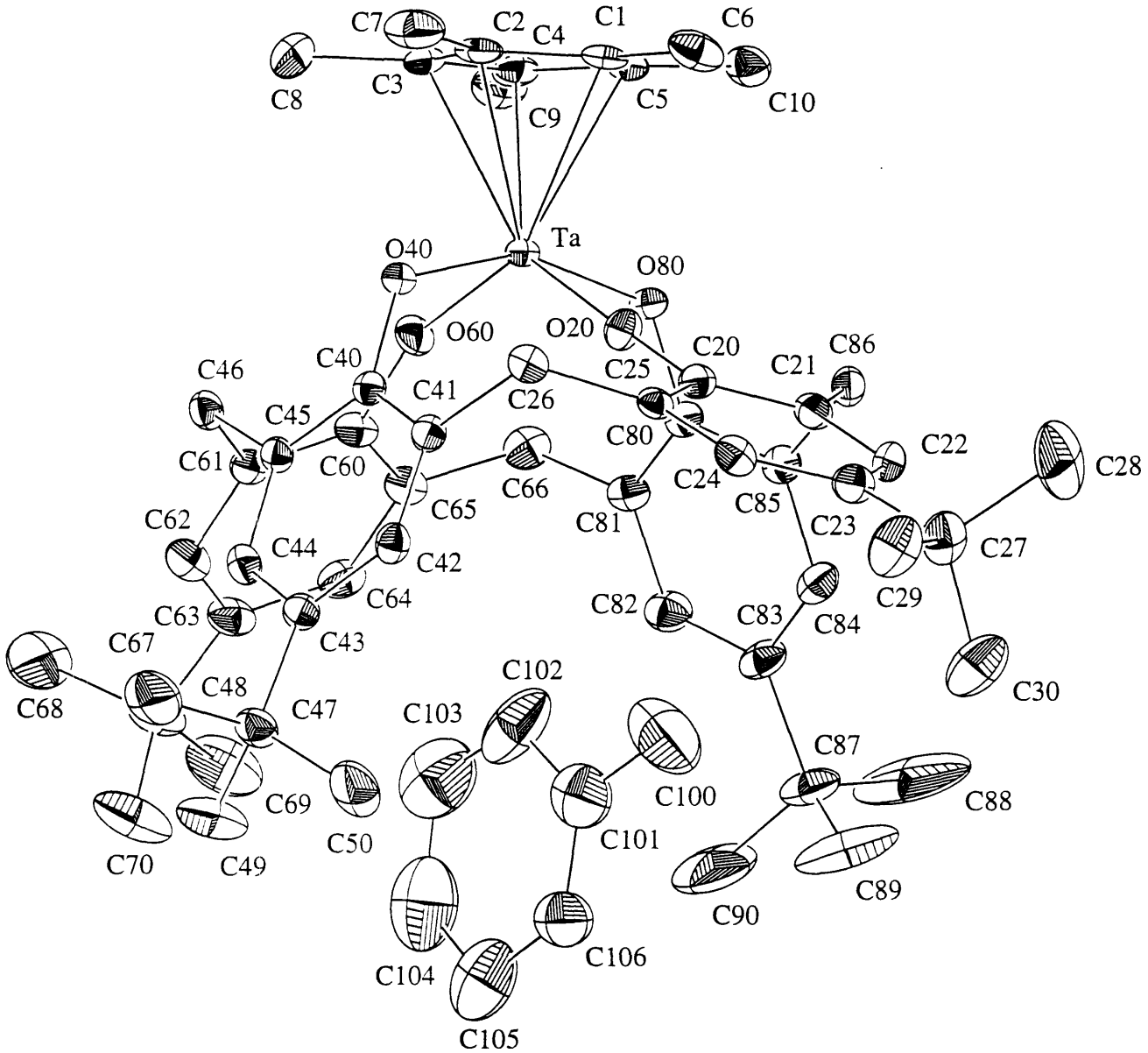

Figure 4.4. An ORTEP drawing of [Cp*Ta(*p-tert*-butylcalix[4]arene)]·toluene, (**2a**)·toluene, showing the atom labeling scheme and the 40% probability ellipsoids.

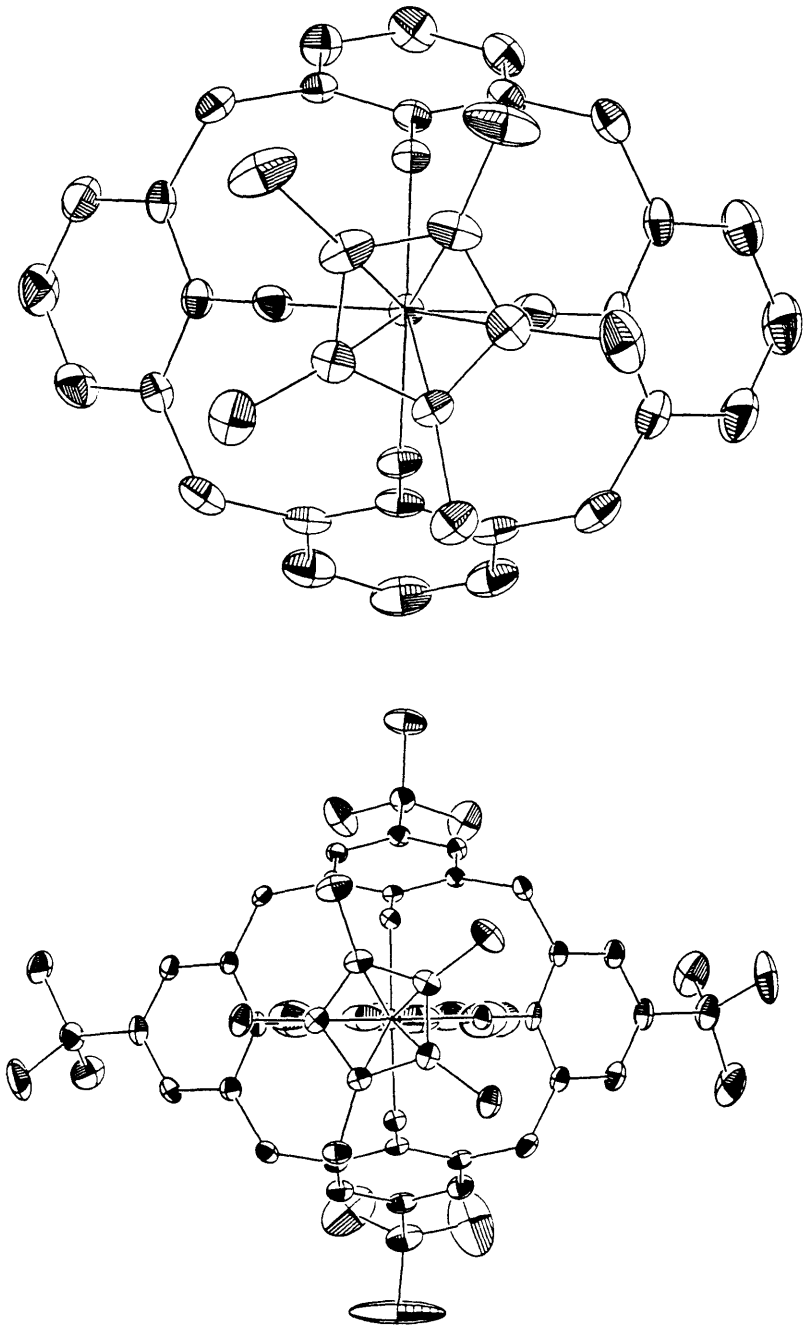

Figure 4.5. Top view of ORTEP diagrams of and [Cp*Ta(calix[4]arene)] (**1**) and [Cp*Ta(*p-tert*-butylcalix[4]arene)]·toluene (**2a**)·toluene .

bend angles.[26] An approximately linear relationship can be seen in a graph of Ta-O_{calix} distances versus Ta-O-C_{calix} angles in the top of Figure 4.6. As will be discussed later, Fenske-Hall calculations support the prediction that π electron donation from the phenoxide oxygen atoms O20 and O60 ameliorates the electron deficiency at the metal centers in **1** and **2a**. This interaction distorts the products from fourfold to twofold symmetry in the solid state. The distortion is more pronounced in **2a**·2 toluene·pentane than in **1**, a difference that can be understood by analysis of intermolecular interactions of these products.

As shown in Figure 4.4, one of the toluene molecules of (**2a**)·2 toluene·pentane is included sideways in the calixarene pocket. This inclusion can be seen more readily in the packing diagram shown in Figure 4.7. Such inclusion of aromatic rings by calixarene macrocycles is precedented[6,16,27,28] and generally attributed to "alkyl-phenyl" or "CH_3-π" interactions.[17] Two types of alkyl-phenyl group interactions are possible between [Cp*Ta(*p-tert*-butyl-calix[4]arene)] (**2a**) and the included toluene molecule: interactions between the methyl group of the toluene molecule, and the phenyl rings of the calixarene, and interactions between the *tert*-butyl methyl groups of the calixarene and the π system of the toluene molecule. In the case of (**2a**)·2 toluene·pentane, the methyl group C100 of the toluene molecule is pointed directly toward the center of the phenyl ring C20-C25 at a distance of 3.59 Å from the plane of the aromatic ring. This distance is similar to that found in other calixarene complexes.[16,20,29] The surprising aspect of the included toluene molecule in (**2a**)·2 toluene·pentane, however, is its sideways orientation (see **I** below). Toluene molecules have previously been found to orient with their methyl group pointed up into the calixarene cone (**II**), as seen in the solid state structures of *p-tert*-butylcalix[4]arene·toluene[16] and [(Ti{*p-tert*-butyl-calix[4]arene})$_2$]·toluene.[6] The sideways inclusion of toluene by the calixarene ligand in **2a** may have been effected by the elliptical distortion of

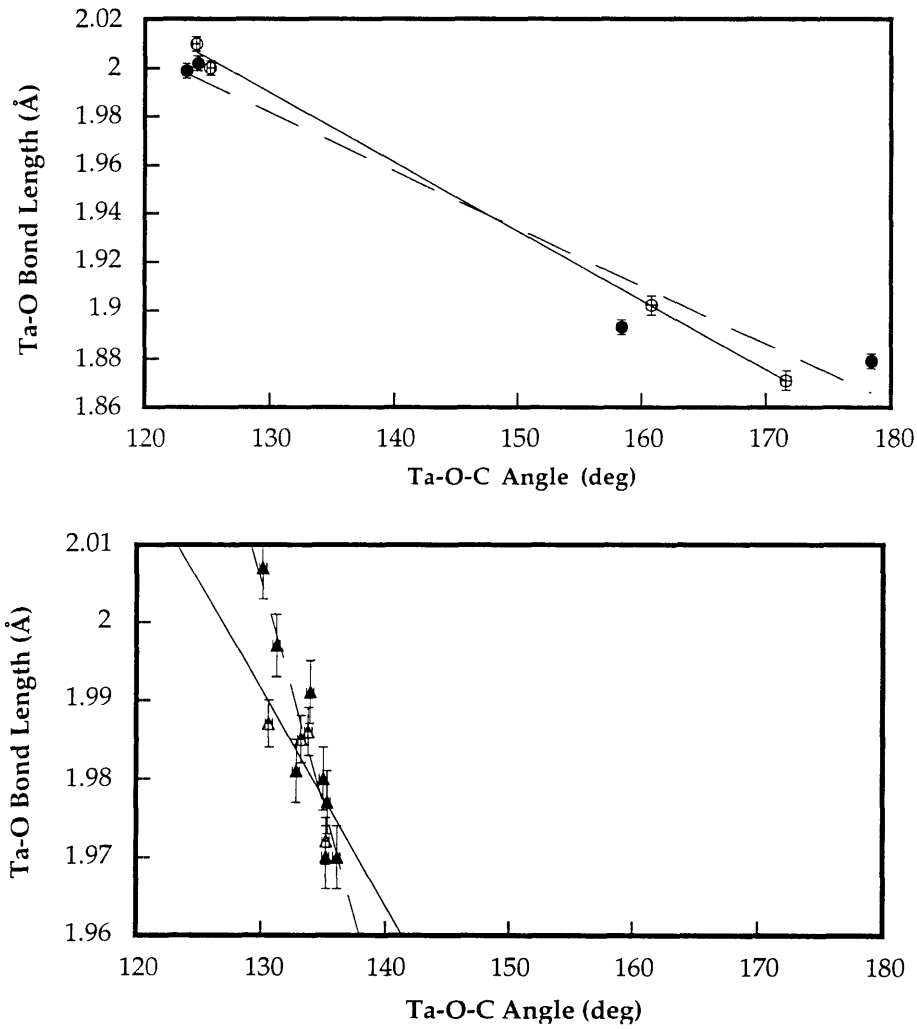

Figure 4.6. Plots of the Ta-O-Ccalix angles versus Ta-Ocalix bond lengths for: [Cp*Ta(calix[4]arene)] (**1**) (open circles) and [Cp*Ta(*p-tert*-butylcalix[4]arene)] (**2a**) (filled circles) in the top graph; and [Cp*Ta($NCCH_3$)(*p-tert*-butylcalix[4]arene)] (**2b**) (open triangles) and [Cp*Ta($NCCH_3$)(*p-tert*-butylcalix[4]arene)] (**2c**) (filled triangles) in the bottom graph. Solid lines represent best least squares fit to a linear relationship. Error bars denote ±1 esd.

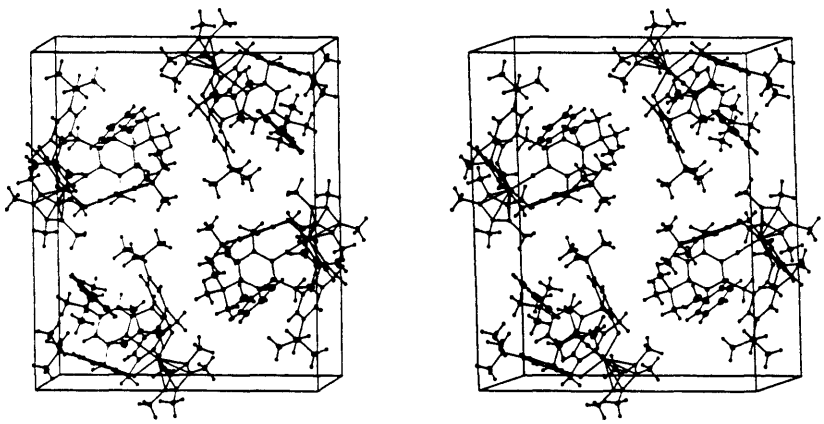

Figure 4.7. A stereo ORTEP packing diagram of [Cp*Ta(*p-tert*-butyl-calix[4]arene)]·toluene (**2a**)·toluene. Toluene and pentane molecules in the lattice were omitted for clarity.

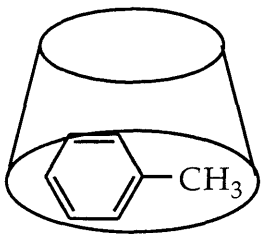

I

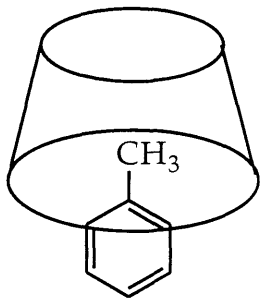

II

the *p-tert*-butylcalix[4]arene induced upon binding of the Cp*Ta moiety to the tetraphenoxide rim of the calixarene basket. Moreover, the shape of **2a** is further distorted by allowing for sideways inclusion of the toluene molecule in the calixarene pocket, reflected in the Ta-O20-C20 angle of 178.4 (3)° versus the Ta-O60-C60 angle of 158.4 (3)°.

Although single crystals of **1** were also grown from a toluene solution, there are no solvent molecules included in the calixarene pocket in the solid state structure. The only difference between **1** and **2a** is the absence of *tert*-butyl groups in **1**. Whereas the methyl groups of the *tert*-butyl moieties of *p-tert*-butylcalix[4]arene may contribute to the alkyl phenyl interactions in (**2a**)·2 toluene·pentane, these sterically demanding residues would also be expected to inhibit the *endo*-calix interaction of larger guests. In fact, intermolecular interactions do occur in the extended lattice of **1**, as shown in the packing diagrams (Figures 4.8 and 4.9). The methyl groups C6 and C7 of the Cp* moiety

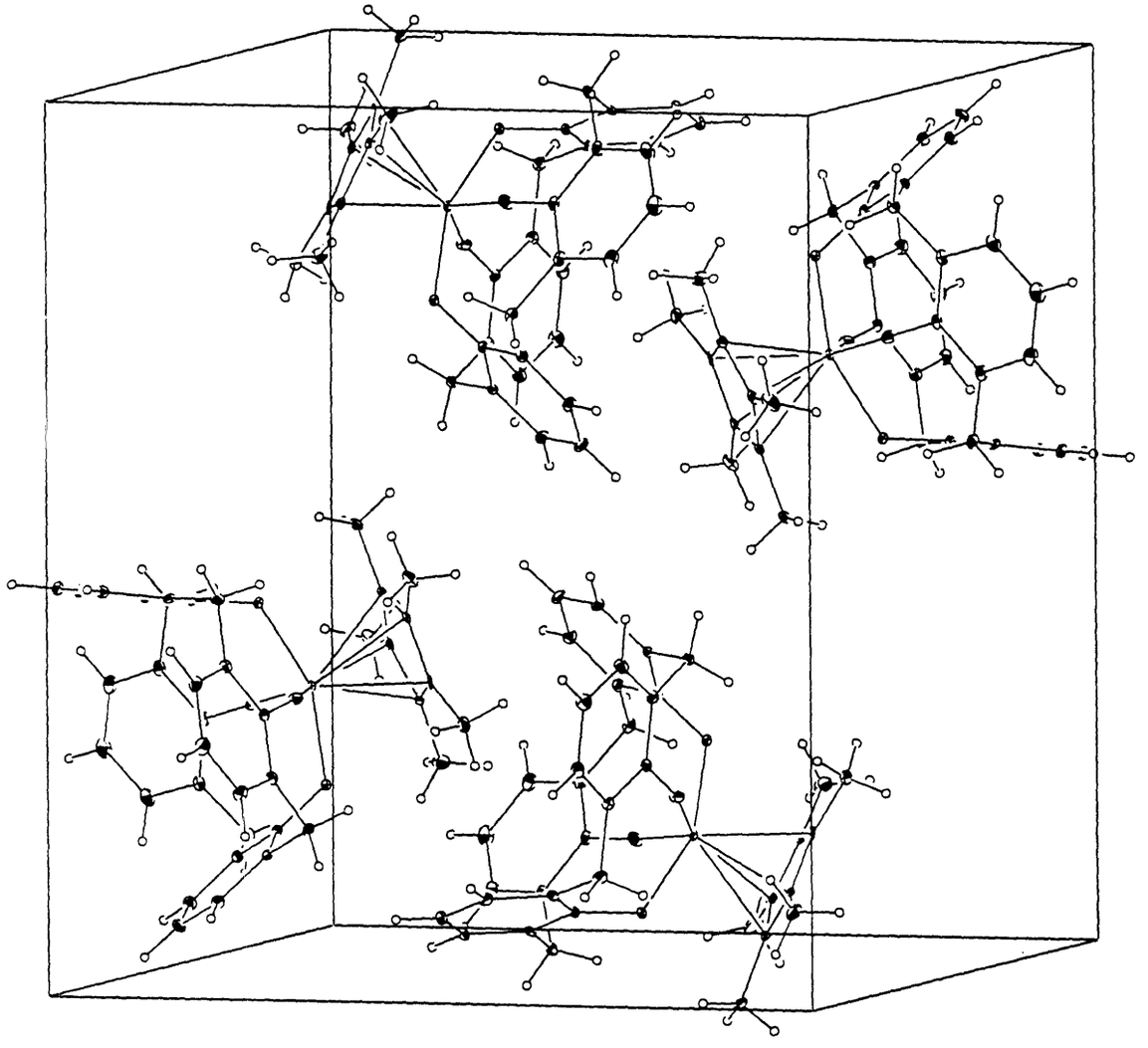

Figure 4.8. Packing diagram of [Cp*Ta(calix[4]arene)] (**1**).

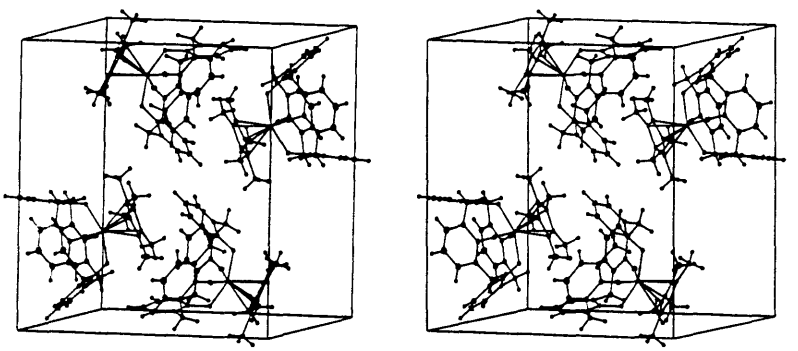

Figure 4.9. Packing diagram in stereo view of [Cp*Ta(calix[4]arene)] (**1**).

of [Cp*Ta(calix[4]arene)] (**1**) enter the calixarene pocket of the neighboring molecule. *Endo*-calix interactions ranging from 3.49 Å to 3.81 Å occur between C6 and the carbon atoms of the phenyl ring C20-C25 and between C7 and the carbon atoms of the phenyl ring C60-C65.

Preparation and Structural Characterization of [Cp*Ta(OH_2)(*p-tert*-butylcalix[4]arene)] (2b) and [Cp*Ta($NCCH_3$)(*p-tert*-butylcalix[4]arene)] (2c). If the metal center of [Cp*Ta(*p-tert*-butylcalix[4]arene)] (**2a**) is considered to have approximate C_{4v} symmetry in solution, simple symmetry analysis[30] predicts that two of the three metal orbitals of A_1 symmetry (s, p_z, and d_{z2}) are involved in σ boding to the calixarene ligand, leaving one orbital available for binding in the *endo*-calix site. More accurately, Fenske Hall calculations on the representative complex [Cp*Ta(calix[4]arene)] (**1**) show that the two lowest unoccupied molecular orbitals (LUMO) are predominantly d_{xy} and d_{z2} in character as shown on the left side of Figure 4.10. The steric bulk of the pentamethyl-cyclopentadienyl ligand prohibits reactions in the *exo*-calix position involving either orbital. Of the two LUMO's, which are very close in energy, only the d_{z2} orbital is geometrically available, and it is of appropriate symmetry to bind nucleophiles in the *endo*-calix position. Accordingly, when exposed to the small molecule nucleophiles H_2O and $NCCH_3$, **2a** formed the complexes [Cp*Ta(OH_2)(*p-tert*-butylcalix[4]arene)] (**2b**) and [Cp*Ta($NCCH_3$)(*p-tert*-butylcalix[4]arene)] (**2c**), with each nucleophile bound through its heteroatom to the tantalum center in the *endo*-calix position.

The bound H_2O molecule of [Cp*Ta(OH_2)(*p-tert*-butylcalix[4]arene)] (**2b**) gives rise to O-H stretches at 3480 and 3425 cm^{-1} in the IR spectrum and a broad resonance at 2.23 ppm in the ^1H NMR spectrum, shifted downfield from the 1.5 ppm resonance of free H_2O in $CDCl_3$. The solid state structure was confirmed by X-ray crystallography. An ORTEP drawing of **2b** is shown in Figure 4.11, and

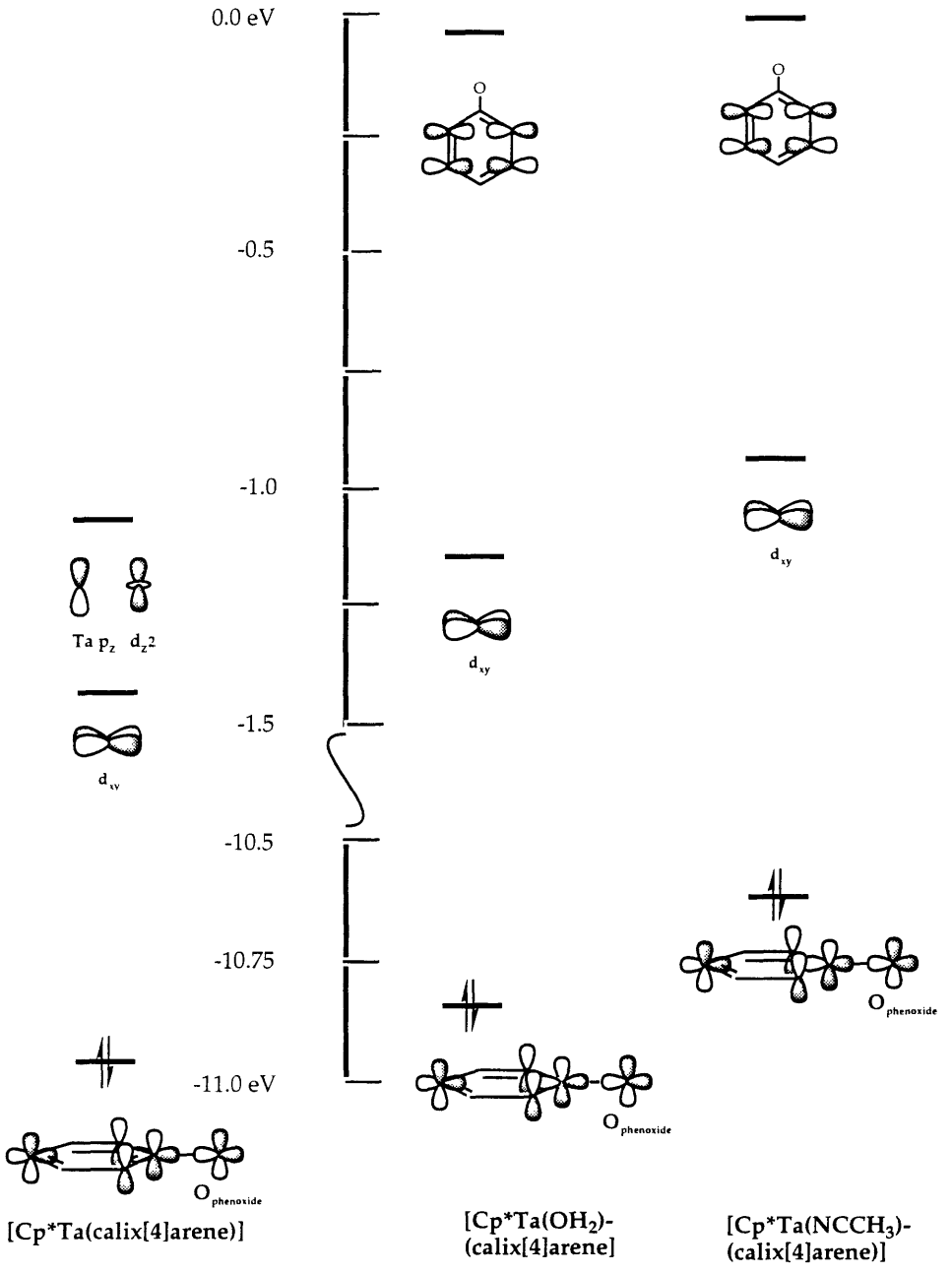

Figure 4.10. HOMO and LUMO representations for [Cp*Ta(calix[4]arene] (**1**), [Cp*Ta(OH_2)(calix[4]arene], and [Cp*Ta($NCCH_3$)(calix[4]arene] from Fenske-Hall calculations.

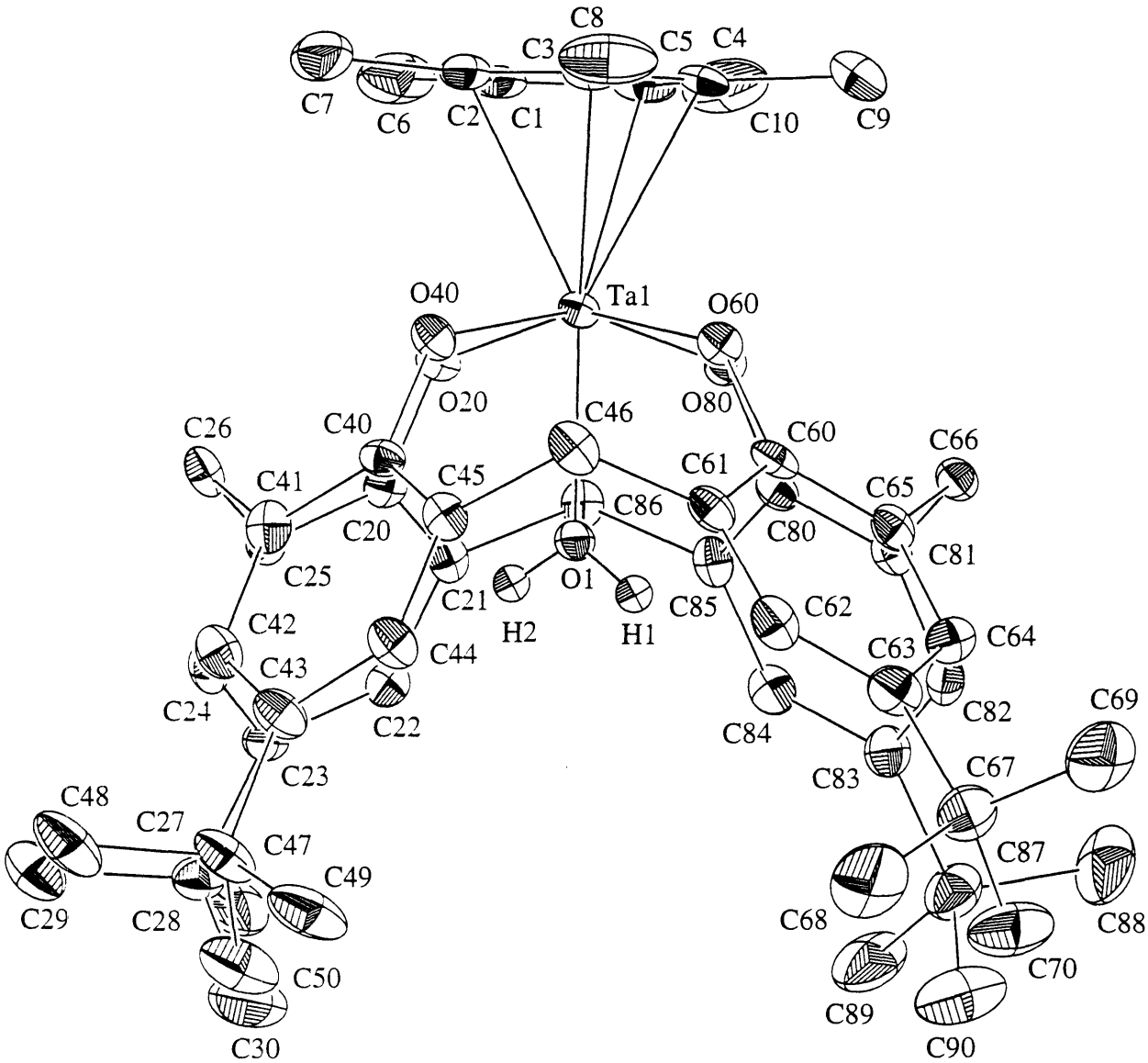

Figure 4.11. An ORTEP drawing of [Cp*Ta(OH_2)(*p-tert*-butylcalix[4]arene)] (**2b**) showing 50% probability ellipsoids and atom labeling scheme.

selected bond distances and angles are given in Table 4.12. The Ta-OH_2 distance of 2.188 (3) Å in **2b** is significantly shorter than the Mo-OH_2 distance of 2.408 (16) Å in [(*p-tert*-butylcalix[4]arene)·(*p-tert*-butylcalix[4]arene)(Mo=O)·H_2O·$PhNO_2$],[18] reflecting the labilization of H_2O bound to a metal center with an oxo group in the trans position[31-33] in the latter complex, as well as the relative electron deficiency of the Ta center in **2b** and in the precursor **2a**. The overall structural difference between the precursor complex **2a** and the H_2O adduct **2b**, is the increased symmetry associated with the *endo*-calix ligation. The *p-tert*-butylcalix[4]arene ligand in **2b** again has approximate fourfold symmetry. The *endo*-calix angles O20-Ta-O60 (156.3 (1)°) and O40-Ta-O80 (157.2 (1)°) are similar, as are the Ta-O_{calix} distances (1.972 (3)-1.987 (3) Å) and Ta-O_{calix}-C_{calix} angles (130.6 (3)°-135.2 (3)°). In addition to the obvious steric requirements of an *endo*-calix ligand, the rounding of the calixarene pocket is also due to the electronic satisfaction provided to the tantalum center by an additional ligand, alleviating the necessity for PhO→Ta π electron donation afforded through calixarene twisting. Fenske-Hall calculations support this theory and will be discussed below.

Similarly, addition of $NCCH_3$ to **2a** provided the complex [Cp*Ta($NCCH_3$)(*p-tert*-butylcalix[4]arene)] (**2c**). Whereas complexes **1** and **2a** show no peaks in the IR spectrum from 1600-2900 cm^{-1}, the IR spectrum of the product **2c** showed bands at 2302 and 2332 cm^{-1} for the crystalline product. The infrared spectrum of free acetonitrile[34] has bands at 2254 and 2293 cm^{-1}, assigned respectively, to the C≡N stretching frequency and a combination band. The combination band results from the coupling of the symmetric CH_3 deformation and C-C stretching, probably enhanced by Fermi resonance. The shift of these bands to higher frequency upon metal complexation is precedented.[33,35,36] The room temperature ^1H NMR of the product showed a broad resonance at -0.28

ppm for the $NCCH_3$ protons, shielded from the position of free $NCCH_3$ in $CDCl_3$ (1.9 ppm). Although binding to a transition metal center might be expected shift the $NCCH_3$ proton resonance downfield, the solid state structure of **2c** revealed the probable shielding effects of *endo*-calix binding. An ORTEP diagram of one of the molecules in the asymmetric unit of **2c**·2.5 (CH_2Cl_2) is given in Figure 4.12, and selected bond angles and distances are provided in Table 4.13. One molecule of $NCCH_3$ is bound to the tantalum center through the nitrogen atom, leaving the methyl group in the center of the calixarene pocket at an average distance of 3.91 Å from the plane of any of the four aromatic rings. The closest *endo*-calix interactions for the methyl carbons C11 and C12 of the two molecules in the asymmetric unit of **2c**·2.5 CH_2Cl_2 occur with phenyl carbons C123 and C223, respectively, at distances of 3.83 Å and 3.98 Å. In this position, the protons contained on the methyl group would experience the shielding of four aromatic rings when exposed to an external magnet. Although this analysis is restricted to the solid state, shielding was also evidenced experimentally in solution in the ^1H NMR spectrum. The solution behavior of **2c** is further discussed below.

The Ta-N distances are 2.246 (5) Å for Ta(100)-N(10) and 2.236 (5) Å for Ta(200)-N(20). The distances and angles associated with the $NCCH_3$ ligand suggest minimal perturbation from the bonding involved in a free molecule of $NCCH_3$, which is not surprising since the d^0 Ta center in **2c** could not participate in π backbonding with the anti-bonding π^* molecular orbital of $NCCH_3$.[37] The N-C distances of N10-C10 (1.110 (7) Å) and N20-C20 (1.124 (7) Å) and N-C-C angles of 177.9 (7)° for N10-C10-C11 and 179.7 (7)° for N20-C20-C21 indicate an N-C bond order of three. Although no other Ta(V) adducts of acetonitrile have been crystallographically characterized, similar features were observed in the solid state structures of other d^0, V(V) and Nb(V), complexes with acetonitrile,

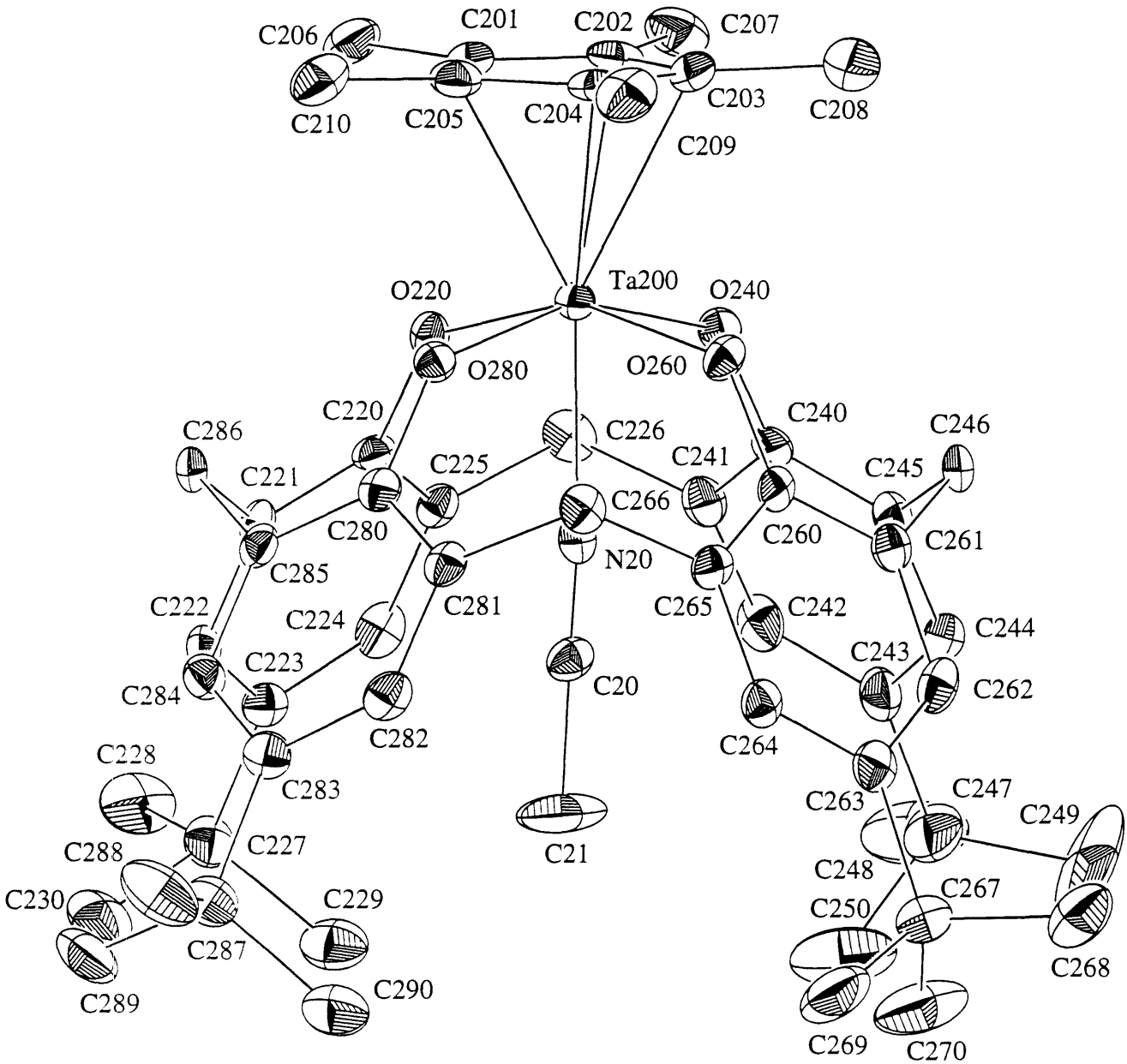

Figure 4.12. An ORTEP drawing of one of the molecules in the asymmetric unit of [Cp*Ta($NCCH_3$)(*p-tert*-butylcalix[4]arene)] (**2c**) showing 40% ellipsoids for non-hydrogen atoms and atom labeling scheme. The other molecule contains the atoms Ta100, N10, C10, C11, O120, O140, O160, O180, C120-130, etc.

such as $[VO(NO_3)_3 \cdot CH_3CN]$ (V-N = 2.24 (3) Å)[38] and $[Nb(NCCH_3)_2Cl_3O]$ (Nb-N = 2.44 (2) and 2.245 (9) Å)[36].

The calixarene pocket of **2c** has approximately fourfold symmetry like **2b**. The *endo*-calix angles O120-Ta100-O160 (155.8 (2)°) and O140-Ta100-O180 (155.3 (2)°) are similar, as are the corresponding angles O20-Ta200-O60 (155.2 (2)°) and O40-Ta200-O80 (155.7 (2)°) on the second molecule in the asymmetric unit. The Ta-O_{calix} distances also fall in a narrow range (1.970 (4) Å to 2.007 (4) Å). Similarly, the Ta-O_{calix}-C_{calix} angles vary only slightly also, ranging from 130.1 (3)° to 136.1 (3)°. There is also an approximately linear relationship between the Ta-O_{calix} distances and Ta-O-C_{calix} angles in complexes **2b** and **2c** as depicted graphically in the bottom of Figure 4.6, but with a narrow distribution of values compared to those of the more distorted complexes **1** and **2a** shown in the top graph of Figure 4.6.

As in the solid state structure of **2a**·2 toluene·pentane, the presence of a Cp*Ta moiety on the rim of the calixarene pocket had a profound effect on the positioning of the included $NCCH_3$ molecule in the complex **2c**. In the case of **2c**, the electron deficient metal center at the lower rim coordinates the lone pair of the N atom of acetonitrile, orienting it as indicated by **III**, below. This orientation is opposite to that of previous inclusion of acetonitrile by a calixarene macrocycle in the complex [*tetra*-ethyl-*p*-*tert*-butylcalix[4]arene tetracarbonate]·-$NCCH_3$, depicted below as **IV**.[29] Positioned with the methyl group of the acetonitrile slightly deeper into the calixarene pocket, the closest *endo*-calix interaction of this organic clathrate is 3.80 Å, and occurs between a bridgehead aromatic carbon and the acetonitrile methyl carbon. The closet bridgehead carbon to methyl carbon distance in either of the two molecules of **2c** is 4.06 Å.

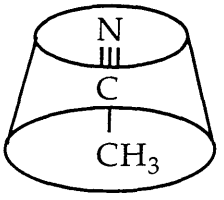

III

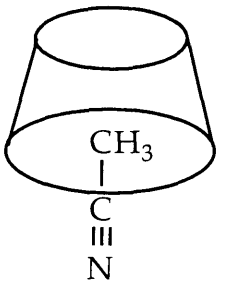

IV

The results of Fenske-Hall calculations on the representative complexes [Cp*Ta(OH_2)(calix[4]arene)] and [Cp*Ta($NCCH_3$)(calix[4]arene)] are shown on the right side of Figure 4.10. The bonding interaction of a nucleophile with complexes such as [Cp*Ta(calix[4]arene)] (**1**), shown on the left side of Figure 4.10, is predominantly through the d_{z2} orbital, as predicted. Upon the addition of a nucleophile to **1**, the bonding interactions of the d_{xy} orbital are virtually unperturbed, whereas the d_{z2} orbital is now involved in bonding with the nucleophile lone pair and is substantially lowered in energy, so much that it is no longer a part of the frontier orbital manifold.

Fenske-Hall calculations also provided insight into the PhO→Ta interactions proposed for complexes **1** and **2a-c**. The relative partial charge on each phenoxide oxygen atom is a measure of the degree of this interaction since less negative charge results from more electron donation to the metal center, and *vice versa*. A summary of these partial charges, or Mulliken atomic charges, is presented in Table 4.14. The partial charges for O20 and O60 are distinctly less negative than those on O40 and O80 for the "empty pocket" complex [Cp*Ta(calix[4]arene)] (**1**). In contrast, the partial charges on O20-O80 for the

complexes [Cp*Ta(OH_2)(calix[4]arene)] and [Cp*Ta($NCCH_3$)(calix[4]arene)] containing ligands in the *endo*-calix site are all essentially the same and are more negative than the charges on O20 and O60 of **1**. These data support our intuition that O20 and O60 in the "empty pocket" and electron deficient complexes **1** and **2a** donate more electron density than O40 and O80, distorting the calixarene macrocycle from fourfold to twofold symmetry in the solid state. These interactions are possible given the bonding picture of **1** in Figure 4.13 below, showing the alternate in-phase and out-of-phase overlap of the in-plane phenoxide oxygen p orbitals with the d_{xy} orbital of the tantalum center. Less PhO→Ta electron donation and hence less distortion of the calixarene ligand is present in the "filled pocket" and more electron dense complexes **2b** and **2c**.

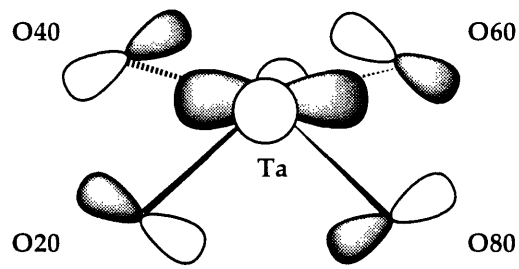

Figure 4.13. Molecular bonding picture of **1** showing the in-plane p orbitals of the phenoxide oxygen atoms and the d_{xy} orbital of the tantalum center.

Space filling diagrams of the calixarene pockets of **1**, **2a**, **2b**, and **2c**, are shown in Figures 4.14-4.17, highlighting the elliptical shapes of **1** and **2a** compared with the circular nature of **2b** and **2c**. It is also clear that the toluene, water, and acetonitrile molecules are nestled tightly in the calixarene pockets in **2a-c**, at least in the solid state. In the Cp(*)Mcalixarene (M = Ta, Nb) complexes,

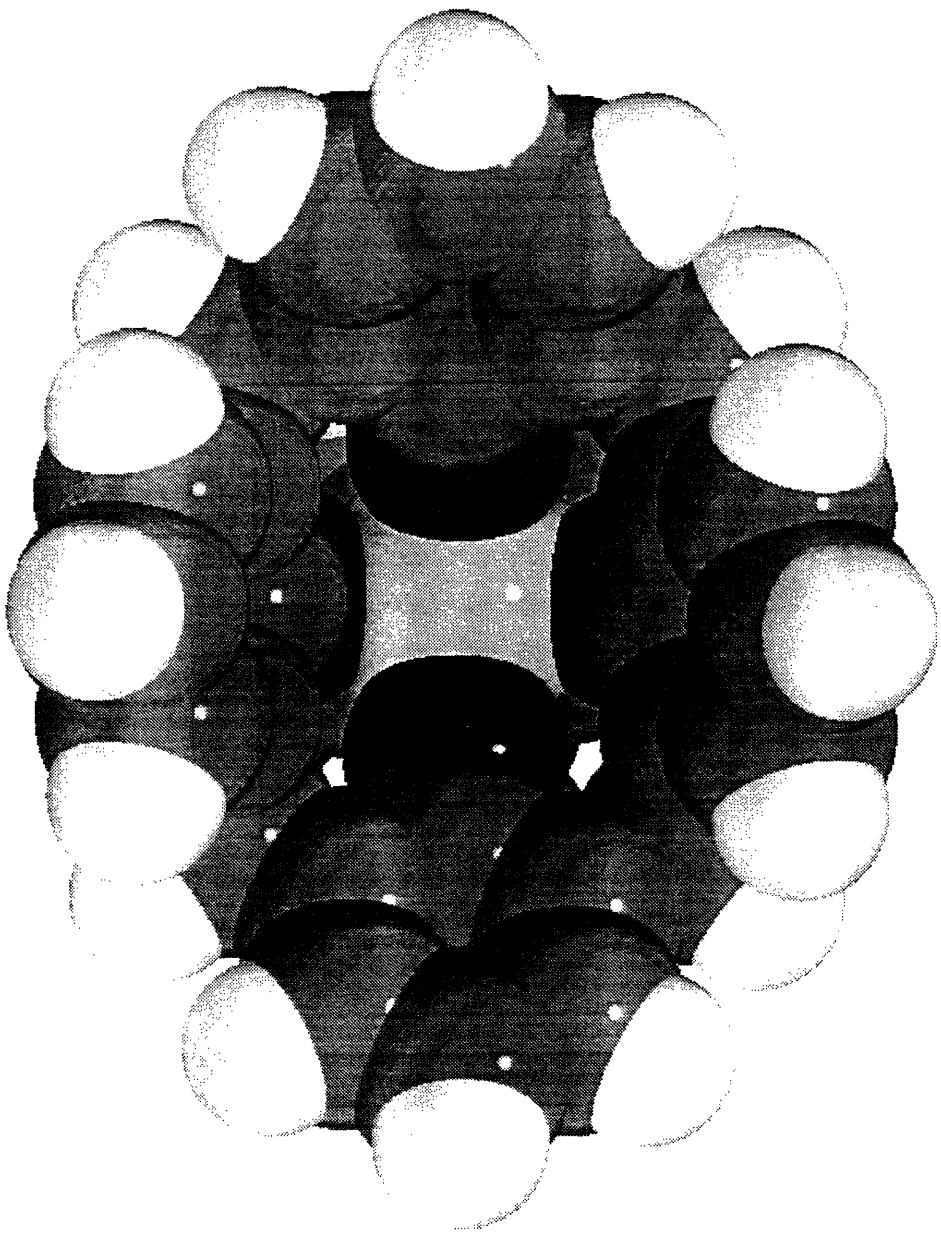

Figure 4.14. A space filling diagram of [Cp*Ta(calix[4]arene)] (**1**) looking into the empty calixarene pocket.

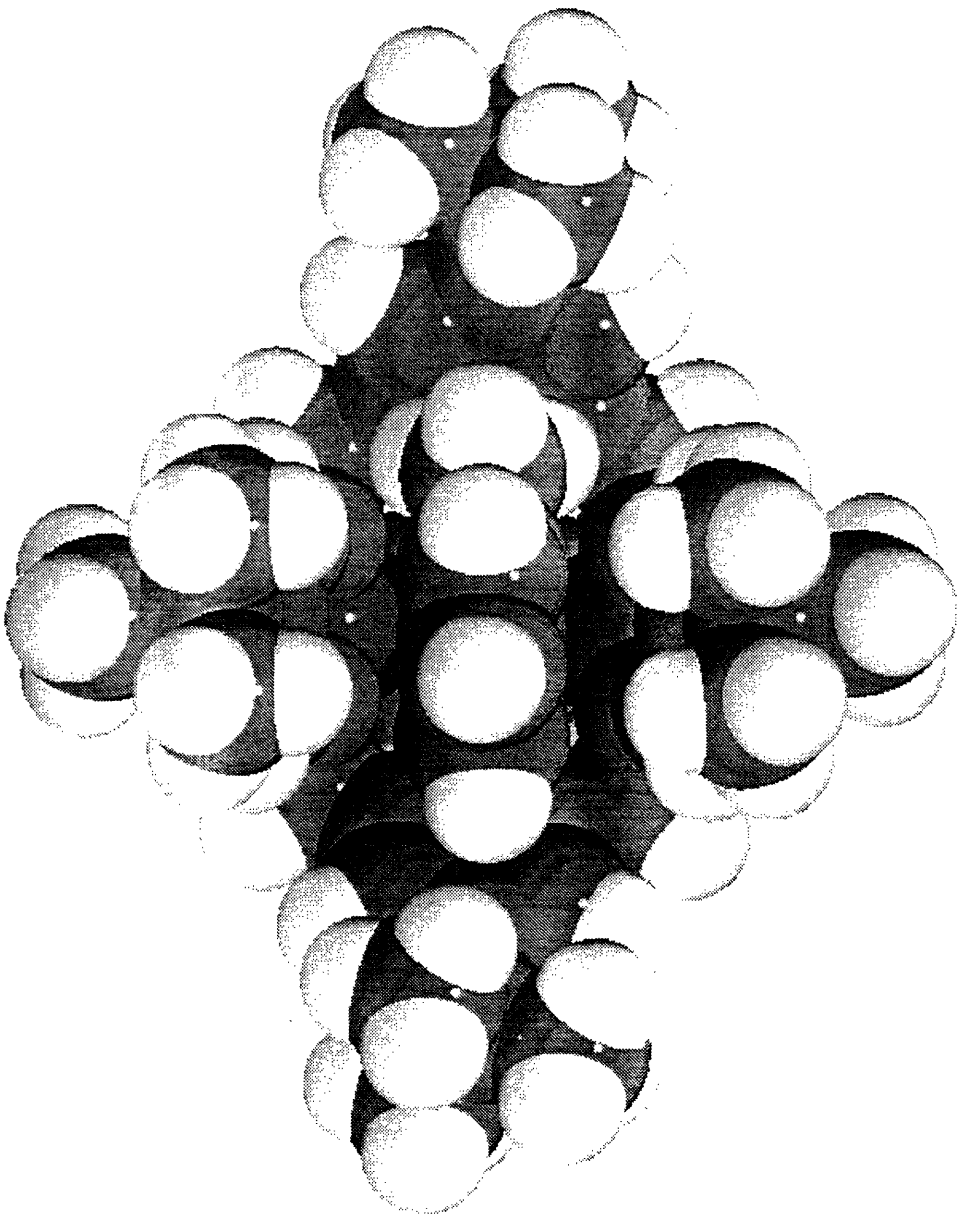

Figure 4.15. A space filling diagram of [Cp*Ta(*p-tert*-butyl-calix[4]arene)]·toluene (**2a**)·toluene, looking into the calixarene pocket at the included toluene molecule.

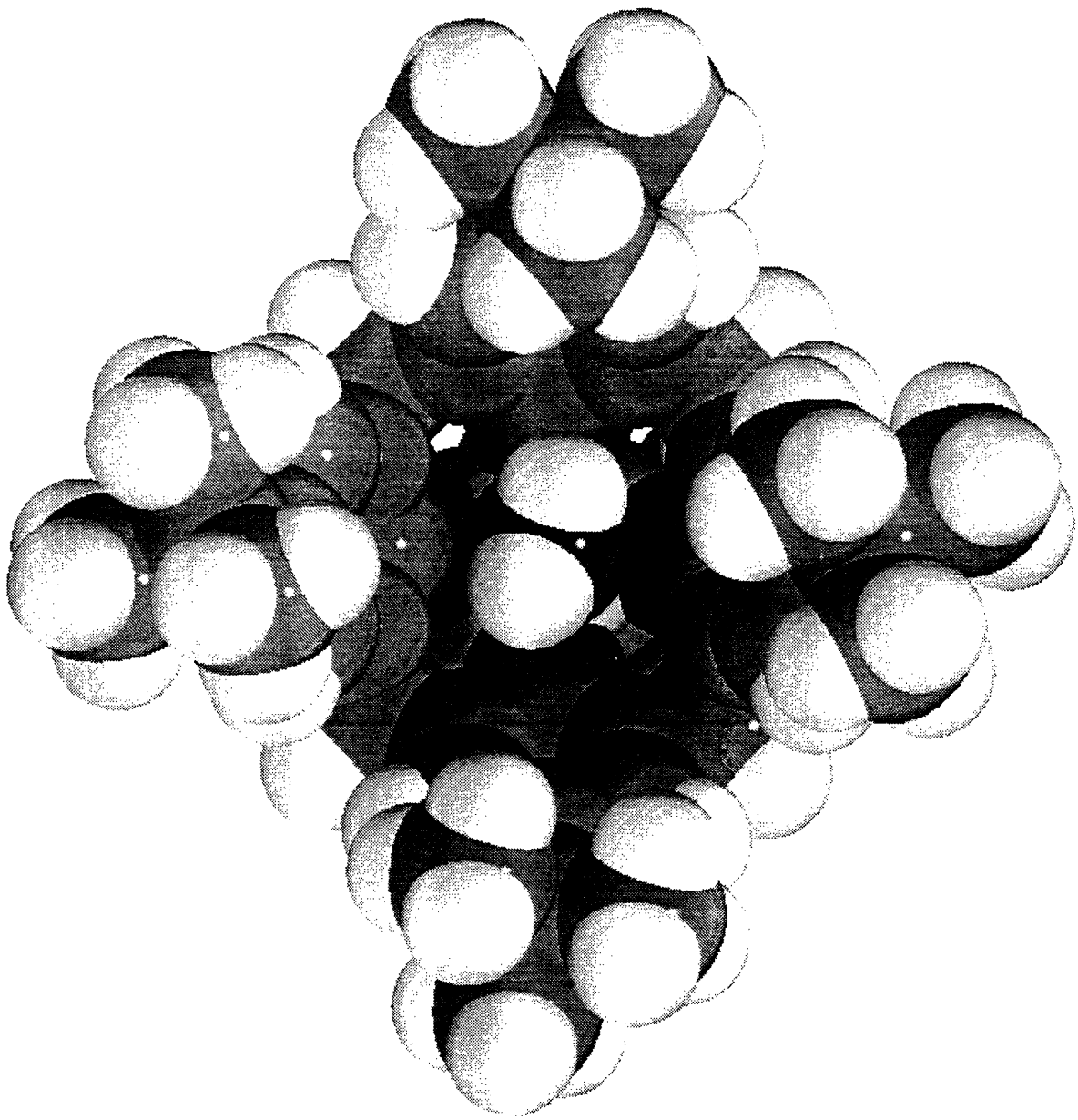

Figure 4.16. A space filling diagram of [Cp*Ta(OH_2)(*p-tert*-butyl-calix[4]arene)] (**2b**), looking into the filled calixarene pocket.

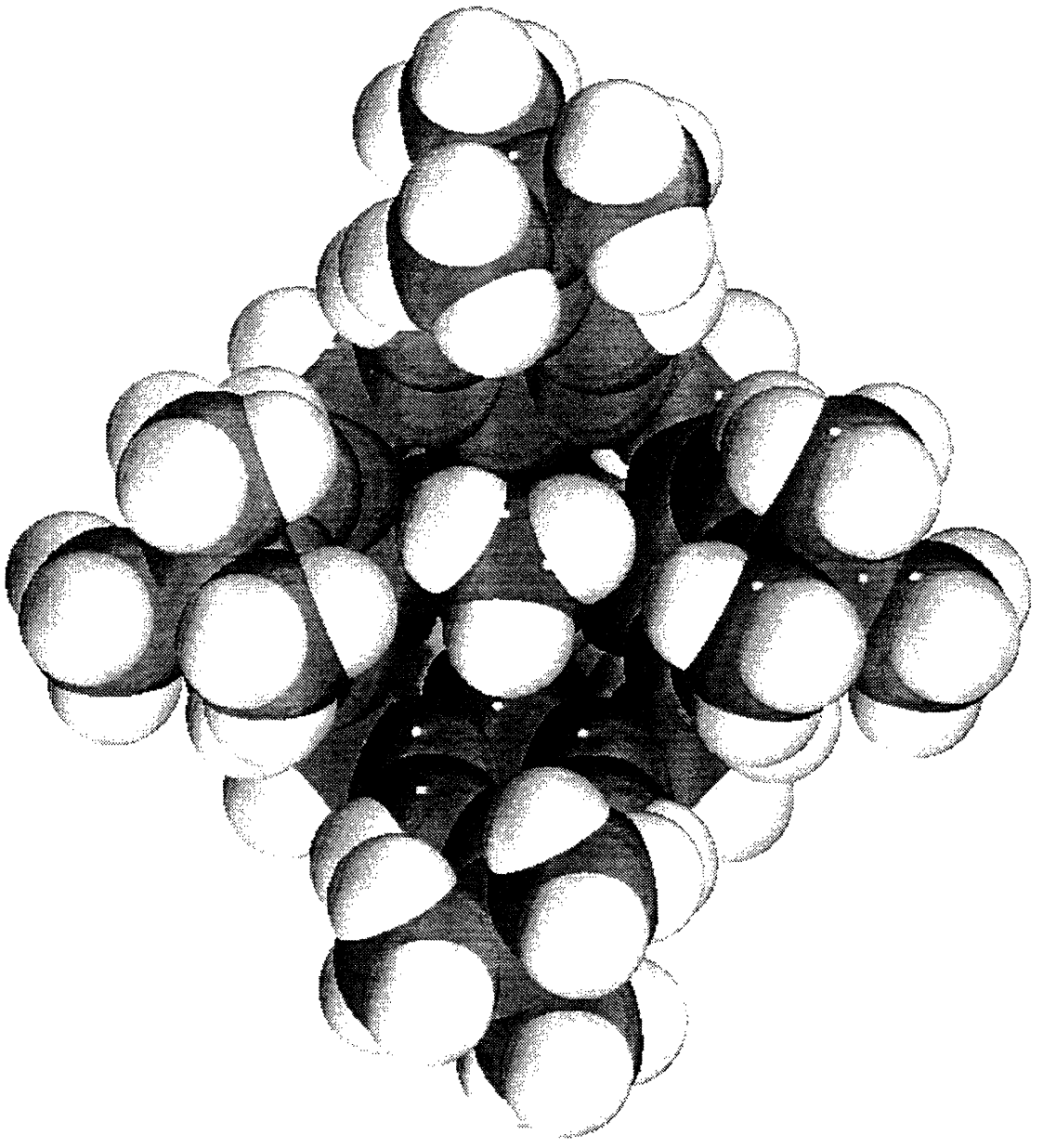

Figure 4.17. A space filling drawing of [Cp*Ta($NCCH_3$)(*p-tert*-butyl-calix[4]arene)] (**2c**), looking into the filled calixarene pocket.

two interactions are primarily responsible for holding small molecules within the pocket of the calixarene: 1) interactions between the electron deficient metal centers of these 14 e$^-$ complexes and the nucleophiles and 2) secondary attractive forces previously seen within calixarene macrocycles, the "alkyl-phenyl" or "CH_3-π" interactions.[17] In order to understand more about the *endo*-calix inclusion of Cp(*)Mcalixarene complexes, we undertook variable temperature solution ^2H NMR studies of [Cp*Ta($NCCD_3$)(*p-tert*-butylcalix[4]arene)] (**2c-d_3**), for which both metal-$NCCD_3$ and calixarene-$NCCD_3$ interactions are expected to occur.

Variable Temperature ^2H NMR Study of [Cp*Ta($NCCD_3$)(*p-tert*-butylcalix[4]arene)] (2c-d_3). Although there is a plethora of examples of inclusion by calixarene macrocycles in the solid state,[39] evidence for such interactions in solution is slim.[40-42] The breadth of the resonance corresponding to the NCCH_3 protons in the room temperature ^1H NMR of **2c** in $CDCl_3$ suggested a dynamic process. In order to slow down the exchange and observe the resonance of the included molecule unobstructed by resonances from other (i.e., *tert*-butyl) nuclei, a variable temperature ^2H NMR study of **2c-d_3** was carried out. The ^2H NMR spectra of **2c-d_3** in the presence of excess CD_3CN at T = 25 °C, 2 °C, -12 °C, and -56 °C are shown in Figure 4.18. At -56 °C, there are two resonances at 1.62 ppm and -0.95 ppm corresponding to the free and bound CD_3CN, respectively. With increasing temperature, the peaks broadened and then coalesced at 2 °C. The coalescence temperature was independent of the concentration of CD_3CN, supporting a dissociative process shown below (eq. 1).

[Cp*Ta($NCCD_3$)(*p-tert*-butylcalix[4]arene)] $\rightleftharpoons$

[Cp*Ta(*p-tert*-butylcalix[4]arene)] + $NCCD_3$ **(1)**

Given the size of the calixarene pocket, this mechanism is also intuitively most

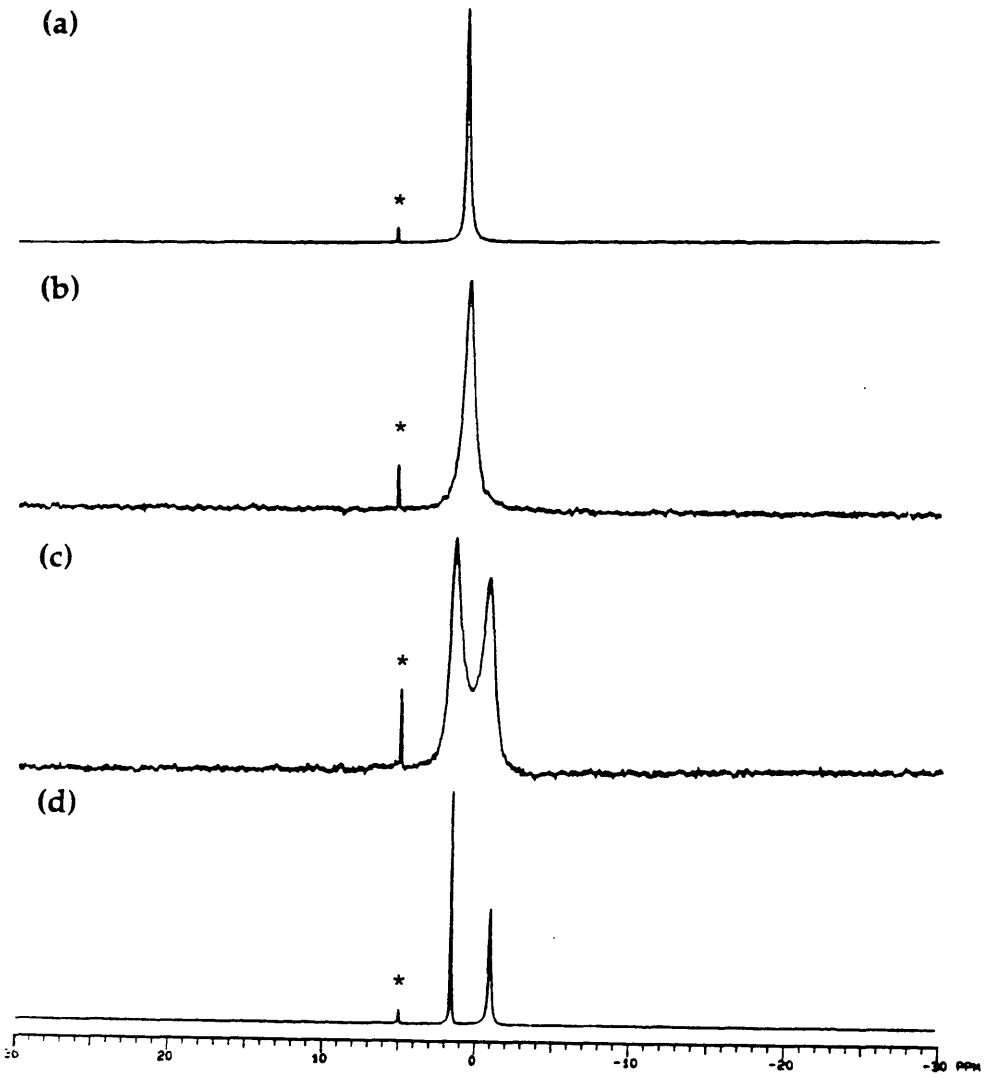

Figure 4.18. ^2H NMR (CH_2Cl_2) spectra of [Cp*Ta($NCCD_3$)(*p-tert*-butyl-calix[4]arene)] (**2c-d$_3$**) in the presence of excess CD_3CN at: (a) 25 °C, (b) 2 °C, (c) -12 °C, and (d) -56 °C. The peak labeled with an asterisk arises from CH_2Cl_2.

reasonable. Assuming equal populations of bound and free $NCCD_3$, an estimate for the rate constant for exchange at the coalescence temperature of 2 °C, given by $k = [\pi(\Delta\upsilon)]/[2]^{0.5}$ for $\Delta\upsilon$ = 780 Hz, was calculated to be 1700 s^{-1}. From the Eyring equation, $k = (\kappa T/h)e^{-\Delta G^{\ddagger}/RT}$, where R = 1.987 x 10^{-3} kcal/(mol)(K), κ = 1.38054 x 10-16 erg/K, h = 6.6256 x 10^{-27} erg sec, and T = 275 K, the free energy of activation $\Delta G^{\ddagger}$ = 8.9 kcal/mol.

Whereas evidence for inclusion of neutral molecules by *p-tert*-butylcalix[4]arene in solution has been elusive, the interactions with the *p-tert*-butylcalix[4]arene ligand in **2c-d$_3$** are augmented by coordination of the guest $NCCD_3$ by the tantalum metal center and can be observed on the NMR time scale at only moderately low temperatures. The influence of the Cp*Ta moiety is dominated by the bonding of the heteroatom of $NCCD_3$ to the electron deficient tantalum center. Moreover, the calixarene pocket adopts a cone conformation in solution in all of the Cp(*)Mcalixarene complexes **1**, **2a**, and **3**, as evidenced by the sharp resonances for their methylene doublets in the room temperature ^1H NMR spectra (see Figure 4.2, for example). In this conformation, the calixarene pocket is well-suited to accommodate small molecule guests. The presence of an electron deficient metal center at the top of the calixarene pocket promotes the observable solution inclusion of the neutral molecule, acetonitrile-d_3.

Deprotonation of $NCCH_3$ inside the calixarene cavity: reaction of [Cp*Ta($NCCH_3$)(*p-tert*-butylcalix[4]arene)] (2c) with butyllithium. When **2c** was stirred in a THF solution containing one equivalent of n-butyllithium, a yellow hue developed. A ^1H NMR spectrum of the product revealed many of the features present in the spectrum of **2c**, with one major difference: the peak corresponding to the *endo*-calix methyl group had disappeared from its position of δ -0.28 ppm, and a new, sharper resonance occurred upfield at δ -0.48 ppm, which integrated to 2 protons (Figure 4.19). Although deprotonation of the

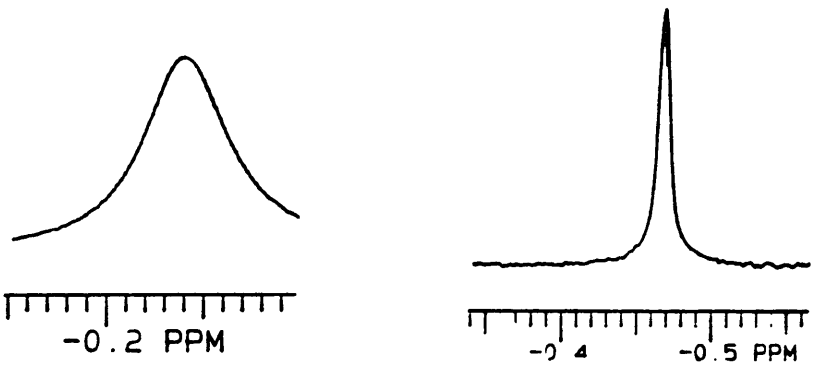

Figure 4.19. A comparison of the upfield region of the ^1H NMR spectra ($CDCl_3$) for (a) [Cp*Ta($NCCH_3$)(*p-tert*-butylcalix[4]arene)] (**2c**) and (b) the product of deprotonation of **2c** with n-butyllithium.

Ta-$NCCH_3$ moiety to produce Ta-$NCCH_2$ might be expected to produce a downfield shift of these proton resonances, it should be considered that the room temperature spectrum of **2c** represents the average of exchanging free and bound acetonitrile molecules. The chemical shift of the $NCCH_3$ proton resonances of the inclusion complex **2c** occurs upfield of the averaged peak. Sharpening of the upfield resonance upon deprotonation suggests that the host-guest interaction is no longer dynamic, as would be expected for the complex Li[Cp*Ta($NCCH_2$)(*p-tert*-butylcalix[4]arene)]. This preliminary result is, therefore, consistent with deprotonation of acetonitrile within the calixarene pocket. This result suggests the potential utility of transition metal calixarene complexes like **1**, **2a**, and **3** which preferentially bind small molecules in the *endo*-calix position. A Lewis acidic metal center will attract small molecule nucleophiles, which can then be activated within the protective barrier of a calixarene pocket. Further reaction would depend on the size of subsequent reagents.

Conclusions

Transition metal calixarene complexes [Cp*Ta(calix[4]arene)] (**1**), [Cp*Ta(*p-tert*-butylcalix[4]arene)] (**2a**), and [CpNb(*p-tert*-butylcalix[4]arene)] (**3**) have been prepared. These mononuclear products have electron deficient metal centers which are protected from reaction in the *exo*-calix position by the bulky cyclopentadienyl and pentamethylcyclopentadienyl ligands but have an available site for nucleophile binding in the *endo*-calix site. The structural characterization of [Cp*Ta(calix[4]arene)] (**1**) and [Cp*Ta(*p-tert*-butylcalix[4]-arene)] (**2a**) revealed an elliptical distortion of the fourfold symmetry of the starting calixarene macrocycles in the solid state upon binding the electron

deficient tantalum center. Insight into the distortion of the calixarene ligand in **1** and **2a** was provided by Fenske-Hall calculations. This distortion facilitates the unusual sideways positioning of toluene in the *endo*-calix toluene position in [Cp*Ta(*p-tert*-butyl-calix[4]arene)]·2 toluene·pentane (**2a**)·2 toluene·pentane. Intermolecular interactions occur in the solid state structure of **1**, in which the Cp* methyl groups penetrate the calixarene pocket of a neighboring complex. Nucleophile binding in the endo-calix site occurs in the solid state structures of [Cp*Ta(OH_2)(*p-tert*-butyl-calix[4]arene)] (**2b**) and [Cp*Ta($NCCH_3$)(*p-tert*-butylcalix[4]arene)] (**2c**). Variable temperature ^2H NMR studies revealed the inclusion of acetonitrile-d_3 in the complex [Cp*Ta($NCCD_3$)(*p-tert*-butylcalix[4]arene)] (**2c-d$_3$**) in solution. The deprotonation of acetonitrile in the *endo*-calix position was accomplished by addition of butyllithium to **2c**. These transition metal calixarene products combine the attractive forces of the ligand pocket with the electrophilicity of an electron deficient metal center to promote binding within the calixarene basket. This strategy represents a novel contribution to transition metal calixarene chemistry.

References

(1) Gutsche, C. D. *Calixarenes*; The Royal Society of Chemistry: Cambridge, 1989; Vol. 1.

(2) Baeyer, A. *Chem. Ber.* **1872**, *5*, 25.

(3) Baeyer, A. *Chem. Ber.* **1872**, *5*, 280.

(4) Baeyer, A. *Chem. Ber.* **1872**, *5*, 1094.

(5) Preparations of standard calix[4,6,8]arenes: (a) Gutsche, C. D.; Iqbal, M. *Org. Synth.*, **1989**, *68*, 234. (b) Gutsche, C. D.; Dhawan, B.; Leonis, M.; Stewart, D. *Org. Synth.* **1989**, *68*, 238. (c) Munch, J. H.; Gutsche, C. D. *Org. Synth.* **1989**, *68*, 243.

(6) Olmstead, M. M.; Sigel, G.; Hope, H.; Xu, X.; Power, P. P. *J. Am. Chem. Soc.* **1985**, *107*, 8087.

(7) Bott, S. G.; Coleman, A. W.; Atwood, J. L. *J. Chem. Soc., Chem. Commun.* **1986**, 610.

(8) Hofmeister, G. E.; Hahn, F. E.; Pedersen, S. F. *J. Am. Chem. Soc.* **1989**, *111*, 2318.

(9) Hofmeister, G. E.; Alvarado, E.; Leary, J. A.; Yoon, D. J.; Pedersen, S. F. *J. Am. Chem. Soc.* **1990**, *112*, 8843.

(10) Furphy, B. M.; Harrowfield, J. M.; Kepert, D. L.; Skelton, B. W. *Inorg. Chem.* **1987**, *26*, 4231.

(11) Andreetti, G. D.; Calestani, G.; Ugozzoli, F.; Arduini, A. *J. Incl. Phenom.* **1987**, *5*, 123.

(12) Englehardt, L. M.; Furphy, B. M.; Harrowfield, J. M.; White, A. H. *Aust. J. Chem.* **1988**, *41*, 1465.

(13) Furphy, B. M.; Harrowfield, J. M.; Ogden, M. I. *J. Chem. Soc., Dalton Trans.* **1989**, 2217.

(14) Corazza, F.; Floriani, C.; Angiola, C. V.; Guastini, C. *J. Chem. Soc., Chem. Commun.* **1990**, 1083.

(15) For some examples, see: (a) Gutsche, C. D. *Acc. Chem. Res.* **1983**, *16*, 161. (b) Gutsche, C. D. *Top. Curr. Chem.* **1984**, *123*, 1. (c) Andreetti, G.D.; Ugozzoli, F.; Ungaro, R.; Pochini, A. in *Inclusion Compounds*; Atwood, J. L., ed.; Oxford Science: New York, **1984**; Vol 4. (d) Atwood, J.L.; Orr, G.W.; Juneja, R.K.; Bott, S.G.; Hamada, F. *Pure & Appl. Chem.* **1993**, *65*, 1471.

(16) Andreetti, G. D. *J. Chem. Soc., Chem. Commun.* **1979**, 1005.

(17) Andreetti, G. D.; Ori, O.; Ugozzoli, F.; Alfieri, C.; Pochini, A.; Ungaro, R. *J. Incl. Phenom.* **1988**, *6*, 523.

(18) Corazza, F.; Floriani, C.; Chiesi-Villa, A.; Guastini, C. *J. Chem. Soc., Chem. Commun.* **1990**, 640.

(19) Corazza, F.; Floriani, C.; Chiesi-Villa, A.; Rizzoli, C. *Inorg. Chem.* **1991**, *30*, 4465.

(20) Acho, J. A.; Lippard, S. J. *Inorg. Chim. Acta.* **1994**, *in press*,

(21) Gutsche, C. D.; Levine, J. A.; Sujeeth, P. K. *J. Org. Chem.* **1985**, *50*, 5802.

(22) Gutsche, C. D.; Iqbal, M. *Org. Synth.* **1989**, *68*, 234.

(23) Carnahan, E. M.; Rardin, R. L.; Bott, S. G.; Lippard, S. J. *Inorg. Chem.* **1992**, *31*, 5193.

(24) *International Tables for Crystallography, Volume A*; Hahn, T., Ed.; Kluwer Academic Publishers: Dordrecht, 1989.

(25) Nakamoto, K. *Infrared and Raman Spectra of Inorganic and Coordination Compounds;* 3rd edn. ; Wiley-Interscience: New York, 1977.

(26) Chisholm, M. H.; Rothwell, I. P. In *Comp. Coor. Chem.*; G. Wilkinson, Ed.; Pergamon Books: New York, 1987; Vol. 2: Ligands; 335.

(27) Bott, S. G.; Coleman, A. W.; Atwood, J. L. *J. Am. Chem. Soc.* **1986**, *108*, 1709.

(28) Coruzzi, M.; Andreetti, G. D.; Bocchi, V.; Pochini, A.; Ungaro, R. *J. Chem. Soc., Perkin Trans. 2* **1982**, 1133.

(29) McKervey, M. A.; Seward, E. M. *J. Org. Chem.* **1986**, *51*, 3581.

(30) Cotton, F. A. *Chemical Applications of Group Theory;* 3rd Edn. ; John Wiley and Sons: New York, 1993.

(31) Cotton, F. A.; Lippard, S. J. *Chem. Commun. (London)* **1965**, 245.

(32) Cotton, F. A.; Lippard, S. J. *Inorg. Chem.* **1965**, *4*, 1621.

(33) Cotton, F. A.; Lippard, S. J. *Inorg. Chem.* **1966**, *5*, 9.

(34) Venkatesarlu, P. *J. Chem. Phys.* **1951**, *19*, 293.

(35) Kepert, D. L.; Nyholm, R. S. *J. Chem. Soc.* **1965**, 2871.

(36) Chavant, C.; Daran, J.; Jeannin, Y.; Constant, G.; Morancho, R. *Acta Cryst., Sect B.* **1975**, *31*, 1828.

(37) Collman, J. P.; Hegedus, L. S.; Norton, J. R.; Finke, R. G. *Principles and Applications of Organotransition Metal Chemistry;* University Science Books: Mill Valley, Calif., 1987.

(38) Einstein, F. W. B.; Enwall, E.; Morris, D. M.; Sutton, D. *Inorg. Chem.* **1971**, *10*, 678.

(39) Andreetti, G. D.; Ugozzoli, F. In *Calixarenes, A Versitile Class of Macrocyclic Compounds;* J. Vicens and V. Böhmer, Ed.; Kluwer Academic Publishers: Dordrecht, 1991; 87-123.

(40) Pochini, A.; Ungaro, R. *Gazz. Chim. Ital.* **1989**, *119*, 335.

(41) Kobayashi, K.; Asakawa, Y.; Kikuchi, Y.; Toi, H.; Aoyama, Y. *J. Am. Chem. Soc.* **1993**, *115*, 2648.

(42) Andreetti, G. D.; Ugaro, R. *J. Chem. Soc., Chem. Commun.* **1994**, *4*, 529.

Table 4.1. X-ray Crystallographic Information for [Cp*Ta(calix[4]arene)] (1), [Cp*Ta(*p-tert*-butylcalix[4]arene)]·2 toluene·pentane (2a)·2 toluene·pentane, [Cp*Ta(OH_2)(*p-tert*-butylcalix[4]arene)]·acetone (2b)·acetone, and [Cp*Ta($NCCH_3$)(*p-tert*-butylcalix[4]arene)]·2.5 CH_2Cl_2 (2c)·2.5 CH_2Cl_2.[a]

	(1)	(2a)·2 toluene ·pentane	(2b)·acetone	(2c)·2.5 CH_2Cl_2
formula	$C_{38}H_{35}O_4Ta$	$C_{71}H_{83}O_4Ta$	$C_{57}H_{75}O_6Ta$	$C_{58.5}H_{75}NO_4Cl_5Ta$
a (Å)	11.270 (3)	13.678 (2)	11.168 (3)	20.21 (1)
b (Å)	18.168 (4)	19.404 (2)	22.211 (6)	22.70 (1)
c (Å)	15.655 (2)	23.230 (2)	20.957 (5)	13.346 (4)
α (deg)				95.10 (2)
β (deg)	110.86 (1)	94.790 (9)	91.17 (1)	97.62 (3)
γ (deg)				108.67 (4)
V (Å^3)	2995 (1)	6144 (1)	4963 (2)	5691 (4)
T (°C)	-83.1	-73.8	-78.1	-110
fw	736.64	1181.38	961.16	1214.46
Z	4	4	4	4
ρ_{calc} (g/cm^3)	1.63	1.276	1.39	1.42

Table 4.1 (cont). X-ray Crystallographic Information for [Cp*Ta(calix[4]arene)] (1), [Cp*Ta(*p-tert*-butylcalix[4]arene)]·2 toluene·pentane (2a)·2 toluene·pentane, [Cp*Ta(OH_2)(*p-tert*-butylcalix[4]arene)]·acetone (2b)·acetone, and [Cp*Ta($NCCH_3$)(*p-tert*-butylcalix[4]arene)]·2.5 CH_2Cl_2 (2c)·2.5 CH_2Cl_2.[a]

	(1)	(2a)·2 toluene ·pentane	(2b)·acetone	(2c)·2.5 CH_2Cl_2
space group	$P2_1/c$	$P2_1/c$	$P2_1/n$	$P\bar{1}$
2θ limits (deg)	3-50	3-51	3-50	3-50
data limits	$+h+k\pm l$	$+h+k\pm l$	$+h+k\pm l$	$+h\pm k\pm l$
μ (cm^{-1})	37.07	18.32	22.35	22.08
no. of total data	5862	12585	11039	21134
no. of unique data	5480	11995	8970	19825
R(merge)[b]	3.0	5.1	2.8	2.5
no. of unique observed[c] data	4184	8636	6798	14108
no. of LS params	388	670	577	1252
p factor	0.03	0.03	0.03	0.03
R^d =	0.028	0.030	0.031	0.036
R_w =	0.034	0.038	0.037	0.040

Table 4.1 (cont). X-ray Crystallographic Information for [Cp*Ta(calix[4]arene)] (1), [Cp*Ta(*p-tert*-butylcalix[4]arene)]·2 toluene·pentane (2a)·2 toluene·pentane, [Cp*Ta(OH_2)(*p-tert*-butylcalix[4]arene)]·acetone (2b)·acetone, and [Cp*Ta($NCCH_3$)(*p-tert*-butylcalix[4]arene)]·2.5 CH_2Cl_2 (2c)·2.5 CH_2Cl_2.[a]

---

[a] Data were collected on an Enraf Nonius CAD-4F kappa geometry diffractometer using Mo K_α radiation.

[b] R(merge) = $\Sigma_{i=1}^{n}\Sigma_{j=1}^{m} | \langle F_i^2\rangle - F_{ij}^2 | / \Sigma_{i=1}^{n} m \times \langle F_i^2\rangle$ where n = number of reflections observed more than once, m = number of times a given reflection was observed, and $\langle F_i^2\rangle$ is the average value of F^2 for reflection i.

[c] Observation criterion $I > 3\sigma(I)$. [d] $R = \Sigma | |F_o| - |F_c| | / \Sigma |F_o|$, $R_w = [\Sigma w (|F_o| - |F_c|)^2 / \Sigma w |F_o|^2]^{1/2}$, where $w = 1/\sigma(F)$, as defined in Carnahan, E. M.; Rardin, R. L.; Bott, S. G.; Lippard, S. J. *Inorg. Chem.* **1992**, *31*, 5193.

Table 4.2. Final Positional Parameters and B(eq) for [Cp*Ta(calix[4]arene)] (1).[a]

atom	x	y	z	B(eq) Å^{2} [b]
Ta	0.272613(19)	0.170703(10)	0.255635(13)	1.336(8)
O(20)	0.43571(34)	0.19934(19)	0.33792(24)	2.3(1)
O(40)	0.24878(31)	0.27897(18)	0.22866(21)	1.6(1)
O(60)	0.11815(38)	0.17836(20)	0.27442(29)	2.9(2)
O(80)	0.29900(34)	0.08092(18)	0.33415(22)	1.9(1)
C(1)	0.33845(58)	0.16962(29)	0.12416(35)	2.4(2)
C(2)	0.20398(58)	0.17678(29)	0.08891(34)	2.4(2)
C(3)	0.14909(52)	0.11117(30)	0.10848(34)	2.1(2)
C(4)	0.25122(50)	0.06265(26)	0.15441(33)	1.7(2)
C(5)	0.36752(51)	0.09917(29)	0.16583(34)	2.0(2)
C(6)	0.43237(75)	0.22438(35)	0.11549(47)	4.0(3)
C(7)	0.13385(80)	0.24118(36)	0.03456(42)	4.6(3)
C(8)	0.01202(59)	0.09430(37)	0.08075(43)	3.7(3)
C(9)	0.23853(54)	-0.01407(30)	0.18329(38)	2.5(2)
C(10)	0.49769(59)	0.06804(33)	0.20926(44)	3.2(3)
C(20)	0.52714(47)	0.22576(28)	0.41247(33)	1.6(2)
C(21)	0.58726(48)	0.17743(28)	0.48493(35)	1.9(2)
C(22)	0.68451(54)	0.20552(32)	0.56024(36)	2.6(2)
C(23)	0.71916(56)	0.27902(35)	0.56468(39)	3.0(2)
C(24)	0.65661(54)	0.32531(31)	0.49231(40)	2.6(2)
C(25)	0.55986(47)	0.29984(29)	0.41543(35)	1.8(2)
C(26)	0.48276(50)	0.34960(28)	0.33936(35)	1.9(2)
C(40)	0.24296(48)	0.33069(27)	0.29034(33)	1.6(2)
C(41)	0.35483(48)	0.36752(26)	0.34471(32)	1.6(2)
C(42)	0.34699(53)	0.42050(29)	0.40710(36)	2.3(2)
C(43)	0.23326(56)	0.43784(30)	0.41560(38)	2.6(2)
C(44)	0.12445(52)	0.40283(30)	0.36044(37)	2.4(2)
C(45)	0.12519(50)	0.34971(28)	0.29764(34)	1.9(2)
C(46)	0.00120(52)	0.31506(30)	0.23768(36)	2.2(2)
C(60)	0.01649(47)	0.18765(30)	0.30029(35)	1.9(2)
C(61)	-0.04549(47)	0.25464(31)	0.28432(34)	2.0(2)
C(62)	-0.14692(57)	0.26267(35)	0.31390(42)	3.1(3)

Table 4.2 (cont). Final Positional Parameters and B(eq) for [Cp*Ta(calix[4]arene)] (1).[a]

atom	x	y	z	B(eq) Å^{2} [b]
C(63)	-0.18408(60)	0.20496(41)	0.35740(49)	3.8(3)
C(64)	-0.12036(58)	0.13874(37)	0.37206(44)	3.3(3)
C(65)	-0.01652(51)	0.12834(31)	0.34603(37)	2.3(2)
C(66)	0.06232(56)	0.05893(31)	0.36382(40)	2.6(2)
C(80)	0.30328(53)	0.07995(26)	0.42323(34)	1.9(2)
C(81)	0.18972(54)	0.06714(27)	0.43931(36)	2.1(2)
C(82)	0.19904(60)	0.06187(30)	0.53068(40)	2.7(2)
C(83)	0.31331(66)	0.06949(31)	0.60207(40)	3.1(3)
C(84)	0.42257(59)	0.08184(30)	0.58440(37)	2.7(2)
C(85)	0.41931(53)	0.08779(27)	0.49500(36)	2.1(2)
C(86)	0.54392(54)	0.09807(29)	0.47887(36)	2.4(2)

[a]Numbers in parentheses are estimated standard deviations of the last significant figure. See Figure 4.3 for atom labeling scheme. [b]$B_{eq} = 4/3\ [a^2\beta_{11} + b^2\beta_{22} + c^2\beta_{33} + 2ab\cos(\gamma)\beta_{12} + 2ac\cos(\beta)\beta_{13} + 2bc\cos(\alpha)\beta_{23}]$

Table 4.3. Complete Anisotropic Thermal Parameters for [Cp*Ta(calix[4]arene)] (1).[a]

atom	U11	U22	U33	U12	U13	U23
Ta	0.02169(12)	0.01771(12)	0.01349(11)	0.000649(86)	0.008871(83)	-0.000590(82)
O(20)	0.0283(22)	0.0229(19)	0.0254(20)	-0.0006(16)	-0.0026(17)	0.0017(16)
O(40)	0.0260(20)	0.0194(18)	0.0155(17)	0.0007(14)	0.0091(15)	0.0000(13)
O(60)	0.0379(25)	0.0311(23)	0.0527(27)	0.0085(18)	0.0308(21)	0.0129(19)
O(80)	0.0361(22)	0.0201(19)	0.0183(18)	-0.0002(16)	0.0140(16)	0.0031(14)
C(1)	0.0543(39)	0.0297(30)	0.0194(27)	-0.0072(27)	0.0300(27)	-0.0076(23)
C(2)	0.0508(38)	0.0265(30)	0.0112(25)	0.0077(26)	0.0077(24)	-0.0029(22)
C(3)	0.0339(33)	0.0304(30)	0.0153(26)	0.0013(24)	0.0076(23)	-0.0101(22)
C(4)	0.0318(31)	0.0175(26)	0.0201(26)	-0.0028(21)	0.0143(23)	-0.0079(20)
C(5)	0.0338(32)	0.0284(30)	0.0189(27)	0.0040(24)	0.0169(24)	-0.0056(22)
C(6)	0.0878(57)	0.0368(37)	0.0518(43)	-0.0121(36)	0.0533(42)	-0.0076(31)
C(7)	0.1008(62)	0.0368(39)	0.0210(32)	0.0167(38)	0.0005(35)	0.0042(27)
C(8)	0.0331(38)	0.0557(43)	0.0399(38)	0.0042(31)	-0.0027(30)	-0.0205(32)
C(9)	0.0415(35)	0.0225(28)	0.0341(31)	-0.0042(26)	0.0189(27)	-0.0125(24)
C(10)	0.0391(38)	0.0396(37)	0.0479(39)	-0.0015(28)	0.0213(31)	-0.0181(29)
C(20)	0.0173(27)	0.0266(28)	0.0205(26)	-0.0007(21)	0.0091(21)	-0.0018(21)
C(21)	0.0185(27)	0.0272(29)	0.0266(29)	0.0034(22)	0.0071(22)	0.0006(22)
C(22)	0.0309(34)	0.0415(35)	0.0209(29)	0.0050(27)	0.0034(25)	0.0075(24)
C(23)	0.0287(34)	0.0504(39)	0.0262(32)	-0.0075(29)	-0.0030(26)	-0.0002(27)
C(24)	0.0283(32)	0.0357(33)	0.0348(33)	-0.0082(26)	0.0106(26)	0.0002(26)
C(25)	0.0162(28)	0.0296(29)	0.0265(29)	-0.0003(22)	0.0101(23)	-0.0020(22)
C(26)	0.0282(30)	0.0228(28)	0.0235(27)	-0.0074(22)	0.0113(23)	0.0009(21)
C(40)	0.0258(28)	0.0203(26)	0.0160(25)	0.0023(22)	0.0074(21)	0.0028(21)
C(41)	0.0252(29)	0.0173(26)	0.0189(26)	-0.0005(21)	0.0084(22)	0.0030(20)
C(42)	0.0317(33)	0.0268(29)	0.0229(29)	-0.0043(24)	0.0042(24)	-0.0044(22)
C(43)	0.0408(37)	0.0276(31)	0.0287(31)	0.0043(26)	0.0118(27)	-0.0096(24)
C(44)	0.0296(32)	0.0307(32)	0.0312(32)	0.0093(25)	0.0115(26)	0.0004(24)
C(45)	0.0256(30)	0.0258(29)	0.0210(27)	0.0042(22)	0.0063(22)	0.0043(22)
C(46)	0.0245(29)	0.0336(32)	0.0214(28)	0.0071(24)	0.0032(23)	-0.0021(23)
C(60)	0.0130(26)	0.0373(32)	0.0231(28)	-0.0037(22)	0.0094(22)	-0.0056(23)
C(61)	0.0154(28)	0.0390(32)	0.0183(26)	-0.0020(23)	0.0018(21)	-0.0052(22)
C(62)	0.0286(34)	0.0520(40)	0.0395(36)	0.0087(29)	0.0143(28)	-0.0038(30)

Table 4.3 (cont). Complete Anisotropic Thermal Parameters for [Cp*Ta(calix[4]arene)] (1).[a]

atom	U11	U22	U33	U12	U13	U23
C(63)	0.0272(35)	0.0661(48)	0.0596(45)	0.0028(32)	0.0277(33)	-0.0005(36)
C(64)	0.0304(35)	0.0536(41)	0.0477(39)	-0.0084(30)	0.0226(30)	0.0020(32)
C(65)	0.0239(30)	0.0374(33)	0.0285(30)	-0.0082(25)	0.0130(24)	-0.0057(25)
C(66)	0.0403(36)	0.0307(32)	0.0369(34)	-0.0109(26)	0.0247(29)	0.0009(25)
C(80)	0.0432(35)	0.0169(26)	0.0180(27)	0.0058(23)	0.0174(25)	0.0049(20)
C(81)	0.0416(35)	0.0166(27)	0.0259(28)	-0.0022(23)	0.0165(26)	0.0057(21)
C(82)	0.0507(40)	0.0279(31)	0.0347(34)	-0.0036(27)	0.0281(31)	0.0053(25)
C(83)	0.0673(48)	0.0293(33)	0.0266(32)	-0.0004(30)	0.0255(33)	0.0036(25)
C(84)	0.0489(40)	0.0252(31)	0.0244(31)	0.0021(27)	0.0079(28)	0.0012(23)
C(85)	0.0394(35)	0.0153(26)	0.0250(29)	0.0049(23)	0.0116(25)	0.0061(21)
C(86)	0.0342(34)	0.0261(30)	0.0246(30)	0.0115(25)	0.0033(25)	0.0031(23)

[a] Numbers in parentheses are estimated standard deviations in the last significant digit. The anisotropic temperature factors are of the form $\exp[-2\pi^2(U_{11}h^2a^{*2} \ldots +2U_{12}hka^*b^* = \ldots)]$.

Table 4.4. Final Positional Parameters and B(eq) for [Cp*Ta(*p-tert*-butylcalix[4]arene)]·2 toluene·pentane (2a)·2 toluene·pentane.[a]

atom	x	y	z	B(eq) Å^{2} [b]
Ta	1.26382(1)	-0.091543(8)	0.582985(7)	1.323(7)
O20	1.3421(2)	-0.1606(1)	0.6198(1)	1.9(1)
O40	1.2940(2)	-0.0421(1)	0.6582(1)	1.6(1)
O60	1.1311(2)	-0.0765(2)	0.5965(1)	2.2(1)
O80	1.2124(2)	-0.1692(1)	0.5325(1)	1.7(1)
C1	1.4031(3)	-0.0553(2)	0.5306(2)	1.9(2)
C2	1.3726(3)	0.0033(2)	0.5604(2)	2.1(2)
C3	1.2768(3)	0.0207(2)	0.5381(2)	2.2(2)
C4	1.2477(3)	-0.0264(2)	0.4929(2)	2.1(2)
C5	1.3270(3)	-0.0722(2)	0.4876(2)	1.8(2)
C6	1.5001(3)	-0.0903(3)	0.5413(2)	2.9(2)
C7	1.4333(4)	0.0430(3)	0.6057(2)	3.5(2)
C8	1.2174(5)	0.0809(3)	0.5569(2)	3.7(3)
C9	1.1507(4)	-0.0285(3)	0.4573(2)	3.0(2)
C10	1.3294(4)	-0.1272(3)	0.4428(2)	2.5(2)
C20	1.4000(3)	-0.2102(2)	0.6451(2)	1.7(2)
C21	1.4044(3)	-0.2735(2)	0.6167(2)	1.9(2)
C22	1.4668(3)	-0.3232(2)	0.6425(2)	2.1(2)
C23	1.5226(3)	-0.3117(2)	0.6944(2)	2.3(2)
C24	1.5125(3)	-0.2482(2)	0.7215(2)	2.0(2)
C25	1.4520(3)	-0.1962(2)	0.6974(2)	1.5(2)
C26	1.4432(3)	-0.1248(2)	0.7232(2)	1.7(2)
C27	1.5913(4)	-0.3692(3)	0.7197(2)	2.9(2)
C28	1.6609(5)	-0.3916(4)	0.6747(3)	5.5(3)
C29	1.6538(4)	-0.3469(3)	0.7738(2)	3.7(3)
C30	1.5290(5)	-0.4310(3)	0.7352(3)	4.4(3)
C40	1.2738(3)	-0.0676(2)	0.7107(2)	1.5(2)
C41	1.3434(3)	-0.1075(2)	0.7437(2)	1.7(2)
C42	1.3218(3)	-0.1297(2)	0.7981(2)	1.8(2)

Table 4.4 (cont). Final Positional Parameters and B(eq) for [Cp*Ta(*p-tert*-butylcalix[4]arene)]·2 toluene·pentane (2a)·2 toluene·pentane.[a]

atom	x	y	z	B(eq) Å^{2} [b]
C43	1.2341(3)	-0.1147(2)	0.8214(2)	1.8(2)
C44	1.1671(3)	-0.0754(2)	0.7874(2)	1.9(2)
C45	1.1850(3)	-0.0517(2)	0.7327(2)	1.5(2)
C46	1.1067(3)	-0.0077(2)	0.6996(2)	1.9(2)
C47	1.2147(3)	-0.1357(2)	0.8833(2)	2.3(2)
C48	1.2449(5)	-0.0765(3)	0.9240(2)	4.6(3)
C49	1.1072(4)	-0.1517(3)	0.8886(3)	4.5(3)
C50	1.2719(5)	-0.1997(3)	0.9026(2)	4.6(3)
C60	1.0441(3)	-0.0861(2)	0.6196(2)	1.9(2)
C61	1.0261(3)	-0.0504(2)	0.6688(2)	1.8(2)
C62	0.9344(3)	-0.0584(3)	0.6898(2)	2.3(2)
C63	0.8629(3)	-0.1012(2)	0.6637(2)	2.5(2)
C64	0.8863(3)	-0.1380(2)	0.6153(2)	2.4(2)
C65	0.9765(3)	-0.1317(2)	0.5920(2)	2.0(2)
C66	1.0032(3)	-0.1733(2)	0.5413(2)	2.3(2)
C67	0.7607(4)	-0.1059(3)	0.6866(2)	3.3(2)
C68	0.7118(4)	-0.0354(4)	0.6813(4)	6.0(4)
C69	0.6949(4)	-0.1571(4)	0.6518(3)	5.7(4)
C70	0.7701(5)	-0.1298(4)	0.7483(3)	5.6(4)
C80	1.1735(3)	-0.2277(2)	0.5533(2)	1.7(2)
C81	1.0723(3)	-0.2321(2)	0.5581(2)	1.9(2)
C82	1.0344(3)	-0.2929(2)	0.5789(2)	2.5(2)
C83	1.0918(4)	-0.3501(2)	0.5942(2)	2.5(2)
C84	1.1911(4)	-0.3446(2)	0.5875(2)	2.3(2)
C85	1.2335(3)	-0.2850(2)	0.5674(2)	1.8(2)
C86	1.3424(3)	-0.2837(2)	0.5606(2)	1.9(2)
C87	1.0462(4)	-0.4180(3)	0.6128(2)	3.4(2)
C88	1.031(1)	-0.4625(4)	0.5626(3)	14.3(8)
C89	1.1113(6)	-0.4537(4)	0.6603(4)	8.0(5)
C90	0.9484(7)	-0.4069(4)	0.6381(5)	10.3(6)

Table 4.4 (cont). Final Positional Parameters and B(eq) for [Cp*Ta(*p-tert*-butylcalix[4]arene)]·2 toluene·pentane (2a)·2 toluene·pentane.[a]

atom	x	y	z	B(eq) Å^{2} [b]
C100	1.2740(6)	-0.3240(5)	0.7595(4)	7.8(5)
C101	1.1721(5)	-0.3111(4)	0.7681(3)	5.2(4)
C102	1.1227(7)	-0.2592(3)	0.7356(3)	6.5(4)
C103	1.0242(8)	-0.2455(5)	0.7410(4)	7.5(5)
C104	0.9748(6)	-0.2852(5)	0.7798(4)	7.6(5)
C105	1.0210(6)	-0.3368(4)	0.8156(4)	6.5(4)
C106	1.1209(5)	-0.3480(3)	0.8066(3)	4.4(3)
C200	0.1416(7)	0.1904(6)	0.0748(5)	11.6(7)
C201	0.2393(5)	0.2066(4)	0.0567(4)	6.1(4)
C202	0.3130(6)	0.2234(5)	0.0952(4)	7.1(5)
C203	0.4071(8)	0.2368(5)	0.0849(4)	8.5(6)
C204	0.4245(7)	0.2334(5)	0.0269(5)	8.3(6)
C205	0.3581(8)	0.2172(5)	-0.0168(4)	7.4(5)
C206	0.2604(7)	0.2023(5)	-0.0004(4)	7.7(5)
C207	0.600(1)	-0.0325(9)	0.9261(7)	16.9(6)
C208	0.552(1)	-0.016(1)	0.9658(9)	19.8(7)
C209	0.487(2)	0.0263(9)	0.993(1)	7.9(5)

[a]Numbers in parentheses are estimated standard deviations of the last significant figure. See Figure 4.4 for atom labeling scheme. [b]$B_{eq} = 4/3\ [a^2\beta_{11} + b^2\beta_{22} + c^2\beta_{33} + 2ab\cos(\gamma)\beta_{12} + 2ac\cos(\beta)\beta_{13} + 2bc\cos(\alpha)\beta_{23}]$

Table 4.5. Complete Anisotropic Thermal Parameters for [Cp*Ta(*p-tert*-butylcalix[4]arene)]·2 toluene·pentane (2a)·2 toluene·pentane.[a]

atom	U11	U22	U33	U12	U13	U23
Ta	0.0161(1)	0.0176(1)	0.0166(1)	-0.00110(8)	0.00207(6)	0.00343(8)
O20	0.024(2)	0.023(2)	0.026(2)	0.005(1)	-0.002(1)	0.002(1)
O40	0.021(2)	0.019(1)	0.020(2)	-0.001(1)	0.004(1)	0.001(1)
O60	0.018(2)	0.031(2)	0.033(2)	-0.002(1)	0.007(1)	-0.003(1)
O80	0.024(2)	0.019(2)	0.022(2)	-0.003(1)	0.003(1)	0.003(1)
C1	0.024(2)	0.029(2)	0.022(2)	-0.008(2)	0.008(2)	0.009(2)
C2	0.034(3)	0.027(2)	0.021(2)	-0.013(2)	0.007(2)	0.006(2)
C3	0.038(3)	0.020(2)	0.026(3)	-0.005(2)	0.011(2)	0.007(2)
C4	0.030(3)	0.027(2)	0.022(2)	0.000(2)	0.002(2)	0.013(2)
C5	0.026(2)	0.025(2)	0.020(2)	-0.005(2)	0.006(2)	0.005(2)
C6	0.022(2)	0.054(3)	0.035(3)	-0.000(2)	0.006(2)	0.011(3)
C7	0.052(3)	0.047(3)	0.033(3)	-0.025(3)	0.004(3)	0.002(3)
C8	0.070(4)	0.026(3)	0.049(3)	0.010(3)	0.020(3)	0.009(2)
C9	0.032(3)	0.045(3)	0.037(3)	0.003(2)	-0.001(2)	0.014(3)
C10	0.041(3)	0.035(3)	0.021(3)	-0.006(2)	0.005(2)	-0.002(2)
C20	0.017(2)	0.022(2)	0.026(2)	0.003(2)	0.004(2)	0.005(2)
C21	0.024(2)	0.027(2)	0.023(2)	0.001(2)	0.006(2)	0.002(2)
C22	0.029(3)	0.020(2)	0.031(3)	0.007(2)	0.007(2)	0.002(2)
C23	0.023(2)	0.031(3)	0.034(3)	0.007(2)	0.005(2)	0.010(2)
C24	0.019(2)	0.033(3)	0.024(2)	0.002(2)	0.000(2)	0.002(2)
C25	0.015(2)	0.023(2)	0.022(2)	-0.001(2)	0.005(2)	0.002(2)
C26	0.017(2)	0.028(2)	0.020(2)	-0.002(2)	-0.003(2)	-0.001(2)
C27	0.043(3)	0.037(3)	0.031(3)	0.015(2)	-0.004(2)	0.005(2)
C28	0.064(4)	0.084(5)	0.060(4)	0.051(4)	0.003(3)	0.002(4)
C29	0.044(3)	0.043(3)	0.051(4)	0.014(3)	-0.016(3)	0.007(3)
C30	0.067(4)	0.036(3)	0.061(4)	0.006(3)	-0.018(3)	0.011(3)
C40	0.020(2)	0.018(2)	0.018(2)	-0.002(2)	0.000(2)	-0.002(2)
C41	0.017(2)	0.020(2)	0.027(2)	-0.001(2)	0.002(2)	-0.002(2)
C42	0.026(2)	0.022(2)	0.021(2)	0.003(2)	-0.001(2)	-0.002(2)
C43	0.027(2)	0.023(2)	0.018(2)	0.001(2)	0.002(2)	0.001(2)

Table 4.5 (cont). Complete Anisotropic Thermal Parameters for [Cp*Ta(*p-tert*-butylcalix[4]arene)]·2 toluene·pentane (2a)·2 toluene·pentane.[a]

atom	U11	U22	U33	U12	U13	U23
C44	0.021(2)	0.026(2)	0.026(2)	0.002(2)	0.004(2)	-0.003(2)
C45	0.023(2)	0.020(2)	0.015(2)	0.003(2)	0.001(2)	0.000(2)
C46	0.025(2)	0.025(2)	0.023(2)	0.007(2)	0.005(2)	0.002(2)
C47	0.034(3)	0.034(3)	0.020(2)	0.003(2)	0.005(2)	0.003(2)
C48	0.090(5)	0.060(4)	0.027(3)	-0.013(4)	0.017(3)	-0.012(3)
C49	0.049(4)	0.081(5)	0.042(4)	-0.009(3)	0.013(3)	0.023(3)
C50	0.085(5)	0.062(4)	0.031(3)	0.033(4)	0.022(3)	0.019(3)
C60	0.014(2)	0.030(2)	0.029(2)	0.003(2)	0.001(2)	0.011(2)
C61	0.019(2)	0.025(2)	0.025(2)	0.004(2)	0.003(2)	0.007(2)
C62	0.024(2)	0.040(3)	0.025(3)	0.007(2)	0.002(2)	0.008(2)
C63	0.018(2)	0.039(3)	0.038(3)	0.003(2)	0.006(2)	0.011(2)
C64	0.019(2)	0.030(3)	0.041(3)	-0.003(2)	-0.001(2)	0.009(2)
C65	0.019(2)	0.031(3)	0.024(2)	0.002(2)	-0.002(2)	0.006(2)
C66	0.019(2)	0.031(3)	0.035(3)	-0.007(2)	-0.004(2)	-0.000(2)
C67	0.024(3)	0.059(4)	0.045(3)	-0.002(2)	0.012(2)	0.012(3)
C68	0.034(3)	0.070(5)	0.130(7)	0.017(3)	0.039(4)	0.025(5)
C69	0.025(3)	0.108(6)	0.086(5)	-0.015(4)	0.015(3)	0.004(4)
C70	0.045(4)	0.116(6)	0.054(4)	-0.009(4)	0.022(3)	0.020(4)
C80	0.026(2)	0.020(2)	0.017(2)	-0.005(2)	-0.001(2)	-0.001(2)
C81	0.029(2)	0.026(2)	0.015(2)	-0.006(2)	-0.002(2)	0.000(2)
C82	0.029(3)	0.032(3)	0.034(3)	-0.010(2)	0.003(2)	-0.001(2)
C83	0.041(3)	0.022(2)	0.031(3)	-0.013(2)	-0.002(2)	-0.001(2)
C84	0.040(3)	0.021(2)	0.024(3)	-0.001(2)	-0.003(2)	0.001(2)
C85	0.026(2)	0.024(2)	0.018(2)	-0.004(2)	-0.002(2)	-0.002(2)
C86	0.032(3)	0.022(2)	0.019(2)	0.006(2)	0.003(2)	0.000(2)
C87	0.059(4)	0.031(3)	0.039(3)	-0.021(3)	0.001(3)	0.007(2)
C88	0.41(2)	0.089(6)	0.049(5)	-0.17(1)	0.045(8)	-0.025(5)
C89	0.117(7)	0.073(5)	0.109(7)	-0.051(5)	-0.019(5)	0.056(5)
C90	0.105(7)	0.056(5)	0.24(1)	-0.018(5)	0.087(8)	0.048(6)
C100	0.091(6)	0.117(7)	0.092(6)	-0.033(5)	0.038(5)	-0.041(5)

Table 4.5 (cont). Complete Anisotropic Thermal Parameters for [Cp*Ta(*p-tert*-butylcalix[4]arene)]·2 toluene·pentane (2a)·2 toluene·pentane.[a]

atom	U11	U22	U33	U12	U13	U23
C101	0.080(5)	0.063(4)	0.055(4)	-0.021(4)	0.009(4)	-0.024(4)
C102	0.141(8)	0.039(4)	0.060(5)	-0.005(5)	-0.030(5)	-0.005(3)
C103	0.118(8)	0.083(6)	0.082(7)	-0.011(6)	-0.014(6)	-0.011(5)
C104	0.092(6)	0.095(7)	0.098(7)	0.005(6)	-0.018(5)	-0.036(6)
C105	0.095(6)	0.062(5)	0.085(6)	-0.009(4)	-0.023(5)	-0.026(4)
C106	0.073(5)	0.055(4)	0.042(4)	-0.015(3)	0.009(3)	-0.009(3)
C200	0.075(6)	0.17(1)	0.20(1)	0.011(7)	0.057(7)	0.07(1)
C201	0.052(4)	0.081(5)	0.097(6)	-0.004(4)	0.004(4)	0.019(5)
C202	0.074(6)	0.109(7)	0.086(6)	-0.009(5)	0.006(5)	-0.020(5)
C203	0.119(8)	0.101(7)	0.106(8)	-0.009(6)	0.035(6)	-0.010(6)
C204	0.100(7)	0.071(6)	0.15(1)	-0.001(5)	0.061(7)	0.025(6)
C205	0.103(7)	0.101(7)	0.078(6)	0.016(6)	0.008(5)	0.006(5)
C206	0.102(7)	0.114(7)	0.074(6)	0.021(6)	-0.007(5)	0.023(5)

[a] Numbers in parentheses are estimated standard deviations in the last significant digit. The anisotropic temperature factors are of the form $\exp[-2\pi^2(U_{11}h^2a^{*2} \ldots +2U_{12}hka^*b^* = \ldots)]$.

Table 4.6. Final Positional Parameters and B(eq) for [Cp*Ta(OH_2)(*p-tert*-butylcalix[4]arene)]·acetone (2b)·acetone.[a]

atom	x	y	z	B(eq) Å^{2} [b]
Ta	0.07787(2)	0.721543(8)	0.572945(8)	1.110(8)
O(1)	0.1706(3)	0.7358(1)	0.4831(1)	1.4(1)
O(20)	0.2032(2)	0.6552(1)	0.5765(1)	1.3(1)
O(40)	0.2019(3)	0.7838(1)	0.5999(1)	1.5(1)
O(60)	-0.0131(3)	0.7928(1)	0.5360(1)	1.3(1)
O(80)	-0.0135(2)	0.6655(1)	0.5138(1)	1.3(1)
O(100)	0.7650(5)	0.1900(2)	0.6114(2)	6.2(3)
C(1)	0.0504(4)	0.6596(2)	0.6755(2)	1.9(2)
C(2)	0.0739(4)	0.7236(3)	0.6926(2)	2.0(2)
C(3)	-0.0215(4)	0.7608(2)	0.6685(2)	1.7(2)
C(4)	-0.1042(4)	0.7206(2)	0.6371(2)	1.8(2)
C(5)	-0.0595(4)	0.6583(2)	0.6418(2)	2.0(2)
C(6)	0.1250(5)	0.6037(3)	0.6937(3)	3.5(3)
C(7)	0.1787(5)	0.7448(3)	0.7325(3)	3.5(3)
C(8)	-0.0359(6)	0.8305(3)	0.6772(3)	3.7(3)
C(9)	-0.2219(5)	0.7399(3)	0.6075(3)	3.5(3)
C(10)	-0.1230(6)	0.6000(3)	0.6187(3)	3.5(3)
C(20)	0.2913(4)	0.6376(2)	0.5367(2)	1.3(2)
C(21)	0.2686(4)	0.5921(2)	0.4896(2)	1.3(2)
C(22)	0.3629(4)	0.5736(2)	0.4513(2)	1.4(2)
C(23)	0.4785(4)	0.5990(2)	0.4579(2)	1.5(2)
C(24)	0.4954(4)	0.6456(2)	0.5038(2)	1.6(2)
C(25)	0.4045(4)	0.6661(2)	0.5433(2)	1.3(2)
C(26)	0.4258(4)	0.7190(2)	0.5901(2)	1.7(2)
C(27)	0.5820(4)	0.5780(2)	0.4153(2)	1.8(2)
C(28)	0.5619(5)	0.5111(3)	0.3890(2)	2.9(2)
C(29)	0.7008(4)	0.5770(3)	0.4533(3)	2.5(2)
C(30)	0.5944(5)	0.6247(3)	0.3601(3)	4.0(3)
C(40)	0.2889(4)	0.8129(2)	0.5657(2)	1.3(2)
C(41)	0.4010(4)	0.7836(2)	0.5604(2)	1.5(2)
C(42)	0.4877(4)	0.8129(2)	0.5244(2)	1.7(2)

Table 4.6 (cont). Final Positional Parameters and B(eq) for [Cp*Ta(OH_2)(*p-tert*-butylcalix[4]arene)]·acetone (2b)·acetone.[a]

atom	x	y	z	B(eq) Å^{2} [b]
C(43)	0.4678(4)	0.8692(2)	0.4918(2)	1.8(2)
C(44)	0.3556(4)	0.8973(2)	0.4981(2)	1.7(2)
C(45)	0.2654(4)	0.8700(2)	0.5342(2)	1.4(2)
C(46)	0.1420(4)	0.9007(2)	0.5363(2)	1.6(2)
C(47)	0.5658(4)	0.8960(2)	0.4496(3)	2.3(2)
C(48)	0.6792(5)	0.9095(3)	0.4896(3)	3.1(3)
C(49)	0.5271(5)	0.9560(3)	0.4149(3)	3.3(3)
C(50)	0.5952(5)	0.8469(3)	0.3981(3)	3.5(3)
C(60)	-0.0076(4)	0.8271(2)	0.4812(2)	1.4(2)
C(61)	0.0611(4)	0.8824(2)	0.4804(2)	1.6(2)
C(62)	0.0587(4)	0.9187(2)	0.4251(2)	1.7(2)
C(63)	-0.0061(4)	0.9017(2)	0.3704(2)	1.9(2)
C(64)	-0.0697(4)	0.8447(2)	0.3728(2)	1.6(2)
C(65)	-0.0711(4)	0.8073(2)	0.4265(2)	1.4(2)
C(66)	-0.1401(4)	0.7448(2)	0.4257(2)	1.4(2)
C(67)	-0.0113(5)	0.9417(2)	0.3097(2)	2.4(2)
C(68)	0.0898(6)	0.9907(3)	0.3088(3)	4.4(3)
C(69)	-0.1316(5)	0.9769(3)	0.3069(3)	3.5(3)
C(70)	-0.0009(6)	0.9003(3)	0.2501(3)	3.7(3)
C(80)	-0.0040(4)	0.6520(2)	0.4512(2)	1.2(2)
C(81)	-0.0653(4)	0.6888(2)	0.4053(2)	1.3(2)
C(82)	-0.0569(4)	0.6733(2)	0.3413(2)	1.5(2)
C(83)	0.0123(4)	0.6221(2)	0.3203(2)	1.8(2)
C(84)	0.0741(4)	0.5884(2)	0.3669(2)	1.6(2)
C(85)	0.0691(4)	0.6019(2)	0.4318(2)	1.3(2)
C(86)	0.1442(4)	0.5647(2)	0.4794(2)	1.3(2)
C(87)	0.0163(5)	0.6072(3)	0.2488(2)	2.4(2)
C(88)	-0.1082(5)	0.5864(3)	0.2246(3)	4.0(3)
C(89)	0.1045(6)	0.5555(3)	0.2340(3)	4.1(3)
C(90)	0.0535(6)	0.6665(3)	0.2115(3)	4.4(3)
C(91)	0.7189(5)	0.2153(3)	0.6565(3)	3.1(3)
C(92)	0.686(1)	0.2828(4)	0.6533(4)	6.9(5)

Table 4.6 (cont). Final Positional Parameters and B(eq) for [Cp*Ta(OH_2)(*p-tert*-butylcalix[4]arene)]·acetone (2b)·acetone.[a]

atom	x	y	z	B(eq) Å^{2} [b]
C(93)	0.6880(6)	0.1777(4)	0.7129(3)	4.7(3)
H(1)	0.1468	0.7513	0.4506	2.1
H(2)	0.2347	0.7186	0.4784	2.1

[a]Numbers in parentheses are estimated standard deviations of the last significant figure. See Figure 4.9 for atom labeling scheme. [b]$B_{eq} = 4/3\ [a^2\beta_{11} + b^2\beta_{22} + c^2\beta_{33} + 2ab\cos(\gamma)\beta_{12} + 2ac\cos(\beta)\beta_{13} + 2bc\cos(\alpha)\beta_{23}]$

Table 4.7. Complete Anisotropic Thermal Parameters for [Cp*Ta(OH_2)(*p-tert*-butylcalix[4]arene)]·acetone (2b)·acetone.[a]

atom	U11	U22	U33	U12	U13	U23
Ta	0.0142(1)	0.0131(1)	0.0150(1)	-0.00070(8)	0.00304(7)	0.00030(8)
O(1)	0.015(2)	0.021(2)	0.016(2)	0.005(1)	0.002(1)	0.003(1)
O(20)	0.016(2)	0.016(2)	0.017(2)	0.001(1)	0.005(1)	0.001(1)
O(40)	0.017(2)	0.016(2)	0.023(2)	-0.001(1)	0.002(1)	-0.001(1)
O(60)	0.017(2)	0.013(2)	0.020(2)	-0.001(1)	0.002(1)	0.001(1)
O(80)	0.017(2)	0.017(2)	0.015(2)	-0.001(1)	-0.000(1)	0.001(1)
O(100)	0.127(5)	0.048(3)	0.062(3)	0.031(3)	0.060(3)	0.015(3)
C(1)	0.027(3)	0.029(3)	0.018(2)	0.003(2)	0.011(2)	0.007(2)
C(2)	0.022(2)	0.039(3)	0.015(2)	-0.007(2)	0.006(2)	0.002(2)
C(3)	0.028(3)	0.022(3)	0.016(2)	-0.001(2)	0.010(2)	-0.003(2)
C(4)	0.017(2)	0.033(3)	0.017(2)	-0.001(2)	0.010(2)	0.004(2)
C(5)	0.029(3)	0.027(3)	0.019(2)	-0.009(2)	0.013(2)	-0.001(2)
C(6)	0.053(4)	0.046(4)	0.036(3)	0.014(3)	0.017(3)	0.022(3)
C(7)	0.036(3)	0.071(4)	0.024(3)	-0.023(3)	0.002(2)	0.004(3)
C(8)	0.077(5)	0.025(3)	0.040(3)	0.001(3)	0.032(3)	-0.006(3)
C(9)	0.021(3)	0.080(5)	0.035(3)	0.004(3)	0.010(2)	0.011(3)
C(10)	0.065(4)	0.039(4)	0.030(3)	-0.031(3)	0.011(3)	-0.001(3)
C(20)	0.019(2)	0.013(2)	0.017(2)	0.002(2)	0.001(2)	0.004(2)
C(21)	0.016(2)	0.012(2)	0.022(2)	0.001(2)	-0.001(2)	0.004(2)
C(22)	0.021(2)	0.016(2)	0.018(2)	0.002(2)	-0.001(2)	-0.001(2)
C(23)	0.020(2)	0.019(2)	0.017(2)	0.005(2)	0.003(2)	0.004(2)
C(24)	0.015(2)	0.019(2)	0.026(2)	-0.003(2)	-0.002(2)	0.004(2)
C(25)	0.017(2)	0.014(2)	0.018(2)	0.003(2)	-0.001(2)	0.003(2)
C(26)	0.012(2)	0.026(3)	0.027(2)	-0.002(2)	0.000(2)	0.000(2)
C(27)	0.025(3)	0.025(3)	0.019(2)	0.002(2)	0.005(2)	-0.002(2)
C(28)	0.030(3)	0.045(4)	0.037(3)	0.007(3)	0.010(2)	-0.016(3)
C(29)	0.024(3)	0.030(3)	0.042(3)	0.002(2)	0.009(2)	-0.008(3)
C(30)	0.046(4)	0.062(4)	0.043(4)	0.016(3)	0.021(3)	0.018(3)
C(40)	0.018(2)	0.016(2)	0.015(2)	-0.004(2)	0.004(2)	-0.003(2)
C(41)	0.021(2)	0.012(2)	0.023(2)	-0.002(2)	-0.003(2)	-0.006(2)
C(42)	0.018(2)	0.018(2)	0.030(3)	0.002(2)	0.001(2)	-0.004(2)

Table 4.7 (cont). Complete Anisotropic Thermal Parameters for [Cp*Ta(OH$_2$)(*p-tert*-butylcalix[4]arene)]·acetone (2b)·acetone.[a]

atom	U11	U22	U33	U12	U13	U23
C(43)	0.020(3)	0.017(2)	0.032(3)	-0.003(2)	0.006(2)	-0.000(2)
C(44)	0.020(2)	0.015(2)	0.031(3)	-0.001(2)	0.004(2)	0.002(2)
C(45)	0.018(2)	0.013(2)	0.023(2)	-0.001(2)	0.001(2)	-0.006(2)
C(46)	0.020(2)	0.010(2)	0.032(3)	0.002(2)	0.004(2)	-0.002(2)
C(47)	0.021(3)	0.025(3)	0.043(3)	-0.002(2)	0.013(2)	0.005(2)
C(48)	0.024(3)	0.033(3)	0.063(4)	-0.005(2)	0.015(3)	0.010(3)
C(49)	0.039(3)	0.032(3)	0.056(4)	0.005(3)	0.027(3)	0.017(3)
C(50)	0.040(3)	0.042(4)	0.052(4)	0.005(3)	0.022(3)	0.002(3)
C(60)	0.014(2)	0.015(2)	0.023(2)	0.004(2)	0.008(2)	0.006(2)
C(61)	0.016(2)	0.018(2)	0.026(2)	0.005(2)	0.005(2)	-0.003(2)
C(62)	0.018(2)	0.015(2)	0.032(3)	0.002(2)	0.002(2)	0.006(2)
C(63)	0.025(3)	0.021(3)	0.029(3)	0.003(2)	0.005(2)	0.008(2)
C(64)	0.024(3)	0.018(2)	0.019(2)	0.003(2)	0.001(2)	0.001(2)
C(65)	0.015(2)	0.015(2)	0.024(2)	0.005(2)	0.003(2)	0.001(2)
C(66)	0.015(2)	0.019(2)	0.019(2)	0.001(2)	0.002(2)	0.002(2)
C(67)	0.035(3)	0.027(3)	0.030(3)	-0.000(2)	0.001(2)	0.010(2)
C(68)	0.061(4)	0.056(4)	0.052(4)	-0.027(3)	-0.004(3)	0.034(3)
C(69)	0.053(4)	0.037(3)	0.043(3)	0.013(3)	-0.002(3)	0.016(3)
C(70)	0.068(4)	0.039(4)	0.033(3)	0.004(3)	0.014(3)	0.015(3)
C(80)	0.013(2)	0.015(2)	0.019(2)	-0.003(2)	0.003(2)	0.000(2)
C(81)	0.014(2)	0.012(2)	0.022(2)	-0.002(2)	0.001(2)	0.002(2)
C(82)	0.017(2)	0.020(3)	0.021(2)	-0.001(2)	-0.004(2)	0.003(2)
C(83)	0.021(2)	0.022(3)	0.024(2)	-0.003(2)	-0.002(2)	-0.002(2)
C(84)	0.020(2)	0.018(2)	0.024(2)	-0.001(2)	0.001(2)	-0.006(2)
C(85)	0.015(2)	0.011(2)	0.025(2)	-0.005(2)	-0.002(2)	-0.000(2)
C(86)	0.018(2)	0.012(2)	0.021(2)	0.001(2)	-0.001(2)	-0.002(2)
C(87)	0.036(3)	0.032(3)	0.024(3)	0.007(2)	-0.002(2)	-0.004(2)
C(88)	0.047(4)	0.067(5)	0.039(3)	0.015(3)	-0.014(3)	-0.029(3)
C(89)	0.061(4)	0.070(5)	0.024(3)	0.031(4)	0.003(3)	-0.010(3)
C(90)	0.082(5)	0.056(4)	0.031(3)	0.007(4)	0.013(3)	0.005(3)
C(91)	0.036(3)	0.048(4)	0.034(3)	0.015(3)	0.010(2)	0.004(3)

Table 4.7 (cont). Complete Anisotropic Thermal Parameters for [Cp*Ta(OH_2)(*p-tert*-butylcalix[4]arene)]·acetone (2b)·acetone.[a]

atom	U11	U22	U33	U12	U13	U23
C(92)	0.152(9)	0.049(5)	0.064(5)	0.029(5)	0.046(5)	-0.002(4)
C(93)	0.070(5)	0.070(5)	0.038(4)	0.021(4)	0.022(3)	0.015(3)

[a] Numbers in parentheses are estimated standard deviations in the last significant digit. The anisotropic temperature factors are of the form $\exp[-2\pi^2(U_{11}h^2a^{*2} \ldots +2U_{12}hka^*b^* = \ldots)]$.

Table 4.8. Final Positional Parameters and B(eq) for [Cp*Ta(NCCH$_3$)(*p-tert*-butylcalix[4]arene)]·2.5 CH_2Cl_2 (2c)·2.5 CH_2Cl_2.[a]

atom	x	y	z	B(eq) Å$^{2\,b}$
Ta(100)	0.781243(13)	0.371406(11)	0.801468(18)	1.42(1)
Ta(200)	0.225222(13)	0.074523(11)	0.598623(18)	1.51(1)
Cl(1)	0.91348(23)	0.16225(16)	0.68612(29)	11.2(2)
Cl(2)	0.97050(18)	0.25168(15)	0.55403(31)	10.3(2)
Cl(3)	0.96179(12)	0.41493(11)	0.31943(18)	5.5(1)
Cl(4)	0.98300(12)	0.30408(11)	0.22078(21)	6.1(1)
Cl(5)	0.54250(17)	0.13285(12)	0.50590(24)	8.1(1)
Cl(6)	0.51307(14)	0.23982(11)	0.43257(16)	6.2(1)
Cl(7)	0.16629(17)	0.16876(15)	0.17558(24)	8.9(2)
Cl(8)	0.09106(16)	0.22199(13)	0.30458(25)	8.3(1)
Cl(9)	0.15198(19)	0.35651(14)	0.53838(29)	9.6(2)
Cl(10)	0.08208(14)	0.44353(14)	0.59496(22)	7.9(1)
O(120)	0.86071(20)	0.44919(17)	0.86116(29)	1.7(1)
O(140)	0.76203(20)	0.41584(18)	0.68608(28)	1.7(1)
O(160)	0.67951(20)	0.31545(17)	0.76540(29)	1.7(1)
O(180)	0.77817(20)	0.34926(17)	0.94061(28)	1.6(1)
O(220)	0.26158(20)	0.14861(17)	0.70474(29)	1.7(1)
O(240)	0.14009(21)	0.04603(18)	0.66525(29)	1.9(2)
O(260)	0.20371(21)	-0.01538(17)	0.54258(29)	1.8(1)
O(280)	0.32452(20)	0.08744(17)	0.58156(28)	1.6(1)
N(10)	0.72542(25)	0.43279(22)	0.86762(36)	1.4(2)
N(20)	0.26569(25)	0.03639(22)	0.73358(39)	1.6(2)
C(10)	0.69961(33)	0.46329(30)	0.90449(49)	2.1(2)
C(11)	0.66830(45)	0.50517(42)	0.95370(87)	7.3(5)
C(20)	0.28924(34)	0.02049(28)	0.80277(48)	1.9(2)
C(21)	0.31949(50)	-0.00039(41)	0.89211(60)	5.4(4)
C(101)	0.89345(32)	0.35297(29)	0.76667(48)	2.2(2)
C(102)	0.85901(38)	0.30523(33)	0.82134(50)	2.8(3)
C(103)	0.79497(37)	0.26824(30)	0.75986(58)	2.9(3)
C(104)	0.78866(34)	0.29328(30)	0.66655(49)	2.4(3)
C(105)	0.85042(32)	0.34583(28)	0.67167(45)	1.8(2)

Table 4.8 (cont). Final Positional Parameters and B(eq) for [Cp*Ta(NCCH$_3$)(*p-tert*-butylcalix[4]arene)]·2.5 CH_2Cl_2 (2c)·2.5 CH_2Cl_2.[a]

atom	x	y	z	B(eq) Å^{2} [b]
C(106)	0.96447(36)	0.40219(37)	0.79841(59)	4.1(3)
C(107)	0.88817(48)	0.29303(44)	0.92387(59)	5.2(4)
C(108)	0.74354(46)	0.20992(35)	0.78689(76)	5.5(4)
C(109)	0.72920(39)	0.26566(38)	0.57832(58)	4.3(3)
C(110)	0.86813(41)	0.38448(35)	0.58714(54)	3.6(3)
C(120)	0.86348(29)	0.50462(27)	0.91194(46)	1.7(2)
C(121)	0.86827(30)	0.51182(27)	1.01886(44)	1.6(2)
C(122)	0.86498(31)	0.56702(29)	1.06796(46)	2.1(2)
C(123)	0.86025(32)	0.61699(29)	1.01651(51)	2.3(3)
C(124)	0.85845(32)	0.60861(27)	0.91195(48)	1.9(2)
C(125)	0.85934(32)	0.55396(28)	0.85786(47)	2.1(2)
C(126)	0.84989(33)	0.54510(27)	0.74259(46)	2.0(2)
C(127)	0.85615(37)	0.67814(31)	1.07249(55)	3.0(3)
C(128)	0.91952(55)	0.73260(43)	1.0651(11)	9.5(6)
C(129)	0.79084(58)	0.69055(48)	1.02125(92)	8.5(6)
C(130)	0.84774(81)	0.67376(47)	1.18249(84)	10.0(7)
C(140)	0.73129(32)	0.46046(27)	0.67113(41)	1.6(2)
C(141)	0.77318(31)	0.52416(28)	0.69310(43)	1.7(2)
C(142)	0.74003(35)	0.56818(28)	0.67195(44)	2.1(2)
C(143)	0.66926(34)	0.55276(28)	0.63370(45)	2.1(2)
C(144)	0.62947(32)	0.48854(30)	0.61561(44)	2.0(2)
C(145)	0.65857(31)	0.44218(27)	0.63429(43)	1.6(2)
C(146)	0.61283(32)	0.37406(28)	0.61947(44)	1.8(2)
C(147)	0.63242(37)	0.60109(32)	0.61170(52)	2.9(3)
C(148)	0.60485(57)	0.59292(43)	0.49895(67)	6.4(4)
C(149)	0.57283(45)	0.59310(36)	0.67259(74)	5.2(4)
C(150)	0.68462(44)	0.66864(36)	0.64302(67)	4.6(4)
C(160)	0.61943(30)	0.32603(26)	0.78507(44)	1.6(2)
C(161)	0.58505(30)	0.35413(26)	0.71571(43)	1.6(2)
C(162)	0.52672(30)	0.36837(26)	0.74085(43)	1.6(2)
C(163)	0.50188(31)	0.35693(26)	0.83263(45)	1.7(2)

Table 4.8 (cont). Final Positional Parameters and B(eq) for [Cp*Ta($NCCH_3$)(*p-tert*-butylcalix[4]arene)]·2.5 CH_2Cl_2 (2c)·2.5 CH_2Cl_2.[a]

atom	x	y	z	B(eq) Å^{2} [b]
C(164)	0.53724(31)	0.32925(26)	0.89858(43)	1.7(2)
C(165)	0.59528(29)	0.31266(25)	0.87675(42)	1.3(2)
C(166)	0.63476(30)	0.28593(26)	0.95584(43)	1.6(2)
C(167)	0.43932(33)	0.37753(28)	0.85739(47)	2.2(2)
C(168)	0.37306(36)	0.34200(34)	0.77851(56)	3.4(3)
C(169)	0.42215(38)	0.36457(34)	0.96251(55)	3.4(3)
C(170)	0.45736(38)	0.44845(33)	0.85327(57)	3.4(3)
C(180)	0.75466(31)	0.36814(26)	1.02463(43)	1.5(2)
C(181)	0.68477(32)	0.33667(26)	1.03881(42)	1.6(2)
C(182)	0.66125(32)	0.35532(28)	1.12515(44)	1.8(2)
C(183)	0.70477(32)	0.40409(28)	1.20030(45)	1.8(2)
C(184)	0.77264(32)	0.43447(27)	1.18284(43)	1.7(2)
C(185)	0.79851(30)	0.41859(27)	1.09711(44)	1.6(2)
C(186)	0.87082(32)	0.45813(28)	1.07694(45)	1.9(2)
C(187)	0.68008(35)	0.42322(32)	1.29823(47)	2.5(3)
C(188)	0.72565(50)	0.41046(45)	1.38904(55)	5.4(4)
C(189)	0.69139(55)	0.49311(44)	1.30938(68)	6.1(4)
C(190)	0.60370(48)	0.38854(51)	1.30034(67)	7.1(4)
C(201)	0.20885(33)	0.16668(28)	0.51602(45)	2.0(2)
C(202)	0.14164(34)	0.12124(30)	0.50977(45)	2.2(2)
C(203)	0.13924(34)	0.06634(28)	0.44702(45)	2.1(2)
C(204)	0.20537(33)	0.07836(29)	0.41488(44)	1.9(2)
C(205)	0.24908(34)	0.14029(30)	0.45727(45)	2.2(2)
C(206)	0.23210(38)	0.23182(30)	0.57119(51)	2.9(3)
C(207)	0.08140(37)	0.13077(33)	0.55786(53)	3.2(3)
C(208)	0.07533(38)	0.00758(32)	0.41501(51)	3.1(3)
C(209)	0.22615(38)	0.03552(31)	0.34259(47)	2.9(3)
C(210)	0.32141(38)	0.17332(31)	0.43779(50)	2.9(3)
C(220)	0.29395(33)	0.16013(26)	0.80302(43)	1.7(2)
C(221)	0.36762(31)	0.17712(25)	0.82568(43)	1.5(2)
C(222)	0.39997(31)	0.18644(26)	0.92779(45)	1.7(2)

Table 4.8 (cont). Final Positional Parameters and B(eq) for [Cp*Ta(NCCH$_3$)(*p*-*tert*-butylcalix[4]arene)]·2.5 CH_2Cl_2 (2c)·2.5 CH_2Cl_2.[a]

atom	x	y	z	B(eq) Å^{2} [b]
C(223)	0.36082(32)	0.17796(27)	1.00745(44)	1.8(2)
C(224)	0.28745(34)	0.16141(28)	0.98132(46)	2.1(2)
C(225)	0.25273(31)	0.15140(26)	0.88103(45)	1.6(2)
C(226)	0.17197(33)	0.12762(29)	0.85597(46)	2.2(2)
C(227)	0.39560(34)	0.18694(29)	1.11925(45)	2.3(2)
C(228)	0.38767(45)	0.24570(34)	1.17547(50)	3.9(3)
C(229)	0.35942(38)	0.12999(34)	1.16998(50)	3.2(3)
C(230)	0.47383(39)	0.19490(37)	1.13044(50)	3.8(3)
C(240)	0.12713(30)	0.01926(28)	0.75070(46)	1.8(2)
C(241)	0.14071(32)	0.05714(29)	0.84578(48)	2.1(2)
C(242)	0.12783(33)	0.02750(31)	0.93122(47)	2.4(3)
C(243)	0.10291(33)	-0.03715(31)	0.92934(49)	2.5(3)
C(244)	0.09126(32)	-0.07269(29)	0.83382(48)	2.3(2)
C(245)	0.10322(31)	-0.04640(28)	0.74471(45)	1.9(2)
C(246)	0.09631(32)	-0.08796(28)	0.64542(47)	2.2(2)
C(247)	0.09475(41)	-0.06746(35)	1.02665(53)	3.6(3)
C(248)	0.06887(52)	-0.03042(50)	1.10461(66)	6.3(5)
C(249)	0.04543(81)	-0.13508(53)	1.00501(71)	13.5(7)
C(250)	0.16699(56)	-0.06763(47)	1.07630(65)	6.1(4)
C(260)	0.21539(32)	-0.06405(26)	0.58699(42)	1.7(2)
C(261)	0.16438(33)	-0.10156(27)	0.63738(44)	1.9(2)
C(262)	0.17928(34)	-0.14864(27)	0.68648(47)	2.2(2)
C(263)	0.24260(34)	-0.16004(27)	0.68790(47)	2.2(2)
C(264)	0.29170(32)	-0.12272(27)	0.63477(46)	1.9(2)
C(265)	0.27969(32)	-0.07546(26)	0.58432(43)	1.7(2)
C(266)	0.33749(32)	-0.03299(27)	0.53580(44)	1.9(2)
C(267)	0.25830(37)	-0.20982(31)	0.74778(52)	2.9(3)
C(268)	0.20586(41)	-0.27461(33)	0.70006(59)	3.7(3)
C(269)	0.33231(43)	-0.21246(38)	0.74610(72)	5.2(4)
C(270)	0.24844(55)	-0.19810(37)	0.85898(60)	5.5(4)
C(280)	0.38062(31)	0.07675(27)	0.63576(44)	1.6(2)

Table 4.8 (cont). Final Positional Parameters and B(eq) for [Cp*Ta(NCCH$_3$)(*p-tert*-butylcalix[4]arene)]·2.5 CH_2Cl_2 (2c)·2.5 CH_2Cl_2.[a]

atom	x	y	z	B(eq) Å^{2} [b]
C(281)	0.39118(32)	0.01922(27)	0.61334(42)	1.7(2)
C(282)	0.44839(33)	0.00936(28)	0.67095(47)	2.0(2)
C(283)	0.49541(33)	0.05384(28)	0.74819(46)	2.0(2)
C(284)	0.48278(32)	0.11054(28)	0.76694(44)	2.0(2)
C(285)	0.42636(31)	0.12247(27)	0.71242(44)	1.7(2)
C(286)	0.41227(31)	0.18353(26)	0.74141(43)	1.6(2)
C(287)	0.55620(34)	0.03900(31)	0.80946(51)	2.6(3)
C(288)	0.60740(40)	0.02945(40)	0.73879(60)	4.4(3)
C(289)	0.59791(38)	0.09071(35)	0.89756(57)	3.9(3)
C(290)	0.52493(40)	-0.02190(35)	0.85563(58)	3.9(3)
C(300)	0.89639(48)	0.20740(43)	0.59578(71)	5.8(4)
C(301)	0.95642(43)	0.36974(39)	0.20341(62)	4.5(3)
C(302)	0.51679(42)	0.19755(37)	0.53513(59)	4.1(3)
C(303)	0.10605(44)	0.15582(40)	0.25728(61)	4.6(4)
C(304)	0.11742(55)	0.41171(47)	0.50158(67)	6.4(4)

[a]Numbers in parentheses are estimated standard deviations of the last significant figure. See Figure 4.10 for atom labeling scheme. [b]$B_{eq} = 4/3\ [a^2\beta_{11} + b^2\beta_{22} + c^2\beta_{33} + 2ab\cos(\gamma)\beta_{12} + 2ac\cos(\beta)\beta_{13} + 2bc\cos(\alpha)\beta_{23}]$

Table 4.9. Complete anisotropic thermal parameters for [Cp*Ta(NCCH$_3$)(*p*-*tert*-butylcalix[4]arene)]·2.5 CH_2Cl_2 (2c)·2.5 CH_2Cl_2.[a]

atom	U11	U22	U33	U12	U13	U23
Ta(100)	0.01728(16)	0.01835(15)	0.02023(15)	0.00789(12)	0.00523(11)	0.00166(11)
Ta(200)	0.02054(16)	0.01913(15)	0.01697(15)	0.00621(12)	0.00157(12)	0.00340(11)
Cl(1)	0.1983(42)	0.1037(26)	0.1404(31)	0.0666(27)	0.0345(29)	0.0408(23)
Cl(2)	0.1032(26)	0.0971(24)	0.1955(38)	0.0214(20)	0.0556(26)	0.0363(24)
Cl(3)	0.0620(15)	0.0719(16)	0.0725(16)	0.0209(13)	0.0038(12)	0.0056(13)
Cl(4)	0.0567(15)	0.0568(15)	0.1272(22)	0.0262(12)	0.0239(15)	0.0263(14)
Cl(5)	0.1207(25)	0.0732(18)	0.1387(26)	0.0469(18)	0.0706(21)	0.0122(17)
Cl(6)	0.0934(19)	0.0686(16)	0.0462(13)	-0.0075(14)	0.0015(13)	0.0144(11)
Cl(7)	0.1164(26)	0.1240(25)	0.1083(24)	0.0363(21)	0.0716(21)	0.0068(19)
Cl(8)	0.1019(23)	0.0921(21)	0.1424(27)	0.0597(19)	0.0366(20)	-0.0019(19)
Cl(9)	0.1249(28)	0.0902(22)	0.1679(33)	0.0499(21)	0.0475(25)	0.0243(22)
Cl(10)	0.0691(18)	0.1271(25)	0.0932(20)	0.0277(17)	0.0212(15)	-0.0351(18)
O(120)	0.0184(24)	0.0189(24)	0.0250(24)	0.0069(19)	0.0032(19)	-0.0015(19)
O(140)	0.0226(24)	0.0261(24)	0.0207(23)	0.0129(20)	0.0049(19)	0.0015(18)
O(160)	0.0177(24)	0.0214(23)	0.0240(24)	0.0052(19)	0.0043(19)	0.0014(18)
O(180)	0.0169(23)	0.0227(23)	0.0199(23)	0.0063(19)	0.0042(19)	0.0017(18)
O(220)	0.0164(23)	0.0217(23)	0.0262(26)	0.0051(19)	0.0073(19)	0.0038(19)
O(240)	0.0225(25)	0.0268(25)	0.0208(24)	0.0048(20)	0.0027(19)	0.0053(19)
O(260)	0.0277(25)	0.0150(22)	0.0255(24)	0.0064(20)	0.0055(20)	0.0031(19)
O(280)	0.0205(24)	0.0210(23)	0.0179(22)	0.0068(19)	0.0039(19)	0.0032(18)
N(10)	0.0128(28)	0.0181(29)	0.0196(29)	0.0012(24)	0.0014(23)	0.0013(23)
N(20)	0.0173(29)	0.0178(29)	0.0246(31)	0.0053(24)	0.0049(24)	-0.0020(24)
C(10)	0.0146(36)	0.0238(38)	0.0348(41)	0.0006(32)	0.0001(31)	-0.0018(32)
C(11)	0.0391(55)	0.0635(63)	0.166(11)	0.0248(49)	0.0179(61)	-0.0520(65)
C(20)	0.0324(41)	0.0193(36)	0.0219(38)	0.0099(32)	0.0046(32)	0.0029(30)
C(21)	0.0971(75)	0.0744(63)	0.0446(52)	0.0460(58)	-0.0031(49)	0.0317(47)
C(101)	0.0198(37)	0.0304(40)	0.0336(40)	0.0146(32)	0.0006(32)	-0.0105(32)
C(102)	0.0447(49)	0.0486(47)	0.0304(41)	0.0370(41)	0.0158(37)	0.0086(36)
C(103)	0.0337(45)	0.0256(40)	0.0637(53)	0.0225(36)	0.0222(40)	0.0064(37)
C(104)	0.0277(41)	0.0333(41)	0.0349(42)	0.0185(35)	0.0085(33)	-0.0048(33)
C(105)	0.0224(38)	0.0273(37)	0.0252(37)	0.0172(32)	0.0079(30)	-0.0017(29)

Table 4.9 (cont). Complete Anisotropic Thermal Parameters for [Cp*Ta(NCCH$_3$)(*p-tert*-butylcalix[4]arene)]·2.5 CH_2Cl_2 (2c)·2.5 CH_2Cl_2.[a]

atom	U11	U22	U33	U12	U13	U23
C(106)	0.0177(41)	0.0695(57)	0.0646(55)	0.0186(40)	0.0032(38)	-0.0254(44)
C(107)	0.0857(69)	0.1129(77)	0.0451(51)	0.0848(64)	0.0234(48)	0.0312(51)
C(108)	0.0685(64)	0.0311(47)	0.1317(86)	0.0229(45)	0.0700(62)	0.0222(50)
C(109)	0.0335(46)	0.0671(56)	0.0518(51)	0.0192(42)	-0.0030(39)	-0.0333(43)
C(110)	0.0565(53)	0.0610(52)	0.0419(46)	0.0356(44)	0.0372(41)	0.0114(39)
C(120)	0.0097(33)	0.0210(37)	0.0332(40)	0.0021(28)	0.0073(29)	0.0056(30)
C(121)	0.0117(34)	0.0239(37)	0.0249(37)	0.0050(28)	-0.0000(27)	0.0009(29)
C(122)	0.0147(35)	0.0325(41)	0.0250(37)	-0.0017(30)	0.0031(29)	-0.0044(31)
C(123)	0.0177(37)	0.0239(39)	0.0442(46)	0.0034(30)	0.0073(32)	0.0054(33)
C(124)	0.0217(37)	0.0160(36)	0.0375(42)	0.0054(29)	0.0082(31)	0.0097(30)
C(125)	0.0183(37)	0.0260(39)	0.0334(40)	0.0027(30)	0.0099(30)	0.0074(31)
C(126)	0.0295(40)	0.0211(36)	0.0303(39)	0.0089(31)	0.0112(31)	0.0123(29)
C(127)	0.0333(44)	0.0297(41)	0.0491(48)	0.0095(35)	0.0111(36)	-0.0008(34)
C(128)	0.0713(76)	0.0448(60)	0.224(14)	-0.0071(54)	0.0626(85)	-0.0510(73)
C(129)	0.0915(86)	0.0828(78)	0.150(11)	0.0614(70)	-0.0155(76)	-0.0449(72)
C(130)	0.258(17)	0.0650(73)	0.0872(84)	0.0834(94)	0.0650(98)	0.0027(61)
C(140)	0.0295(40)	0.0265(38)	0.0114(32)	0.0127(33)	0.0114(28)	0.0055(27)
C(141)	0.0195(36)	0.0276(39)	0.0206(35)	0.0099(31)	0.0078(28)	0.0071(28)
C(142)	0.0373(44)	0.0212(36)	0.0200(35)	0.0068(32)	0.0107(31)	0.0081(28)
C(143)	0.0318(43)	0.0267(39)	0.0242(37)	0.0128(33)	0.0098(31)	0.0087(29)
C(144)	0.0218(37)	0.0395(43)	0.0176(34)	0.0126(33)	0.0055(28)	0.0054(30)
C(145)	0.0221(38)	0.0236(36)	0.0175(34)	0.0080(30)	0.0049(28)	0.0021(27)
C(146)	0.0218(36)	0.0264(37)	0.0239(36)	0.0112(30)	0.0054(29)	0.0016(29)
C(147)	0.0389(45)	0.0365(43)	0.0409(44)	0.0191(36)	0.0086(36)	0.0110(34)
C(148)	0.1288(93)	0.0753(68)	0.0616(62)	0.0739(68)	-0.0078(60)	0.0096(51)
C(149)	0.0557(58)	0.0391(50)	0.1172(80)	0.0277(45)	0.0349(56)	0.0129(50)
C(150)	0.0596(58)	0.0398(49)	0.0891(67)	0.0286(44)	0.0206(50)	0.0225(46)
C(160)	0.0154(35)	0.0126(33)	0.0232(36)	-0.0027(27)	0.0011(28)	-0.0061(27)
C(161)	0.0166(35)	0.0159(33)	0.0199(34)	0.0005(28)	-0.0066(28)	-0.0024(27)
C(162)	0.0172(35)	0.0166(34)	0.0219(35)	0.0012(28)	-0.0029(28)	0.0038(27)
C(163)	0.0175(35)	0.0121(33)	0.0308(38)	0.0042(28)	-0.0001(29)	-0.0014(28)

Table 4.9 (cont). Complete Anisotropic Thermal Parameters for [Cp*Ta(NCCH$_3$)(*p-tert*-butylcalix[4]arene)]·2.5 CH_2Cl_2 (2c)·2.5 CH_2Cl_2.[a]

atom	U11	U22	U33	U12	U13	U23
C(164)	0.0197(36)	0.0186(34)	0.0216(35)	0.0023(29)	0.0047(28)	-0.0016(27)
C(165)	0.0153(34)	0.0100(31)	0.0201(34)	-0.0009(26)	0.0017(27)	0.0001(25)
C(166)	0.0172(35)	0.0162(33)	0.0223(35)	-0.0005(27)	0.0063(28)	0.0040(27)
C(167)	0.0240(38)	0.0276(38)	0.0322(39)	0.0103(31)	0.0076(31)	0.0032(30)
C(168)	0.0233(41)	0.0535(50)	0.0573(51)	0.0199(37)	0.0087(37)	0.0109(40)
C(169)	0.0376(47)	0.0552(51)	0.0507(49)	0.0276(40)	0.0206(38)	0.0119(39)
C(170)	0.0390(46)	0.0370(44)	0.0587(51)	0.0193(37)	0.0128(39)	0.0025(37)
C(180)	0.0213(37)	0.0188(34)	0.0178(34)	0.0090(29)	0.0032(28)	0.0058(27)
C(181)	0.0277(39)	0.0205(35)	0.0139(33)	0.0130(30)	-0.0004(28)	0.0053(27)
C(182)	0.0229(37)	0.0277(38)	0.0227(36)	0.0133(31)	0.0039(30)	0.0080(30)
C(183)	0.0236(38)	0.0247(36)	0.0241(36)	0.0137(31)	0.0037(30)	0.0035(29)
C(184)	0.0284(39)	0.0227(35)	0.0153(34)	0.0119(31)	-0.0019(29)	-0.0006(27)
C(185)	0.0109(33)	0.0209(35)	0.0248(36)	0.0032(28)	-0.0021(28)	0.0053(29)
C(186)	0.0241(38)	0.0260(37)	0.0227(36)	0.0102(30)	-0.0032(29)	0.0013(28)
C(187)	0.0329(42)	0.0440(45)	0.0232(38)	0.0183(36)	0.0055(32)	0.0010(32)
C(188)	0.0895(73)	0.1169(79)	0.0243(44)	0.0614(64)	0.0254(45)	0.0163(47)
C(189)	0.1150(88)	0.0779(68)	0.0663(63)	0.0621(66)	0.0363(60)	0.0028(51)
C(190)	0.0542(63)	0.1349(94)	0.0570(61)	0.0069(62)	0.0290(50)	-0.0374(59)
C(201)	0.0289(40)	0.0249(38)	0.0227(36)	0.0088(33)	0.0003(30)	0.0097(29)
C(202)	0.0338(42)	0.0341(41)	0.0172(35)	0.0174(35)	-0.0033(30)	0.0083(30)
C(203)	0.0307(41)	0.0241(37)	0.0227(36)	0.0058(32)	0.0024(30)	0.0097(30)
C(204)	0.0293(40)	0.0300(40)	0.0183(35)	0.0142(33)	0.0024(30)	0.0118(30)
C(205)	0.0281(40)	0.0364(42)	0.0207(36)	0.0112(34)	0.0015(31)	0.0123(31)
C(206)	0.0491(49)	0.0236(39)	0.0386(43)	0.0117(36)	0.0022(36)	0.0121(33)
C(207)	0.0351(45)	0.0470(47)	0.0439(45)	0.0245(38)	-0.0015(36)	0.0085(36)
C(208)	0.0414(47)	0.0391(44)	0.0352(43)	0.0104(37)	0.0005(35)	0.0074(34)
C(209)	0.0515(49)	0.0394(44)	0.0207(38)	0.0135(38)	0.0113(34)	0.0060(32)
C(210)	0.0457(48)	0.0354(42)	0.0324(41)	0.0124(37)	0.0125(35)	0.0144(33)
C(220)	0.0311(41)	0.0158(34)	0.0139(35)	0.0048(29)	-0.0002(30)	0.0044(26)
C(221)	0.0221(37)	0.0104(32)	0.0229(36)	0.0032(28)	0.0054(29)	-0.0006(26)
C(222)	0.0177(35)	0.0150(34)	0.0279(38)	0.0022(27)	-0.0003(30)	0.0012(27)

Table 4.9 (cont). Complete Anisotropic Thermal Parameters for [Cp*Ta(NCCH$_3$)(*p-tert*-butylcalix[4]arene)]·2.5 CH_2Cl_2 (2c)·2.5 CH_2Cl_2.[a]

atom	U11	U22	U33	U12	U13	U23
C(223)	0.0270(40)	0.0187(34)	0.0217(35)	0.0097(30)	0.0035(30)	0.0004(27)
C(224)	0.0342(43)	0.0212(36)	0.0252(38)	0.0104(31)	0.0145(32)	-0.0014(28)
C(225)	0.0207(36)	0.0171(34)	0.0275(38)	0.0087(29)	0.0080(30)	0.0053(28)
C(226)	0.0285(40)	0.0334(40)	0.0236(36)	0.0156(33)	0.0075(30)	-0.0021(30)
C(227)	0.0324(41)	0.0317(40)	0.0193(36)	0.0056(33)	0.0036(30)	0.0003(29)
C(228)	0.0806(63)	0.0445(48)	0.0211(40)	0.0251(45)	-0.0037(39)	-0.0121(34)
C(229)	0.0463(48)	0.0536(49)	0.0267(40)	0.0215(40)	0.0093(35)	0.0122(35)
C(230)	0.0408(49)	0.0713(57)	0.0221(40)	0.0093(42)	-0.0013(35)	0.0093(37)
C(240)	0.0091(33)	0.0312(40)	0.0311(40)	0.0081(29)	0.0027(29)	0.0112(32)
C(241)	0.0169(36)	0.0307(40)	0.0314(40)	0.0078(31)	0.0050(30)	0.0039(32)
C(242)	0.0215(38)	0.0416(46)	0.0261(39)	0.0034(34)	0.0095(31)	0.0046(33)
C(243)	0.0205(38)	0.0348(43)	0.0324(42)	-0.0004(32)	0.0037(31)	0.0068(33)
C(244)	0.0213(38)	0.0290(39)	0.0319(41)	0.0014(31)	0.0037(31)	0.0122(33)
C(245)	0.0157(35)	0.0263(38)	0.0260(37)	0.0041(29)	0.0031(28)	0.0023(29)
C(246)	0.0170(36)	0.0231(37)	0.0325(39)	-0.0050(29)	-0.0020(30)	0.0075(30)
C(247)	0.0523(53)	0.0472(49)	0.0305(43)	0.0030(41)	0.0094(38)	0.0157(36)
C(248)	0.0894(76)	0.1354(92)	0.0549(59)	0.0685(71)	0.0430(55)	0.0530(61)
C(249)	0.250(17)	0.1010(90)	0.0386(60)	-0.1042(98)	-0.0041(79)	0.0338(60)
C(250)	0.1100(86)	0.1053(80)	0.0508(57)	0.0697(70)	0.0274(56)	0.0370(54)
C(260)	0.0279(39)	0.0124(33)	0.0164(33)	0.0017(29)	-0.0002(28)	-0.0045(27)
C(261)	0.0283(39)	0.0157(35)	0.0210(35)	0.0028(30)	-0.0020(29)	-0.0049(28)
C(262)	0.0321(42)	0.0159(35)	0.0306(39)	0.0018(31)	0.0073(32)	-0.0009(29)
C(263)	0.0307(42)	0.0164(35)	0.0314(39)	0.0059(31)	-0.0011(32)	-0.0041(29)
C(264)	0.0237(37)	0.0167(35)	0.0287(37)	0.0065(30)	0.0024(30)	-0.0012(29)
C(265)	0.0293(39)	0.0133(33)	0.0193(34)	0.0061(29)	0.0011(29)	-0.0023(27)
C(266)	0.0281(39)	0.0198(35)	0.0226(36)	0.0095(30)	0.0038(30)	-0.0038(28)
C(267)	0.0394(46)	0.0316(42)	0.0408(45)	0.0133(36)	0.0030(36)	0.0129(34)
C(268)	0.0534(53)	0.0334(44)	0.0639(54)	0.0194(40)	0.0212(43)	0.0180(39)
C(269)	0.0475(55)	0.0562(57)	0.1091(76)	0.0234(46)	0.0164(51)	0.0561(54)
C(270)	0.1317(90)	0.0453(52)	0.0414(50)	0.0477(57)	0.0036(53)	0.0121(41)
C(280)	0.0189(36)	0.0251(37)	0.0197(34)	0.0062(30)	0.0096(29)	0.0074(29)

Table 4.9 (cont). Complete Anisotropic Thermal Parameters for [Cp*Ta(NCCH$_3$)(*p-tert*-butylcalix[4]arene)]·2.5 CH_2Cl_2 (2c)·2.5 CH_2Cl_2.[a]

atom	U11	U22	U33	U12	U13	U23
C(281)	0.0264(38)	0.0210(36)	0.0157(33)	0.0051(30)	0.0085(29)	0.0039(27)
C(282)	0.0282(39)	0.0207(36)	0.0325(39)	0.0124(31)	0.0095(32)	0.0044(30)
C(283)	0.0238(38)	0.0260(38)	0.0283(38)	0.0105(31)	0.0057(31)	0.0034(30)
C(284)	0.0227(38)	0.0274(38)	0.0201(35)	0.0024(31)	0.0013(29)	0.0038(29)
C(285)	0.0214(36)	0.0191(35)	0.0221(35)	0.0025(29)	0.0073(30)	0.0070(29)
C(286)	0.0177(35)	0.0150(33)	0.0233(35)	-0.0013(27)	-0.0000(28)	0.0003(27)
C(287)	0.0249(39)	0.0365(42)	0.0387(42)	0.0137(33)	0.0034(33)	0.0071(33)
C(288)	0.0341(48)	0.0822(63)	0.0581(54)	0.0344(46)	-0.0014(40)	0.0016(46)
C(289)	0.0351(46)	0.0504(50)	0.0537(51)	0.0143(39)	-0.0182(39)	0.0028(40)
C(290)	0.0456(51)	0.0492(50)	0.0545(51)	0.0216(42)	-0.0064(40)	0.0144(40)
C(300)	0.0608(64)	0.0743(66)	0.0818(69)	0.0252(53)	0.0165(53)	-0.0277(54)
C(301)	0.0496(54)	0.0675(59)	0.0594(56)	0.0253(47)	0.0012(43)	0.0218(46)
C(302)	0.0520(53)	0.0582(54)	0.0517(51)	0.0213(44)	0.0195(42)	0.0117(41)
C(303)	0.0620(60)	0.0737(61)	0.0554(55)	0.0379(50)	0.0159(45)	0.0244(46)
C(304)	0.0959(81)	0.1010(80)	0.0507(58)	0.0428(67)	0.0154(54)	0.0018(54)

[a] Numbers in parentheses are estimated standard deviations in the last significant digit. The anisotropic temperature factors are of the form $\exp[-2\pi^2(U_{11}h^2a^{*2} \ldots +2U_{12}hka^*b^* = \ldots)]$.

Table 4.10. Selected Interatomic Bond Distances (Å) and Angles (deg) for [Cp*Ta(calix[4]arene)] (1).[a]

Bond Distances	
Ta-O(20)	1.902(4)
Ta-O(40)	2.010(3)
Ta-O(60)	1.871(4)
Ta-O(80)	2.000(3)
Ta-C(1)	2.424(5)
Ta-C(2)	2.447(5)
Ta-C(3)	2.476(5)
Ta-C(4)	2.480(5)
Ta-C(5)	2.425(5)
Bond Angles	
O(20)-Ta-O(40)	84.3(1)
O(20)-Ta-O(60)	127.0(2)
O(20)-Ta-O(80)	84.8(1)
O(40)-Ta-O(60)	84.1(1)
O(40)-Ta-O(80)	155.1(1)
O(60)-Ta-O(80)	84.7(1)
Ta-O(20)-C(20)	160.8(4)
Ta-O(40)-C(40)	124.1(3)
Ta-O(60)-C(60)	171.6(4)
Ta-O(80)-C(80)	125.2(3)

[a]Estimated standard deviations in the least significant figure are given in parentheses.

Table 4.11. Selected Interatomic Bond Distances (Å) and Angles (deg) for [Cp*Ta(*p-tert*-butylcalix[4]arene)]·toluene (2a)·toluene.[a]

Bond Distances

Ta-O(20)	1.879(3)
Ta-O(40)	2.002(3)
Ta-O(60)	1.893(3)
Ta-O(80)	1.999(3)
Ta-C(1)	2.451(4)
Ta-C(2)	2.450(4)
Ta-C(3)	2.429(4)
Ta-C(4)	2.437(4)
Ta-C(5)	2.473(4)

Bond Angles

O(20)-Ta-O(40)	83.0(1)
O(20)-Ta-O(60)	123.6(1)
O(20)-Ta-O(80)	83.5(1)
O(40)-Ta-O(60)	84.9(1)
O(40)-Ta-O(80)	155.2(1)
O(60)-Ta-O(80)	85.3(1)
Ta-O(20)-C(20)	178.4(3)
Ta-O(40)-C(40)	124.2(2)
Ta-O(60)-C(60)	158.4(3)
Ta-O(80)-C(80)	123.3(2)

[a]Estimated standard deviations in the least significant figure are given in parentheses.

Table 4.12. Selected Interatomic Bond Distances (Å) and Angles (deg) for [Cp*Ta(OH_2)(*p-tert*-butylcalix[4]arene)]·acetone (2b)·acetone.[a]

Bond Distances

Ta-O(1)	2.188(3)
Ta-O(20)	1.986(3)
Ta-O(40)	1.987(3)
Ta-O(60)	1.972(3)
Ta-O(80)	1.985(3)
Ta-C(1)	2.543(5)
Ta-C(2)	2.509(5)
Ta-C(3)	2.455(4)
Ta-C(4)	2.461(4)
Ta-C(5)	2.516(5)

Bond Angles

O(20)-Ta(1)-O(40)	88.5(1)
O(20)-Ta(1)-O(60)	156.3(1)
O(20)-Ta(1)-O(80)	87.2(1)
O(40)-Ta(1)-O(60)	87.3(1)
O(40)-Ta(1)-O(80)	157.2(1)
O(60)-Ta(1)-O(80)	87.7(1)
Ta(1)-O(20)-C(20)	133.8(3)
Ta(1)-O(40)-C(40)	130.6(3)
Ta(1)-O(60)-C(60)	135.2(3)
Ta(1)-O(80)-C(80)	133.2(3)
O(1)-Ta(1)-O(20)	77.6(1)
O(1)-Ta(1)-O(40)	79.2(1)
O(1)-Ta(1)-O(60)	78.7(1)
O(1)-Ta(1)-O(80)	78.0(1)

[a]Estimated standard deviations in the least significant figure are given in parentheses.

Table 4.13. Selected Interatomic Bond Distances (Å) and Angles (deg) for [Cp*Ta(NCCH$_3$)(*p-tert*-butylcalix[4]arene)]·2.5 CH_2Cl_2 (2c)·2.5 CH_2Cl_2.

Bond Distances

Ta(100)-N(10)	2.246(5)	Ta(200)-N(20)	2.236(5)
N(10)-C(10)	1.110(7)	N(20)-C(20)	1.124(7)
C(10)-C(11)	1.46(1)	C(20)-C(21)	1.453(9)
Ta(100)-O(120)	1.981(4)	Ta(200)-O(220)	1.970(4)
Ta(100)-O(140)	1.977(4)	Ta(200)-O(240)	1.991(4)
Ta(100)-O(160)	2.007(4)	Ta(200)-O(260)	1.997(4)
Ta(100)-O(180)	1.970(4)	Ta(200)-O(280)	1.980(4)
Ta(100)-C(101)	2.527(6)	Ta(200)-C(201)	2.522 (7)
Ta(100)-C(102)	2.504(6)	Ta(200)-C(202)	2.495(6)
Ta(100)-C(103)	2.469(6)	Ta(200)-C(203)	2.437(6)
Ta(100)-C(104)	2.466(6)	Ta(200)-C(204)	2.446(6)
Ta(100)-C(105)	2.505(6)	Ta(200)-C(205)	2.510(6)

Bond Angles

Ta(100)-N(10)-C(10)	176.8(5)	Ta(200)-N(20)-C(20)	175.9(5)
N(10)-C(10)-C(11)	177.9(7)	N(20)-C(20)-C(21)	179.7(7)
O(120)-Ta(100)-O(140)	87.5(2)	O(220)-Ta(200)-O(240)	87.5(2)
O(120)-Ta(100)-O(160)	155.8(2)	O(220)-Ta(200)-O(260)	155.2(2)
O(120)-Ta(100)-O(180)	87.9(2)	O(220)-Ta(200)-O(280)	88.0(2)
O(140)-Ta(100)-O(160)	87.3(2)	O(240)-Ta(200)-O(260)	87.3(2)
O(140)-Ta(100)-O(180)	155.3(2)	O(240)-Ta(200)-O(280)	155.7(2)
O(160)-Ta(100)-O(180)	87.0(2)	O(260)-Ta(200)-O(280)	86.9(2)
Ta(100)-O(120)-C(120)	132.8(3)	Ta(200)-O(220)-C(220)	135.2(3)
Ta(100)-O(140)-C(140)	135.3(3)	Ta(200)-O(240)-C(240)	133.9(3)
Ta(100)-O(160)-C(160)	130.1(3)	Ta(200)-O(260)-C(260)	131.2(3)
Ta(100)-O(180)-C(180)	136.1(3)	Ta(200)-O(280)-C(280)	135.0(3)

Table 4.13 (cont). Selected Interatomic Bond Distances (Å) and Angles (deg) for [Cp*Ta(NCCH$_3$)(*p-tert*-butylcalix[4]arene)]·2.5 CH_2Cl_2 (2c)·2.5 CH_2Cl_2.

O(120)-Ta(100)-N(10)	77.5(2)	O(220)-Ta(200)-N(20)	77.3(2)
O(140)-Ta(100)-N(10)	77.7(2)	O(240)-Ta(200)-N(20)	77.9(2)
O(160)-Ta(100)-N(10)	78.3(2)	O(260)-Ta(200)-N(20)	78.0(2)
O(180)-Ta(100)-N(10)	77.6(2)	O(280)-Ta(200)-N(20)	77.8(2)

[a]Estimated standard deviations in the least significant figure are given in parentheses.

Table 4.14. Mulliken Atomic Charges for Oxygen Atoms from Fenske-Hall Calculations for [Cp*Ta(calix[4]-arene)] (1), [Cp*Ta(OH_2)(calix[4]arene)], and [Cp*Ta-($NCCH_3$)(calix[4]arene)]

atom	[Cp*Ta(calix[4]-arene)] (1)	[Cp*Ta(OH_2)-(calix[4]arene)]	[Cp*Ta($NCCH_3$)-(calix[4]arene)]
δ_{O20}	-0.526	-0.591	-0.587
δ_{O40}	-0.602	-0.618	-0.597
δ_{O60}	-0.499	-0.584	-0.599
δ_{O80}	-0.594	-0.588	-0.581

About the Author

I was born and raised in Michigan by my parents Peter and Barbara Acho. He is an independent business man, and she is a private therapist. From very early on, they emphasized the importance of education to my brother Michael and me and encouraged us to pursue whatever would make us happy.

Although all children are naturally scientific, this can be fostered or discouraged as they grow. Interest in science in adulthood can usually be traced to positive experiences along the way. I am not different. My interest in chemistry was sparked in high school and fueled at the University of Michigan in Ann Arbor where I began learning about scientific research with Professor Seyhan Ege. Her enthusiasm was contagious, and I decided to pursue graduate studies in chemistry at MIT. She and I also share a passion for teaching. Her influence on my teaching philosophy is obvious, and it is certainly a credit to her as well as one of my greatest joys that students awarded me the institute-wide Goodwin Medal for "conspicuously effective teaching by a graduate student at MIT" in the Spring of 1992.

I carried out scientific research under the direction of Professor Stephen J. Lippard while at MIT, learning much about science and life. My career in the Lippard laboratories did have a turning point. Because it is so much a part of this thesis, I feel it is appropriate to tell the story here: in the second year of graduate study in inorganic chemistry at MIT, students are required to undergo oral examinations. As a part of this exercise a novel proposal for original research is required. I found the very intriguing calixarene ligands and produced a proposal which truly excited me and subsequently caught the interest of my advisor. We agreed then that it would be worthwhile to pursue transition metal calixarene chemistry. I was so grateful then for such freedom and still am. The rest is history, written on the preceding pages.

I have made a decision that leads me away from scientific research not because I did not enjoy myself here, but because I am inspired now to pursue other interests. Following a vacation spending time with family and friends, I will be working in the Chicago office of the consulting firm, McKinsey & Company, Inc. Although my experience in reductive coupling chemistry and transition metal calixarenes will probably not be called upon in the near future, the time I spent learning to be a scientific researcher is now deeply a part of who I am. There are those who believe that what we take from education is not so much information as it is the process of learning and teaching ourselves. The strength of this experience should apply to any pursuit. In the years to come, I hope to find that they are right.

Jacqueline Ann Acho

October 17, 1994